UNIVERSITEIT VAN PRETORIA
UNIVERSITY OF PRETORIA
YUNIBESITHI YA PRETORIA

Heat transfer and pressure drop in annuli with non-uniform internal wall temperatures in the transition flow regime

by

Dickson Daniel Ndenguma

Thesis submitted in partial fulfilment of the requirements for the degree

PhD in Mechanical Engineering

in the Faculty of Engineering, Built

Environment and Information Technology

UNIVERSITY OF PRETORIA

Supervisors: Prof J Dirker and Prof JP Meyer

December 2017

© University of Pretoria

Abstract

It is common practice to design heat exchangers that are operated in either the laminar or the turbulent flow regime and not in the transition flow regime. This could mainly be due to a lack of knowledge on the behaviour in the transition flow regime for several reasons. However, due to factors such as design constraints, heat exchangers may indeed operate in the transition flow regime.

An experimental study was conducted to determine the lower and upper Reynolds number limits of the transition flow regime, and the characteristics of the heat transfer coefficients and friction factors for annular passages with different geometric dimensions. The inner wall of the annular passage had different degrees of non-uniform temperature, while the outer wall was insulated. Both heated and cooled flow applications with water as fluid (cold fluid and hot fluid respectively) were investigated. The isothermal condition investigation was also conducted for pressure drop. Four horizontal concentric counter-flow tube-in-tube heat exchangers with conventional inlet geometries were considered to obtain the required data. The hydraulic diameters of the test sections were 26.2 mm, 23 mm, 20.2 mm and 17 mm, their respective annular diameter ratios were 0.327, 0.409, 0.386 and 0.483 and their length-to-hydraulic ratios were 193, 221, 251 and 299 respectively. The flow was both hydrodynamic and thermally developing. Test data of laminar, transition and turbulent flow regimes was collected. However, the transition flow regime was the main area of interest for this study. The transition flow regime was found to exhibit either mixed or forced convection types. Average heat transfer coefficients were obtained for both heating and cooling cases, while friction factors were obtained for heating, cooling and isothermal conditions. Uncertainties in the friction factor and Nusselt number were on average below 5.6% and 10.5%, respectively.

The geometric size of the annular passage, degree of wall temperature uniformity and direction of the heat flux (heating and cooling cases of annular fluid) had a significant influence on the heat transfer coefficients, friction factors and Reynolds number span of the transition flow regime. New correlations for predicting the transition flow regime Reynolds number spans, Nusselt numbers and friction factors were developed for the transition flow regime and predicted most of the data to within ±10%.

Acknowledgements

I would like to acknowledge the following people and institutions for their support:

Publications originating from this investigation

Journal papers:

1) Ndenguma, D.D., Dirker, J., and Meyer, J.P., "Transitional flow regime heat transfer and pressure drop in an annulus with non-uniform wall temperatures", *International Journal of Heat and Mass Transfer*, 108, pp 2239–2252, 2017.
2) Ndenguma, D.D., Dirker, J., and Meyer, J.P., "Heat transfer and pressure drop in annuli with approximately uniform internal wall temperatures in the transitional flow regime", *International Journal of Heat and Mass Transfer*, 111, pp 429–441, 2017.

Peer reviewed International conference papers:

3) Ndenguma, D.D., Dirker, J., and Meyer, J.P. "Heat transfer and pressure drop characteristics of a horizontal annular passage in the transitional flow regime", 11th International Conference on Heat Transfer, Fluid Mechanics and Thermodynamics, HEFAT 2015, Kruger National Park, South Africa, Paper Number: 1570073907, 20-23 July 2015.
4) Ndenguma, D.D., Dirker, J., and Meyer, J.P. "Transitional flow regime heat transfer in a horizontal annular passage associated with mixed-convection and non-uniform wall temperature boundary condition", 12th International Conference on Heat Transfer, Fluid Mechanics and Thermodynamics, HEFAT 2016, Costa del Sol, Spain, Paper Number: 1570248845, 11–13 July 2016.

Journal paper prepared for review:

5) Ndenguma, D.D., Dirker, J., and Meyer, J.P. "Correlating Heat Transfer and Pressure Drop in Annuli for Different Non-Uniform Internal Wall Temperature Boundary Conditions and Annular Diameter Ratios in the Transitional Flow Regime".

Table of contents

Results of the influence of the degree of wall temperature uniformity............................... 142

List of figures

xiv

List of tables

Nomenclature

A_c	Cross-section area	[m^2]
A_s	Surface area	[m^2]
c_p	Specific heat	[J/kgK]
D	Diameter	[m]
DAQ	data acquisition	
DNS	Direct numerical simulations	
D_0	Inner diameter of outer tube of heat exchanger	[m]
D_1	Outer diameter of inner tube of heat exchanger	[m]
D_i	Inside diameter of the inner tube	[m]
e	Surface roughness	[mm]
E	Modulus of elasticity	[Pa]
g	Acceleration due to gravity	[m/s^2]
h	Convection heat transfer coefficient	[W/m^{2}K]
HEST	High Education, Science and Technology	
I_x	Second moment of area	[m^4]
k	Thermal conductivity	[W/mK]
L_{dp}	Pressure drop length	[m]
L_{hx}	Heat exchange length	[m]
$L_{unsupported}$	Unsupported axial length of tube	[m]
LMTD	Logarithmic mean temperature difference	
$\dot{m}$	Mass flow rate	[kg/s]
Δp	Pressure drop	[kPa]
RMSD	Root mean square deviation	

$\dot{Q}$	Heat transfer rate	[W]
T	Temperature	[°C]
$\bar{T}$	Averaged temperature	[°C]
UHF	Uniform heat flux	
UWT	Uniform wall temperature	
$\bar{V}$	Average cross-sectional velocity	[m/s]
w	Distributed load	[N/m]
x	Axial coordinate along heat exchanger	[m]
y_{max}	Maximum allowable vertical displacement	[mm]

Dimensionless parameters

a	annular diameter ratio (D_1/D_0)	
B	coefficients	
C	coefficients	
F	factor to take into account the dependence on a	
f	Friction factor	
Gr	Grashof number	
Gz	Graetz number	
K	factor to consider the temperature dependence of fluid properties	
m	exponent for Re	
n	exponents for λ	
Nu	Nusselt number	
Nu_l	Nusselt number in the laminar regime	
Nu_t	Nusselt number in the turbulent regime	

Nu_{trans} Nusselt number in the transition regime

p exponent for τ

Pr   Prandtl number

Ra   Rayleigh number (Gr.Pr)

Re   Reynolds number

Re^{*} adjusted Reynolds number

Re_1 Reynolds number at transition starting point

Re_2 Reynolds number at transition ending point

u exponents for Gr

v exponents for Pr

z_1, z_2 exponent for (GrPr/Re)

z_3 exponent for ($\mathrm{Gr}^u \mathrm{Pr}^v$)

Greek symbols

β coefficient of thermal expansion   [1/K]

λ annular geometric parameter   [-]

μ dynamic viscosity   [kg/m.s]

ρ density   [kg/m^3]

τ degree of wall temperature uniformity   [-]

υ kinematic viscosity $= \mu / \rho$ [m^2/s]

Subscripts

0   outer wall of annulus

1   inner wall of annulus

am   arithmetic mean value

b   bulk property

ca   for a cooled annulus

cu   copper

d   diabatic

F   pure forced convection

h   hydraulic

ha   for a heated annulus

i   inner flow passage

in   inlet

iso   for isothermal conditions

iw   inner annular wall

lm   logarithmic mean temperature difference

max   maximum

min   minimum

o   annular flow passage

out   outlet

Re$_2$ for the upper Reynolds number limit of the transitional flow regime

ΔRe   for the transition flow regime Reynolds number span

Chapter 1

Introduction

1.1 Background

Throughout the years, extensive heat transfer and pressure drop studies were performed on fluids flowing in tubes. From about 1840, it was realised that the flow of a fluid could be of different kinds. By observing the behaviour of a stream of dye in flowing water, Reynolds was able to distinguish between two distinct flow regimes, which he called direct and sinuous (Reynolds, 1883). These flow regimes are known in modern terms as laminar and turbulent flows. The process of a laminar flow becoming turbulent, or vice versa, is known as transition flow. This is an extraordinarily complicated process, which is not fully understood. Whether the flow is laminar, transition or turbulent can be correlated to the Reynolds number[1].

In about 1840, a German engineer, GHL Hagen, and a French physicist, JLM Poiseuille, conducted independent experimental investigations of isothermal flow in straight pipes with a circular cross-section (Massey, 2006). They found that the pressure drop in a tube is directly proportional to the shear stress at the tube wall and inversely proportional to the diameter of the tube. From these relationships, a dimensionless term known as friction factor was derived. The friction factor is widely used in the design of pipe systems and in heat exchangers to determine the pumping power consumption required for a system,

Besides circular tubes, thermal engineers are also interested in other flow passages, including annular flow passages. Annular passages are important to applications such as tube-in-tube heat exchangers, condensers for sea water distillation, boilers, cooling channels of nuclear reactors, thermal storage, solar energy systems, gas-cooled electrical cables, thermal insulation, food processes, chemical processing and many more (Dawood, Muhammed, Sidik, Munisamy and

---

[1] The Reynolds number is a ratio of inertia to viscous forces.

Wahid, 2015; Passerini, Ferrario and Thäter, 2007; Sambamurthy, Shaija, Narasimham and Murthy, 2008). A tube-in-tube heat exchanger is one of the simplest types of heat exchanger to construct. It consists of two concentric pipes of different diameters that form an annular passage between them. Normally the fluids in the inner tube and the annular passage flow in opposing directions. Such heat exchangers are commonly used in a wide range of cooling and heating applications, and are vital to the energy sector.

A good heat exchanger can be described as one that maximises the heat transferred between the two fluids at a relatively low pumping power. The flow rate of fluid plays an important role in the heat transfer performance. The heat transfer rate to or from the fluid depends on its flow rate. Laminar flow is normally associated with a low pressure drop and heat transfer, while turbulent flow is associated with a high pressure drop and heat transfer. Pressure drop translates into head loss, which accounts for extra cost for pumping the fluid. A compromise between the heat transfer ability and the pressure drop penalty is often sought.

When sizing heat exchanger components, thermal designers often rely on design correlations to predict the heat transfer coefficients and fluid flow friction factors. The correlations are simplified models that aim to describe complicated fluid and thermal interactions. Therefore, they are developed for particular thermal and flow conditions. Notably, the flow regime has a major impact on the mathematical format of the correlation. For instance, when considering circular tubes, most of these correlations are available for turbulent flow, followed by the correlations for laminar flow and relatively little is available in the transition flow regime (Abraham, Sparrow and Tong, 2009; Gnielinski, 2013; Kakaç, Shah and Aung, 1987).

Aside from the flow regimes' major impact on the performance of heat transfer and pressure drop, other factors are also known to have a large impact on heat transfer coefficients, friction factors and the Reynolds number limits of the transition flow regime. Some of these factors include the thermal boundary condition on the heat transfer surface, the type of convection (free, forced or mixed), the geometry and angle of orientation of the fluid passage, the fluid velocity and temperature profiles as determined by the entrance conditions (developing or fully developed flows) and the roughness of the wall surfaces. These factors are discussed in detail in Chapter 2.

Generally, most heat exchangers are designed to be operated in either the laminar or the turbulent flow regime, and not in the transition regime. This could mainly be due to a lack of knowledge on the behaviour in the transition flow regime, the need for higher heat transfer rates associated with turbulent flow or system limitations.

Even though turbulent flow is generally favoured during the design phase of heat exchangers, there are several reasons why heat exchangers are operated in the transition flow regime. These include design constraints, operating constraints and energy requirements (Meyer, 2014; Nunner, 1956; Obot, Esen and Rabas, 1990; Withers, 1980; Manglik and Bergles, 1993; Olivier and Meyer, 2010; Everts and Meyer, 2015a; Everts and Meyer, 2015b). In some cases, the best compromise between a high heat transfer coefficient and relative low pressure drop is found in the transition flow regime.

For this reason, several studies have been conducted on heat transfer and pressure drop in the transition regime for several flow passage geometries. Notably, the most attention has been devoted to circular tubes. Unfortunately, relatively little to no information is available for annular passages (Meyer, 2014), even though it is a common flow passage geometry. Some specific research effort has been devoted to the heat transfer behaviour in annuli (Hattori, 1979; Kotake and Hattori, 1985; Dirker, Van der Vyver and Meyer, 2004; Prinsloo, Dirker and Meyer 2014; Van Zyl, Dirker and Meyer, 2013; Dawood et al., 2015; Ciampi, Faggiani, Grassi and Tuoni, 1987; Mohammed, Campo and Saidur, 2010; Lu and Wang, 2008a; Lu and Wang, 2008b) but additional work is necessary.

1.2 Problem statement

Based on the literature (also see Chapter 2), it is clear that there is a knowledge gap with regard to heat transfer and pressure drop characteristics, especially in the transition flow regime of annular passages, when the thermal boundary condition is not uniform and the flow is of a mixed convection developing type. As a result, heat exchanger designs have to be made from estimations that could be incorrect. This study was conducted to bring to light the characteristics of heat transfer coefficients and pressure drop in the transition flow regime of an annular passage.

1.3 Objectives

In light of the previous discussion, the objectives of this study are as follows:

- Obtain heat transfer and friction factor data for Reynolds numbers spanning the laminar, transition and turbulent flow regimes for a smooth annular passage using water as the working fluid.
- Investigate the impact of various magnitudes of non-uniform wall temperatures on the behaviour of transition flow regime Reynolds number spans, heat transfer coefficients and friction factors in the annular passage.
- Investigate the impact of different geometrical dimensions of the annular passage on the transition flow regime Reynolds number spans, heat transfer coefficients and friction factors in the transition regime.
- Determine the lower and upper Reynolds number limits of transition regimes for the various magnitudes of non-uniform wall temperatures and geometrical dimensions of the annular passage.
- Compare and contrast the Reynolds number limits of transition regimes, heat transfer coefficients and friction factors between heating and cooling annular fluid processes.
- Develop correlations or algebraic relationships for predicting transition flow regime Reynolds number spans, heat transfer coefficients and friction factors for a transition flow regime in the annular passage.

1.4 Thesis layout

This thesis consists of eight chapters. Chapter 2 reviews the available literature regarding heat transfer coefficients and friction factor in the different flow regimes of annular passages. The literature for circular tubes that was deemed relevant to this study is also covered. Chapter 3 describes the experimental facility and the test sections (tube-in-tube heat exchangers). Included in this chapter is the procedure that was followed to collect the required data. Chapter 4 describes the method for calculating heat transfer coefficients and friction factors. Chapter 5 describes the method for identifying the lower and upper Reynolds number limits of transition flow regime and classifies the convection types in the entire flow range and particularly in the transition flow

regimes. It also demonstrates how the data collection method and analysis procedure are validated. The results of the uncertainty analysis are also included in this chapter. The study findings are presented in chapters 6 and 7. The effects of the inner wall thermal boundary on the behaviour of the transition regime, heat transfer coefficients and friction factors are discussed in Chapter 6, while the effects of annular passage dimensions are discussed in Chapter 7. In these chapters, correlations for determining transition flow regime Reynolds number spans, heat transfer coefficients and friction factors for the various degrees of wall temperature uniformity and annular passage dimensions are also proposed. Chapter 8 contains the conclusions of the study. Some relevant additional information is included in the appendices.

Chapter 2

Literature study

2.1 Introduction

This chapter contains some published literature that is related to this study. The previous chapter mentioned that several factors can influence the lower and upper Reynolds number limits of the transition regime, heat transfer coefficients and friction factors. Consequently, correlations are developed for particular thermal, fluid flow and geometry conditions. In this chapter, some of the important factors that affect the Reynolds number limits of the transition flow regime, heat transfer coefficients and friction factors are discussed. It was challenging to present the discussion of these factors separately from each other as several of these factors affect most of the research outputs. Therefore, the literature is discussed according to specific research reports. This chapter also discusses some literature on circular tubes that relates to heat transfer behaviour and fluid flow in the annular passage. The last part of this chapter discusses some correlations for the prediction of Nusselt numbers and friction factors that are relevant to this study.

2.2 Factors that influence the heat transfer coefficient, pressure drop and Reynolds number limits of the transition flow regime

Different thermal boundary conditions may exist at the heat transfer surface, which influence the heat transfer and pressure drop characteristics of the fluid passing through the conduit, especially for low Reynolds numbers. In literature, most investigations for heat transfer and pressure drop in annular passages are carried out at either uniform heat flux (UHF) or uniform wall temperature (UWT) conditions (Dawood et al., 2015). It is accepted in the literature that heat transfer coefficients for a fully developed laminar flow in a circular tube due to UHF and UWT are different. The Nusselt number (Nu) for UHF is 4.36 and that for UWT is 3.66. However, heat transfer coefficients in the annular passage depend on the annular diameter ratio (defined as the inner wall diameter over the outer wall diameter), as shown by Kays and Perkins (1972).

Generally, in many practical applications, heat exchangers exhibit thermal boundary condition types that are neither UHF nor UWT. This is especially so if the relative flow rates of the heat

transfer fluids are such that there is a significant change in the temperature of both of the fluids along the flow passages. In most cases, either the UHF or the UWT is assumed, which does not give accurate results. To get more accurate results, one needs to find an improved method of treating real-life thermal boundaries.

The heat transfer direction (heating or cooling) to or from a fluid flowing in a horizontal concentric annular passage affects the heat transfer and pressure drop performances differently. Petukhov, Polyakov and Strigin (1969) found that the heat transfer correlation that was developed for a heated fluid could not apply to a cooled fluid. Van Zyl et al. (2013) and Van Zyl (2012) found that, for the turbulent flow regime in horizontal annuli, the heat transfer coefficients were higher for the heated cases than for the cooled cases. Friction factors were also higher for cooled cases than for heated cases. This phenomenon was attributed to the bulk temperature differences during the heating and cooling processes that were considered. For instance, the viscosity near the wall is lower for a heated case and is relatively higher for a cooled case. This results in low pressure drop in a heated case and high pressure drop in a cooled case. The results showed that a heated annulus had Nusselt numbers that were on average 35% higher than those for the cooled case and that the friction factors for a heated annulus were on average 9% lower than for a cooled annulus. Van Zyl et al. (2013) went further to express the heat transfer results in terms of the *j*-factor. By taking the effects of the Prandtl number (Pr) into account, the results for a heated and a cooled annulus were in close agreement to the average percentage difference of only 2.6%. Prinsloo et al. (2014) also found similar results for a similar investigation with a different procedure and for different test section dimensions.

For lower Reynolds numbers, the impact of buoyancy-driven flow is also important, as is evident for diabatic conditions where thermal-driven secondary flow is produced. For example, due to lower fluid density at a higher temperature, the fluid near a hot tube surface circulates upward, while the fluid near the centre of the pipe, having a lower temperature and a higher density, circulates downward. The secondary flow due to buoyancy force can significantly affect the lower and upper Reynolds number limits of transition regime, heat transfer coefficients and friction factors (Ghajar and Tam, 1994; Martinell, Southwell, Alves, Craig, Weinberg, Lansing and Boelter, 1942).

In practice, most flows in the low Reynolds numbers are either free or mixed (a combination of free and forced) convection, while for higher Reynolds numbers, the flows exhibit forced convection. The flow regime in free convection is governed by the Grashof number (Gr), which represents the ratio of the buoyancy force to the viscous force acting on the fluid. The presence of both forced and free convection results in a better fluid mix and improved heat transfer coefficients of the mixed convection. In a vertical circular tube, a laminar mixed-convection heat transfer coefficient in a buoyancy-assisted flow can be up to five times higher than its value in pure forced convection (Martinell et al*., 1942)*. However, in buoyancy-opposed flow, the laminar mixed-convection heat transfer coefficient can be lower than its value in pure forced convection.

Tam and Ghajar (1997) conducted experiments to investigate the effect of heat flux and the inlet configuration on the fully developed friction factor in the transition flow regime. The experiments were conducted in a horizontal circular straight tube with re-entrant, square-edged and bell-mouth inlets under isothermal and non-isothermal (uniform wall heat flux) flow conditions. When different heat flux values of 3, 8 and 16 kW/m^2 were applied, the friction factors increased significantly with the heating rate in the laminar and transition flow regimes. However, heat flux did not significantly affect the magnitude of friction factors in the turbulent flow region. Similarly, the experimental Nusselt number values were also significantly higher when compared with the fully developed pipe flow forced convection heat transfer coefficient for laminar flow (Nu = 4.36). The significant influence of the heating rate on the Nusselt numbers and friction factors in the laminar and transition flow regions were attributed to buoyancy-driven secondary flows. It was also shown that various values of heat flux affected the Reynolds number limits of the transition region. The isothermal transition flow ranges for re-entrant, square-edged and bell-mouth inlets were 2 900 to 3 500, 3 100 to 3 700, and 5 100 to 6 100, respectively. When a heat flux of 3 kW/m^2 was applied, both the lower and upper Reynolds number limits of the transition flow region increased to between 3 060 and 3 890 for the re-entrant inlet, between 3 500 and 4 180 for the square-edged inlet, and between 5 930 and 8 730 for the bell-mouth inlet. These Reynolds number limits continued to increase when the heating rate was adjusted to 8 kW/m^2 and 16 kW/m^2. The strength of the buoyancy-driven secondary flows were found to increase with heat flux and were thought to be the cause of change in the Reynolds number limits of the transition flow regime.

It is important to realise that buoyancy forces can significantly influence heat transfer in annular passages, especially at low Reynolds numbers. Existing results on mixed convection in concentric annulus are derived mainly from theoretical studies. Several experimental studies are also available in the literature.

In separate works by Hattori (1979) and Nguyen, Vasseur, Robillard and Chandra (1988), it has been indicated that the secondary flows of mixed convection in a horizontal concentric annulus can strongly distort the velocity and temperature profiles and consequently increase the heat transfer coefficients. Mohammed et al. (2010) conducted an experimental study on forced and free convective heat transfer for thermally developing and thermally fully developed laminar air flow inside horizontal concentric annuli in the thermal entrance length. The thermal boundary on the inner wall was UHF, while the outer annular wall was insulated. The investigation covered a Reynolds number range from 200 to 1 000. They found that buoyancy-driven secondary flow significantly increased the heat transfer coefficients. The heat transfer coefficients for thermally developing flow were considerably greater than the corresponding values for fully developed flow over a significant portion of the annulus.

Islam, Gaitonde and Sharma (2001) conducted numerical and experimental investigations on the steady laminar mixed convection heat transfer in a horizontal concentric annulus by using air and water. The inner tube of the annular passage was 1 m long with an outer diameter of 38.1 mm. The numerical study was conducted within the annular diameter range of 0.10 to 0.67 and the Reynolds number range of 200 to 1 000. As the fluid moved from the entrance, the buoyancy forces became stronger and affected the temperature field at the upper half, which caused a noticeable distortion. The secondary flow was more intense in the upper part of the annulus than in the lower part and increased throughout the cross-section until the intensity reached a maximum value. Increasing the Prandtl number decreased the Nusselt number. The Nusselt number first decreased rapidly after a certain distance and then gradually increased before remaining uniform.

Ciampi et al. (1987) conducted experiments to investigate mixed convection and heat transfer in a horizontal, concentric tube annulus. The study focused on determining the circumferential variations in the local Nusselt numbers. Their wall boundary condition was constant heat flux, and the Reynolds number range was between 2 200 and 5 000. The visual inspection showed the flow

to be laminar and helicoidal for Reynolds numbers less than the critical value, while for Reynolds numbers above the critical value, the helicoidal motion vanished with a subsequent transition to turbulence in the top and side regions of the annular passage. The helicoidal flow in the laminar regime and slightly above the critical Reynolds number was described as the manifestation of secondary flows due to buoyancy forces.

The investigations discussed so far indicate that the presence of buoyancy-driven secondary flows in a horizontal annular passage influences the Reynolds number limits of the transition, the flow regime, the heat transfer coefficients and the friction factors. Whenever one deals with heat transfer, it is essential to know the operating convection type prevalent in the fluid flow for specified operating conditions. Methods for determining convection types are presented in section 2.3.

Conduit geometry, in terms of shape and size, has also been found to influence the lower and upper Reynolds number limits of the transition flow regime, heat transfer coefficients and friction factors. For instance, length to hydraulic diameter ratio on L/D_h is used in the correlation of heat transfer coefficients of several heat exchangers, and annular diameter ratio is used for heat transfer coefficient predictions in the annular passage.
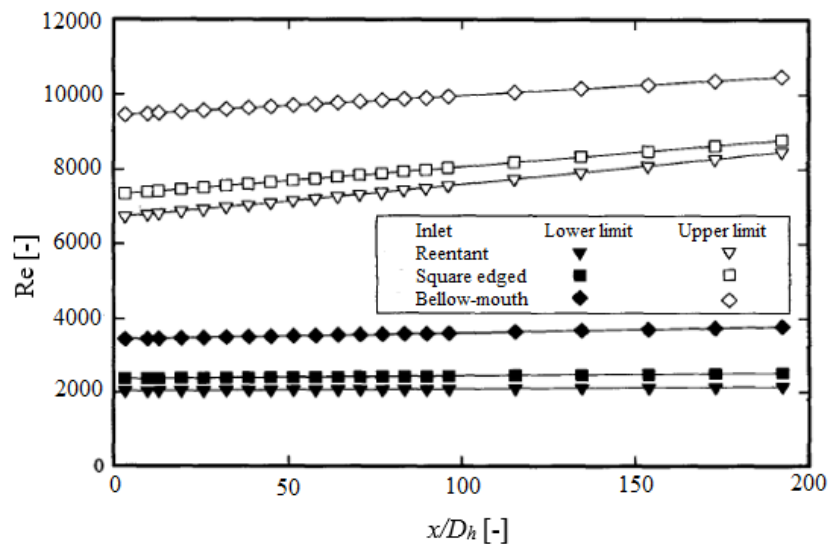
Figure 2.1: Variation of the lower and the upper limits of the heat transfer transition Reynolds number along a pipe for three different inlet configurations (Ghajar and Tam, 1994)

10

Ghajar and Tam (1994) found that the Reynolds number limits of the transition flow regime depend on x/D_h, where x represents the axial distance from the inlet. Based on the local Reynolds number along the pipe, they showed that these limits of the transition flow regime increase linearly with an increase in x/D_h (Ghajar and Tam, 1994). See Figure 2.1.

Several researchers investigated the effects of varying annular diameter ratio and the ratio of hydraulic diameter to heat transfer length, (D_h/L_{hx}), both numerically and experimentally. Some of their findings are presented in this section.

In the process of improving the Nusselt number correlation, which he developed earlier for fully developed flow, Gnielinski (1976) multiplied it with a correction factor to account for entrance effects. Hausen (1943) developed the entrance correction factor earlier and expressed it in terms of the tube diameter ratio, *D,* to length, *L,* as follows:
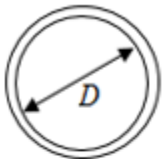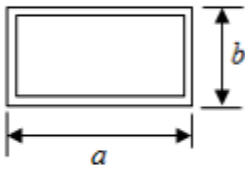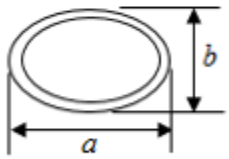
$$1+\left(D/L\right)^{2/3} \tag{2.1}$$

By substituting the tube diameter with the hydraulic diameter, the correlation could also be applied to a concentric annular passage.

Different cross-sections may result in different heat transfer coefficients and friction factors based on the hydraulic diameter, $D_h = 4A_c/p$, where A_c is the cross-section area of the tube, and *p* is the wetted perimeter. For example, some friction factor and Nusselt number relations for fully developed laminar flow of various cross-sections are shown in Table 2.1 (Çengel and Ghajar, 2011).

Abed, Shareef and Najeeb (2010) conducted a numerical study of the natural convection heat transfer in a two-dimensional (2D) region that is formed by a horizontal tube with UHF concentrically located in a cooled horizontal cylinder. The annular diameter ratio ranged from 0.1 to 0.2, and the orientation angles ranged from 0° to 90°. The results showed that the average Nusselt number increased when the annular diameter ratio was increased.

Table 2.1: Nusselt numbers and friction factors for fully developed laminar flow in tubes of various cross-sections ($D_h = 4A_c/p$)

Tube Geometry	a/b or θ°	Nusselt number		Friction factor
		UWT	UHF	
	-	3.66	4.36	64.00/Re
	a/b			
	1	2.98	3.61	56.92/Re
	2	3.39	4.12	62.20/Re
	3	3.96	4.79	68.36/Re
	4	4.44	5.33	72.92/Re
	6	5.14	6.05	78.80/Re
	8	5.60	6.49	82.32/Re
	∞	7.54	8.24	96.00/Re
	a/b			
	1	3.66	4.36	64.00/Re
	2	3.74	4.56	67.28/Re
	4	3.79	4.88	72.96/Re
	8	3.72	5.09	76.60/Re
	16	3.65	5.18	78.16/Re
	θ			
	10°	1.61	2.45	50.80/Re
	30°	2.26	2.91	52.28/Re
	60°	2.47	3.11	53.32/Re
	90°	2.34	2.98	52.60/Re
	120°	2.00	2.68	50.96/Re

Heaton, Reynolds and Kays (1964) studied laminar flow heat transfer in the concentric annuli of various annular diameter ratios with simultaneously developing velocity and temperature distributions. One wall was heated at a constant wall heat flux, while the other was insulated. For the same Prandtl number and normalised axial coordinate, $\bar{x}$ (where $\bar{x} = x/RePrD_h$), Nusselt number values were larger for the smaller annular diameter ratio than for larger the annular diameter ratio. For example, for $\bar{x} = 0.0001$ with Pr = 0.7 and a heated inner wall, the Nusselt

number values were 61.2, 55.4 and 53.5 for the annular diameter ratios of 0.1, 0.25 and 0.5, respectively.

Nada (2007) conducted experiments to investigate natural convection heat transfer and the fluid flow characteristics of buoyancy-driven flow in horizontal and inclined annuli bound by concentric tubes. Unlike Heaton et al. (1964) and Abed et al. (2010), he based the results on the annular gap size. The results showed that increasing the annulus gap width results in significant increases in the heat transfer rate.

Van Zyl (2012) and Van Zyl et al. (2013) experimentally investigated the annular diameter ratios of 0.483, 0.579, 0.593 and 0.712 with respective hydraulic diameters of 17.01 mm, 13.84 mm, 10.88 mm and 7.71 mm. As previously discussed, they agreed with all the other researchers that the heat transfer and friction factor were found to depend on the annular diameter ratio (see Figure 2.2a and Figure 2.2b).

However, the Nusselt numbers for an annular diameter ratio of 0.593 were found to be larger than that of 0.579. The line fits that are inserted in Figure 2.2 reveal that the relationship between the Nusselt numbers and the friction factors to the annular diameter ratio is not well defined. This is contrary to the findings of Heaton et al. (1964) and Abed et al. (2010). Prinsloo et al. (2014) performed an experimental investigation on the heat transfer coefficient and pressure drop in the turbulent flow regime of horizontal annuli with annular diameters ratios of 0.327, 0.409 and 0.483, and found similar results to that of Van Zyl (2012) and Van Zyl et al. (2013) . This suggests that annular diameter ratio alone may not be the best dimensionless factor to optimise the influence of geometry on the heat transfer and friction factor. Jones and Leung (1981) came to a similar conclusion.
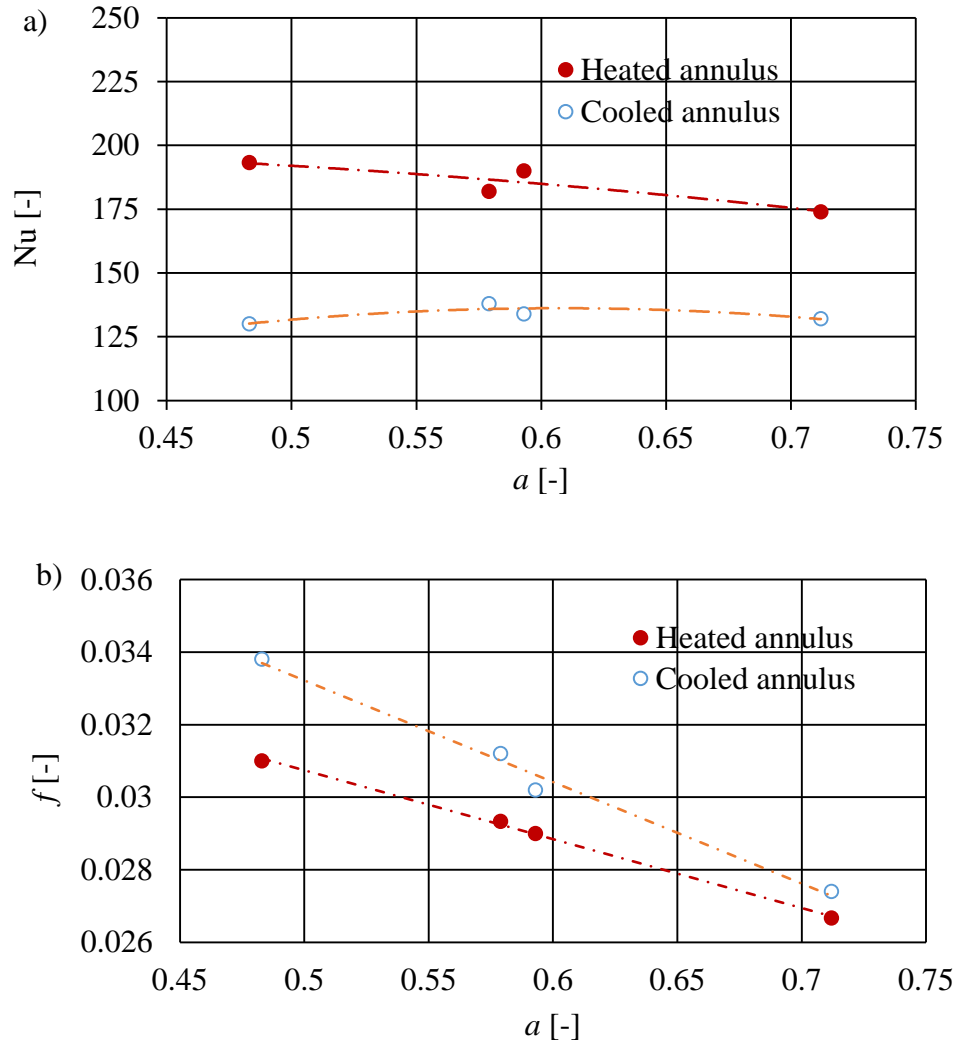
Figure 2.2: A comparison of different annular ratios: (a) for Nusselt numbers; and (b) friction factors for heated and cooled annulus cases (Van Zyl, 2012)

2.3 Methods for determining the convection types

The necessity of knowledge of the convection types in the fluid flow for specified operating conditions was mentioned in the previous section. Different methods for determining whether buoyancy-driven secondary flows should be considered in a forced flow are available in the literature. The first and second methods that are presented below are applicable to circular tubes, while the third is applicable to the annular passage.

a) Flow regime map

Flow regime maps are used to determine whether the convection is of a forced or mixed type. Augmenting the results of other researchers with their own, Metais and Eckert (1964) recommended the use of flow regime maps. The two maps can also be found in the handbook of single-phase convective heat transfer (Kakaç et al., 1987). One flow regime map is for flow in vertical circular tubes. Its results are valid for both up-flow and down-flow, and for UHF and UWT boundary conditions. The other map is for flow in a horizontal circular tube and UWT boundary condition only. A flow regime map made specifically for an annular passage was not found.

b) Peripheral heat transfer ratio

In this method, the boundary between mixed and forced convection is determined from the local heat transfer data. The ratio of the local peripheral heat transfer coefficient at the top of the tube to the local peripheral heat transfer coefficient at the bottom of the tube (h_t/h_b) is used. For mixed convection to be considered, this ratio must be less than 0.8. Forced convection is considered when the ratio is within 0.8 to 1.0. In their respective investigations for circular tubes, Ghajar and Tam (1994, 1995) and Everts, Ayres, Houwer, Vanderwagen, Kotze and Meyer (2014) used this method to determine the boundary between mixed and forced convection.

c) Richardson number method

The type of convection may also be determined by the Richardson number (Ri). Both the free and forced convections are considered when $0.1 \leq \mathrm{Ri} \leq 10$. For $\mathrm{Ri} > 10$, the flow is treated as free convection. The pure forced convection is considered when $\mathrm{Ri} < 0.1$.

2.4 Correlations

In order to determine the dimensions of heat exchangers during the design phase, equations are required to estimate heat transfer coefficients and friction factors. Due to the complexities of transition flow, correlations for predicting Nusselt numbers and friction factors for an annular passage have not been developed yet. However, correlations are available both in the laminar and turbulent flow regimes of an annular passage. Laminar and turbulent correlations have been used

before to develop correlations for the transition flow regime of a circular tube. For example, Gnielinski (2013) and Abraham et al. (2009) used an interpolation formula to bridge the Nusselt number or friction factor between the limiting cases of laminar and fully turbulent flows. Since no correlations are available for the transition regime, laminar and turbulent correlations are relevant for the validation of the experimental procedure and calculation method. For this reason, the correlations in the laminar and turbulent regimes of the annular passage are presented as follows:

2.4.1   Nusselt number correlations

 (i) Laminar flow

It was mentioned that buoyancy-driven secondary flow is usually present in the low Reynolds number range of the heat transfer process. Therefore, the Grashof number is included in the correlations of such flows to account for the buoyancy effects.

Mohammed et al. (2010) proposed a Nusselt number correlation for mixed convection in the thermal entry region of horizontal concentric annuli covering $200 \leq \text{Re} \leq 1\,000$, $62 \times 10^5 \leq \text{Gr} \leq 1.2 \times 10^7$ for air given as the following:

$$\text{Nu} = 2.964\left(\frac{\text{GrPr}}{\text{Re}}\right)^{0.0326}$$

(2.2)

Equation 2.2 was developed for a single annular diameter ratio of 0.5. Depending on their application, heat exchangers are designed in various sizes. Therefore, it is necessary that correlations should consider the geometric dimension. Hattori (1979) considered varying annular diameter ratio as shown in Equation 2.3. The correlation was developed for hydrodynamically fully developed laminar flow for a case where the inner wall was heated at UHF and the outer wall was insulated as follows:

$$\text{Nu} = 0.44\text{Gr}^{0.2}\,\text{Pr}^{0.28}\left(\frac{D_0}{D_1}\right)^{0.35}$$

(2.3)

The range of applicability of Equation 2.3 was not specified.

(ii) Turbulent flow

For horizontal tubes, experimental evidence indicates that the effect of buoyancy is negligible in turbulent flow (Kakaç et al., 1987). This may also apply to turbulent flow in the annular passages, as most of the available correlations disregard buoyancy effects. Correlations for turbulent flow are obtained from experimental data. Some correlations for predicting Nusselt numbers in the annulus are summarised in Table 2.2. The letter a that is appearing in most of the correlations is annular diameter ratios (defined as the ratio of the inner wall diameter to the outer wall diameter), $a = D_1/D_0$.

Table 2.2: Equations available in the literature that describe the Nusselt number in a smooth, concentric annulus for forced convection in fully developed turbulent flow

Author(s)	Correlation	Equation	Diameter ratio range	Reynolds number range	Working fluid
Gnielinski (2015)	$$\mathrm{Nu} = \frac{(f/8)(\mathrm{Re}-1000)\mathrm{Pr}_b}{1+12.7\sqrt{(f/8)}\left(\mathrm{Pr}_b^{2/3}-1\right)}\left[1+\left(\frac{D_h}{L}\right)^{2/3}\right]$$ $$(0.75a^{-0.17})\left(\frac{\mathrm{Pr}_b}{\mathrm{Pr}_w}\right)^{0.11}$$ Where $f = \left(1.8\log_{10}\mathrm{Re}^* - 1.5\right)^{-2}$ And $\mathrm{Re}^* = \mathrm{Re}\dfrac{\left(1+a^2\right)\ln a + \left(1-a^2\right)}{\left(1-a\right)^2 \ln a}$	2.4	Not specified	Re ≥ 4 000	Water
Dirker and Meyer (2005)	$$\mathrm{Nu} = C_o\,\mathrm{Re}_{Dh}^{P}\,\mathrm{Pr}^{1/3}\left(\frac{\mu_b}{\mu_{iw}}\right)^{0.14}$$ Where $P = 1.013e^{-0.067a}$ and $C_o = \dfrac{0.003a^{1.86}}{0.063a^3 - 0.0674a^2 + 2.225a - 1.157}$	2.5	0.3125 – 0.588	4 000 – 30 000	Water

Author(s)	Correlation	Equation	Diameter ratio range	Reynolds number range	Working fluid
Davis (1953)	$^2\,\mathrm{Nu} = 0.038 a^{-0.15} \left(\dfrac{1}{a}-1\right)^{0.2} \mathrm{Re}_{Dh}^{0.8}\,\mathrm{Pr}_o^{1/3}\left(\dfrac{\mu_b}{\mu_w}\right)_o^{0.14}$	2.6	0.00147 – 0.847	Not specified	All media
McAdams (1954)	$\mathrm{Nu} = 0.03105 a^{-0.15} \left(\dfrac{1}{a}-1\right)^{0.2} \mathrm{Re}_{Dh}^{0.8}\,\mathrm{Pr}_o^{1/3}\left(\dfrac{\mu_b}{\mu_w}\right)_o^{0.14}$	2.7	0.00147 – 0.847	Not specified	All media
Foust and Christian (1940)	$^2\,\mathrm{Nu} = \dfrac{0.04 a}{(1/a+1)^{0.2}}\,\mathrm{Re}_{Dh}^{0.8}\,\mathrm{Pr}_o^{0.4}$	2.8	0.543 – 0.833	3 000 – 60 000	Water
McAdams (1954)	$\mathrm{Nu} = 0.023\,\mathrm{Re}_{Dh}^{0.8}\,\mathrm{Pr}_o^{1/3}\left(\dfrac{\mu_b}{\mu_w}\right)_o^{0.14}$	2.9	Not specified	Not specified	Not specified
Monrad and Pelton (1942)	$^2\,\mathrm{Nu} = 0.023\left[\dfrac{2\ln\frac{1}{a}-a^{-2}+1}{\frac{1}{a}-a-2\frac{1}{a}\ln\frac{1}{a}}\right]\mathrm{Re}_{Dh}^{0.8}\,\mathrm{Pr}_o^{n}$	2.10	0.606, 0.408, 0.0588	12 000 – 220 000	Water, air
Wiegand, McMillen and Larson (1945)	$^3\,\mathrm{Nu} = 0.023 a^{-0.45}\,\mathrm{Re}_{Dh}^{0.8}\,\mathrm{Pr}_o^{n}\left(\dfrac{\mu}{\mu_w}\right)_o^{0.14}$	2.11	0.1 – 1	Not specified	Fluids with $\mu_{material} \leq 2\mu_{water}$

---

[2] Original equations rewritten as to have the Reynolds and Nusselt numbers based on the hydraulic diameter, $D_h = D_0 - D_1$.

[3] The exponent $n = 0.4$ for a heated annulus and $n = 0.3$ for a cooled annulus.

Author(s)	Correlation	Equation	Diameter ratio range	Reynolds number range	Working fluid
Kays and Leung (1963)	Results listed in tables for various conditions	2.12	0 – 1	$10^4 - 10^6$	Not specified
Petukhov (1970)	$\mathrm{Nu} = 0.027\,\mathrm{Re}^{0.8}\,\mathrm{Pr}^{1/3}\left(\dfrac{\mu_b}{\mu_w}\right)^{0.14}$	2.13		$3\,000 - 5 \times 10^6$	Water
Petukhov and Roizen (1964)	$^2\mathrm{Nu} = \dfrac{0.06759 a^{-0.16}}{(1/a + 1)^{0.2}}\, \zeta\,\mathrm{Re}_{Dh}^{0.8}$ Where $\zeta = 1 + 1.75\left[\dfrac{1/a - 5}{(1/a - 1)\mathrm{Re}_{Dh}}\right]^{0.6}$ for $a \geq 5$, $\zeta = 1$ for $a \leq 5$	2.14	1 – 14.3	$10^4 - 3 \times 10^5$	Air
Stein and Begell (1958)	$\mathrm{Nu}_f = 0.02 a^{-0.5}\,\mathrm{Re}_{Dh,f}^{0.8}\,\mathrm{Pr}_f^{1/3}$	2.15	0.812, 0.684, 0.59	$30\,000 - 390\,000$	Water
Crookston, Rothfus and Kemode (1968)	$\mathrm{Nu} = 0.23 a^{-0.25}\,\mathrm{Re}_{D_h}^{0.75}\,\mathrm{Pr}^{1/3}$	2.16	0.1, 0.0625, 0.0323	$17\,000 - 100\,000$	Air
Dittus and Boelter (1930)	$^3\mathrm{Nu} = 0.23\mathrm{Re}_{D_h}^{0.8}\,\mathrm{Pr}^n$	2.17	Not specified	Not specified	Not specified

In the correlations represented by equations 2.4, 2.5, 2.6, 2.7, 2.8, 2.10, 2.11, 2.14, 2.15 and 2.16, the annular diameter ratio is included to consider the effect of geometric dimensions, while equations 2.10 and 2.17 can predict Nusselt numbers for both heating and cooling processes by substituting the exponent n of the Prandtl number with 0.4 and 0.3, respectively. The ratio of viscosity of the bulk fluid to viscosity on the wall, which appears in some correlations, considers the variation of fluid properties with temperature.

Equation 2.4 is one of the recent correlations for predicting Nusselt numbers in the turbulent flow regime. The main advantage of this correlation is that it can be used for tubes and annuli. Only different correlations for the friction factor are required and the relevant hydraulic diameter must be used.

2.4.2   Friction factor correlations

(ii) Laminar flow

Many correlations accurately describe the friction factor in circular tubes. Several correlations are also available for laminar and turbulent flow regimes in annular passages. However, correlations were not found for the transition flow of the annular passage. It has been shown in some instances that, by substituting the diameter of a circular tube with the hydraulic diameter, correlations originally developed for circular tubes could be adopted for annular passages. For this reason, a few correlations for circular tubes, especially those that consider the influence of buoyancy force, are presented in this section.

The friction factor for a fully developed laminar flow in a circular tube without heat transfer is given as follows:

$$f = \frac{64}{\mathrm{Re}}$$

(2.18)

The friction factor with heat transfer is given by Equation 2.19, where the effects of temperature on the isothermal friction factor in Equation 2.18 are taken into account with the variation of viscosity with temperature.

$$f = \frac{64}{\text{Re}} \left(\frac{\mu_b}{\mu_w} \right)^n$$
(2.19)

Sun, Sun and Yan (2004) indicated that the friction factor for a fully developed laminar flow in the annular passage without heat transfer is given as follows:

$$f = \frac{64}{\text{Re}^*}$$
(2.20)

Where Re^* is defined as follows:

$$\text{Re}^* = \text{Re} \frac{\left(1 + a^2\right) \ln a + \left(1 - a^2\right)}{\left(1 - a\right)^2 \ln a}$$
(2.21)

And a in Equation 2.21 is annular diameter ratios, $a = D_1/D_0$.

No friction factor correlation that considers the entrance and buoyancy force effects in the laminar and transition regimes of the annuli was found. However, Ghajar and Tam (1997) developed a friction factor correlation for the laminar flow of a circular tube, which is expressed as follows:

$$f = \frac{64}{\text{Re}} \left(\frac{\mu_b}{\mu_w} \right)^m$$
(2.22)

Where the effects of buoyancy force are considered by exponent m as follows:

$$m = 1.65 - 0.013 \text{Gr}^{0.17} \text{Pr}^{0.84}$$
(2.23)

(ii) Turbulent flow

A summary of some known correlations for predicting friction factors in annular passages is presented in the Table 2.3.

22

Monrad and Pelton (1942) observed that the friction factor for annular passages is relatively larger than that for a circular tube. This should be the case, since the velocity profiles in these two conduits are different and the surface area in the annular passage is relatively larger.

Kaneda, Yu, Ozoe and Churchill (2003) performed Direct Numerical Simulations (DNS) on flow inside an annulus and proposed Equation 2.25, which is based on wall shear stresses.

Observing that the pressure drop in an annular passage does not depend on the hydraulic diameter alone, but also on the annular diameter ratio, Jones and Leung (1981) proposed a friction factor correlation in Equation 2.26. Similarly, Gnielinski (2009) modified an original correlation (Equation 2.24) for a circular tube by Konakov (1946) in an effort to improve the Nusselt number correlation. The Reynolds number in the original correlation was substituted for its annular passage equivalent given by Equation 2.21.

$$f = \left(1.8\log_{10}\mathrm{Re}-1.5\right)^{-2} \qquad (2.24)$$

Equation 2.28 is a modification of a well-known friction factor in the smooth tubes of Blasius (Çengel and Ghajar, 2011). The Reynolds number is modified to a Reynolds number based on the hydraulic diameter for annular flow.

Table 2.3: Equations available from literature describing friction factors in a smooth concentric annulus for forced convection in fully developed turbulent flow

Author(s)	Correlation	Equation	Diameter ratio range	Reynolds number range	Working fluid
Kaneda et al. (2003)	$$\frac{f}{8} = \left[1.61 + 2.3 \ln \left(\frac{\mathrm{Re}_{Dh}}{\sqrt{8/f}} \right) - \frac{550}{\mathrm{Re}\sqrt{8/f}} \right]^{-2}$$	2.25	0.0 – 1.0	Re > 10 000	Not specified
Jones and Leung (1981)	$$\frac{1}{f} = \left[2 \log_{10} \mathrm{Re}^* \sqrt{f} - 0.8 \right]$$ $$\mathrm{Re}^* = \mathrm{Re} \frac{\left(1+a^2\right)\ln a + \left(1-a^2\right)}{\left(1-a\right)^2 \ln a}$$	2.26	0.0 – 1.0	$10^4 \le \mathrm{Re} \le 10^6$	Not specified
Gnielinski (2007)	$$f = \left(1.8 \log_{10} \mathrm{Re}^* - 1.5\right)^{-2}$$ $$\mathrm{Re}^* = \mathrm{Re} \frac{\left(1+a^2\right)\ln a + \left(1-a^2\right)}{\left(1-a\right)^2 \ln a}$$	2.27	Not specified	Not specified	All media
Blasius (Çengel and Ghajar, 2011)	$$f = 0.3164 \, \mathrm{Re}_{D_h}^{-0.2}$$	2.28	Not specified	Not specified	All media

2.5 Summary

The reviewed literature reveals several aspects that affect the Reynolds number limits of the transition flow regime, heat transfer coefficients and friction factors. Some of these, which include the type and the degree of heat flux on the heat transfer surface, buoyancy-driven secondary flow, the shape and size of the flow space geometry, the heat transfer direction and the flow inlet configuration, are discussed in detail. Some of the methods that are used to identify cut-off points of different convection types in a convection heat transfer flow were also discussed.

Correlations for predicting heat transfer coefficients and friction factors in the laminar and turbulent flow regimes were presented for both circular tubes and annular passages. Correlations were also presented for the transition flow regime of a circular tube. No correlation for predicting heat transfer coefficients and friction factors in the transition regime of annular passage was found in the literature.

For this reason, it is of great interest to obtain correlations for the transition regime of an annular passage, considering thermal boundary conditions, geometric dimensions and other important parameters. Of further interest would be to study the effect buoyancy-driven secondary flow would have on the characteristics of the transition flow regime.

In the next chapter, the experimental set-up and the procedure that was used to collect the required data are discussed.

Chapter 3

Experimental set-up and procedure

3.1 Introduction

In the preceding chapter, some factors that influence the Reynolds number limits of the transition flow regime, heat transfer coefficients and pressure drop were reviewed from the available literature. Some correlations that predict heat transfer coefficients and friction factors were also discussed. In this investigation, data is gathered through experiments. Therefore, details on the experimental set-up, which comprised the test facility and the test section, are presented and discussed in this chapter. An overview of the components and measuring instruments of the test facility, as well as the design of the tube-in-tube heat exchangers, which acted as the test sections, is detailed. The procedure that was used to get the required data is also discussed.

3.2 Experimental facility

Figure 3.1 shows the schematic layout of the experimental facility that consisted of two closed water loops, one for hot water (with components labelled 1) and the other for cold water (with components labelled 2). The components of the experimental facility, which are abbreviated in the figure, are given in the following list:

A	Accumulator	P	Pump
BV	Bypass valve	PG	Pressure gauge
F	Filter	PT	Pressure transducer
M	Flow meter	R	Water reservoir
NV	Non-return valve	V	Valve
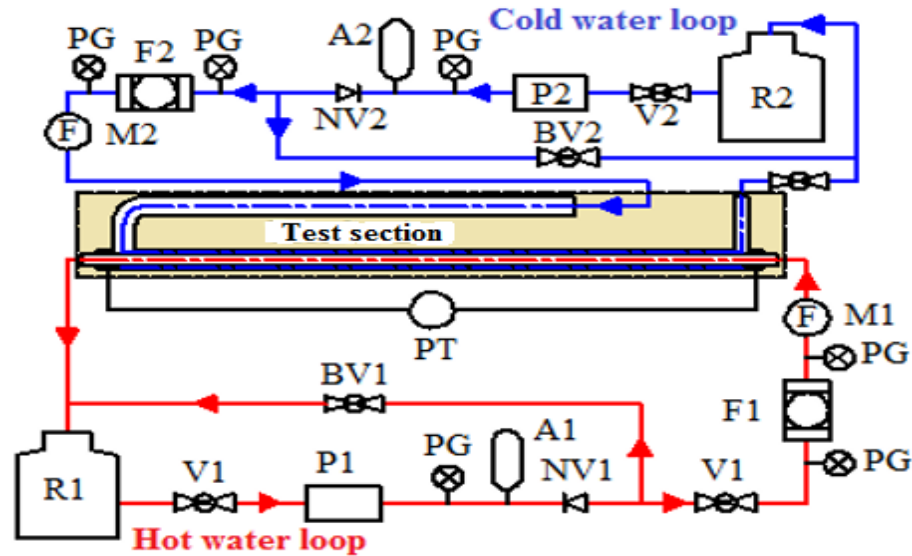
Figure 3.1: Schematic diagram of an experimental set-up with test section

The hot water loop (red line in Figure 3.1) was connected to a 1 000 litre reservoir (item R1) fitted with a 36 kW electrical resistance heater. The water was heated to a preselected temperature of up to 50 °C and thermostatically controlled to a temperature of within ±1 °C of the selected temperature. A pump (item P1) was used to circulate the water through the loop. Two different positive displacement pumps were employed according to flow rate requirements and had delivery ranges of 0.03 to 0.775 kg/s and 0.3 to 1.6 kg/s. Since flow rates that were much less than the pumps were rated for were often required, a bypass line with a hand-operated valve (item BV1) was utilised to control the flow rate through the test section. An accumulator (item A1) was installed downstream of the pump to dampen mass flow pulsations and small pressure pulsations to the inlet of the test section.

The mass flow rates in the water loop were measured using one of two possible Coriolis mass flow meters (item M1), each having different rated mass flow ranges of 0 to 0.607 kg/s and 0 to 1.833 kg/s respectively, and measurement error uncertainties of ±0.1% each. The flow meters were selected depending on the required flow rate of a specific test.

The cold water loop (blue line in Figure 3.1) consisted of components very similar to the hot water loop. The cold water was, however, supplied from a 5 000 litre reservoir (item R2) connected to a 45 kW chiller unit. The water was cooled to a preselected temperature as low as 20 °C, and

thermostatically controlled to a temperature of within ±1 °C of the selected temperature. The same types of pumps and flow meters that were utilised for the hot water loop were used in the cold water loop. In addition, both loops were fitted with filters (items F1 and F2), pressure gauges (PG), non-return valves (items NV1 and NV2), valves (V1, V2), pressure relief valves, and appropriate pipes and pipe fittings.

Heat was exchanged between the two flow loops via a fitted tube-in-tube heat exchanger test section. By switching the connections between the test section inlets and outlets, and the two water loops, the operating test requirements of either hot water or cold water in the annulus could be investigated. For the heated annulus cases (configuration shown schematically in Figure 3.1), cold water flowed in the annular passage and hot water in the inner tube, while for cooled annulus cases, it was the opposite.

3.3 Test sections

Four tube-in-tube heat exchanger test sections with different annular diameter ratios and hydraulic diameters were used. A schematic diagram of a typical test section is shown in Figure 3.2. It consisted of circular inner and outer tubes, inlets and outlets, temperature and pressure measuring stations, a fluid mixer, pipe connectors and elastomeric foam insulation sheet (not shown in the figure).

Two inner tubes with outside diameters of 12.7 mm and 15.9 mm (D_0) and two outer tubes with inside diameters of 32.9 mm and 38.88 mm (D_1) made of hard drawn copper were used to assemble the test sections. Tube diameters were measured with a vernier calliper with an uncertainty on the measurement of 20 μm. Since all the tubes were made of copper, the surface roughness ($e = 0.0015$ mm) was the same for all the test sections and could not influence the results. Alternating the outer tubes and inner tubes resulted in four test sections with hydraulic diameters ($D_h = D_0 - D_1$) of 26.2 mm, 23 mm, 20.2 mm and 17 mm, and corresponding annular diameter ratios, $a = D_1/D_0$, of 0.327, 0.409, 0.386 and 0.483, respectively.
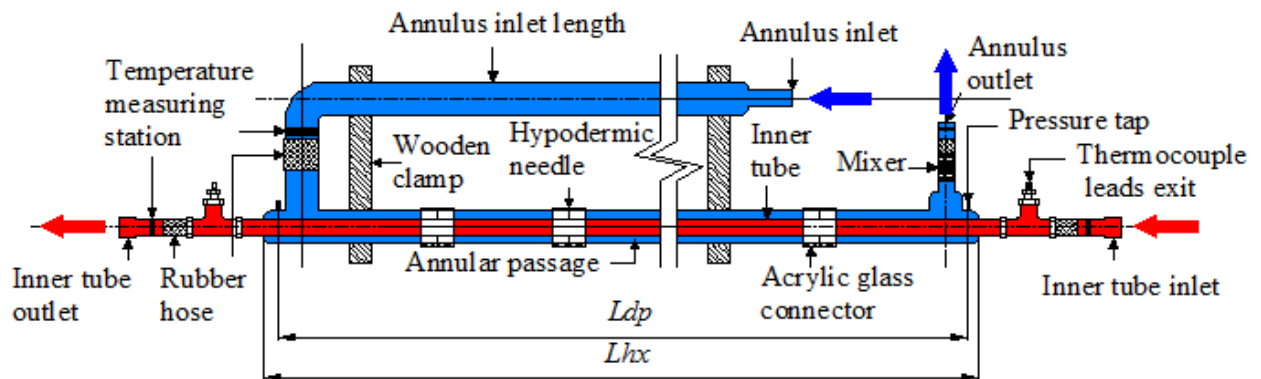
Figure 3.2: Schematic diagram of the test section similar in configuration to a tube-in-tube heat exchanger

The heat transfer lengths (L_{hx}), based on the wetted annulus surface area over which heat transfer could occur, were either 5.06 m or 5.08 m, and resulted in length-to-diameter ratios (L_{hx}/D_h) ranging from 193 to 299. The heat transfer length of approximately 5 m was chosen due to the fact that larger heat exchange lengths produce larger temperature differences across the length of the tube. These larger temperature differences produce larger heat transfer values, which reduces the uncertainties. The lengths were measured by a measuring tape with an uncertainty on the measurement of ±2.5 mm.

The pressure drop length (L_{pd}) between the two pressure taps (shown in Figure 3.2) were either 5.04 m or 5.06 m. These also resulted in length-to-diameter ratios (L_{pd}/D_h) between 193 and 298. The pressure taps were positioned on the top of the annular passage, and each had an inner diameter of 1 mm. They were positioned in the stagnant flow regions 30 mm (centre distance) before and after the inlet and outlet, respectively. The diameters of the taps were far smaller than the recommended 10% of the hydraulic diameter of the annulus to avoid significant influence on the pressure readings (Rayle, 1959). When drilling the holes into the outside wall of the outer tube for the pressure taps, special care was taken to ensure that no burrs were left behind and that the tube was smooth on the inside. The pressure drops were measured with a 2.2 kPa pressure transducer (item PT in Figure 3.1) with a measurement uncertainty of ±0.0055 kPa.

Table 3.1 provides the various tube diameters and the resulting hydraulic diameters, annular diameter ratios and length-to-diameter ratios (L_{hx}/D_h) for the four test sections. In the rest of this document, these test sections are identified by the numbers TS 1, TS 2, TS 3 and TS 4.

Table 3.1: Test section dimensions

Test section (TS)	D_1[mm]	D_0[mm]	L_{hx}[mm]	L_{dp}[mm]	D_h [mm]	a [-]	L_{hx}/D_h [-]
1	12.7	38.88	5 060	5 040	26.2	0.327	193
2	15.9	38.88	5 060	5 040	23	0.409	221
3	12.7	32.9	5 080	5 060	20.2	0.386	251
4	15.9	32.9	5 080	5 060	17	0.483	299

3.3.1. Inner tube construction

The inner tubes were made of hard drawn copper of 5.28 m long. The outer diameters for the two inner tubes are given in Table 3.1. It was necessary to measure the temperature of the inner wall of the annular passage. This was achieved by using T-type thermocouples that were embedded in the wall. Each thermocouple had a measurement uncertainty of 0.106 °C. The thermocouples were located at nine stations that were separated from each other by a distance of 550 mm (see Figure 3.3). Each station had two thermocouples; one was inserted at the top and the other at the bottom. Two thermocouples were used to reduce the measurement uncertainty of the axial average temperature, as will be discussed in section 4.4.

All dimensions in millimeter
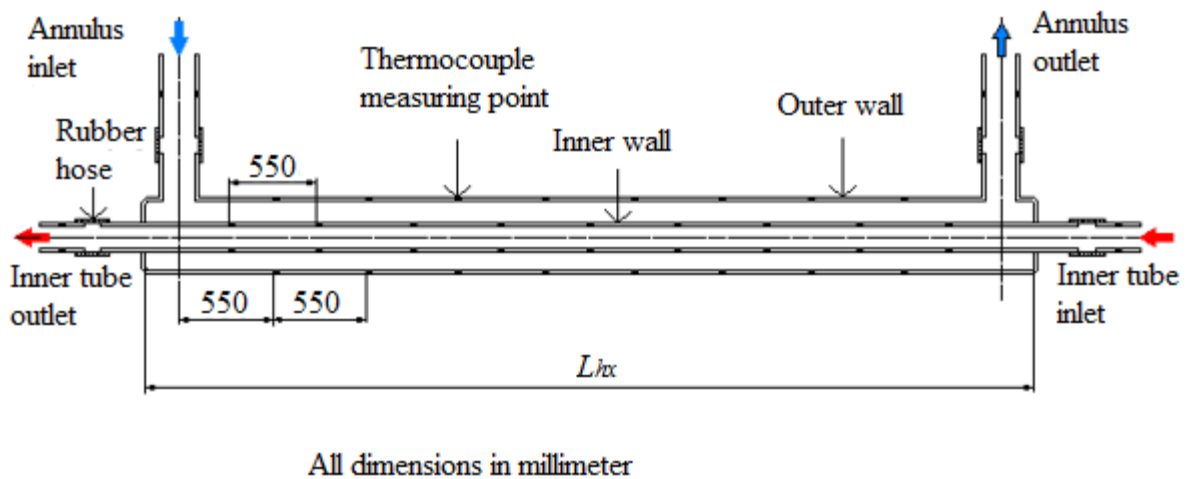
Figure 3.3: Thermocouple measuring points on the inner and outer tube walls (the figure is not drawn to scale)

A method of attaching the thermocouples to the inner tube wall, as recommended by Van Zyl (2012) and Van Zyl et al. (2013) was adopted. This method was the best among three different methods of attaching thermocouples to the inner tube that they had investigated. Figure 3.4 illustrates the attachment method of thermocouples. A groove 10 mm long and 1.2 mm wide with a depth of 0.46 mm was machined into the wall of the tube. A thermocouple junction was inserted into the groove and soldered. The thermocouple cable was then fed through a hole with a diameter of 1.2 mm that was drilled at one end of the groove to run inside the tube and retrieved at the end of the tube. This was done in order to keep the annular passage, which was the focus of this study, clear, as is the case in operating heat exchangers. The protrusions due to soldering were filed down to avoid fin effects[4]. Then the rest of the groove and hole was sealed with epoxy called Araldite 2000. This type of epoxy was used because it bonds well with copper and can withstand high temperature and pressure. In order to keep the annular passage dimensions constant, it was

---

[4] In the study of heat transfer, a fin is a protrusion from an object that increases the rate of heat transfer to or from an environment by increasing convection.

31

ideal to sand down the excess epoxy to wall surface level. Since the pressure in the inner tube of this investigation was too high for the flush seal to withstand, the excess epoxy was only sanded down to a height of approximately 0.5 mm to ensure a strong seal. The seal protrusion was rounded off at the edges to minimise the effect it could have on the fluid flow.
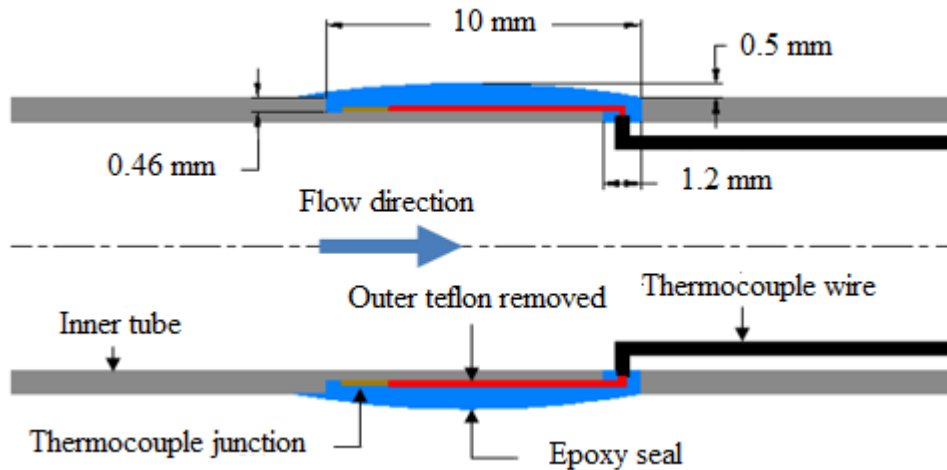
Figure 3.4: A cross-section of the inner tube wall showing the method that was used to attach the thermocouples

The inlet and outlet ends of the inner tube (see Figure 3.5) were identical and each had two main parts. The first part, with a T-shape, was designed to provide the exit port for thermocouple leads out of the inner tube. Each thermocouple lead exit port was perpendicular to the inner tube and was constructed of a copper tube with the same diameter as the inner tube, but it was 30 mm long. Then, compression couplings comprising a body, sleeve and nut through which the thermocouple leads were extracted were fitted. The inner diameter of the sleeve was 3 mm, which was big enough to take 10 thermocouple leads that were wrapped with thread tape. From the inner tube, thermocouple leads entered one end of the tee fitting, then came out through the exit port. At the section around the sleeve, each thermocouple lead was split after removing the outer Teflon cover and the thread tape was wound around each wire separately before bundling them together. This was done to prevent leakages from occurring during the experiments. The tee fittings at the inlet and outlet sections were connected to the inner tubes with straight compression couplings at one end and a 100 mm-long copper tube of the same diameter as the inner tube at the other end.
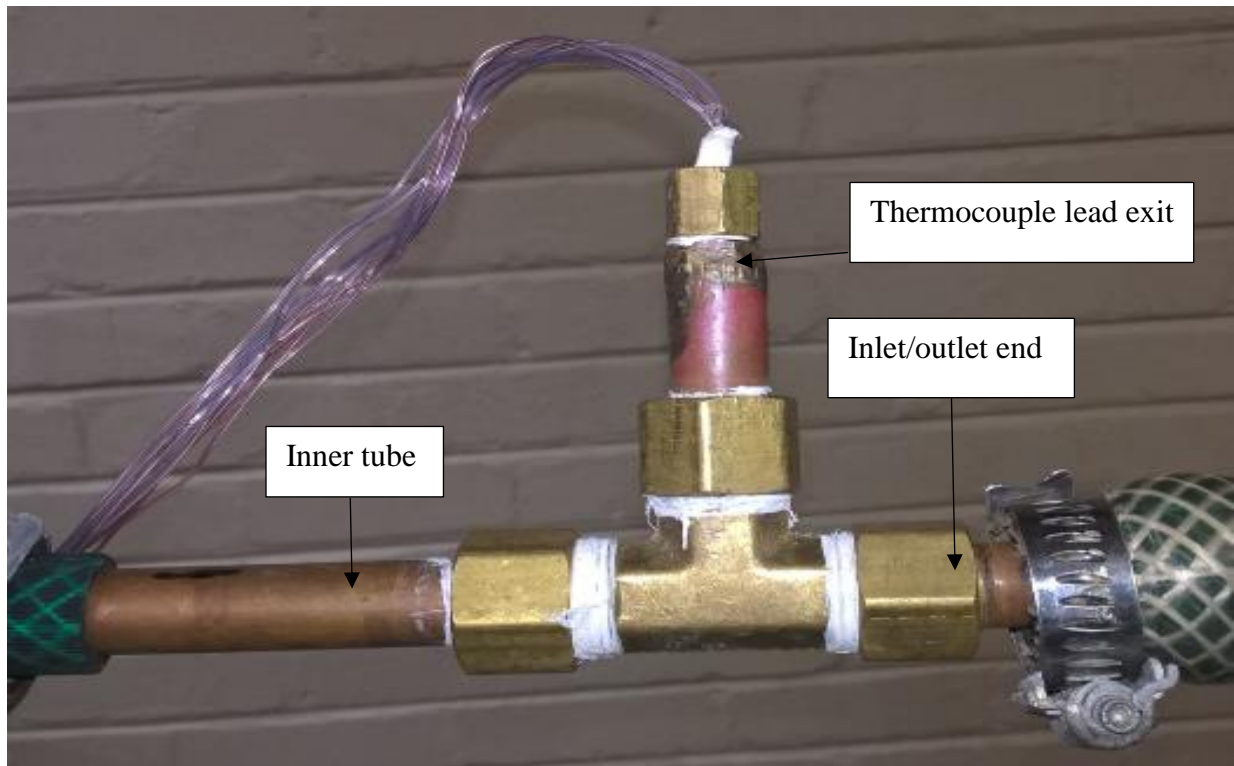
Figure 3.5: The inlet and outlet ends of the inner tube with the thermocouple lead exit mechanism

It was necessary to measure the inlet and outlet temperatures of the water passing through the inner tube during each test. Therefore, temperature measuring stations were installed at the inlet and outlet sides of the two tee fittings. These stations are labelled as temperature measuring stations in Figure 3.2. The measuring stations were made of copper tube with the same diameter as the inner tube (100 mm). This part had four thermocouples that measured the inlet and outlet temperature of the water flowing in the inner tube. Four thermocouples were attached 90° apart on the periphery of each tube and reduced the measurement uncertainty of the inlet and outlet fluid temperatures, as discussed in section 4.4. The thermocouples were attached to the copper tube with silver tape. Thermally, these measuring stations were insulated from the heat exchanger by means of rubber hoses to prevent axial conduction. The average of the four thermocouples was used as the mean inlet and outlet temperatures. This design therefore ensured that the temperature taken was that of the water only.

3.3.2.   Outer tube construction

As mentioned, two outer tubes were constructed from hard drawn copper tube with inner diameters as provided in Table 3.1. Considering the length of the test section, the inner tube would sag due to its own weight if it was only supported at the two ends of the annular passage. Therefore, supports for the inner tube were considered along the outer tube length in order to ensure concentricity of the annulus. The outer tube was split into eight modular sections of 550 mm each, which were linked to each other via the carefully manufactured acrylic glass connectors, such that the outer wall of the annular passage was smooth and straight. The distance between the support locations was determined by a bending analysis of the inner tube, as illustrated in section 3.3.3. Four equally spaced 0.8 mm holes were drilled around the acrylic glass connectors to fit hypodermic needles that would support the inner tube centrally. Clear acrylic glass was used to allow visual inspection of concentricity during assembly. Hypodermic needles with a diameter as small as 0.8 mm were used to avoid disturbing the flow in the annular passage. The insertion of the inner tube into the outer tube was achieved by using a wooden bush with inner and outer diameters equal to the inner tube's outer diameter and the outer tube's inner diameter, respectively. Starting from one end of the outer tube, the bush was pulled from the other end until it reached the first acrylic glass connector. Then four needles were inserted into the small holes 90° apart through the connector until they touched the surface of the inner tube. Next, the needles were cut and the holes were sealed with epoxy. Finally, the needles were held firm by a metal hose clamp before moving the wooden bush to the next location. Figure 3.6 shows the cross-sectioned view of the connector with the inner tube centrally assembled. To measure the local outer wall temperature profiles along the length of the annular passage, two thermocouples were attached to each of the eight measuring stations on the outer surface of the outer tube wall at intervals exactly midway between the inner tube's measuring stations. At each measuring station, one thermocouple was placed on top and the other at the bottom of the tube as shown in Figure 3.3.
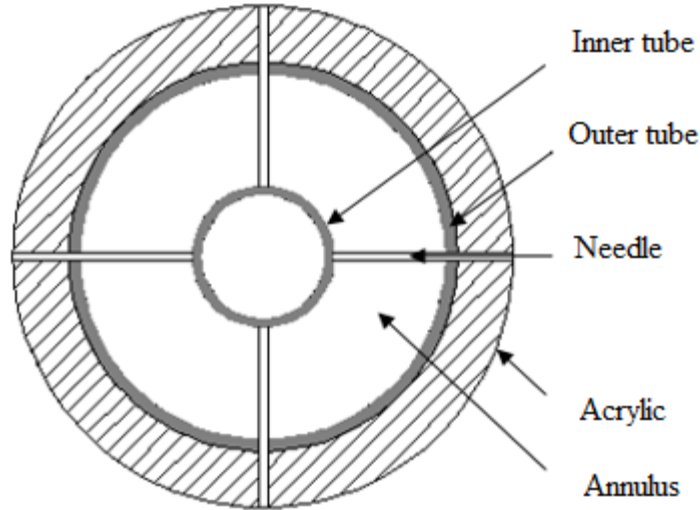
Figure 3.6: A cross-section image of the inner tube support mechanism

3.3.3. Determination of positions for inner tube support

As mentioned, the heat exchangers were long enough for the inner tube to sag if it was only supported at the ends. The sagging could make the annulus eccentric. Therefore extra supports were needed along the length of the inner tube to ensure concentricity. Just enough supports were needed to minimise the obstruction of flow in the annulus. Therefore, a bending analysis (Shigley, Mischke and Budynas, 2004) was performed on the inner tube where a maximum allowable vertical displacement of the inner tube of 1 mm was used. This displacement translates into an allowable shift of approximately 5% for the smallest hydraulic diameter. The vertical deflection of a tube is given by Shigley et al. (2004) as follows:

$$y_{max} = \frac{5wx}{384EI_x} \quad y_{max} = \frac{wx}{24EI_x}\left(2l_{un\,sup\,ported}x^2 - x^3 - L_{un\,sup\,ported}^3\right) \tag{3.1}$$

where y_{max} is the maximum allowable vertical displacement of the inner tube, x is the distance along the tube length and $L_{unsupported}$ is the total unsupported tube length. The second moment of area, I_x, is given as follows:

$$I_x = \frac{\pi}{64}\left(D_1^4 - D_i^4\right) \qquad (3.2)$$

where D_i is the inside diameter of the inner tube.

The modulus of elasticity for copper is given by Shigley et al. (2004) as $E = 119 \times 10^9$ Pa. The uniformly distributed load, w, is the weight of the inner tube, given as follows:

$$w = Mg \qquad (3.3)$$

where M is the mass of the tube per metre and g the gravitational acceleration. The mass of copper tube is the product of its volume and density. Therefore, Equation 3.3 can be expressed in terms of density and volume as follows:

$$w = xg\rho_{cu}A_c \qquad (3.4)$$

Where A_c is the cross-sectional area, x is the supported length and ρ_{cu} is the density of the copper.

With Equation 3.1 and Equation 3.2, an iterative process is used to determine the maximum distance between the inner tube's support locations.

The maximum distance between the support locations for the tube with an outer diameter of 12.7 mm is 1 061 mm and 1 143 mm for a tube with an outer diameter of 15.9 mm. However, the hypodermic needle supporting the inner tube was located with the acrylic glass connectors, which were 550 mm from each other. This distance would ensure a smaller vertical deflection not exceeding 0.0375 mm.

3.3.4. Annulus inlet

Since the lower and upper Reynolds number limits of the transition flow regime could be affected by the inlet configuration (Ghajar and Madon, 1992; Ghajar and Tam, 1994; Ghajar and Madon, 1997; Dirker, Meyer and Garach, 2014), two different inlet configurations were investigated for the annular passage flow in order to learn how best to minimise the effects due to the inlet profile. Both configurations were that of a 90° T-section fitting, similar to that found in most practical applications. For inlet geometry 1 (Figure 3.7a), the T-section was preceded by an

adiabatic inlet length that was above and ran parallel to the test section length. The inlet length was long enough to ensure fully hydrodynamic development before the elbow. While for inlet geometry 2 (Figure 3.7b), the inlet length was only 100 mm long and was positioned below the test section length. Section 5.2 will show, for the conditions considered in this study, that the inlet configuration does not have a significant impact on the Reynolds number limits of the transition flow regime. However, inlet geometry 1 was adopted for all the test sections because it was envisaged that the impact the upstream disturbances might have on relative heat transfer and pressure drop characteristics could be reduced within the inlet length. The inlet length of 4.2 m was connected to the annular passage inlets of the test sections, where the outer tube had an inside diameter of 32.9 mm, while a 5 m inlet length was used for tubes with an inside diameter of 38.88 mm.

(a)

(b)
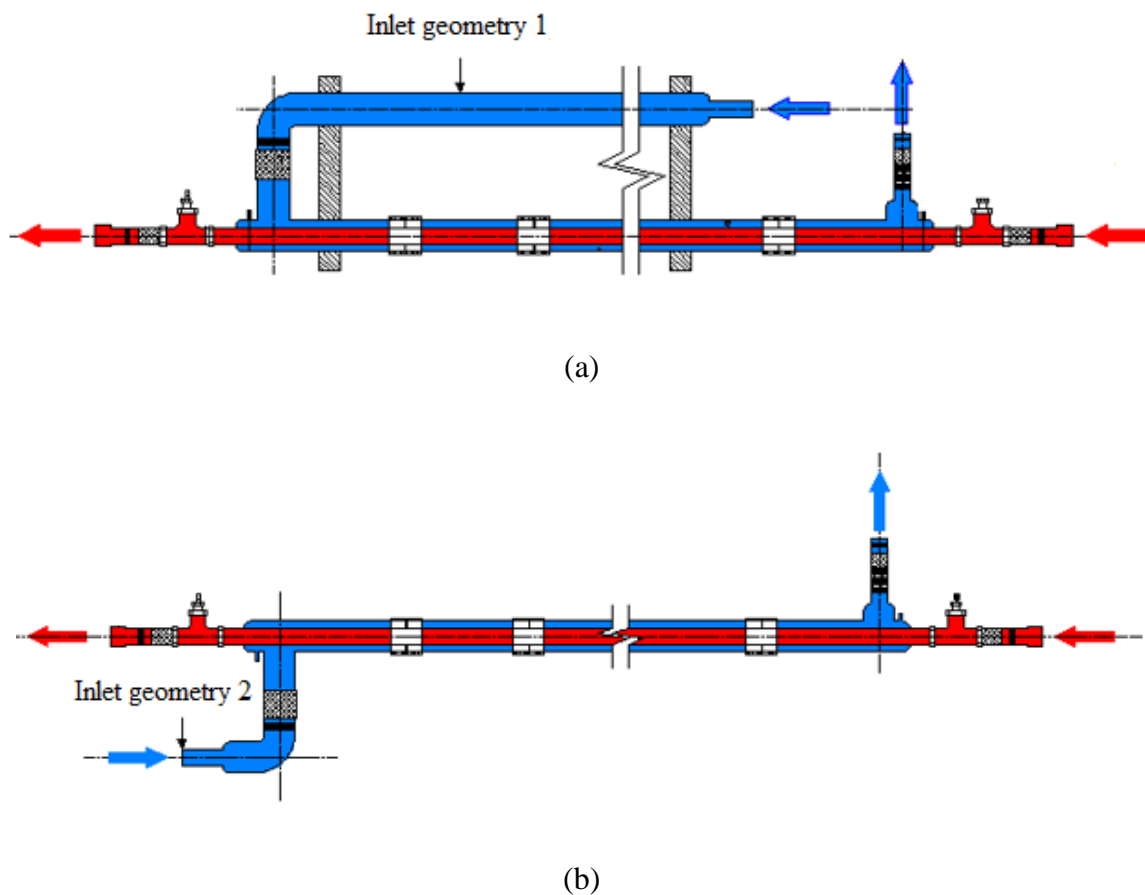
Figure 3.7: Tube-in-tube test sections with different annulus inlet geometries

The annulus inlet length (see Figure 3.7a) was clamped to the outer tube of the heat exchanger by three wooden supports to ensure a fixed relative position between the test section passage and itself. One clamp was placed near the elbow to prevent the inlet tube from slipping off the plastic hose connection due to high pressure at the elbow in the course of the experiments. Since two outer tubes of different diameters were used to assemble the four test sections, their inlets were geometrically proportional to each other to ensure consistency of inlet conditions. The inlet for a test section with an outer annular passage diameter of 32.9 mm (TS 3 and TS 4) had an inlet length of 4.2 m, which was connected to the heat exchanger by an elbow with a mid-pipe radius of 25 mm. This length was calculated by hydrodynamic entry length formulae ($L = 115D$) in the limiting case of Re = 2 300 (Çengel and Ghajar, 2011). However, inlet lengths were made a bit longer to ensure that full hydrodynamic development was indeed attained. The centre line distance between the inlet length and the main test section length was 210 mm, while for an outer annular passage diameter of 38.88 mm (TS 1 and TS 2), the inlet length was 5 m, the connecting elbow had a mid-pipe radius of 30 mm and the centre line distance between the inlet length and the main test section length was 248 mm. The entrance length had thermocouples attached close to the annulus entrance. Therefore, it was also thermally separated from the heat exchanger.

The inlet and outlet temperatures of the water that was passing through the annular passage also had to be measured during each test. Therefore, a temperature measuring station was installed after the inlet length, but before the annular passage entrance (labelled temperature measuring station in Figure 3.2). The position for the measuring station on the annulus outlet side is explained in the next section. As the annular passage was the area of interest in this study, eight thermocouples were installed at the inlet and outlet temperature measuring stations. The eight thermocouples were attached 45° apart on the periphery of each tube and reduced the measurement uncertainty of the inlet and outlet fluid temperatures, as will be discussed in section 4.4. The thermocouples were attached to the copper tube using silver tape. Thermally, these measuring stations were insulated from the heat exchanger by means of rubber hoses to prevent axial conduction. The average of the eight thermocouples was used as the mean inlet and outlet temperatures.

3.3.5. Annulus outlet

The outlet of the annular passage was also made of hard drawn copper tube. Since the outlet temperature readings of the water coming out of the annulus were required from the temperature measuring-station, a spiral in-line mixer was placed before the outlet temperature measuring station to avoid the formation of a thermal boundary layer and to ensure that the average water temperature was captured accurately. The mixer was made of four copper elements of alternating right-hand and left-hand 180° helices inserted in a copper tube with a diameter of 19.8 mm and a length of 120 mm.

3.3.6. Insulation

The test section and inlet and outlet measuring stations were thermally insulated from the environment by covering them with elastomeric foam sheets 50 mm thick with a thermal conductivity of 0.036 W/mK at 23 °C.

3.3.7. Acquisition of data

A computerised data acquisition (DAQ) system was used to gather the data from the respective measuring instruments. The DAQ system consisted of a personal computer using LabVIEW software with which the measurements could be logged and the experimental system could be controlled. The DAQ package used contained the necessary multiplexers, analogue-to-digital converters and terminal blocks to successfully log the data onto the computer.

3.4 Thermocouple and pressure transducer calibration

Before testing took place, the thermocouples and pressure transducers were checked for accuracy. The thermocouples were calibrated *in situ* without any heat transfer occurring between the inner tube and the annular fluid. The heat exchanger was initially modified to a single loop by connecting the outlet of the annulus to the inlet of the inner tube with a plastic pipe. This modification allowed the water entering from the annulus inlet to circulate through the entire heat exchanger and exit through the inner tube outlet. All thermocouples were calibrated against two PT100 probes installed at the inlet of the annulus and outlet of the inner tube. The average

measurement of the two PT100 probes was used in the calibration analysis. Water from a storage tank at different fixed temperatures was circulated for a long period of time through the exchanger until the temperature difference between the two PT100 probes was within ±0.05. The calibrations were done with the water circulated at temperatures between approximately 17 °C and 55 °C, and at intervals of approximately 5 °C. This range covered the minimum and maximum temperatures that were used during experimentation. The calibrations occurred once steady-state conditions were reached, which was when temperature variations of ±0.05 °C occurred for three minutes. Second-order polynomial calibration curves were created, with which measured data was conditioned during the data-processing stages. The calibration results of the thermocouples indicated that they were accurate in absolute terms to within a ±0.1 °C band. The 2.2 kPa pressure transducer was calibrated using a water column and a manometer with an accuracy of 0.0055 kPa. Twelve points from 0 to 2.2 kPa at intervals of 0.2 kPa were used in the calibration. A linear equation was created with which measured data was conditioned during the data-processing stages. The calibration results indicated that they were accurate to within ±0.01 kPa.

3.5 Experimental procedure

Seven different test types of experiments were conducted for each of the four test sections with reference to the fluid in the annular passage: isothermal experiments when no heat transfer occurs (pressure drop experiments only), and six types of diabatic experiments (pressure drop and heat transfer measurements) when the annulus was either heated or cooled (three types for each).

The heated and cooled diabatic annulus tests were performed with reference to the longitudinal inner wall temperature profiles. These temperature profiles were identified in terms of the degree of the wall temperature uniformity, τ, which was defined as the ratio of the inner wall temperature of the annular passage at the outlet, $\bar{T}_{iw,out}$ (measured in degrees Kelvin), to that at the inlet, $\bar{T}_{iw,in}$ (measured in degrees Kelvin), as shown in Equation 3.5. Since the inner wall temperatures at the inlet and outlet were not directly measured (see Figure 3.3), line-fit extrapolations from the measured wall temperature profiles were used, based on the measurements taken at the nine measuring stations on the inner wall. The method that was used to extrapolate the inlet and outlet wall temperature profiles is described in section 4.2.

$$\tau_{ha} = \frac{\overline{T}_{iw,out}}{\overline{T}_{iw,in}} \quad \text{(for a heated annulus)}$$

$$\tau_{ca} = \frac{\overline{T}_{iw,in}}{\overline{T}_{iw,out}} \quad \text{(for a cooled annulus)} \tag{3.5}$$

Since the annular passage was the focus of this investigation, the annular flow rate was the independent property during experimental tests, while the inner tube flow rate was dependent on the annular flow rate in order to create a particular wall temperature uniformity condition. The annular Reynolds number, based on the hydraulic diameter, ranged from slightly above 100 to approximately 14 000. This range was chosen to ensure that the transition flow regime was adequately covered. Specific wall temperature uniformities were achieved by running the water in the inner tube at different rates relative to the flow of the water in the annulus. This would give a constant temperature difference between the inlet and the outlet of the inner tube wall. In this investigation, three different degrees of wall temperature uniformity of 0.99, 0.975 and 0.965, with a precision of ±0.002 (see section 4.4 for the uncertainty analyses associated with the experimental tests) were applied for both heated and cooled annulus cases. The average temperature differences across the length of the inner tubes, which gave the selected degree of wall temperature uniformity, are given in Table 3.2. Due to the small diameter of the inner tube, which limited the maximum mass flow rate in the inner tube, it was challenging to maintain a difference across the inner tube length of 2 °C or less for test sections TS 1 and TS 3, especially for the high Reynolds numbers of the annular flow passage. Therefore, the achievable highest inner tube fluid flow rate limited the annular flow rate to Reynolds numbers of approximately 5 500 for the heated annulus case of TS1 and TS3. To achieve a truly UWT ($\tau = 1$), the wall temperature at the inlet and outlet of the inner tube surfaces would need to be equal. This was, however, difficult to achieve with the experimental facility in this investigation (because a very high inner flow rate would be needed, or a condensing/boiling fluid in the inner tube would have been required). Therefore, a wall temperature uniformity case of $\tau = 0.99$, being within 1% of $\tau = 1$, was treated as an approximate UWT condition. The rest of the ratios were regarded as non-UWT conditions.

Table 3.2: Degree of wall temperature uniformity, τ, for the diabatic tests

Diabatic case	Degree of wall temperature uniformity, τ, [-]	Mean temperature difference on the inner tube wall between the inlet and outlet for the four test sections [°C]			
		TS 1	TS 2	TS 3	TS 4
Heated annulus	0.990	2.71	2.15	2.72	2.07
	0.975	7.44	6.04	6.14	6.09
	0.965	11.52	10.04	10.03	10.14
Cooled annulus	0.990	2.8	2.39	2.82	1.84
	0.975	6.38	6.04	6.20	5.78
	0.965	10.46	9.69	9.63	9.69

Isothermal tests were conducted at a temperature range of 19.15 °C to 20.98 °C (with an average of 20.06 °C based on all tests), while the diabatic tests were conducted with a cold water temperature inlet range of 17.5 °C to 21.0 °C (with an average of 19.28 °C based on all tests) and a hot water inlet temperature range of 48.5 °C to 51.28 °C (with an average of 50.09 °C based on all tests). In all cases, the water in the inner tube and in the annular passage flowed in opposite directions.

During experimentation, the test sections were maintained at a horizontal position in order to avoid the effects of different angles of inclination on the results (Martinell et al., 1942; Lu and Wang, 2008). The data points were logged upon reaching a steady-state condition when the average annular fluid temperature at the outlet changed within ±0.1 °C over one minute. During this period, all other temperatures readings, as well as the mass flow rates for both the inner tube and the annulus, remained constant. Up to 120 data points were collected for each test data point at 10 Hz. Energy balance errors in terms of the heat transfer rates associated with the annular and inner tube fluids were checked and recorded.

An important data integrity check is that of comparing the energy transfer rate obtained based on measurements on the inner tube flow passage and that obtained from measurements on the annular flow passage. Before data was logged, it was attempted to keep the energy balance errors

as low as possible. It was found that achieving low energy balance errors for higher values of τ was more challenging than for cases with lower τ values. This was due to the relative temperature difference magnitude in the inner tube fluid from the inlet to the outlet. More details of the calculation of these errors are given in section 4.4. Smaller temperature differences of this nature resulted in higher measurement uncertainties, which were reflected in poorer energy balances. Since the focus of the investigation was only on the annular side, the energy balance errors were only used as relative data quality indicators. Test case heat transfer rates were based on the annular fluid temperature differences (not those of the inner passage fluid), which had a significant reduced uncertainty associated with the calculated heat transfer rate.

3.6 Summary

In this chapter, the experimental facility and test section set-ups were described in detail. The test sections were concentric tube-in-tube heat exchangers with the main focus being on the annular passage. Four test sections with different annular gap sizes of 26.2 mm, 23 mm, 20.2 mm and 17 mm, and respective annular diameter ratios of 0.327, 0.409, 0.386 and 0.483 were assembled, and were referred to as TS 1, TS 2, TS 3 and TS 4. During the assembly, special attention was given to ensure concentricity of the annulus and consistency of the inlet configuration.

The procedure that was followed to gather the required data was explained in detail. Hot water flowed into the inner tube and cold water flowed into the annulus for a heated annulus case, while the opposite was the case for a cooled annulus. Data was only collected at steady-state condition. In the next chapter, the method that was used to analyse the collected data is discussed.

Chapter 4

Reduction of the results

4.1. Introduction

In the previous chapter, the experimental set-up and the procedure that was used to collect the required data was discussed. In this chapter, methods and equations that were used to analyse the collected data to obtain the heat transfer coefficients and the friction factors are discussed. This chapter also presents the uncertainties of all the measurements and the associated uncertainty propagation analysis.

4.2. Data reduction method

The measured mass flow rates and the average inlet and outlet temperatures of the water passing through the inner tube and the annular passage were used to determine the heat transfer rates in the inner tube, $\dot{Q}_i$, and annular passage, $\dot{Q}_o$, as in Equation 4.1 and Equation 4.2, respectively.

$$\dot{Q}_i = \dot{m}_i c_{p,i} \left(\overline{T}_{in,i} - \overline{T}_{out,i} \right) \tag{4.1}$$

$$\dot{Q}_o = \dot{m}_o c_{p,o} \left(\overline{T}_{in,o} - \overline{T}_{out,o} \right) \tag{4.2}$$

The average inlet and outlet temperatures of the water were obtained from the wall temperature measurements on the inlet and outlet measuring stations. The specific heat values were obtained from the method of Popiel and Wojtkowiak (1998) at the bulk temperature of each stream. The bulk temperature for the inner tube was determined by the arithmetic average between the measured inlet and outlet fluid temperatures. This was acceptable since the inner tube was always operated in highly turbulent flow. This resulted in the arithmetic average temperature being a good representation of the average bulk fluid temperature. The same is true for high Reynolds number cases in the annulus, but not necessarily at low annulus Reynolds numbers. This is because the

annular bulk fluid temperature along the longitudinal direction is not necessarily linear at lower annular flow rates. Thus, it would often have been inaccurate to use the arithmetic average between the measured inlet and outlet bulk fluid temperatures. To increase the accuracy of the calculated fluid properties, it was briefly assumed that the bulk fluid temperature profile and the measured outer wall temperature profiles were approximately the same. Based on this, an improved estimation of effective bulk fluid temperature was obtained as follows:

$$\overline{T}_{b,o} \cong \frac{1}{L_{hx}} \int_{x_{in}}^{x_{out}} \overline{T}_{ow}(x)\,dx$$

$$(4.3)$$

Where $\overline{T}_{ow}(x)$ is a polynomial fit that represents the temperature measurement profile of the outer tube wall.

The energy balance error, EB, was calculated in terms of the average heat transfer rate, $\overline{\dot{Q}}$:

$$EB = \frac{\dot{Q}_o - \overline{\dot{Q}}}{\overline{\dot{Q}}}$$

$$(4.4)$$

Where

$$\overline{\dot{Q}} = \frac{\dot{Q}_i + \dot{Q}_o}{2}$$

$$(4.5)$$

The convection heat transfer rate in the annulus can be expressed with Newton's law of cooling:

$$\dot{Q}_o = hA_s \Delta T_{lm}$$

$$(4.6)$$

Where h is the average convection heat transfer coefficient, A_s is the wetted inner annulus wall surface area where convection heat transfer takes place, and ΔT_{lm} is the logarithmic mean temperature difference between inner annular passage wall temperature and the bulk fluid temperature.

In Equation 4.6, the surface area of the outside wall of the inner tube can be expressed in terms of the heat transfer length, L_{hx}, and inner wall diameter of the annular passage, D_1:

$$A_s = \pi L_{hx} D_1 \tag{4.7}$$

The logarithmic mean temperature difference for the annular flow passage was obtained using the relevant arithmetic averages from the calibrated thermocouple measurements and line extrapolations, as mentioned earlier.

$$\Delta \overline{T}_{lm} = \frac{\left(\overline{T}_{out,iw} - \overline{T}_{in,o}\right) - \left(\overline{T}_{in,iw} - \overline{T}_{out,o}\right)}{\ln\left[\dfrac{\left(\overline{T}_{out,iw} - \overline{T}_{in,o}\right)}{\left(\overline{T}_{in,iw} - \overline{T}_{out,o}\right)}\right]} \tag{4.8}$$

Here, $\overline{T}_{out,iw}$ refers to the inner tube wall outlet temperature, $\overline{T}_{in,iw}$ refers to inner tube wall inlet temperature, $\overline{T}_{in,o}$ refers to annular fluid inlet temperature and $\overline{T}_{out,o}$ refers to annular fluid outlet temperature.

As shown in Figure 3.3, temperature measuring stations on the inner wall of the annular passage were only located within its length. Due to the design of the test section, it was anticipated that heat conduction would greatly compromise temperature measurements at the inlet and outlet ends of the inner wall. Therefore no temperature measuring stations were installed at these locations. However, temperature measurements at the inner wall ends of the annular passage were needed to calculate the wall temperature uniformity and logarithmic mean temperature difference. Therefore, they had to be extrapolated from the temperature measured within the inner wall length. Figure 4.1 shows the method that was used to extrapolate the inlet and outlet inner wall temperatures. The average wall temperatures at the nine measuring stations that were located within the inner wall length were plotted against the heat transfer length (L_{hx}). A polynomial line was used to find a quadratic equation that would best describe the temperature profile along the wall for each test run. Finally, the equation was used to predict the average inner wall temperatures at the inlet and outlet ends, i.e. at $x = 0$ and $x = 5.06$ m, respectively.
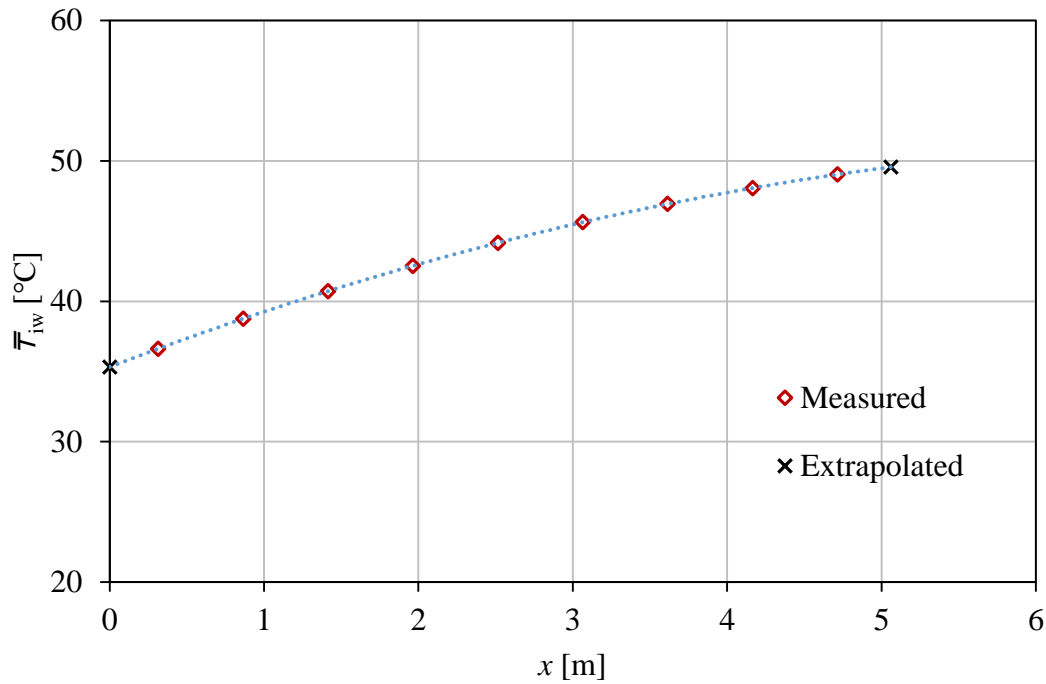
Figure 4.1: Temperature profile on the inner wall of the annular passage showing the extrapolated inlet and outlet temperatures

The mean Nusselt number for the annular passage was based on the hydraulic diameter, and was calculated as follows:

$$\overline{\mathrm{Nu}} = \frac{hD_h}{k}$$

(4.9)

The heat transfer coefficient results may also be presented in terms of the average Colburn *j*-factors. In this type of analysis, the effects of Prandtl number are taken into account. The Colburn *j*-factor is expressed as follows:

$$j = \frac{\mathrm{Nu}}{\mathrm{Re}\,\mathrm{Pr}^{1/3}}$$

(4.10)

The Reynolds number for flow in the annular passage was calculated as follows:

$$\text{Re}_o = \frac{\dot{m}_o D_h}{\mu_o A_o} = \frac{4\dot{m}_o}{\pi \mu_o (D_0 + D_1)} \tag{4.11}$$

It was discussed in Chapter 2 that a convection heat transfer may be influenced by secondary flows due to buoyancy force. This is common in low Reynolds number ranges. One method that is used to determine whether or not buoyancy force should be considered in the forced flow is the Richardson number, which is expressed as follows:

$$\text{Ri} = \frac{\text{Gr}}{\text{Re}^2} \tag{4.12}$$

Here the Grashof number is the dimensionless parameter that represents the free convection effects and is calculated as follows:

$$\text{Gr} = \frac{g\beta(T_{iw} - T_b)D_h^3}{v^2} \tag{4.13}$$

In Equation 4.13, g is acceleration due to gravity, v is the kinematic viscosity (μ/ρ) and β is the volumetric expansion coefficient, which was determined by the method of Popiel and Wojtkowiak (1998) at the bulk fluid temperature.

The average friction factors at different Reynolds numbers were determined from the measured pressure drops, Δp, over the distance between the two pressure taps as follows:

$$\bar{f} = \frac{2D_h \Delta p}{\rho_o L_{pd} V_o^2} \tag{4.14}$$

The velocity of the water in the annulus, V_o, was determined from the measured mass flow rate in the annulus, the cross-sectional annulus area and average fluid density at the bulk temperature.

$$V_o = \dot{m}_o / (\rho_o A_o) \tag{4.15}$$

4.3. Local heat transfer analysis

Even though the approximate axial annular bulk fluid temperature was monitored with the thermocouple measurements on the outer annular wall (as mentioned earlier), the non-thermally developed nature of the flow did not allow for the exact calculation of local bulk fluid temperatures along the heat exchanger length. Therefore, it was not feasible to analyse heat transfer locally; thus, only averaged heat transfer coefficients are presented in this study.

4.4. Uncertainties

An uncertainty analysis of the overall experimental procedures, focusing on the annular side, based on the method of Moffat (1988) was performed. All uncertainties were calculated within the 95% confidence interval. The comprehensive uncertainty analysis is presented in Appendix A. Table 4.1 gives the uncertainties of measuring instruments with their respective range, bias and precision.

Table 4.1: Ranges and uncertainties of instruments used in the experimentation

Instrument	Range	Bias	Precision	Uncertainty
Thermocouple (T-type)	-200 – 350 °C	0.1 °C[5]	0.036 °C	0.106 °C
Coriolis flow meters	0 – 1.833 kg/s	0.1%[6]	0.09%	0.13%
	0 – 0.607 kg/s	0.1%[3]	0.05%	0.11%
Pressure transducer	0 – 2.2 kPa	0.25%[7]	2.19%	2.2%

It was mentioned in the experimental set-up (Chapter 3) that the inlet and outlet measuring stations for the inner tube had four thermocouples each, while those for the annular passage had eight and the inner and outer tube walls had two at each measuring station. This was done to reduce uncertainty of measurement at these points. As annular passage was the area of focus of this study,

---

[5] Calibrated with a PT 100 with an uncertainty of 0.01 °C.
[6] Percentage of reading.
[7] Percentage of full scale value

it had more thermocouples at each measuring station than the others. The uncertainty of measurement at a temperature measuring station with more than one thermocouple is calculated as follows:

$$\delta \overline{T} = \frac{\delta T}{\sqrt{n}}$$

(4.16)

Here, δT is the uncertainty of a thermocouple, which in this case is 0.106 °C, and n is the number of thermocouples at a temperature measuring station. The uncertainty of measurement at different temperature measuring stations is shown in Table 4.2.

Table 4.2: Uncertainty of measurement at different temperature measuring stations

Temperature measuring station	Number of thermocouples	Uncertainty
Inlet and outlet of annular passage	8	0.0376
Inlet and outlet of annular passage	4	0.0531
Inner and outer wall of annular passage	2	0.0752

The uncertainties of the averaged Nusselt numbers and the friction factors of the transition regime, which is the focus of this study, are summarised in Table 4.3 for both the heated and cooled annulus cases.

It was found that the maximum Nusselt number uncertainty was approximately 30% and occurred at a laminar Reynolds number of 128. However, at higher Reynolds numbers, the uncertainties were significantly lower. In this investigation, the highest Nusselt number uncertainties occurred at the lowest Reynolds numbers, where the fluid flow rates were at their lowest. Even though the resulted higher temperature differences associated with lower flow rates tend to cause the heat transfer uncertainty values to drop, the higher uncertainties of flow meter reading at low flow rates resulted in an overall high Nusselt number uncertainty. For the transition flow regime, which is the area of interest of this study, the highest Nusselt number uncertainty of 10.4% was at the lower Reynolds number limit of transition of a test section, TS 4, with the degree of temperature uniformity on the inner wall of 0.965. The lowest Nusselt number uncertainty of

1.2% was at the upper limit of transition of a test section, TS 1, with the degree of temperature uniformity on the inner wall of 0.990.

Table 4.3: Uncertainties of averaged Nusselt numbers and friction factors in the transition flow regime

TS	Annulus case	τ	Heat transfer transition		Friction factor transition	
			Min (%)	Max (%)	Min (%)	Max (%)
TS 1	Isothermal				1.18	3.81
	Heated	0.99	1.21	6.56	1.07	3.16
		0.975	1.28	6.34	1.10	3.26
		0.965	1.45	6.14	1.18	3.42
	Cold	0.99	1.26	6.72	1.08	3.42
		0.975	1.36	7.39	1.14	3.65
		0.965	1.44	8.06	1.20	3.82
TS 2	Isothermal				1.26	3.64
	Heated	0.99	1.21	7.0	1.22	3.81
		0.975	1.25	7.25	1.22	3.90
		0.965	1.36	7.67	1.26	4.06
	Cold	0.99	1.33	6.79	1.21	3.48
		0.975	1.37	7.46	1.25	3.75
		0.965	1.47	8.11	1.32	4.01
TS 3	Isothermal				1.50	4.71
	Heated	0.99	1.43	8.98	1.04	3.58
		0.975	1.44	9.35	1.07	3.66
		0.965	1.51	10.08	1.11	3.76
	Cold	0.99	1.60	8.33	1.45	4.17
		0.975	1.63	9.13	1.51	4.48
		0.965	1.68	9.74	1.53	4.71
TS 4	Isothermal				1.58	4.56
	Heated	0.99	1.50	9.32	1.65	5.52
		0.975	1.51	9.83	1.62	5.54
		0.965	1.64	10.12	1.68	5.58
	Cold	0.99	1.74	8.54	1.49	4.12
		0.975	1.77	9.58	1.52	4.31
		0.965	1.87	10.4	1.55	4.54

For the friction factor, the highest uncertainty was 5.58%. This was also at the lower Reynolds number limit of the transition regime of test section TS 4, with the degree of temperature uniformity on the inner wall of 0.965. The lowest uncertainty of 1.07% was at the upper Reynolds number limit of the transition regime of test section TS 1, with the degree of temperature uniformity on the inner wall of 0.99. The maximum uncertainties of the friction factors were high at low Reynolds numbers due to higher uncertainties of the pressure drop transducer at lower flow rates. As the Reynolds number was increased, thus reducing uncertainties in pressure drop measurement, the friction factor uncertainties reduced as well.

4.5. Summary

In this chapter, the method by which the data that was gathered in Chapter 3 was analysed to get experimental heat transfer coefficients and friction factors was discussed. Only the averaged results were processed in this investigation. Mean Nusselt numbers were determined using the logarithmic mean temperature difference. An uncertainty analysis was performed based on the measurement instruments and data reduction method used. The uncertainties of heat transfer coefficients in the transition regime were between 10.4% and 1.2%, while those of the friction factors were between 5.6% and 1.1%.

In the next chapter, the preliminary analysis of the results is done. This includes a method for identifying the lower and upper Reynolds number limits of the transition flow regime, a discussion of the convection types within the flow regimes and the validation of the experimental results.

Chapter 5

Preliminary data analysis

5.1. Introduction

In the previous chapter, the data reduction method and uncertainty of experimental measurements were discussed. In this chapter, the results of the investigation that was conducted to establish the effect of the inlet configuration on the Reynolds number limits of the transition flow regime are presented first. Then a methodology for identifying laminar, turbulent and transition flow from laminar to turbulent for both the heat transfer and friction factor results is presented. After this, the spread of different convection types within the flow regimes is analysed. Finally, the experimental set-up and procedure are validated with well-known correlations.

5.2. The effect of the annulus inlet configuration on the Reynolds number limits of the transition regime

It was mentioned in section 3.3.4 that two different annular passage inlet configurations were investigated to establish the effects of the inlet geometry on the Reynolds number limits of the transition flow regime (Ghajar and Madon, 1992; Ghajar and Tam, 1994; Ghajar and Madon, 1997; Dirker et al., 2014). Isothermal experiments were done for the two inlet configurations shown in the Figure 3.7. Figure 5.1 gives the mean friction factor results for the two inlet configurations. As can be seen, the results were very similar. Therefore, based on this, the transition flow regime results are repeatable in terms of the impact of the inlet geometry used in this investigation.

5.3. Identification of cut-off points of the flow regimes

Test data encompassing laminar, transition and turbulent regimes was analysed to get the lower and upper Reynolds number limits of transition flow regimes. These lower and upper limits are represented by Re_1 and Re_2, respectively. The lengthwise averaged heat transfer coefficients and friction factors were plotted against the Reynolds number (both on a logarithmic scale) for all test cases.
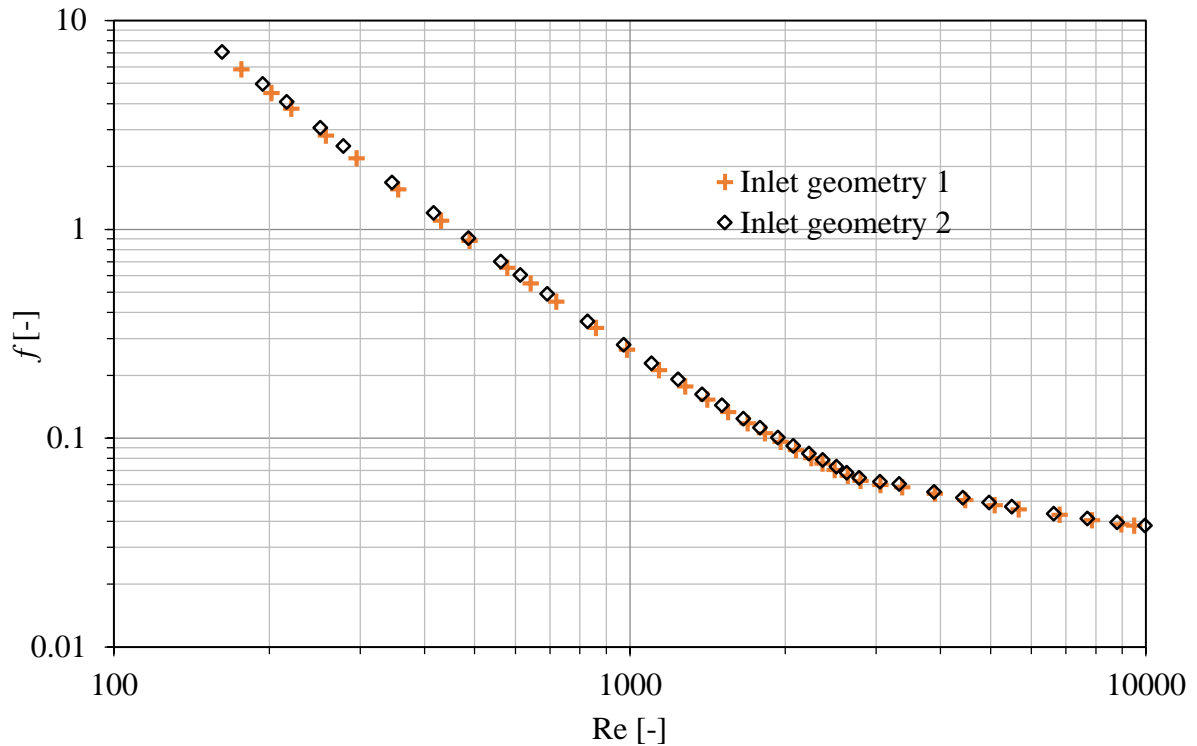
Figure 5.1: Friction factor results for inlet geometries 1 and 2

For both case types of the diabatic investigation (heated and cooled annulus), similar behaviour was observed in the Nusselt number plots. The logarithmic scale gradient of the Nusselt number data points was relatively steep in the low Reynolds number region, less steep in the mid-range of the Reynolds numbers and steeper again in the high Reynolds number range. On inspection, it was observed that the trends of the graph are well described by linear line segments. The best matching set of linear line segments was determined by minimising the overall root mean square error associated with the difference between the experimental data and the trends described by the linear line segments. An example case for the cooled annulus case of a wall temperature uniformity of 0.965 of TS 4 is shown in Figure 5.2. Similar type lines were also used to trace out the flow regime regions for the other wall temperature uniformity cases and test sections. The mid-range region, as defined by the portion between the intersections of the three lines, indicates the transition flow regime range, while the low and high Reynolds number ranges indicate the laminar and turbulent regimes, respectively.
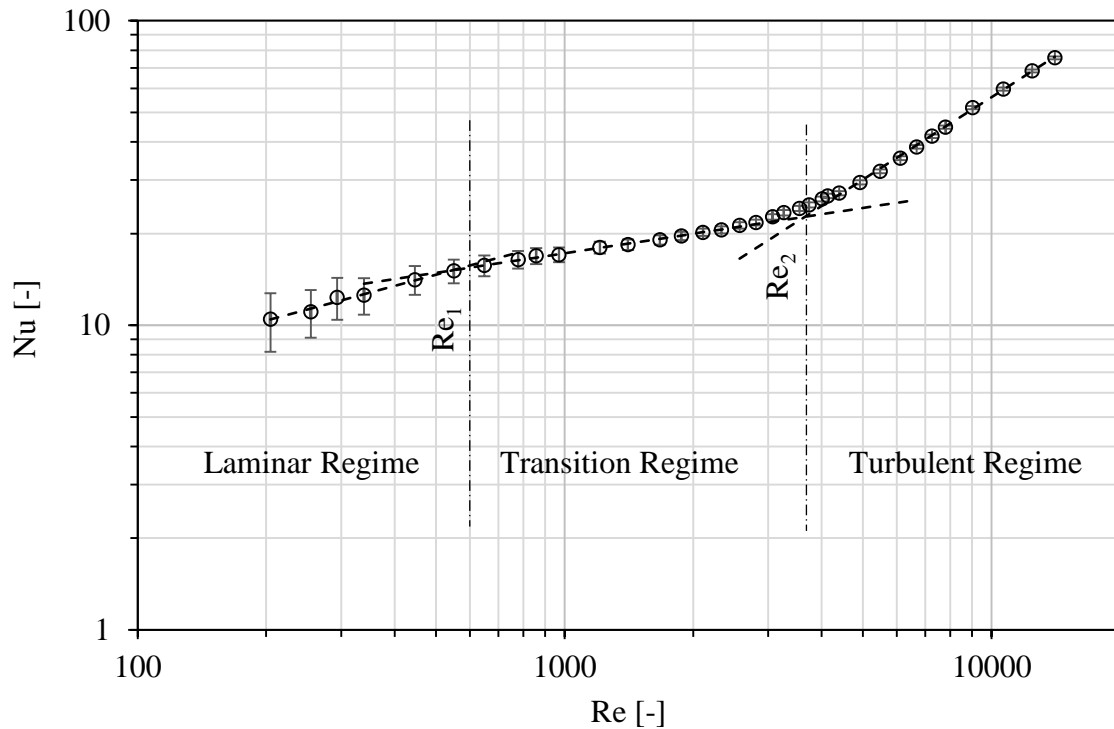
Figure 5.2: A method for identifying flow regime due to heat transfer

Plots of the friction factor against the Reynolds number (both on a logarithmic scale) also gave approximately linear patterns, which could be traced out by straight lines as is shown in Figure 5.3. The friction factors rapidly decreased linearly with increasing Reynolds numbers in the low Reynolds number region, then at a relatively lower rate of decrease in the mid-range of the Reynolds numbers, and finally at the lowest in rate of decrease in the high Reynolds number region. Figure 5.3 shows the pattern of the friction factor against Reynolds numbers for an adiabatic test of TS 4 and a method of identifying different flow regimes. The mid-range region, as defined by the region between the intersections of the three lines, indicates the transition flow regime range, while the low and high Reynolds number ranges indicate the laminar and turbulent regimes, respectively.
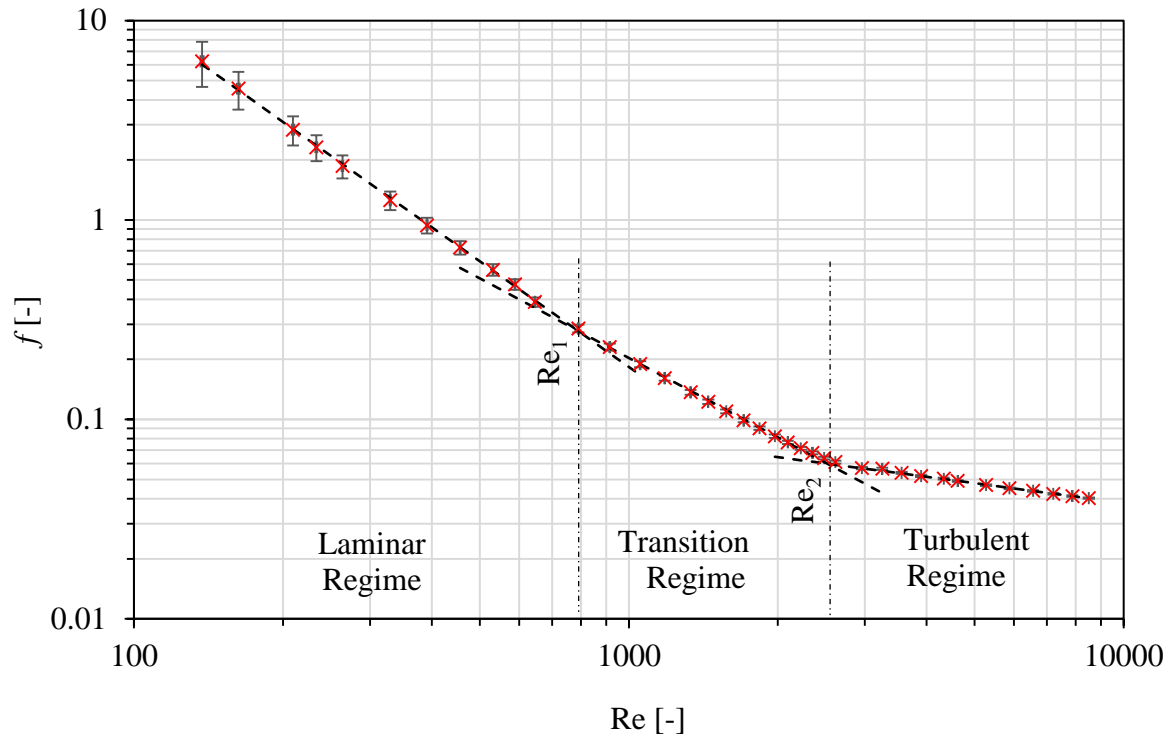
Figure 5.3: A method for identifying flow regime due to friction factor

5.4. Analysis of convection types

A better understanding of convection types (natural, mixed and forced convection) that were present in the flow regimes is required for validation purposes and a better interpretation of the results. The Richardson number method was used to identify convection types. A flow regime map for annular flow could not be found in the literature and the peripheral heat transfer method could not be applied to annular flow. In the Richardson number method of determining convection types, both the free and forced convections (mixed convection) are to be considered when $0.1 \leq Ri \leq 10$. For $Ri > 10$, the flow is treated as free convection. The pure forced convection is considered when $Ri < 0.1$. Figure 5.4 depicts the spread of experimental data within the three convection types and Reynolds number regimes (laminar, transition and turbulent). Figure 5.4a is for TS 1 where data for different degrees of wall temperature uniformity is presented. Similar data for TS 2, TS 3 and TS 4 is presented in Appendix B. Figure 5.4b is for $\tau = 0.99$ where data for different test sections is presented. Similar data for $\tau = 0.975$ and $\tau = 0.965$ is presented in Appendix C. Since each test

had different Re_1 and Re_2 values from the other (as will be presented in section 6.2), average Reynolds number limits have been used in Figure 5.4.
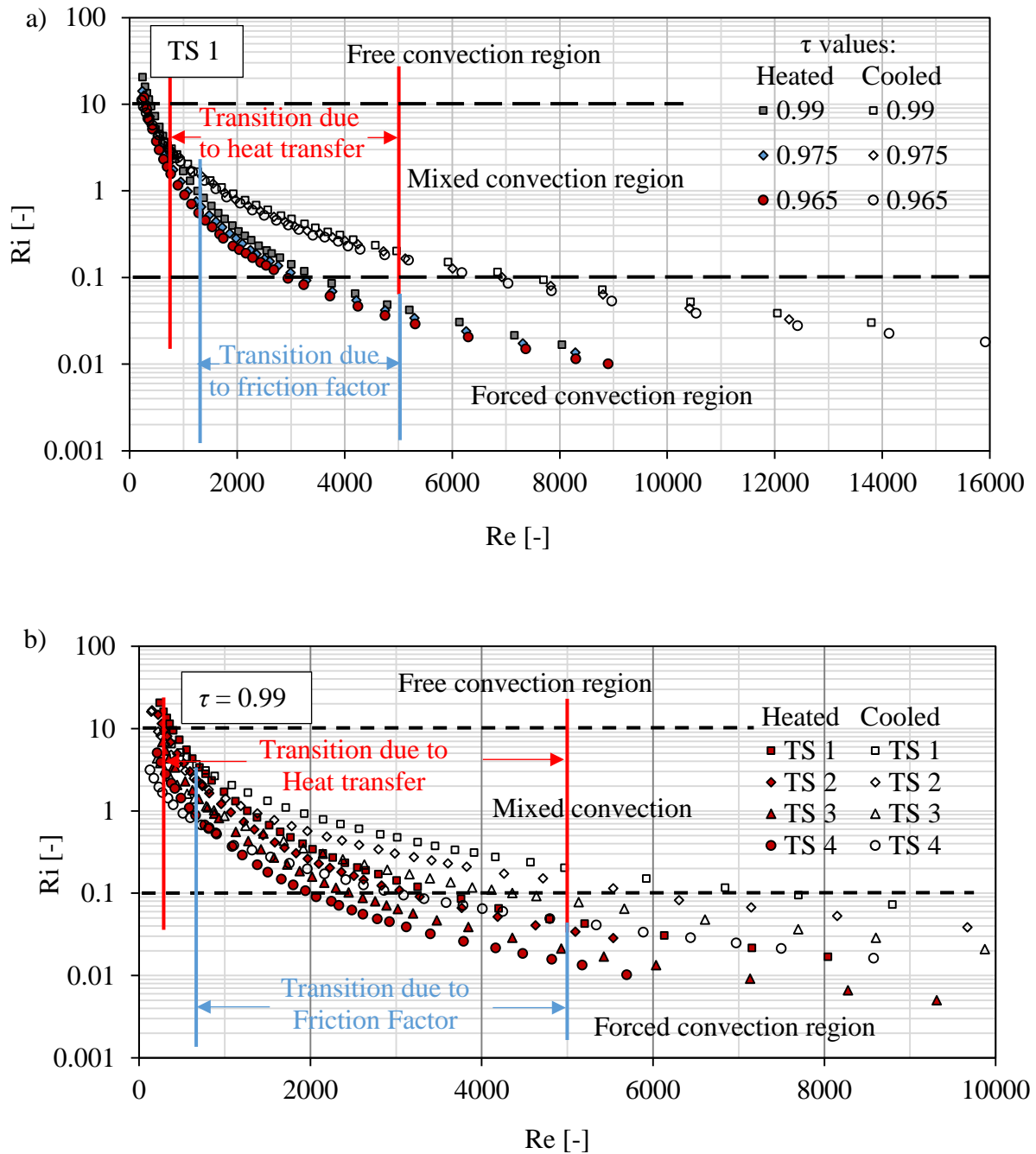
Figure 5.4: Richardson numbers for heated and cooled annulus cases for: (a) different degrees of wall temperature uniformities; and (b) test sections with different annular gaps

Laminar flow, in all the test sections was generally a combination of natural and forced convections ($10 > Ri > 0.1$), although a few data points for test sections TS 1 and TS 2 fell in the free convection region. The transition regime in most of the test sections was partly mixed and forced convection. Turbulent flow was generally forced convection ($Ri < 0.1$), although a few data points of the cooled annulus cases are seen in the mixed-convection region. Buoyancy forces were relatively strong in a case with a higher degree of wall temperature uniformity than with a lower degree of wall temperature uniformity as shown in Figure 5.4a. This means that buoyancy forces were much stronger for $\tau = 0.99$, followed by $\tau = 0.975$, and lastly $\tau = 0.965$. In Figure 5.4b, the test section with a larger annular gap (hydraulic diameter of 26.2 mm) had higher Richardson numbers, followed by the rest in descending order. This means that the buoyancy forces were much stronger in TS 1, followed by TS 2, TS 3 and lastly TS 4. Both in terms of annular gap size and degree of wall temperature uniformity, the cooled annulus case had a stronger buoyancy force than the heated case.

The cut-off points between the mixed and forced convection types were found within the transition regime for most of the tests. As will be discussed later in Chapter 6 and Chapter 7, each test case had different lower (Re_1) and upper (Re_2) Reynolds number limits of transition regime from the other. Since it would be challenging to insert the limits for each test in Figure 5.4, the average Reynolds number limits (Re_1 and Re_2) for all the tests considered were used. Alternatively, the sizes of the mixed-convection portions in the different tests for $\tau = 0.99$ are presented as a percentage of total data points in the transition regime in Table 5.1. Similar information is presented in Appendix C for $\tau = 0.975$ and $\tau = 0.965$.

In Table 5.1, the mixed-convection portion (expressed as a percentage) of the transition flow regime data point is higher for the test sections with larger annular gap sizes. As the annular gap size decreases, the mixed-convection portion of the transition regime data points decreases as well. The size of the mixed-convection portion is also affected by the degree of wall temperature uniformity. The higher the degree of wall temperature uniformity, the larger the mixed-convection portion became. Both in terms of annular gap size and degree of wall temperature uniformity, the cooled annulus case had a larger mixed-convection portion than the heated case.

Table 5.1: Heat transfer and flow transition ranges for heated and cooled annuli and mixed-convection size for the approximately UWT case, $\tau = 0.99$

Heated annulus						
TS	**Transition based on Nusselt number**			**Transition based on friction factor**		
	Re₁	**Re₂**	**Percentage of transition flow regime data points that are of the mixed-convection type**	**Re₁**	**Re₂**	**Percentage of transition flow regime data points that are of the mixed-convection type**
1	720	4 800	87%	1 350	4 000	89%
2	650	4 200	86%	1 100	3 400	85%
3	630	4 000	68%	1 000	3 200	69%
4	570	3 400	57%	900	2 800	58%
Cooled annulus						
1	690	6 400	100%	1 500	6 000	100%
2	610	5 000	100%	1 400	5 000	100%
3	590	4 600	96%	1 350	4 600	97%
4	540	3 800	78%	1 250	4 400	60%

5.5. Validation

Experimental results for the heat transfer coefficients and the friction factors were compared with established heat transfer and friction factor correlations in the turbulent regime. There were no relevant correlations in the literature that could be used to validate the present annular experimental results in the laminar and transition regimes. However, laminar fully developed mixed convection has been included to appreciate the effect of secondary flow on the heat transfer coefficient. Also included is the laminar fully developed forced convection to appreciate the effect of developing flow on the heat transfer coefficient. The validation for friction factor measurements was done for isothermal flow only, as this disregarded any influence of heat transfer on the properties of the fluid.

5.5.1   Friction factor

Figure 5.5 shows the experimental isothermal friction factor results for the test section TS 4. In the figure, the friction factors for a hydrodynamically developing flow are plotted against the annular Reynolds number. Uncertainty bars are also included in the figure. These measurements were made without any heat transfer. Therefore they disregard varying density and viscosity effects. For comparison purposes, a laminar flow Poiseuille relation, as given in Equation 5.1 for an isothermal fluid, was used. This equation is the modified version of the laminar flow Poiseuille relation for a circular tube with a fully developed velocity profile.

$$f = \frac{64}{\mathrm{Re}^*} \tag{5.1}$$

Where
$$\mathrm{Re}^* = \mathrm{Re}\,\frac{(1+a^2)\ln a + (1-a^2)}{(1-a)^2 \ln a} \tag{5.2}$$

And *a* in Equation 5.2 is annular diameter ratios, $a = D_1/D_0$.

Similarly, friction factors in the turbulent regime were compared to an equation by Filonenko (1954), which was later modified for application in annular passages by Gnielinski (2007) as shown in Equation 5.3. The Gnielinski equation (turbulent flow), which is well known for circular tube applications, was adjusted for the annular Reynolds number, Re, based on the hydraulic diameter, in order to suit the present investigation. The adjusted turbulent flow adiabatic equation was given as follows:

$$f = (1.8\log_{10}\mathrm{Re}^* - 1.5)^{-2} \tag{5.3}$$

Here, Re^* is the same as that in Equation 5.2.
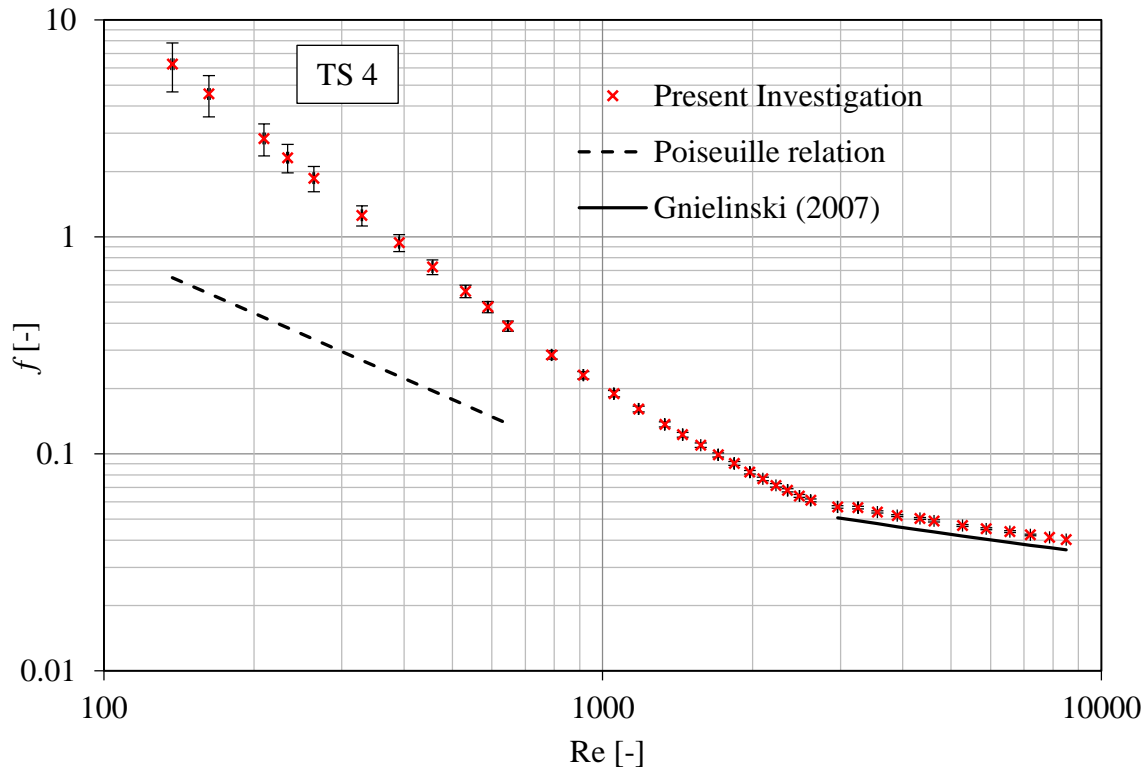
Figure 5.5: Comparison of adiabatic friction factor results with some literature references

The experimental laminar friction factors are much higher than those obtained by the Poiseuille relation (Equation 5.1). This could be due to the entrance effects in the present investigation, since the Poiseuille relation was developed for fully developed flow. In the literature study, it was learnt that the pressure drop is higher in the hydrodynamic entrance region of a developing flow, and hence increases the average friction factor for the whole conduit (Mohammed et al., 2010). The difference between the friction factor values is much less in the turbulent flow than in the laminar flow because the entry length is much shorter for a turbulent flow than for a laminar flow (Çengel and Ghajar, 2011). The Gnielinski equation (Equation 5.2) under-predicted the average experimental friction factors by 23%, 18%, 12% and 9.7% for test sections with an annular diameter ratio of TS 1, TS 2, TS 3 and TS 4, respectively. These differences could be due to the different annular gap sizes of the test section. It is observed that the smaller the annular gap size, the smaller is the prediction error.

Van Zyl (2012) and Van Zyl et al. (2013) investigated the characteristics of the heat transfer coefficients and friction factors in concentric horizontal annuli in fully turbulent flow. Both heated and cooled annuli were examined in the Reynolds number range from 10 000 to 45 000 with water as a working medium. In the investigation, four smooth concentric tube-in-tube heat exchangers of an annular diameter ratio of 0.483, 0.579, 0.593 and 0.712 were employed. Experiments were performed with the inlet temperatures to the annulus and inner tube constant at approximately 20 °C and 55 °C. Like in the present investigation, the annular flow rate was varied but the inner tube flow rate was held constant. In the present investigation, a test section with an annular diameter ratio of 0.483 (TS 4) was also used to investigate the characteristics of the heat transfer coefficients and friction factors by applying an almost similar procedure to that of Van Zyl (2012) and Van Zyl et al. (2013). The Reynolds number range for the present investigation was approximately 100 to 14 000. Since the Reynolds number ranges for these similar but independent investigations (Van Zyl and the present investigation) appear to overlap, the results for the friction factors of the two investigations were plotted together in Figure 5.6 to check whether they overlap as well. As can be seen in Figure 5.6, the data for the present investigation bridges well with that of Van Zyl (2012) and Van Zyl et al. (2013).
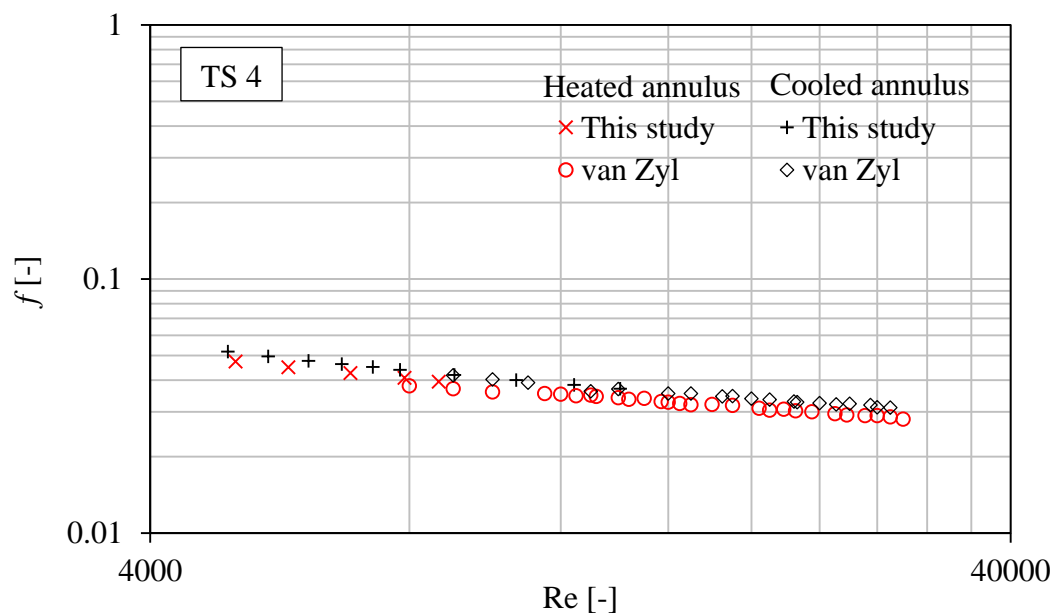
Figure 5.6: Diabatic friction factors for a cooled and heated annulus from two independent but similar investigations

5.5.2   Heat transfer coefficient

The flow in the turbulent regime was generally forced convection, while in the laminar and transition regimes, the convection was of the mixed type. The prevalence of the types of convections in different flow regimes is dealt with in section 5.4. A thermal boundary profile was developing in this investigation. Since correlations for thermally and hydrodynamically developing flow were unavailable in the literature for laminar and transition flow, the measured heat transfer data was compared with the fully developed forced convection correlation of Gnielinski (2015) in the turbulent regime, Equation 2.4, which is repeated here. The correlation is given as follows:

$$Nu_o = \frac{(f/8)(\text{Re}-1000)\text{Pr}_b}{1+12.7\sqrt{(f/8)}\left(\text{Pr}_b^{2/3}-1\right)}\left[1+\left(\frac{D_h}{L}\right)^{2/3}\right]FK$$

$$(5.4)$$

Here $F = 0.75a^{-0.17}$ for the boundary condition of heat transfer at the inner wall with the outer wall insulated, $K = \left(\dfrac{\text{Pr}_b}{\text{Pr}_w}\right)^{0.11}$, and *f* is as in Equation 5.3.

Figure 5.7 contains the Nusselt number results for the heated annulus case of test section TS 4. The results for the degree of wall temperature uniformity, $\tau = 0.965$, were singled out for validation purposes because, despite the high flow rate challenges of the inner tube, as indicated in Chapter 3, higher annular Reynolds numbers were achieved. Therefore, a reasonable amount of experimental data points could be compared with correlations in the turbulent regime. Uncertainty bars are also included in the figure. A comparison between the experimental results and Equation 5.4 (Gnielinski, 2015) indicate good agreement. The experimental Nusselt numbers for TS 1 were within 1.6% (on average) of the predicted heat transfer coefficient, 1.2% for TS 2, 1.0% for TS 3 and 0.8% for TS 4. Similar to the observation that was made for friction factors, the prediction errors for the Nusselt numbers are also proportional to the annular gap size. The smaller the annular gap size, the smaller the prediction error.
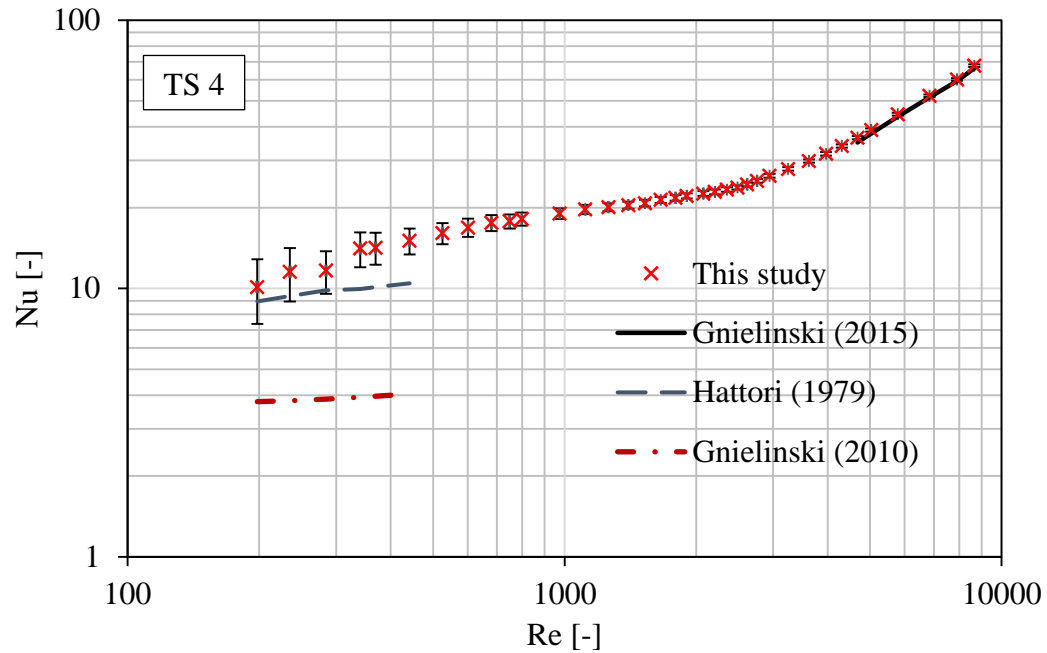
Figure 5.7: Comparison of the Nusselt number results for the four test section with some literature references

In order to appreciate the effect of secondary flows, the measured data in the laminar regime was also compared with the fully developed forced convection correlation by Gnielinski (2010). This correlation is given as follows:

$$
\mathrm{Nu}_o = \left\{ \begin{array}{l} 3.66^3 + 0.7^3 + \left[1.615 \sqrt[3]{\left(\mathrm{Re}_o \, \mathrm{Pr}_b \, D_h / L_{hx} \right)} - 0.7 \right]^3 \\ + \left[\left(\dfrac{2}{1 + 22 \mathrm{Pr}_b} \right)^{1/6} \left(\mathrm{Re}_o \, \mathrm{Pr}_b \, D_h / L_{hx} \right)^{1/2} \right]^3 \end{array} \right\}^{1/3}
\tag{5.5}
$$

The experimental Nusselt numbers were significantly higher than the laminar flow regime predictions of Equation 5.5. This is because Equation 5.5 is for flow free from buoyancy effects, while in the current investigation, significant buoyancy-driven secondary flow was present. This greatly impacts on the heat transfer coefficient, as was observed by Kakaç et al. (1987) and Mohammed et al. (2010).

Hattori (1979) proposed a Nusselt number correlation for an annular passage associated with mixed convection. The correlation given in Equation 5.6 was proposed for a fully developed flow in the laminar regime with a UWT boundary on the inner wall and isothermal condition on the outer wall. In Figure 5.7, the correlation due to Equation 5.6 is close to the experimental results. The difference could be due to several factors, including the effects of thermal boundary development at the entrance for the present investigation.

$$\mathrm{Nu}_o = 0.44 \mathrm{Gr}^{0.2}\,\mathrm{Pr}^{0.28}\left(\frac{D_1}{D_0}\right)^{-0.35} \tag{5.6}$$

As in the case of friction factors, the Nusselt numbers were compared between the measured data of Van Zyl (2012) and that of the present investigation for both the heated and cooled annulus cases for the same test section, TS 4 ($a = 0.483$). The plots of the two similar but independent investigations in Figure 5.8, appear to bridge well, especially for a cooled annulus case. Due to limited data points of the heated case, there is no common range for the two experiments, however, the extrapolation of the present data seems to bridge reasonably well with those of Van Zyl.
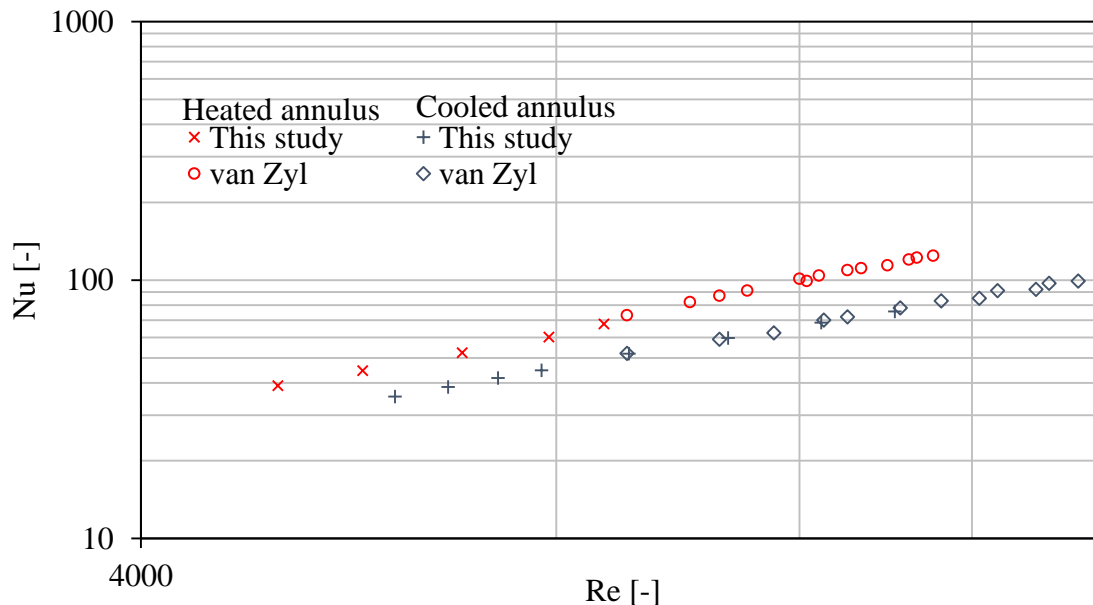
Figure 5.8: Measured mean Nusselt numbers and correlations available in the literature for a cooled annulus with an annular diameter ratio of 0.482

Based on the good agreement of the experimental results with the friction factor and Nusselt number predictions of the well-accepted Gnielinski correlations (Gnielinski, 2007 and Gnielinski, 2015) for the turbulent flow and a comparison between the experimental results of the present investigation and those of van Zyl (2012), the experimental procedure and data reduction method used in this investigation were assumed to be validated.

Repeatability and drift of the experimental test procedure was also checked. Figure 5.9 shows the Nusselt numbers of two sets of data for $\tau_{ha} = 0.99$ that were taken eight months apart, during which time the first set of data (Dataset 1) and the second set of data (Dataset 2) were collected and compared. Very good repeatability was observed with the average difference in values from the two datasets being less than 2.5%, and the maximum difference being 8.2% in the low Reynolds number range.
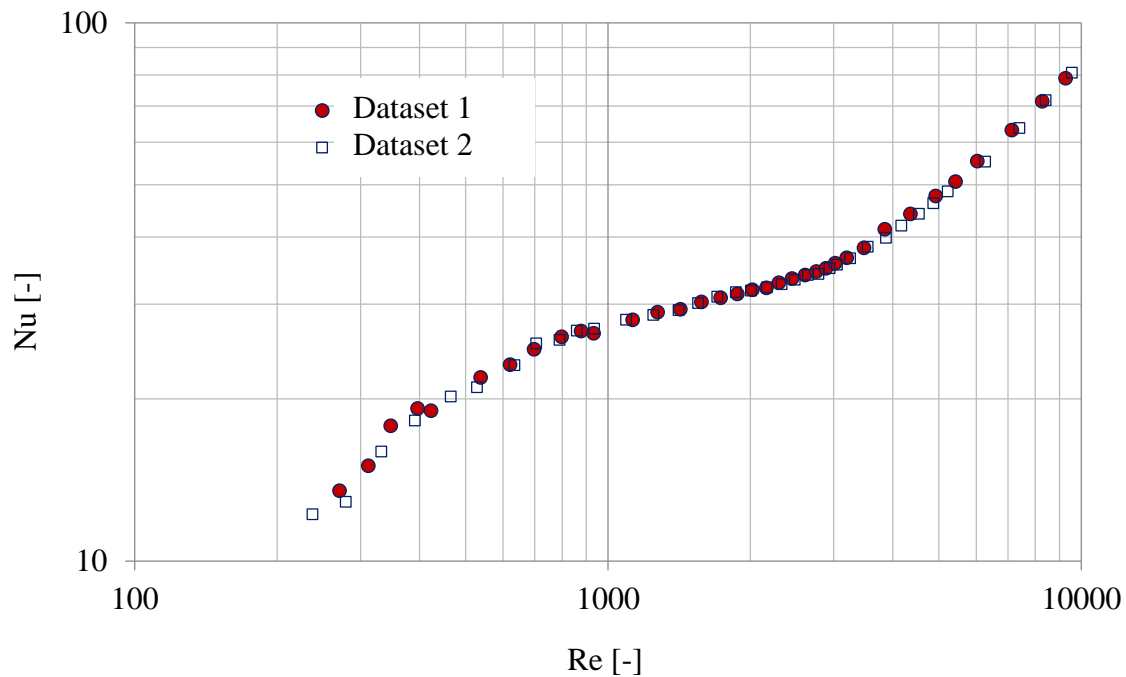
Figure 5.9: Plots of two similar experiments conducted at different periods, eight months apart (the data was for a heated annulus and a degree of wall temperature uniformity of $\tau_{ha} = 0.99$)

5.6. Summary

This chapter started by presenting the results of an investigation of two different inlet configurations on the Reynolds number limits of the transition flow regime. Then a technique used to determine the lower and upper Reynolds number limits of transition flow regimes was described. The types of convection present in the different flow regimes were identified. By using the Richardson method, it was shown that the transition regime was a combination of mixed convection and pure forced convection. The laminar regime was generally mixed convection, while the turbulent regime was pure forced convection. An analysis of the proportions of the mixed to forced convections indicated that the transition was largely mixed convection.

Validation was done by comparing the friction factor and Nusselt number results of the present investigation with well-established correlations. A few data points of the present investigation were also compared with data from a similar experimental set-up. There was good agreement between the heat transfer and pressure drop measurements of the present investigation and the literature. This implied that the experimental procedure and data reduction method that were used to generate results were accurate and could be used with confidence.

In the next two chapters, the results of the effects of the degree of wall temperature uniformity and annular passage dimensions on the lower and upper Reynolds number limits of the transition regime, heat transfer coefficients and friction factors will be discussed. The correlations that predict the Nusselt numbers and the friction factors will be presented as well.

Chapter 6

Influence of the degree of wall temperature uniformity

6.1 Introduction

In the previous chapter, a method for identifying the Reynolds number limits of the transition regime was described, the spread of different convection types within the flow regimes was analysed and the experimental set-up and method were validated. In this chapter, the influence of various degrees of the inner wall temperature on the average Nusselt number, average friction factor and lower and upper Reynolds number limits of the transition regime are analysed. Only the results of test section TS 1, which had a hydraulic diameter of 26.2 mm, annular diameter ratio of 0.327 and length-to-hydraulic diameter ratio of 193 are presented in detail in this chapter. The analyses of the other test sections (TS 2, TS 3 and TS 4) are presented in Appendix B. The results comprise laminar, transition and turbulent flow regimes, but special focus is placed on the transition flow regime. Friction factor results are plotted for isothermal and diabatic wall boundary conditions, while the results of the Nusselt number are (by definition) only plotted for diabatic wall boundary conditions. For the diabatic cases, both heated and cooled conditions are presented – each for the three different longitudinal degrees of wall temperature uniformity. Also included in this chapter are newly developed correlations for the prediction of Nusselt number and friction factor in terms of the degree of wall temperature uniformity and other relevant dimensionless parameters.

6.2 Transition range limits

In this section, the lower and upper Reynolds number limits of the transition flow regime are presented for isothermal and diabatic wall conditions. Table 6.1 shows the lower (Re_1) and upper (Re_2) Reynolds number limits of the transition flow regime for the isothermal cases, as well as the heated and cooled annulus cases for the different degrees of wall temperature uniformity of the four test sections that were considered in this investigation.

Table 6.1: Reynolds number ranges based on heat transfer and flow transition for the isothermal, heated and cooled annuli for various test sections and thermal boundaries

| TS | WTU | Heat transfer transition | | | | Flow transition | | | | | |
| | | Heated annulus | | Cooled annulus | | Heated annulus | | Cooled annulus | | Isothermal | |
		Re_1	Re_2	Re_1	Re_2	Re_1	Re_2	Re_1	Re_2	Re_1	Re_2
1	0.990	790	4 900	660	6 320	1 410	4 170	1 510	5 890	890	2 950
	0.975	700	4 790	540	5 900	1 260	3 560	1 510	5 770		
	0.965	740	4 680	520	5 650	1 240	3 350	1 520	5 640		
2	0.990	600	4 170	590	5 260	1 120	3 160	1 250	4 910	850	2 710
	0.975	680	3 980	575	5 150	1 000	3 020	1 260	4 790		
	0.965	470	3 890	570	5 020	1 000	2 950	1 250	4 680		
3	0.990	550	3 990	500	5 020	1 100	3 090	1 230	4 800	830	2 620
	0.975	570	3 900	470	4 780	1 100	3 000	1 250	4 680		
	0.965	520	3 800	450	4 490	1 070	2 870	1 240	4 570		
4	0.990	490	3 470	400	3 980	1 000	2 820	1 000	3 980	800	2 500
	0.975	430	3 240	360	3 800	1 020	2 700	1 120	3 890		
	0.965	500	3 020	500	3 720	1 000	2 570	1 130	3 800		

For convenience, the transition flow ranges in terms of the Reynold number for TS 1 are represented graphically in Figure 6.1a and Figure 6.1b for the heat transfer and friction factor-based transitions, respectively.

a)

b)
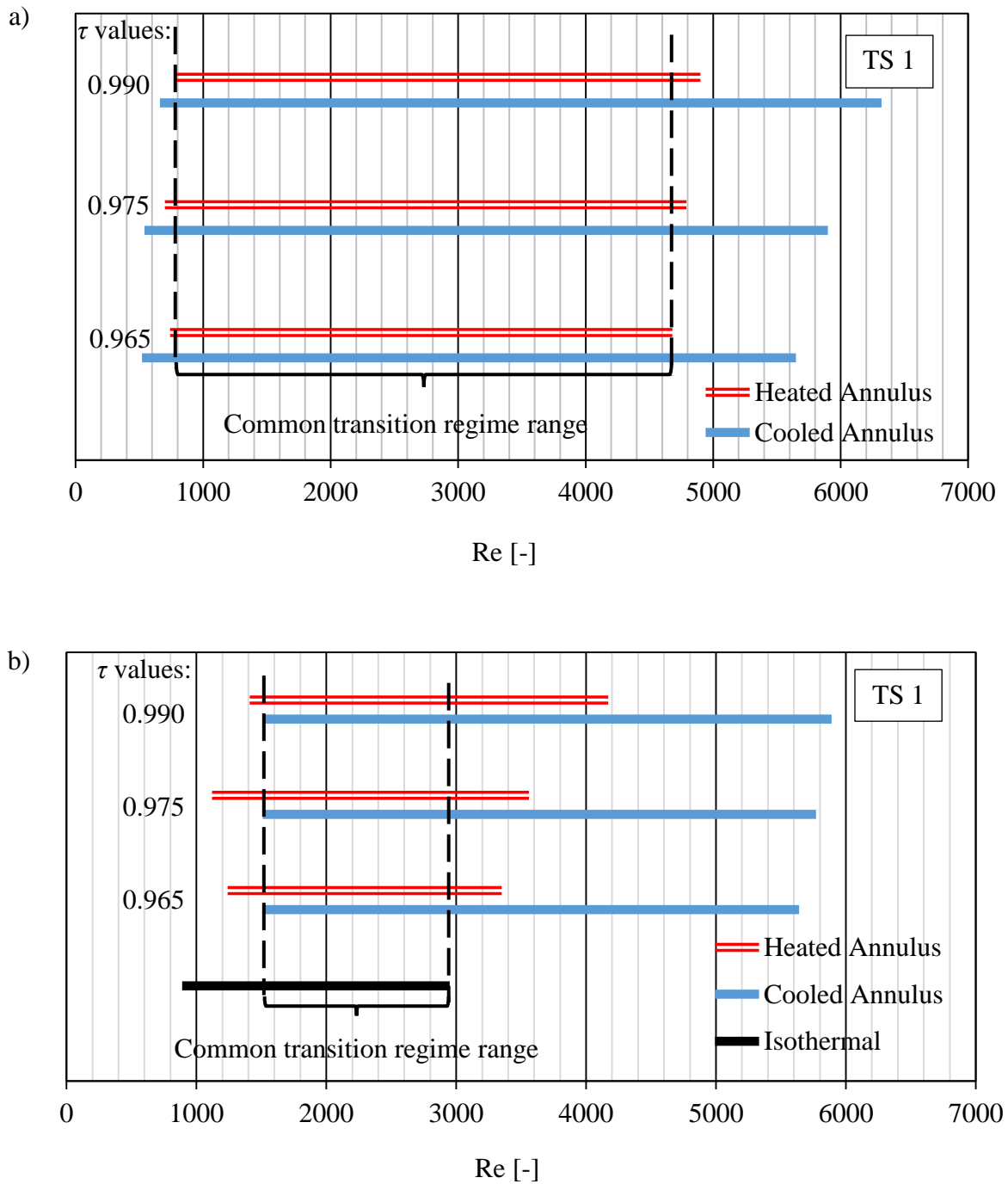
Figure 6.1: A graphic representation of transition ranges for: (a) the heat transfer coefficient; and (b) the friction factor

For all cases that were considered in this investigation, transition based on the heat transfer generally started earlier than transition based on the friction factor. This is different from that observed in circular tubes, where the transition based on the heat transfer coefficient and that based on the friction factor start and end concurrently. Other studies in the annular passage had similar observations (Monrad and Pelton, 1942; Lu and Wang, 2008a). The difference in the behaviour of the two transition regime is due to the fact that the friction factor is influenced by both the outer and inner wall surfaces, while the heat was only transferred at the inner wall surface (the outer wall being adiabatic).

It was observed for the same degree of wall temperature uniformity that the Re_1 values of the heated and cooled cases were closer to each other. However, there was a relatively significant difference in the Re_2 values. For instance, for $\tau = 0.99$, Re_1 was 660 and 790 for the cooled and heated cases respectively, while Re_2 was 4 900 and 6 320, respectively. This means that the transition Reynolds number range (Re_2 to Re_1) for cooled cases was longer than for heated cases. Similarly, this can be observed for $\tau = 0.975$ and 0.965. In Figure 5.4a, it was observed that the Richardson number values for the cooled annulus cases were relatively higher than for the heated case. Secondly, the difference between the Richardson number values for the two cases was small at the lower Reynolds number limit of transition and relatively large at the upper limit. Also, 100% of the cooled case data points in the transition regime were of a mixed-convection type, while only 60% of the heated case data points were of a mixed-convection type. Therefore, the strength of the buoyancy force was generally higher for the cooled case than for the heated case, almost the same at the lower transition regime limit and different at the upper limit. This observed behaviour of buoyancy force corresponds well with that of the Reynolds number limits of transition. Therefore this could be the reason behind the differences in the transition regime range between the cooled and heated annulus cases.

It was also observed for both the heated and cooled cases that Re_2 values were proportionate to the τ values. Higher τ values resulted in higher Re_2 values. This is also reflected in the strength of the buoyancy force as shown in Figure 5.4a. Higher τ values resulted in higher Richardson number values. This suggests that buoyancy forces were stronger at higher τ values, which could be the cause of prolonged transition. Similar characteristics were also observed for the other test sections, as shown in Appendix B.

6.3 Heat transfer coefficients

6.3.1   Nusselt number

Figure 6.2 contains the lengthwise averaged heat transfer coefficients plotted in terms of the Nusselt number with respect to the Reynolds number (both on a logarithmic scale). Figure 6.2a gives the results for a heated annulus, Figure 6.2b gives the results for a cooled annulus, and Figure 6.2c gives the combined results of Figure 6.2a and Figure 6.2b.

In the transition flow regime (refer to Figure 6.2), a definite decrease in the heat transfer coefficients was observed as the degree of wall temperature uniformity decreased. For instance, at a Reynolds number of 2 000, the Nusselt numbers of a heated annulus case for the degrees of wall temperature uniformity of $\tau = 0.975$ and $\tau = 0.965$, were 5.9% and 7.8% lower than the $\tau = 0.99$ case, respectively. This is directly linked to the temperature difference between the wall and the bulk fluid. Figure 6.3, which presents the temperature difference between the wall and the bulk fluid for a heated case at a Reynolds number of 2 000, is used to explain this point. The method that was used to obtain the bulk fluid temperature is described in section 4.2. Because it was challenging to perform all the tests at exactly the same Reynolds number interval values, the temperature differences in this figure were obtained by interpolating between the closest Reynolds number data points. Since the inlet temperatures for the hot and cold water were relatively constant, the temperature differences at the annulus's inlet side of the heat exchanger for the three wall temperatures were close to each other. At annular downstream points, an appreciable difference in the temperature differentials was observed at different τ values. Higher downstream temperature differentials were obtained at higher τ values. Such higher temperature differentials lead to a stronger buoyancy-driven flow, which results in improved fluid mixing and higher heat transfer rates. In their investigation, Ciampi et al. (1987) made a similar observation. For that reason, the dependence of the Nusselt number on τ in Figure 6.2 could have been expected.

Figure 6.2: Nusselt numbers for different degrees of wall temperature uniformity: (a) for heated annulus cases; (b) for cooled annulus cases; and (c) for all cases combined
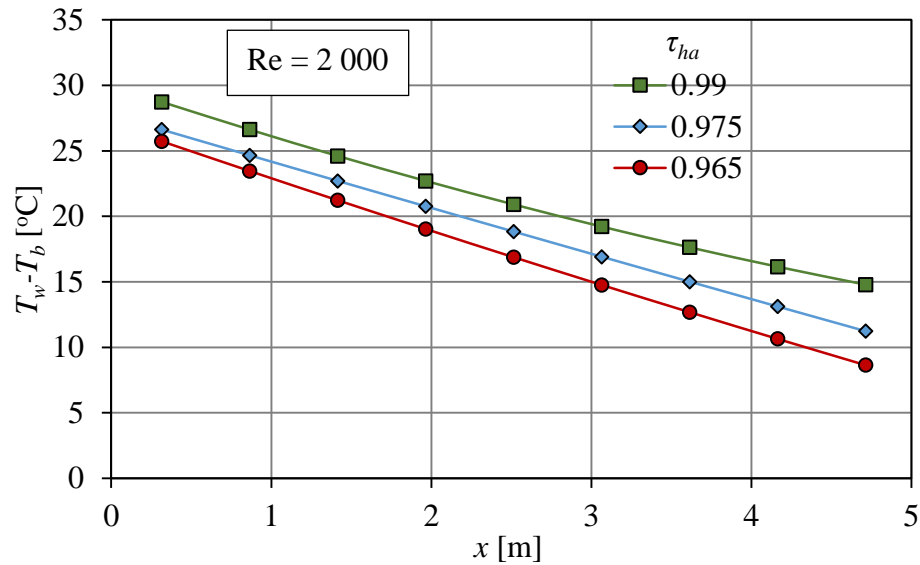
Figure 6.3: Temperature difference between the inner wall and the bulk fluid for different degrees of wall temperature uniformity

In general, all the results (shown in Figure 6.2) followed the same trend in relation to τ. On closer inspection, it was found that 95% of the data points in the transition flow regime exhibited a consistent dependency on τ, which was greater in magnitude than the experimental uncertainty. Therefore, it can be concluded that the observed variation of the Nusselt number in terms of τ is not due to measurement error.

Figure 6.2b shows that the trends for the cooled annulus cases were similar to the heated annulus cases in Figure 6.2a. The case with the highest wall temperature uniformity had the highest Nusselt numbers, followed by the rest in descending order. The gap between the cooled annulus data is closer than that for the heated annulus case. For instance, at a Reynolds number of 2 000, the average Nusselt numbers for the wall temperature uniformities of $\tau = 0.975$ and $\tau = 0.965$ were 2.3% and 4.9% lower than for the $\tau = 0.99$ case, respectively.

Similar to the observations of Van Zyl (2012) and Van Zyl et al. (2013) and Prinsloo et al. (2014), it was found that, for any given Reynolds number, the heat transfer coefficient for heated and cooled cases were different from each other. This is shown in Figure 6.2c, where the heated annulus data of Figure 6.2a is compared to the cooled data of Figure 6.2b. The results show that the Nusselt numbers for the heated cases were higher in value than those for the cooled cases. For

74

instance, at a Reynolds number of 2 000, the Nusselt numbers for heated cases at τ values of 0.99, 0.975 and 0.965 were 23%, 19% and 18% higher, respectively, than their cooled case counterparts. This is caused by the variation in the temperature differences between the bulk annular fluid temperature and the inner wall temperature of the annular passage, as well as the fluid Prandtl and Grashof numbers, which are relatively temperature sensitive.

6.3.2 Colburn j-factor

The heat transfer coefficient results are also presented in terms of the average Colburn *j*-factors in Figure 6.4. The heated annulus results are given in Figure 6.4a, the cooled annulus data is given in Figure 6.4b, and all the results combined are given in Figure 6.4a, Figure 6.4b and Figure 6.4c. The Colburn *j*-factors were found to be proportional to the τ value. Higher τ values produced higher Colburn *j*-factors. For instance, at a Reynolds number of 2 000, the Colburn *j*-factors for the heated cases at $\tau = 0.975$ and $\tau = 0.965$ were 6.5% and 10% lower than at $\tau = 0.99$, respectively. Likewise, for the cooled cases (also at a Reynolds number of 2 000), the average Colburn *j*-factor at $\tau = 0.975$ and $\tau = 0.965$ were 1.6% and 3.3% lower, respectively.

It was also observed from the results in Figure 6.4, that the Colburn *j*-factor values for a cooled annulus case were relatively closer to each other than those for a heated case. The impact of τ was therefore more severe for heated cases than for cooled cases. This could also be due to the variation in temperature differences between the annular bulk fluid and the inner wall during the heating and cooling processes. When the effect of the Prandtl number, which is dependent on the fluid viscosity, is taken into consideration, as is the case when considering the *j*-factors, the data points for the heated and cooled cases moved closer to each other (see Figure 6.4c), than was the case with the Nusselt number results in Figure 6.2c. The percentage difference between the Colburn *j*-factors of the heated and cooled annuli at a Reynolds number of 2 000, for $\tau = 0.99$, 0.975 and 0.965, were +9.5%, +4.0% and +2.2%, respectively, which were significantly smaller than the percentage differences based on the Nusselt number results in Figure 6.2c. This indicates that a large component of the observed differences in the heat transfer coefficients in the heated and cooled cases were, in fact, based on fluid property, and not necessarily based on the direction of the heat flux.
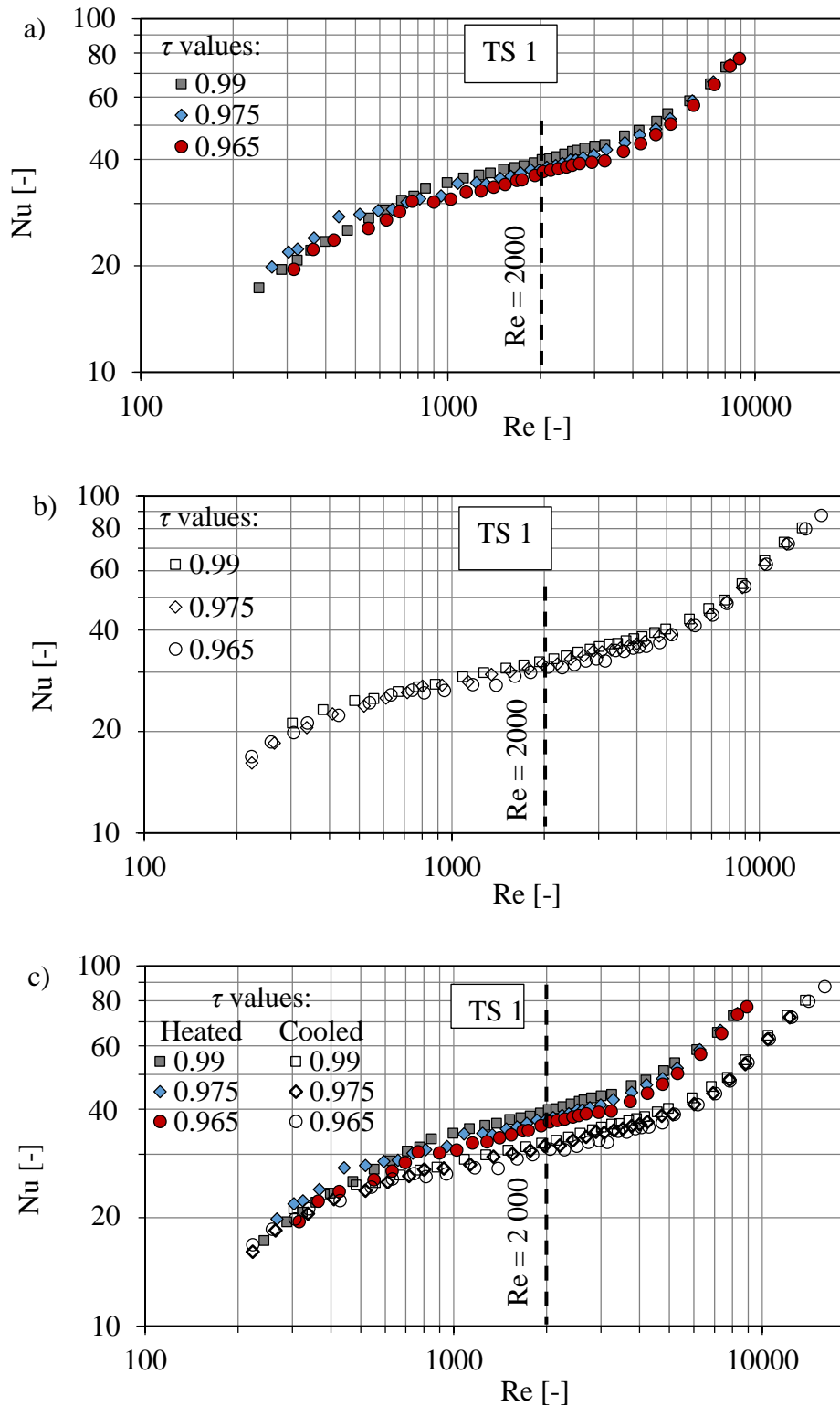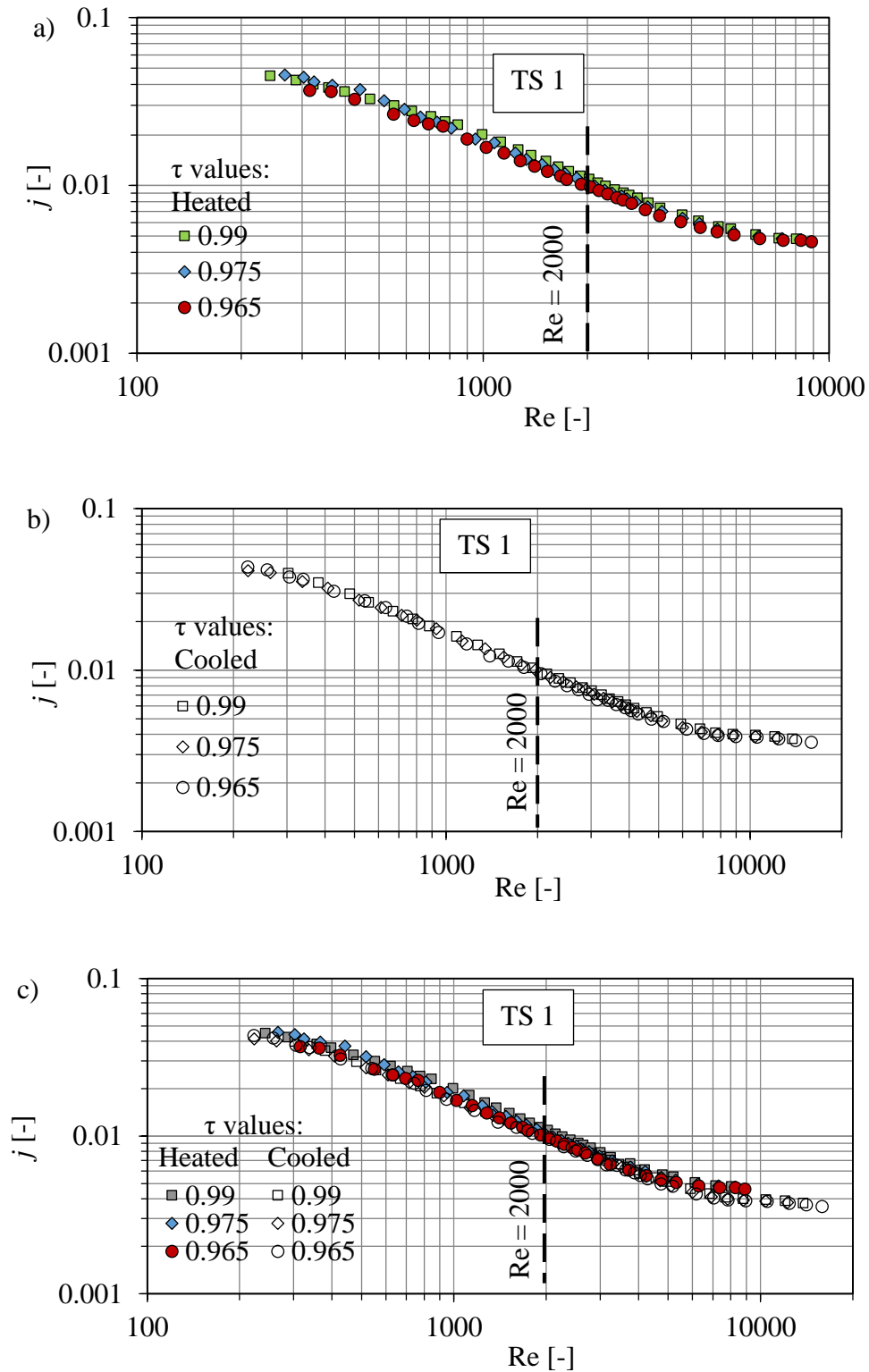
Figure 6.4: Colburn *j*-factors for different degrees of wall temperature uniformity: (a) for heated annulus cases; (b) for cooled annulus cases; and (c) for all cases combined

However, Figure 6.4c shows that the Colburn *j*-factor in the transition regime of the cooled annulus and heated annulus did not fall exactly on one line, as is often the case in fully forced convection turbulent cases (Van Zyl*,* 2012; Van Zyl et al., 2013). This could be due to the presence of secondary flows. It was also noted that, as the degree of wall temperature uniformity decreased, the Colburn *j*-factors for the heated and cooled annulus case types moved much closer together. This could be due to the decrease in the strength of the buoyancy force on the flow as the temperature difference between the inner wall and the bulk fluid decreased, as observed in Figure 5.4a.

6.4 Friction factors

The friction factor results are plotted in Figure 6.5. The heated annulus results are given in Figure 6.5a, the cooled annulus results are given in Figure 6.5b, and all the results of Figure 6.5a and Figure 6.5b are combined in Figure 6.5c. The isothermal friction factor plot is also included for reference purposes.

In the laminar and transition flow regimes, friction factors were higher for the higher τ values, but in the turbulent flow regime, such variations were insignificant. At a Reynolds number of 2 000, the average friction factor for the heated case for τ values of 0.99, 0.975 and 0.965 were 72%, 34% and 24% higher than for the isothermal friction factor case, respectively, while for the cooled annulus case, the average friction factor for τ values of 0.99, 0.975 and 0.965 were 172%, 159% and 153% higher than the isothermal friction factor case, respectively. As was also observed for the Nusselt number and Colburn *j*-factor, the friction factor data between the different cases of τ values is closer to each other in the cooled annulus cases than in the heated annulus cases.
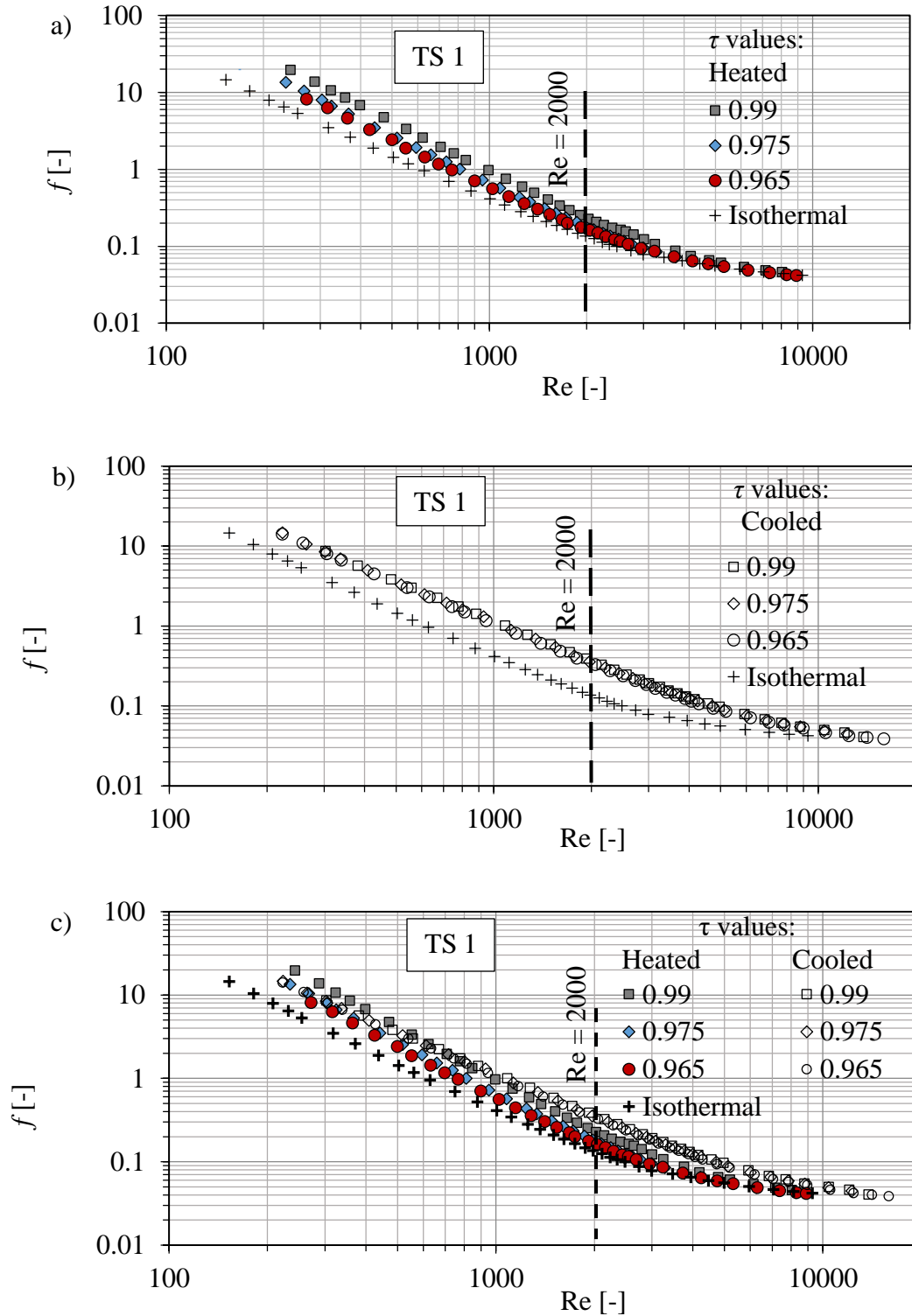
Figure 6.5: Friction factors for different degrees of wall temperature uniformity: (a) for heated annulus cases; (b) for cooled annulus cases; and (c) for all cases combined

This phenomenon could be caused by various factors, including the different values of viscosity on the inner wall as determined by different wall temperature uniformities. For instance, when considering a cooling case (with hot water in the annulus and cold water in the inner tube), a higher value of τ would mean a lower average temperature on the inner wall of the annulus, which would result in higher wall fluid viscosity and higher shear forces on the wall. This would increase the perceived friction factor. As an example, by considering Re = 2000 for a forced convection cooled annulus case, the increases in friction factor based on its dependence on the fluid viscosity and radial velocity gradient, $\mu(dv/dr)$ would be approximately 51%, 42%, and 35% above the isothermal friction factor. As these values are much lower than the increases in the experimental friction factors mentioned earlier, it can be concluded that the increase in friction factors is partly due to the secondary flow in the annulus. The higher the temperature difference between the annulus wall and the bulk fluid temperature, the higher the buoyancy forces and the cooler the annular fluid. This eventually results in higher wall fluid viscosity and friction factors. Figure 6.6 illustrates this phenomenon for a cooled annulus case of TS 1 and $\tau = 0.99$ in the transition Reynolds number range of 1 400 to 3 200.
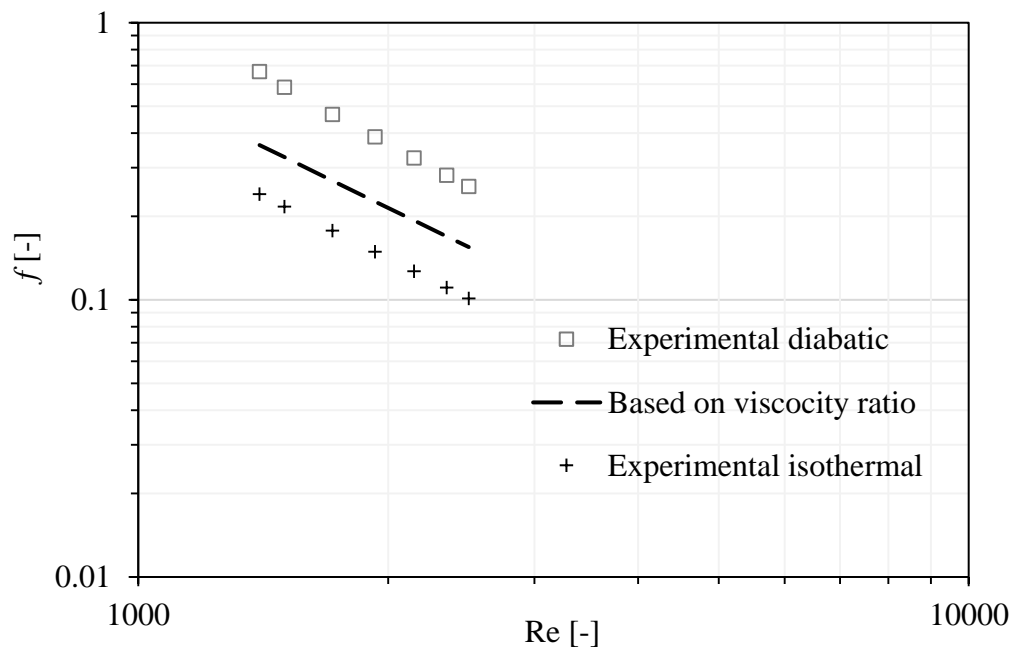
Figure 6.6: Friction factor values for adiabatic and diabatic experimental cases and for forced convection based on the viscosity ratio

In a similar fashion, for a heated case, a reduction in the friction factor would be expected if it was only dependent on viscosity, but in this investigation, these friction factors were found to also increase with an increase in the degree of wall temperature uniformity. Therefore, the presence of buoyancy-induced secondary flow is believed to be the cause of the increased friction factor.

6.5 Development of new correlations to account for the thermal boundary condition

6.5.1   Nusselt number correlation

In cases with internal mixed convection, the heat transfer coefficient depends on the Grashof number, Prandtl number, Reynolds number and the physical properties of the fluid, as well as the geometry of the conduit (Mohammed et al., 2010; Hattori, 1979; Ghajar and Madon, 1997). In this chapter, only one flow passage geometry of TS 1 is considered. The intention is to first correlate the impact of the degree of wall temperature uniformity specifically, before attempting to include geometric influences, which will be dealt with in Chapter 7.

Unlike circular tubes, where transition is metastable and complicated, as explained by Zhipeng (2012), the flow regime transition in the annular passage is more orderly. This conclusion can be drawn judging by the linear appearance of the transition flow regime of the Nusselt number, *j*-factor and friction factor versus the Reynolds number relationships (using logarithmic scales), for instance, in Figure 6.2, Figure 6.4 and Figure 6.5. Mohammed et al. (2010) used Equation 6.1 to develop correlations associated with mixed convection.

$$\mathrm{Nu} = C\left(\frac{\mathrm{Gr\,Pr}}{\mathrm{Re}}\right)^{n} \qquad\qquad (6.1)$$

In this study, Equation 6.1 has been modified to consider different degrees of wall temperature uniformity and is of the following form:

$$\mathbf{Nu} = \left[C\tau^{p}\right]_{ha/ca} \qquad\qquad (6.2)$$

where

$$C = B_1 \left(\frac{\text{Gr Pr}}{\text{Re}} \right)^{z_1} \tag{6.3}$$

and

$$p = B_2 \left(\frac{\text{Gr Pr}}{\text{Re}} \right)^{z_2} \tag{6.4}$$

A common transition flow regime range for the three wall temperature boundaries, as shown in Figure 6.1a, was used for the purposes of deriving the new correlations. The maximum value of all the lower Reynolds number limits and the minimum value of all the upper Reynolds number limits were considered as the lower and upper limits of the common transition regime range, respectively. The values of the Grashof number, the Prandtl number and the Reynolds number were found for each test data for all the three wall temperature boundaries. These were then plotted against experimental Nusselt numbers as shown in Figure 6.7.
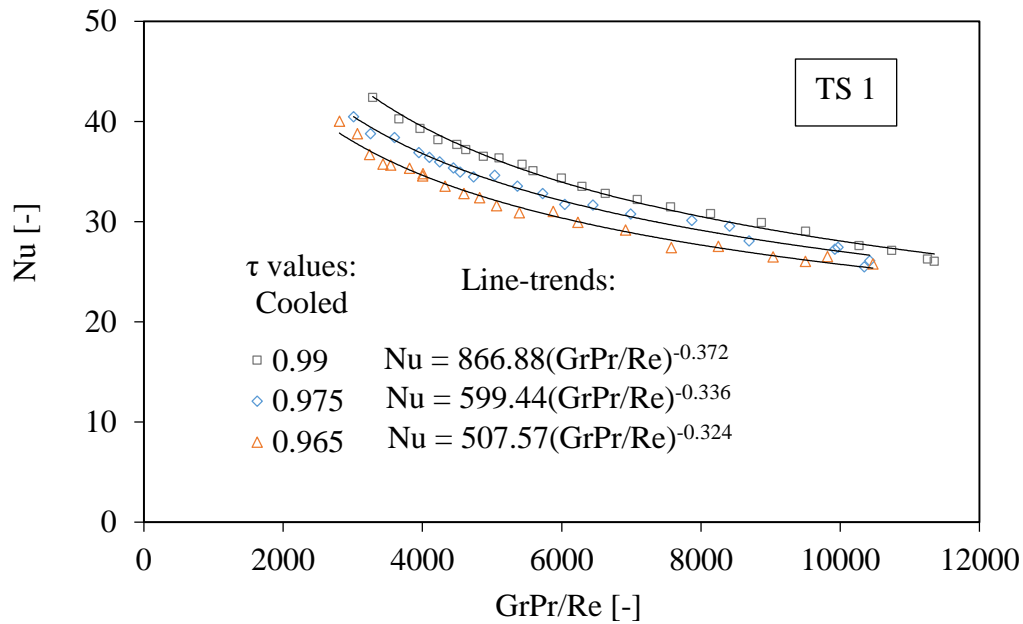
Figure 6.7: Plots of experimental Nusselt numbers against Grashof, Prandtl and Reynolds numbers for different values of τ

Line fits of power form were then used to get equations that best describes the relationships between the Nusselt numbers and the Grashof, Prandtl and Reynolds parameters for each case. The equations are shown in Figure 6.7 and are arranged in the same order as the wall temperature

boundary cases. A relationship between the constant *C* and the Grashof, Prandtl and Reynolds numbers, as well as between the power index *p* and the Grashof, Prandtl and Reynolds numbers, was then established, as shown in Figure 6.8a and Figure 6.8b, respectively.

a)

TS 1

$$C = 1058(GrPr/Re)^{-0.389}$$

b)

TS 1

$$p = 173(GrPr/Re)^{-0.421}$$
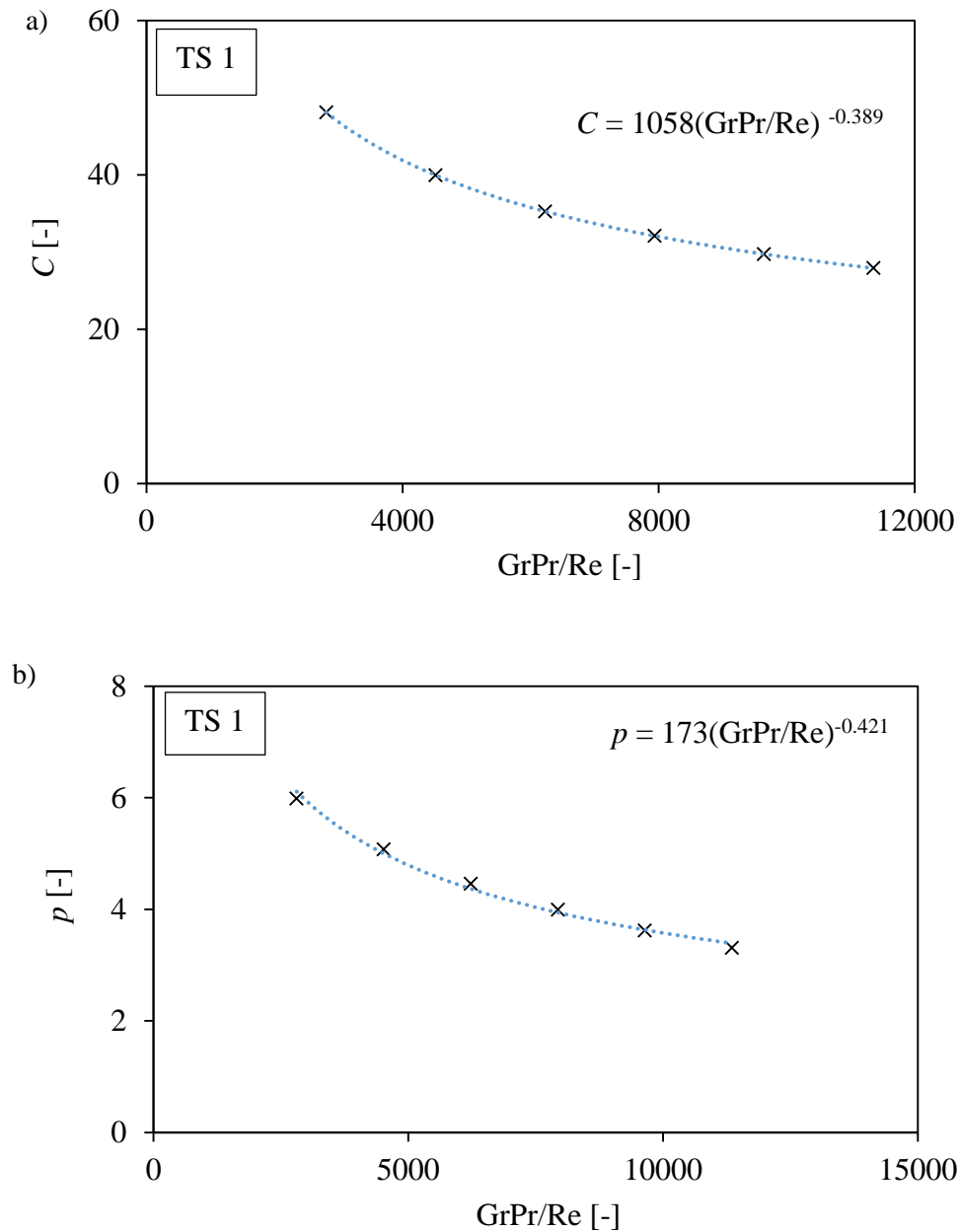
Figure 6.8: Relationships between the Grashof, Prandtl and Reynolds numbers and: (a) parameter C; and (b) exponent *p*

Suitable expressions for the constants and exponents for Equation 6.3 and Equation 6.4 can be written as follows:

For heated annuli:

$$C_{ha} = 260\left(\frac{Gr\,Pr}{Re}\right)^{-0.217} \tag{6.5}$$

$$p_{ha} = 0.29\left(\frac{Gr\,Pr}{Re}\right)^{0.107} \tag{6.6}$$

For cooled annuli:

$$C_{ca} = 1.058\times10^{3}\left(\frac{Gr\,Pr}{Re}\right)^{-0.389} \tag{6.7}$$

$$p_{ca} = 173\left(\frac{Gr\,Pr}{Re}\right)^{-0.421} \tag{6.8}$$

The ranges of applicability for these equations are $800 \leq Re \leq 4\,700$, $4.8 \leq Pr \leq 6.6$, $1.1 \times 10^3 \leq GrPr/Re \leq 10.2 \times 10^3$ and $0.965 \leq \tau \leq 0.990$ for heated annuli and $650 \leq Re \leq 5\,700$, $3.7 \leq Pr \leq 4.8$, $2.8 \times 10^3 \leq GrPr/Re \leq 11.5 \times 10^3$ and $0.965 \leq \tau \leq 0.990$ for cooled annuli.

Figure 6.9 shows the comparison between the experimental results and the predicted Nusselt number for heated and cooled annulus cases. The agreement between the experimental results and the proposed correlations was good, with all the data points for both heated and cooled annulus cases being predicted within a ±4% error band. The correlations for the other test sections (TS 2, TS 3 and TS 4) are presented in Appendix B.
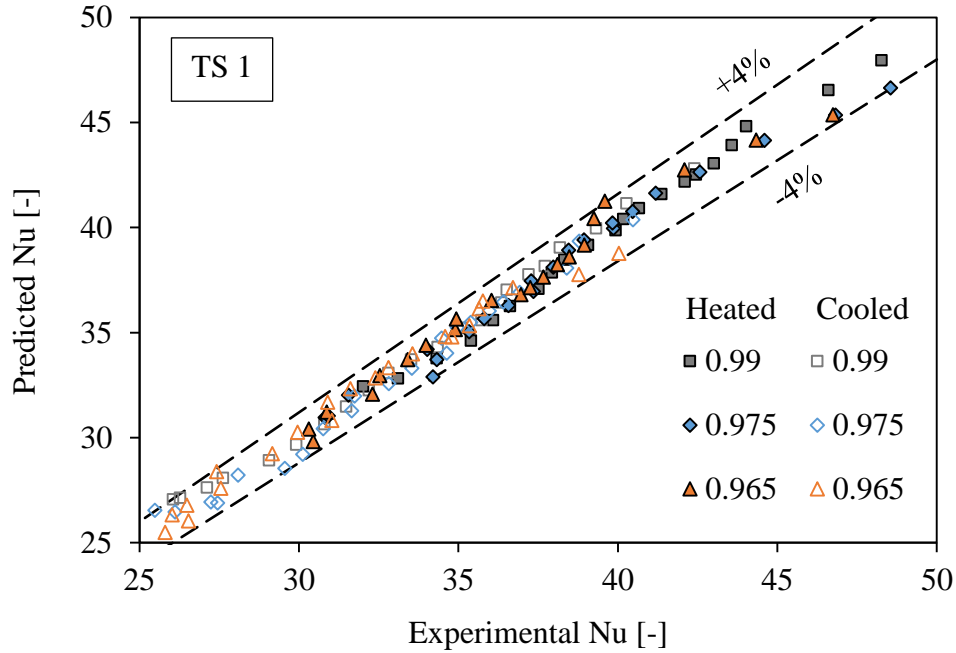
Figure 6.9: Comparison between the results of the experimental and predicted Nusselt numbers

6.5.2   Friction factor correlation

As with the Nusselt number correlation, a common transition regime range for the isothermal case and three wall temperature boundaries of TS 1, as shown in Figure 6.1b, was used for the purposes of deriving the correlations. The maximum value of all the lower Reynolds number limits and the minimum value of all the upper Reynolds number limits were considered as the lower and upper limits of the common transition regime range, respectively.

It was mentioned that the isothermal pressure drop was included in this investigation for referencing purposes. Therefore, its correlation was developed first. The diabatic cases were then developed based on the isothermal correlation. The best line fit in the transition regime of the isothermal friction factor plot was a power form line and is presented in Equation 6.9. This equation represents all the experimental data to within ±5% for $1\,400 \le Re \le 3\,200$.

$$f_{iso} = 7383 Re^{-1.434} \tag{6.9}$$

Since the degree of the wall temperature uniformity affected the friction factors, the correlation for the diabatic transition regime was also developed in terms of the wall temperature uniformity value. Based on the form of the reference Equation 6.9, diabatic correlations were developed in terms of the viscosity ratio (viscosity of the bulk fluid divided by the viscosity of the fluid on the annulus wall), and the wall temperature uniformity value to account for the heat transfer effects. The proposed correlation is of the following form:

$$f_d = f_{iso} C \left(\frac{\mu_b}{\mu_{iw}} \right) \tau^p \tag{6.10}$$

The method for deducing constant C and exponent p is similar to that explained for the Nusselt number correlation. It was shown in Figure 6.6 that friction factor values were much higher than when they were based on their dependence on the fluid viscosity and radial velocity gradient, $\mu(dv/dr)$. This was attributed to the presence of buoyancy force. The dependency of the friction factor on the buoyancy force is taken into account by the Grashof number and the Prandtl number in the constant, C, and the exponent, p, in the following form:

$$C = B_1 \left(Gr^u \, Pr^v \right)^{z_3} \tag{6.11}$$

$$p = B_2 \left(Gr^u \, Pr^v \right) + B_3 \tag{6.12}$$

Suitable expressions for the constants and exponents for Equation 6.11 and Equation 6.12 can be written as follows:

For heated annuli:

$$C = 19.08 \times 10^3 \left(Gr^{0.07} \, Pr^{1.12} \right)^{-3.32} \tag{6.13}$$

$$p = -0.41 \left(Gr^{0.07} \, Pr^{1.12} \right) + 0.88 \tag{6.14}$$

For cooled annuli:

$$C = 0.84 \left(\mathrm{Gr}^{0.07} \, \mathrm{Pr}^{1.12} \right)^{-0.61} \tag{6.15}$$

$$p = -1.1 \left(\mathrm{Gr}^{0.07} \, \mathrm{Pr}^{1.12} \right) + 20 \tag{6.16}$$

The ranges of applicability for these equations are $1\,500 \leq \mathrm{Re} \leq 3\,000$, $18.1 \leq \mathrm{Gr}^u \, \mathrm{Pr}^v \leq 20.8$, $1.38 \leq \mu_b/\mu_{iw} \leq 1.54$ and $0.990 \leq \tau \leq 0.965$ for heated annuli and $1\,500 \leq \mathrm{Re} \leq 3\,000$, $12.95 \leq \mathrm{Gr}^u$ $\mathrm{Pr}^v \leq 14.7$, $0.63 \leq \mu_b/\mu_{iw} \leq 0.75$ and $0.990 \leq \tau \leq 0.965$ for cooled annuli.

Figure 6.10 shows the comparison between the experimental and predicted friction factor for heated and cooled annulus cases. The agreement between the experimental results and proposed correlations was good, with all the data points within a ±6% error band for both the heated and cooled cases. The correlations for the other test sections (TS 2, TS 3 and TS 4) are presented in Appendix B.
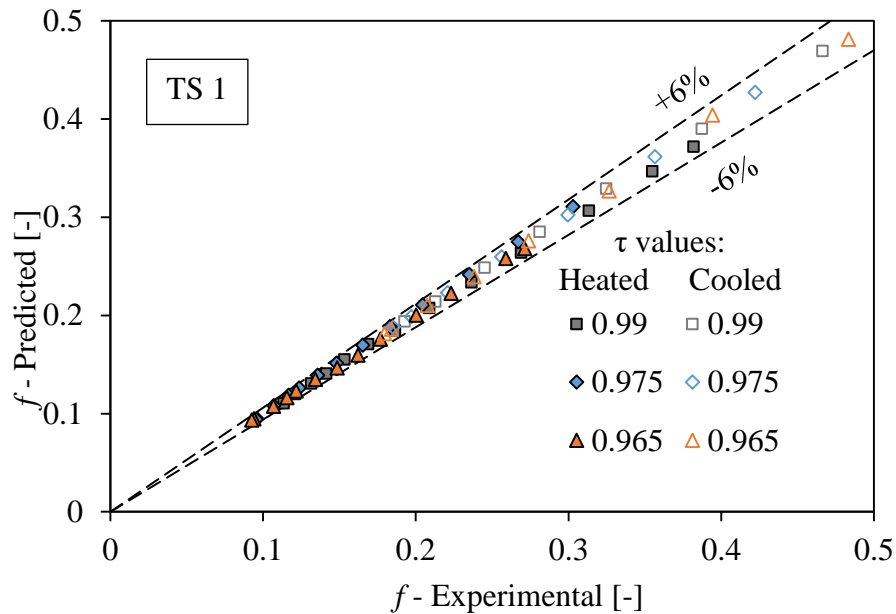
Figure 6.10: Comparison between the results of the experimental and predicted adiabatic friction factor

6.6 Summary

Heat transfer characteristics in a concentric horizontal annular passage (TS 1) were experimentally investigated for developing flow associated with secondary flows in water. The annular diameter ratio for TS 1 was 0.327 and its hydraulic diameter was 26.2 mm. The averaged inlet temperatures for hot and cold water were approximately 50 °C and 19 °C, respectively. The inner surface of the annular passage had non-uniform longitudinal wall temperature profiles that were expressed in terms of a degree of wall temperature uniformity, while the outer wall was isothermal. Heated and cooled annulus cases were investigated in all the heat transfer and fluid flow regimes, but special attention was given to the transition flow regime.

For both heated and cooled annulus cases, heat transfer coefficients in terms of the Nusselt number were found to be directly proportional to the degree of wall temperature uniformity. Cases with high degrees of wall temperature uniformity had higher Nusselt numbers than those with a lower degrees of wall temperature uniformity. Nusselt numbers for heated annulus cases were higher than those for cooled annulus cases and can be attributed to the temperature-dependent bulk fluid properties of the fluid. The heat transfer transitions for different wall temperature uniformity heated annulus cases started almost at the same Reynolds number, but ended at a different Reynolds number.

Friction factors for diabatic cases were higher than for isothermal case in the laminar and transition flow regimes. Furthermore, friction factors for cooled annulus cases were higher than for the heated annulus cases. No significant difference in friction factor values was observed in the turbulent flow regime for all the case types. The friction factors for diabatic cases were also found to be directly proportional to the degree of wall temperature uniformity in the transition flow regime. Another important observation was that the flow regime transition based on the Nusselt number started earlier than the transition based on the friction factor.

New correlations for the Nusselt number and friction factor in the transition flow regime were developed to account for the impact of the thermal boundary condition. For TS1, the Nusselt number correlation predicts all the experimental data within a ±4% error band, while the friction factor correlation predicts all data points within a ±6% error band for both the heated and cooled annulus cases.

This chapter only reported on experimental data produced for a single test section (TS 1). Since mixed-convection flow fields are dependent on the geometrical proportions of the flow passage, the next chapter will report on the impact the diameter ratio and hydraulic diameter will have on the transition flow regime behaviour.

Chapter 7

Influence of annular passage dimensions

7.1 Introduction

In the previous chapter, only experimental data produced for a single test section (TS 1) was reported. Special interest was on the effect the degree of wall temperature uniformity had on the lower and upper Reynolds number limits of the transition flow regime, the heat transfer coefficient and the friction factor. In this chapter, the effects of the annular gap size on the lower and upper Reynolds number limits of the transition flow regime, the heat transfer coefficient and the friction factor are analysed. Only the results of the approximately UWT boundary condition ($\tau = 0.990$) are presented in this chapter. The analyses of other degrees of wall temperature uniformity ($\tau = 0.975$ and $\tau = 0.965$) are presented in Appendix C. The results comprise laminar, transition and turbulent flow regimes, but special focus is placed on the transition regime. The results of the friction factor are plotted for isothermal and diabatic wall conditions, while the results of the Nusselt number are, by definition, only plotted for diabatic wall cases. For the diabatic cases, both heated and cooled conditions are presented for each of the four test sections, TS 1, TS 2, TS 3 and TS 4.

Also included in this chapter are the new correlations developed for the prediction of the Nusselt number and friction factor, which take into account the annular gap size and other relevant dimensionless parameters. After that, a new comprehensive correlation, which considers both the annular gap size and the degree of wall temperature uniformity, was also developed.

7.2 Transition range limits

The method that was used to trace out the lower and upper Reynolds number limits of the transition flow regime (Re_1 and Re_2, respectively) has already been discussed in Chapter 5 and the Reynolds number limits were presented for all the test sections in Table 6.1. For convenience, the Reynolds number transition ranges for the four test sections are represented graphically in Figure 7.1a and Figure 7.1b based on the heat transfer coefficient and the friction factor, respectively.
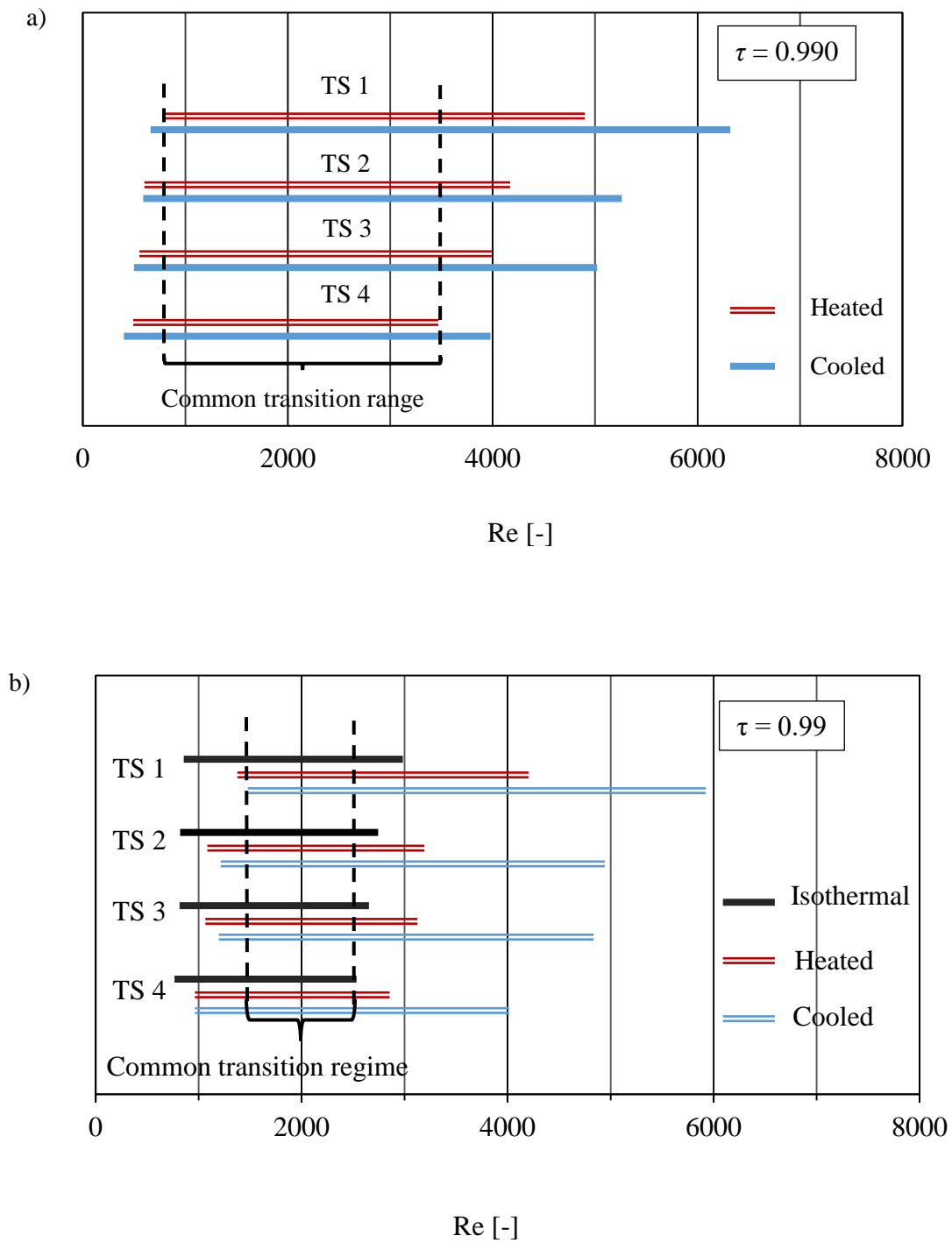
Figure 7.1: A graphic representation of the transition ranges for: (a) heat transfer; and (b) friction factor

As explained in Chapter 6, for all cases considered in this investigation, transition based on the heat transfer coefficient generally started earlier than for fluid flow. This differs from the characteristics of transition in circular tubes where both types of transition occur within the same Reynolds numbers limits.

In all the cases considered, the Re_1 values (based on either the heat transfer coefficient or the friction factor) were higher for TS 1, followed by TS 2, TS 3 and TS 4, consecutively. This trend relates linearly to the hydraulic diameters of these test sections (the larger the hydraulic diameter, the higher the Re_1 value). Similarly, Re_2 was also higher for the test section with larger hydraulic diameters. The difference in the lower Reynolds number limits among the test sections was very small when compared with the upper limits. As a result, the Reynolds number spans of the transition flow regimes (Re_2 to Re_1) were also found to be related to the hydraulic diameters. Larger hydraulic diameters exhibited larger spans and smaller hydraulic diameter exhibited smaller spans.

It was also observed that the Re_1 value based on the friction factor was lowest for isothermal cases, followed by heated cases, and finally cooled cases, which exhibited the largest Re_1 values. The Re_2 to Re_1 ranges for cooled cases were the largest, followed by the heated cases. For isothermal cases, these ranges were the smallest.

By considering, for instance, the friction factor data, the differences in the Re_1 and Re_2 values obtained from the different test sections for the isothermal cases could be due to the changes in annular dimensions. In the diabatic cases, apart from the annular dimensions, changes in the heat transfer coefficient and friction factor values could also be due to a variation in temperature differences between the annular fluid and the inner wall of the annular passage, as well as the fluid viscosity, which is relatively temperature sensitive.

As the annular gap size (hydraulic diameter) and/or heat transfer direction changes, the temperature difference between the annular fluid and the inner wall of the annular passage changes as well. Representative temperature difference profiles for the four test sections that were considered are shown in Figure 7.2 at a Reynolds number value of 2 000 for a heated annulus case. A Reynolds number value of 2 000 was selected because it falls in the middle of the transition range. Buoyancy-driven flow is expected to be stronger at higher temperature differences between

the wall and the bulk fluid than at lower temperature differences, as shown in Figure 5.4b. This could affect the lower and upper Reynolds number of the transition regime.
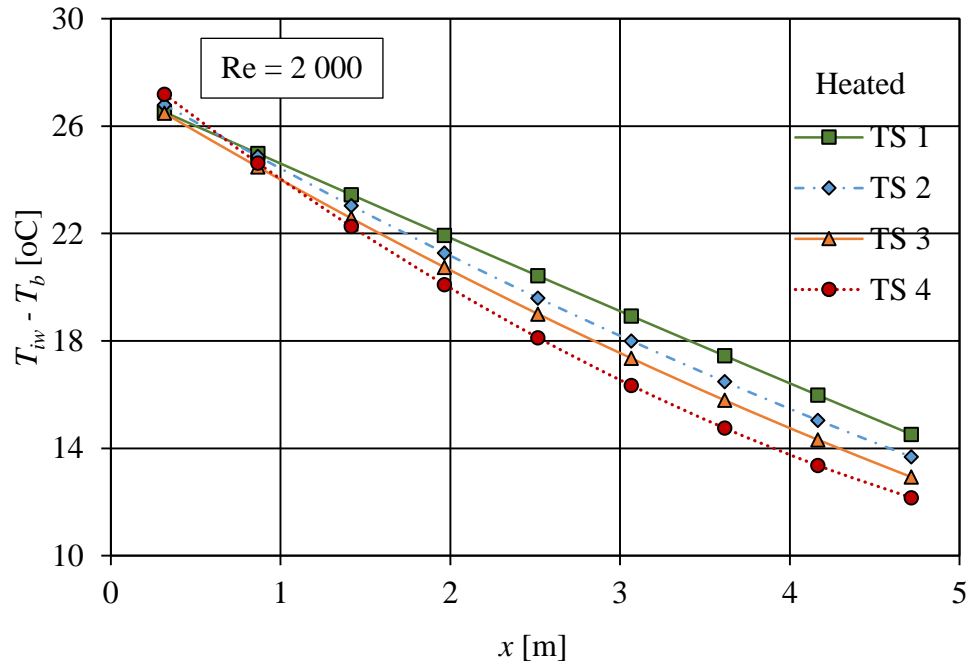
Figure 7.2: Temperature difference between the inner wall and the bulk fluid for different test sections

7.3 Heat transfer coefficients

7.3.1   Nusselt number

The experimental averaged Nusselt numbers for all the test sections are shown in Figure 7.3, based on the Reynolds number. Both the Nusselt and Reynolds numbers are plotted on logarithmic axes. The results, which include all regimes from the laminar to the turbulent, are presented for both heated and cooled cases together.
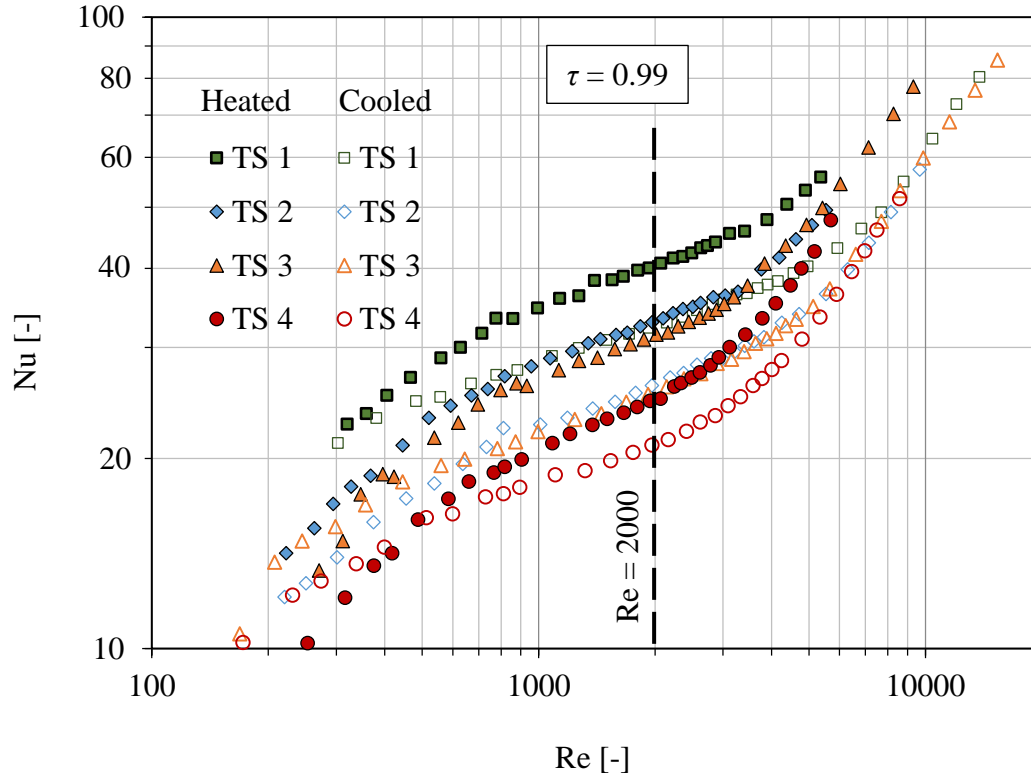
Figure 7.3: Nusselt numbers for different annular diameter ratios for heated and cooled annulus cases

In the transition flow regime, significant differences in the Nusselt numbers were observed among different test sections. TS 1 had the highest Nusselt numbers, followed by TS 2, TS 3 and TS 4. For instance, at a Reynolds number of 2 000, the Nusselt numbers of the heated annulus for TS 2, TS 3 and TS 4 were 16%, 20% and 37% lower than for TS 1, respectively. These differences are directly proportional to the hydraulic diameter of the test sections, even though the hydraulic diameter is already included in the definition of the Nusselt number. Similarly, for the cooled annulus case, the Nusselt number values of TS 2, TS 3 and TS 4 were 17%, 20% and 34% lower than for TS 1, respectively. As was observed in Figure 5.4b concerning types of convections and in Table 5.1 concerning the size of mixed convection in the transition regime, TS 1 had a stronger buoyancy force. Buoyancy forces cause secondary flows, which result in better fluid mixing and higher Nusselt numbers. This phenomenon decreased with hydraulic diameter size.

A comparison between heated and cooled annulus cases for the individual test sections shows that, at any given Reynolds number in the transition flow regime, the Nusselt number for the heated annulus was higher than for the cooled annulus. An analysis of the Nusselt numbers for TS 1, TS 2, TS 3 and TS 4 at a Reynolds number of 2 000 shows that the heat transfer coefficients for the heated annulus cases were higher by 24%, 26%, 23% and 18% than for the cooled annulus cases, respectively. Similar observations were made in Prinsloo et al. (2014) and Van Zyl et al. (2013). This is caused by the variation of the temperature differences between the bulk annular fluid temperature and the inner wall temperature of the annular passage, as well as the fluid Prandtl and Grashof numbers.

7.3.2   Colburn j-factor

The heat transfer results were also presented in terms of an average Colburn *j*-factor. Figure 7.4 shows the averaged Colburn *j*-factors for heated and cooled cases plotted against the Reynolds number on a logarithmic axis. As the case with Nusselt numbers, the *j*-factors are highest for TS 1 followed by TS 2, TS 3 and TS 4. The Colburn *j*-factors were found to be more dependent on the hydraulic diameter. TS 1, with a larger hydraulic diameter, produced higher values of the Colburn *j*-factor. A comparison at a Reynolds number of 2 000 of the Colburn *j*-factors for TS 1 against the other test sections shows that, for TS 2, TS 3 and TS 4, the *j*-factors were 18%, 22% and 38% lower than for TS 1 for the heated annulus case, respectively. For cooled cases, TS 2, TS 3 and TS 4 were 18%, 21% and 35% lower than for TS 1, respectively. It is observed that the comparisons between TS 1 and the other test section for the Nusselt number and the Colburn *j*-factor results are similar. The small differences could be due to measurement uncertainties. This should be expected since both the heat transfer results are obtained from the same test sections and wall temperature boundary conditions.
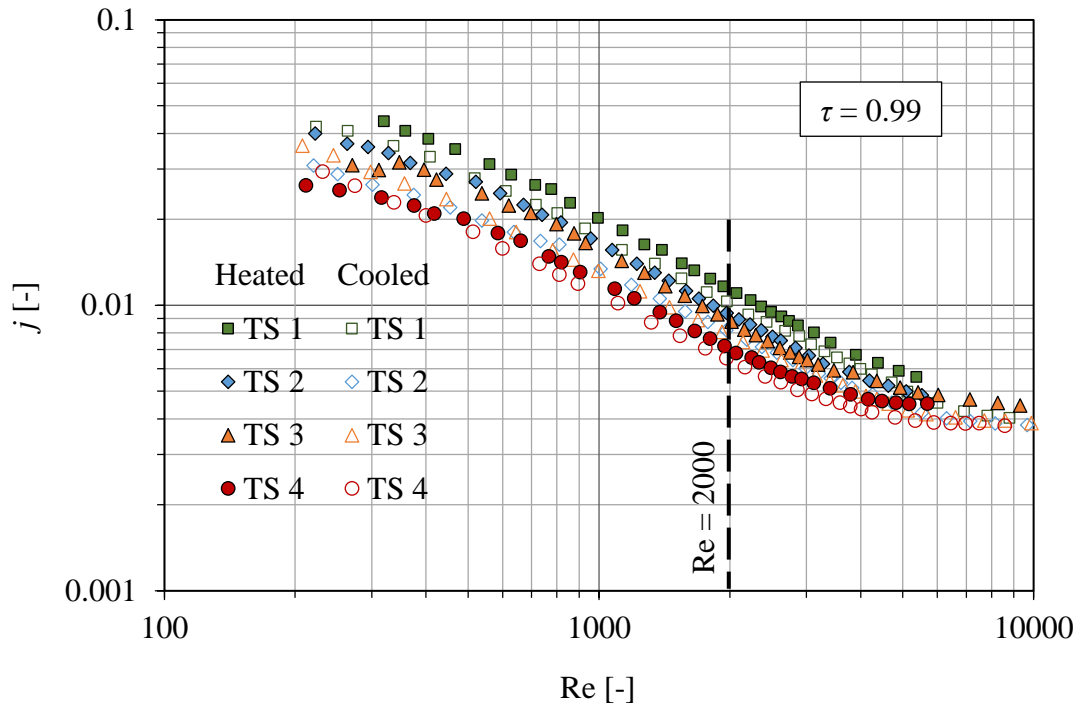
Figure 7.4: Colburn *j*-factor values for the different annular diameter ratios for the heated and cooled annulus cases

A comparison of the Colburn *j*-factors between the heated and the cooled cases, for individual test sections, shows that the Colburn *j*-factors were relatively closer to each other than was the case with the Nusselt number results. The percentage difference between the Colburn *j*-factors of the heated and cooled annuli at a Reynolds number of 2 000 for TS 1, TS 2, TS 3 and TS 4 was 11%, 15%, 12% and 9%, respectively. These were smaller than the percentage differences based on the Nusselt number results, which were 24%, 26%, 23% and 18% for TS 1, TS 2, TS 3 and TS 4, respectively. As mentioned, this indicates that a large component of the observed differences in the heated and cooled case heat transfer coefficients was, in fact, based on fluid property, and not necessarily on the direction of the heat flux.

However, it was observed in Figure 7.4 that the Colburn *j*-factors did not collapse completely as is often the case in fully forced convection turbulent cases (Prinsloo et al., 2014; Van Zyl et al., 2013). For lower degrees of wall temperature uniformity, the comparison of Colburn *j*-factors between the heated and cooled annulus cases for TS 1, TS 2, TS 3 and TS 4 was +4%, +4%, +3%

and +3% for $\tau = 0.975$ and +2.23%, 1.77%, +0.32% and -1.61% for $\tau = 0.965$ (see Appendix C). It is observed that the smaller the degree of wall temperature uniformity, the closer the Colburn *j*-factor values of the heated and cooled annulus cases to each other. This could mean that the relative magnitude effect of the Grashof number in the presence of mixed convection, as observed earlier by the Richardson number analysis, was responsible for this occurrence.

7.4 Friction factors

The friction factors for the isothermal cases of the four heat exchangers are plotted with respect to the Reynolds number on logarithmic axes in Figure 7.5a, while the friction factors for the heated and cooled cases are presented together in Figure 7.5b. In Figure 7.5a, TS 1 has higher friction factors, followed by TS 2, TS 3 and TS 4. In this analysis, the friction factors were also found to be more dependent on the hydraulic diameter. The bigger the annular gap, the higher the friction factor.

A comparison at a Reynolds number of 2 000 of the friction factors (adiabatic case) for TS 1 against the friction factors for the other test sections shows that TS 2, TS 3 and TS 4 had friction factors that were 26%, 31% and 40% lower than for TS 1, respectively. When heat transfer is introduced in the flow, shown in Figure 7.5b, the friction factors remain higher for TS 1 for both the heated and cooled annulus cases. For a heated case, the friction factors of TS 2, TS 3 and TS 4 at Reynolds number of 2 000 were 42%, 43% and 56% lower than for TS 1, respectively. For cooled cases, the friction factors of TS 2, TS 3 and TS 4 were 43%, 51% and 62% lower than for TS 1, respectively. The friction factors for the cooled cases were higher than for the heated cases in all the test sections. Again, at a Reynolds number of 2 000, the cooled annulus case friction factors for TS 1, TS 2, TS 3 and TS 4 were 65%, 60%, 48% and 40% higher than their counterparts for the heated annulus case, respectively. The difference in the friction factors between the isothermal and diabatic cases and also between the cooled and the heated annulus cases for a particular test section could be due to various factors, including the different geometrical dimensions of the annular passages and the viscosity values on the inner wall of the annulus, as determined by wall temperature.

a)

b)
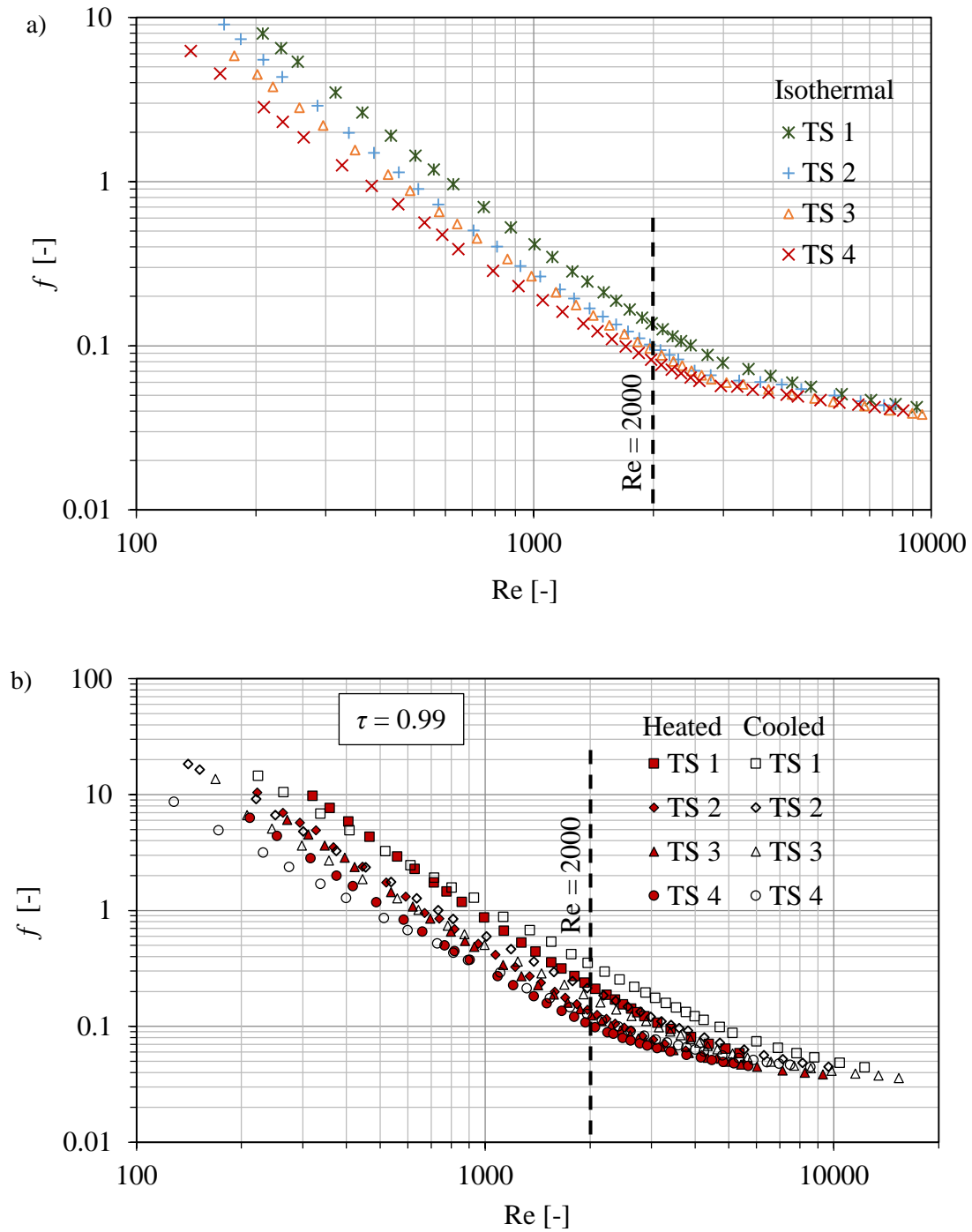
Figure 7.5: Friction factors for different annular diameter ratio values: (a) for the isothermal case; and (b) for the heated and cooled annulus cases

A comparison of the friction factors between the cooled and the isothermal cases for each test section (also at a Reynolds number of 2000) shows that the friction factors for the cooled cases were higher than for the isothermal cases. The friction factors for TS 1, TS 2, TS 3 and TS 4 were 172%, 108%, 94% and 72% higher than for their adiabatic (isothermal) values, respectively. However, the increases in friction factor for forced convection, based on its dependence on the fluid viscosity and radial velocity gradient, $\mu(dv/dr)$, would be approximately 51% above the isothermal friction factor. As discussed in the previous chapter, this value is much lower than the increases in the experimental friction factors mentioned earlier. It can thus be concluded that the increase in friction factors is partly due to the secondary flow in the annulus.

7.5 Development of new correlations to account for the annular dimensions

7.5.1.   Introduction

In this section, correlations for the prediction of the Nusselt numbers and the friction factors in the transition flow regime of an annular passage are proposed. Since the dimensions of an annular passage were found to impact on the behaviour of the transition flow regime, an annular geometric parameter (defined in section 7.5.2) was considered together with other parameters in the development of the correlations. The correlations were developed within the common transition Reynolds number range that covered the experimental data of all the tests. These ranges are illustrated in Figure 7.1a for transition based on the heat transfer coefficient and in Figure 7.1b for transition based on the friction factor. The correlations that are presented in this section are for the approximately UWT boundary condition ($\tau = 0.99$). Those for non-uniform wall boundary conditions ($\tau = 0.975$ and $\tau = 0.965$) can be found in Appendix C. The correlations for the heated and the cooled annulus cases were developed exclusively.

7.5.2.   Annular geometric parameter

In this study, the characteristics of the transition flow regime, heat transfer coefficients and friction factors were observed to be significantly dependent on the annular gap (hydraulic diameter). However, most of the correlations for the annular passage appearing in literature show that heat transfer and friction factor depend on the annular diameter ratio (Prinsloo et al., 2014;

Van Zyl et al., 2013; Swamee, Aggarwal and Aggarwal*,* 2008; Dirker and Meyer, 2005; Davis, 1953; Foust and Christian, 1940; Monrad and Pelton, 1942). Thus, it is evident that both the annular diameter ratio and the hydraulic diameter of the annuli need to be considered when attempting to develop a correlation that can be used to predict the heat transfer coefficient and friction factors in the transition flow regime. In that sense, it is possible to have annular passages that share the same annular diameter ratio, but with different annular gap sizes. Conversely, different annular passages might share the same hydraulic diameter, but may have different annular diameter ratios. The impact of this could unfortunately not be found in the literature.

In addition, it is known that the axial length (heat transfer length and pressure drop length) also affects the heat transfer coefficients and friction factors (Hausen, 1943; Heaton et al.*,* 1964; Ghajar and Madon, 1997; Gnielinski, 2009). The length is usually presented in dimensionless form as a length-to-diameter ratio, L/D_h. For instance, Gnielinski (2015) considered this ratio in Equation 2.4. As mentioned earlier, and as included in Table 3.1, the test sections in this study exhibited different L/D_h ratios. Since lengths for the four test sections were approximately equal, the variations in L/D_h ratio are due to D_h. Based on the datasets, it was found via inspection that a plausible combined effect of the annular diameter ratio, hydraulic diameter and heat transfer and pressure drop length on the heat transfer coefficients and friction factors could be described in dimensionless form as follows:

$$\lambda = \frac{aL_{hx}}{D_h}$$

(7.1)

An example case of the Nusselt number data dependence on the annular diameter ratio, *a*, is shown in Figure 7.6, as well as the annular geometric parameter, λ, in Figure 7.7 at a Reynolds number of 2 000. It can be observed that the dependence of the Nusselt number on the new annular geometric parameter is better defined than on the annular diameter ratio. This Nusselt number to annular geometric parameter trend was evident for all data points in the transition flow regime. Similar behaviour was observed in the friction factor to annular geometric parameter trends shown in Figure 7.8.

99
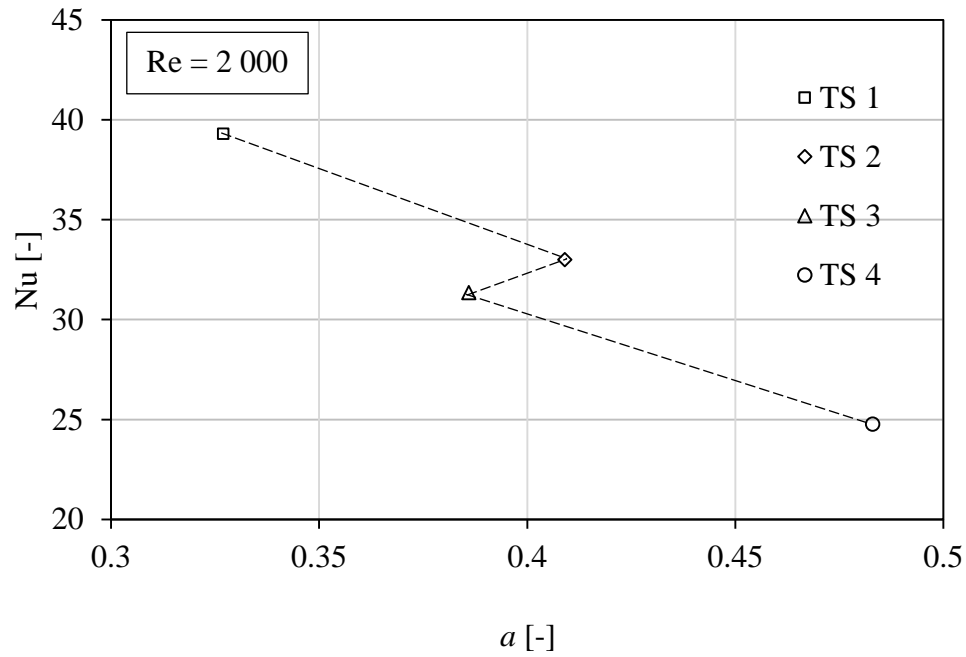
Figure 7.6: Nusselt number values for Re = 2 000 plotted against the annular diameter
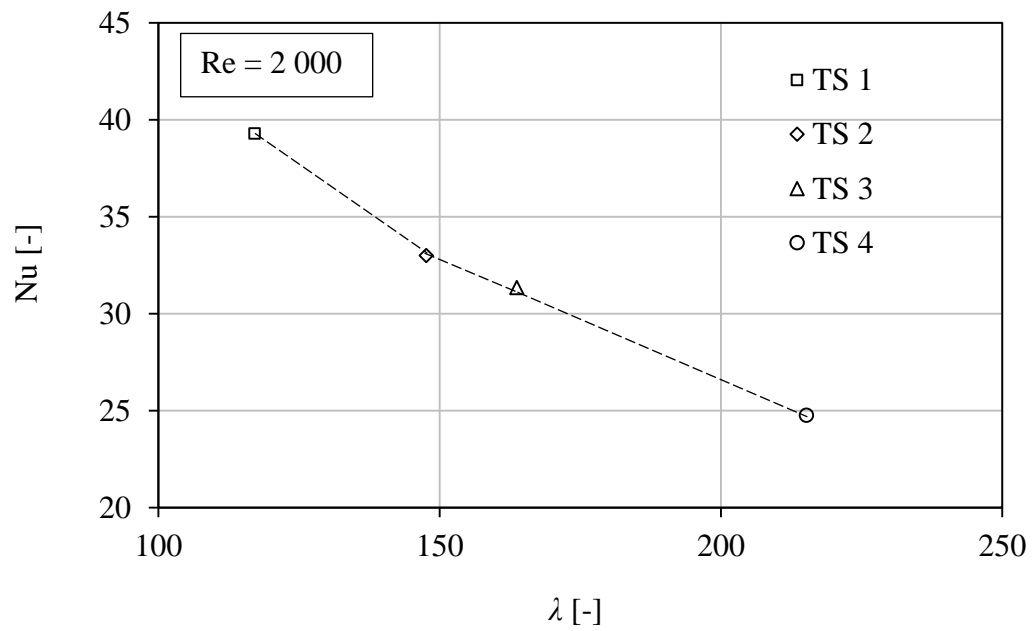
Figure 7.7: Nusselt number values for Re = 2 000 plotted against the annular geometric parameter
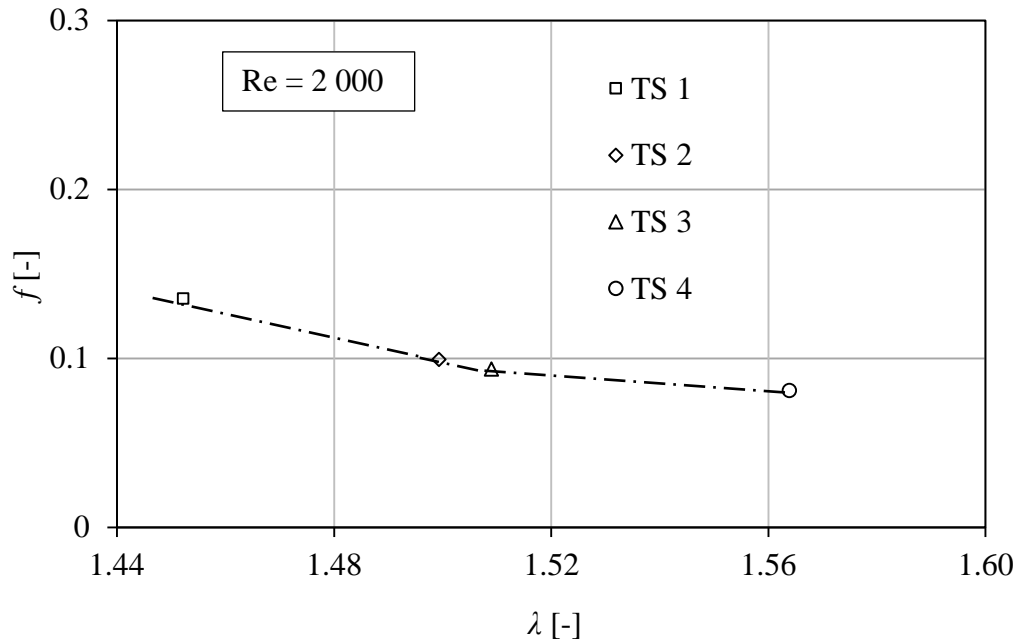
Figure 7.8: Friction factors at Re = 2 000 for the four test sections based on the ratio annular geometric parameter

A comparison of the influence of the annular geometric parameters among the four test sections (see Figure 7.7) indicates that TS 1, which has a lower annular geometric parameter, has the highest Nusselt number value. Since the heat transfer length is constant, the effect on the Nusselt number values could be due to the hydraulic diameter. Figure 5.4b shows that TS 1, which had a larger hydraulic diameter, also had stronger buoyancy forces, thus a better fluid mix than the rest. As the annular geometric parameter increased for TS 2, TS 3 and TS 4, the Nusselt number values decreased.

7.5.3.   Nusselt number and friction factor correlations

From the existing correlations for the circular tubes and annulus operated in mixed-convection conditions, it is known that the Nusselt number is dependent on the Grashof, Prandtl and Reynolds numbers (Ghajar and Madon, 1997; Mohammed et al., 2010; Hattori, 1979). Since most of the data points in the transition flow regime in this investigation were for mixed-convection conditions (see Figure 5.4b), the following form was adopted for the Nusselt number correlation:

$$Nu = C\lambda^{-n} \tag{7.2}$$

Here, heat transfer has some dependence on the annular passage dimensions expressed via the annular geometric parameter, λ. The coefficient C and exponent n consider the effects of the Grashof, Prandtl and Reynolds numbers.

Isothermal friction factors, f_{iso}, were related to the Reynolds number in the following form:

$$f_{iso}C_{iso}(\lambda)\mathrm{Re}^{-m(\lambda)} \tag{7.3}$$

The coefficient $C_{iso}(\lambda)$ and exponent $m(\lambda)$ are dependent on a geometric parameter, λ.

Diabatic friction factors, f_d, were adjusted from the isothermal friction factors by incorporating the Grashof and Prandtl numbers to account for buoyancy and heat transfer effects:

$$f_d = f_{iso}\lambda^n C_d\left(\frac{\mu_b}{\mu_{iw}}\right) \tag{7.4}$$

Coefficient C_d and exponent n are dependent on the Grashof and Prandtl numbers.

To complete the construction of the correlations, expressions for λ, C, C_T, m, C_d and n are needed. This was done iteratively in order to reduce the root mean square deviation (RMSD) of the predicted Nusselt number and friction factor values compared to the experimentally obtained values.

7.5.4.   Coefficients and exponents for the Nusselt number correlations

Expressions for the coefficient and exponent in Equation 7.2 for the heated and cooled annulus cases with $\tau = 0.99$ were obtained as follows:

For heated annuli:

$$C_d = 134 \left(\frac{Gr\,Pr}{Re} \right)^{0.401} \tag{7.5}$$

$$n = 0.32 \left(\frac{Gr\,Pr}{Re} \right)^{0.147} \tag{7.6}$$

For an applicable range of $790 \leq Re \leq 3\,490$, $620 \leq GrPr/Re \leq 9\,700$ and $63 \leq \lambda \leq 145$.

For cooled annuli:

$$C_d = 1183 \left(\frac{Gr\,Pr}{Re} \right)^{0.28} \tag{7.7}$$

$$n = 0.496 \left(\frac{Gr\,Pr}{Re} \right)^{0.122} \tag{7.8}$$

For an applicable range of $660 \leq Re \leq 3\,980$, $1\,000 \leq GrPr/Re \leq 12\,000$ and $63 \leq \lambda \leq 145$.

The mathematical formulation of these coefficients and exponents was purposefully selected to match the formulation in Equation 7.2.

Figure 7.9 shows the comparison between the experimental and predicted Nusselt number for both the heated and cooled annulus cases. The agreement between the experimental results and proposed correlations was good, with all the data points within a ±8% error band.

Figure 7.9: Comparison between the results of the experimental and predicted Nusselt numbers for the heated and cooled annulus cases

7.5.5.   Coefficients and exponents for friction factor correlations

As indicated before, the friction correlation for the isothermal conditions was developed first. From this, the diabatic cases were developed within the common Reynolds number transition range of 1 400 to 2 500, as indicated in Figure 7.1b. The best line fit in the transition regime of the isothermal friction factor plot for all the test sections was a power form. The isothermal friction factor equations for the four test sections, which were developed, are shown in Table 7.1.

Table 7.1: Correlations for the isothermal friction factor of the test sections that were considered in this study

TS	Isothermal friction factors correlation	Equation
1	$7383Re^{-1.43}$	7.9
2	$4032Re^{-1.39}$	7.10
3	$3317Re^{-1.38}$	7.11
4	$989Re^{-1.24}$	7.12

The four equations were then combined into one, expressed with respect to the Reynolds number and annular geometric parameter, and is represented by Equation 7.3. By plotting the coefficients of the four isothermal friction factor correlations against the annular geometric parameters as shown in Figure 7.10a, the overall coefficient in Equation 7.3 was found as in Equation 7.13. Using a similar method as shown in Figure 7.10b, the overall power index, *m,* was also found as in Equation 7.14.

a)

$$C_{iso} = 2.784\lambda^2 - 717.574\lambda + 46\,425.43$$

b)

$$m = -0.00357\lambda + 1.721$$
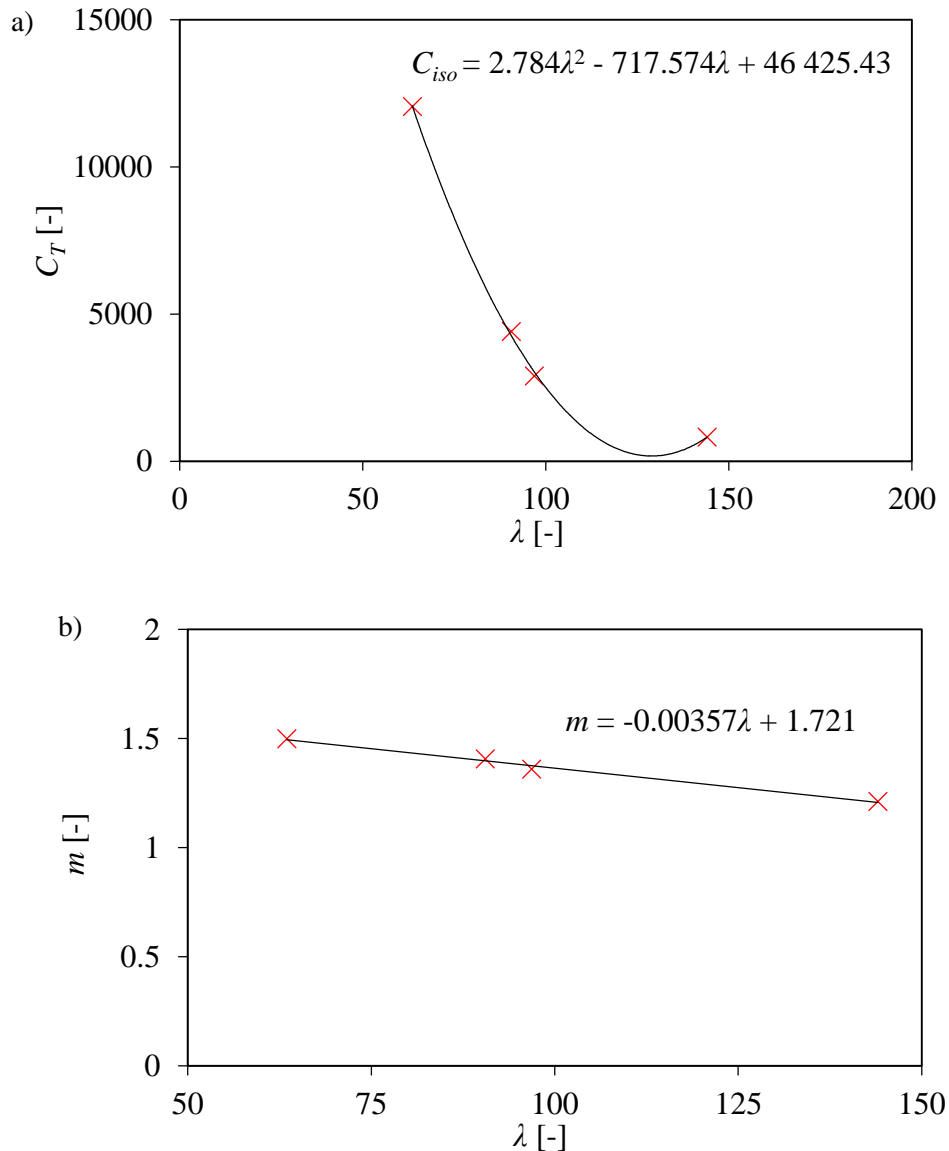
Figure 7.10: Relationships between λ and: (a) coefficient *C;* and (b) power index *m*

$$C_{iso} = 2.784\lambda^2 - 717.574\lambda + 46425.43 \tag{7.13}$$

$$m = -3.57 \times 10^{-3}\lambda + 1.721 \tag{7.14}$$

The isothermal annulus correlation is developed for the transition flow regime cases with $1\,400 \leq \mathrm{Re} \leq 2\,500$, $64 \leq \lambda \leq 114$. The agreement between the experimental results and the proposed correlations was good, with 95% of the data points within $\pm 7\%$ error band, as shown in Figure 7.11.
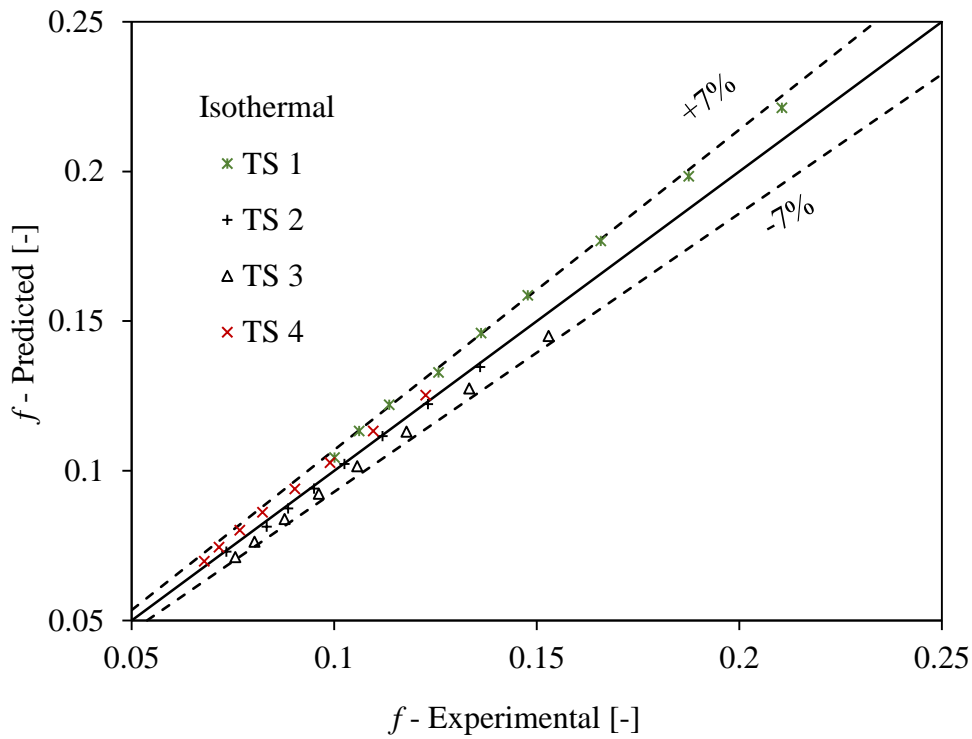
Figure 7.11: Comparison between the experimental and predicted friction factor results for the isothermal case

Expressions for the coefficient and exponent in Equation 7.4 for the heated and cooled annulus cases were obtained as follows:

For heated annuli:

$$C_d = 46.6 \times 10^6 \left(\mathrm{Gr}^{0.01} \, \mathrm{Pr}^{2.9} \right)^{-3.12} \tag{7.15}$$

$$n = 3.8 \times 10^{-3} \left(\mathrm{Gr}^{0.01} \, \mathrm{Pr}^{2.9} \right) - 0.88 \tag{7.16}$$

For an applicable range of $1\,400 \leq \mathrm{Re} \leq 2\,500$, $136 \leq \mathrm{Gr}^{0.01} \, \mathrm{Pr}^{2.9} \leq 187$, $1.35 \leq \mu_b/\mu_{iw} \leq 1.50$ and $64 \leq \lambda \leq 144$.

For cooled annuli:

$$C_d = 10.95 \left(\mathrm{Gr}^{0.01} \, \mathrm{Pr}^{2.9} \right)^{0.19} \tag{7.17}$$

$$n = -0.14 \times 10^{-3} \left(\mathrm{Gr}^{0.01} \, \mathrm{Pr}^{2.9} \right) - 0.45 \tag{7.18}$$

For an applicable range of $1\,400 \leq \mathrm{Re} \leq 2\,500$, $70 \leq \mathrm{Gr}^{0.01} \, \mathrm{Pr}^{2.9} \leq 95$, $0.65 \leq \mu_b/\mu_{iw} \leq 0.69$ and $64 \leq \lambda \leq 144$.

The exponents for the Grashof and Prandtl numbers were done iteratively to reduce the RMSD of the values of the predicted friction factors compared to the experimentally obtained values.

Figure 7.12 shows the comparison between the experimental and predicted friction factors for the heated and cooled annulus cases. The agreement between the experimental results and the proposed correlations was good, with all the data points within a ±8% error band.
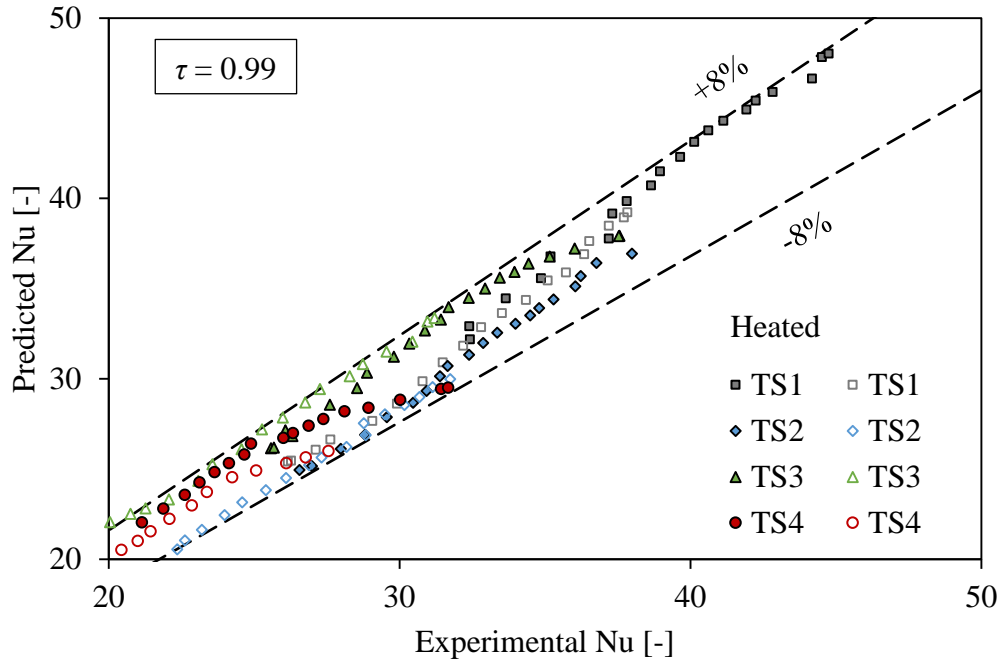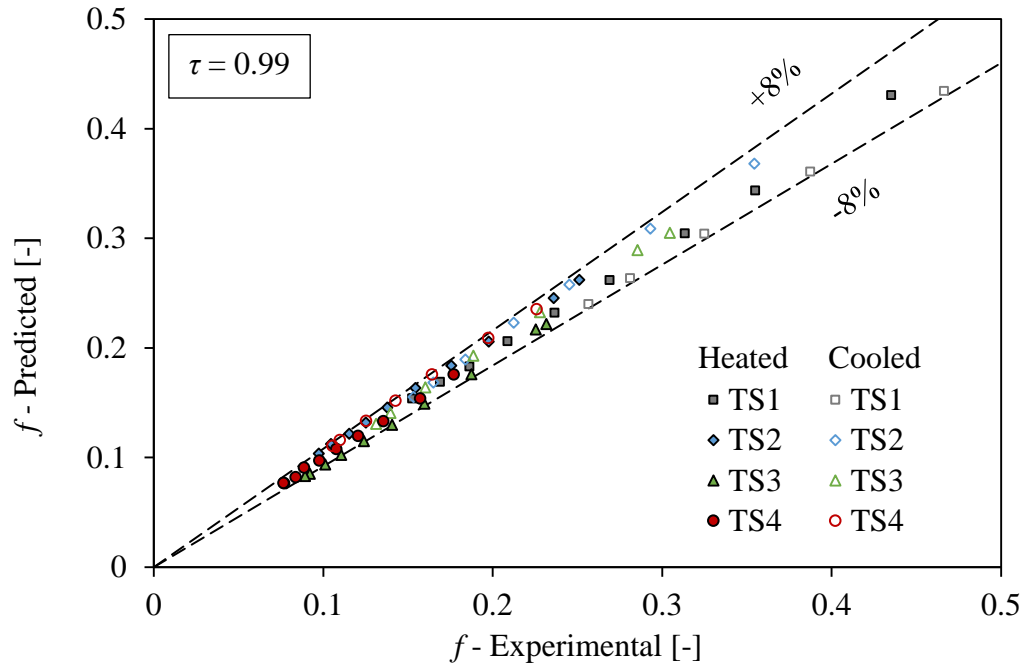
Figure 7.12: Comparison between the results of the experimental and predicted friction factors for the heated and cooled annulus cases

7.6 Comprehensive correlations

It has been learnt in this study that the thermal boundary condition and annular geometric parameter impact on the transition flow regime Reynolds number spans, heat transfer coefficients and friction factors. The effects of the thermal boundary conditions on the transition flow regime and the related Nusselt number and friction factor correlations were discussed in detail in Chapter 6 using the data for TS 1. The effects of the annular geometric parameter and the related correlation were covered earlier in this chapter, based on approximate UWT boundary condition ($\tau = 0.99$). Apart from the thermal boundary and annular dimensions, the presence of buoyancy-driven secondary flows had a significant impact as well. Since the said factors influenced the heat transfer coefficients and friction factors inclusively, it is necessary to have comprehensive correlations that take all the important parameters into account. In this section, correlations for the transition flow regime Reynolds number spans, heat transfer coefficients and friction factors are presented.

7.6.1.   Transitional flow regime Reynolds number spans

As mentioned previously, different transitional Reynolds number spans for the heat transfer coefficients and friction factors were obtained, depending on the test section, degree of wall temperature uniformity and the thermal operating condition (heated, cooled or isothermal). It was found that Re_2, as well as ΔRe, for either the heat transfer coefficient or the friction factor coefficient can conveniently be expressed as follows:

$$Re_2 = \left[C\lambda^n (\tau + 0.01)^p \right]_{Re_2} \tag{7.19}$$

$$\Delta Re = \left[C\lambda^n (\tau + 0.01)^p \right]_{\Delta Re} \tag{7.20}$$

Table 7.2: Transitional flow regime Reynolds number span correlation coefficients and exponent values

	Transition based on the Nusselt number				Transition based on the friction factor					
	Heated		Cooled		Heated		Cooled		Isothermal	
	Re_2	ΔRe	Re_2	ΔRe	Re_2	ΔRe	Re_2	ΔRe	Re_2	ΔRe
C	27 300	20 700	64 800	56 200	27 000	20 000	41 400	29 700	6 700	5 300
n	-0.42	-0.39	-0.56	-0.55	-0.46	-0.49	-0.47	-0.46	-0.2	-0.23
p	2.94	2.9	3.3	3.52	4.42	4.42	1.82	1.82	N/A	N/A
Mean absolute error	2.2%	2.3%	1.5%	1.8%	5.9%	4.4%	1.0%	1.3%	1.2%	1.5%
Maximum absolute error	5.0%	9.8%	4.3%	3.7%	9.2%	8.5%	2.0%	2.5%	2.5%	3.5%

Here, C_{Re2} and $C_{\Delta Re}$ have different numeric values, depending on whether Re_2 or ΔRe is computed. This is also the case for n_{Re2} and $n_{\Delta Re}$, and p_{Re2} and $p_{\Delta Re.}$ A summary of suitable C, n and p values is given in Table 7.2. These values were determined through mathematic regression to minimise the root mean square errors of the predicted values of Re_2 and ΔRe values in terms of the experimentally obtained values. The mean prediction errors, as well as the maximum prediction errors based on our experimental data set, are also supplied. The lower limit of the transitional flow regime can be estimated by subtracting the prediction of ΔRe from the prediction for Re_2. The difference in the heated, cooled and isothermal cases is probably due to the impact of the secondary flow development and growth of the thermal boundary layers. Insufficient data is available in this data set to determine whether these variations can be linked to the Grashof number and to the viscosity ratio between the bulk fluid and the heat transfer wall.

7.6.2.   Nusselt number

Nusselt number correlation was developed for all the test sections for the approximately UWT condition ($\tau = 0.99$) and is represented by Equation 7.2. The variation of fluid properties with temperature is usually taken into account by viscosity ratio, as evidenced in many existing correlation, for instance, equations 2.5, 2.6, 2.7, 2.8, 2.9, 2.11 and 2.13. However, in this case, the temperature effects are taken into account by τ so that Equation 7.2 becomes:

$$\mathrm{Nu} = \left[C\lambda^{-n}\left(\tau + 0.01\right)^{p} \right]_{ha/ca} \tag{7.21}$$

The term $(\tau + 0.01)$ in Equation 7.21 adjusts the heat transfer coefficient for the approximately UWT condition ($\tau = 0.99$) to a hypothetical heat transfer coefficients for $\tau = 1$.

Suitable expressions for C, n and p can be written as follows:

For heated annuli:

$$C_{ha} = 137\left(\frac{\mathrm{Gr\,Pr}}{\mathrm{Re}}\right)^{0.403}, \quad n_{ha} = 0.329\left(\frac{\mathrm{Gr\,Pr}}{\mathrm{Re}}\right)^{0.145} \text{ and } p_{ha} = 6.04$$

$$\tag{7.22}$$

For cooled annuli:

$$C_{ca} = 1180 \left(\frac{\text{Gr Pr}}{\text{Re}} \right)^{0.28}, \quad n_{ca} = 0.475 \left(\frac{\text{Gr Pr}}{\text{Re}} \right)^{0.127} \text{ and } p_{ca} = 4.42$$

(7.23)

The coefficient and exponent values in C and n, as well as the values of p, were obtained iteratively in order to minimise the RMSD of the predicted Nusselt number values compared to the experimentally obtained values. The ranges of applicability for these equations are $790 \leq$ Re $\leq 3\ 490$, $620 \leq$ GrPr/Re $\leq 9\ 700$, $63 \leq \lambda \leq 145$ and $1 \leq \tau \leq 0.965$ for heated annulus cases and $660 \leq$ Re $\leq 3\ 980$, $1\ 000 \leq$ GrPr/Re $\leq 12\ 000$, $63 \leq \lambda \leq 145$ and $1 \leq \tau \leq 0.965$ for cooled annulus cases. The agreement between the experimental results and the proposed correlations was good, with 99% of the data points for all τ values, 0.99, 0.975 and 0.965, falling within a $\pm10\%$ error band as shown in Figure 7.13.
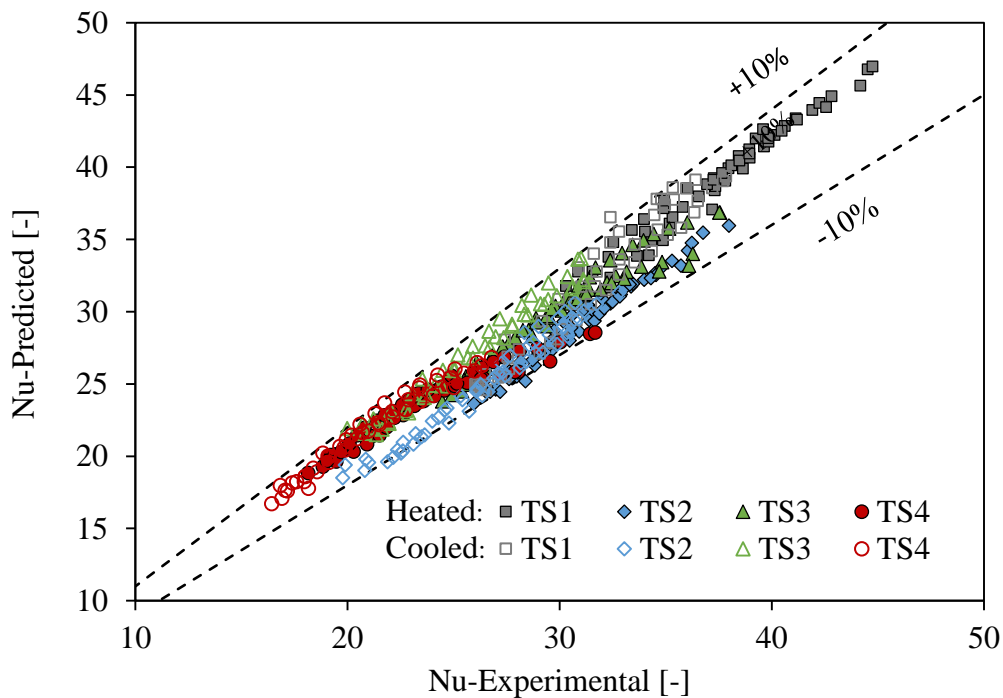
Figure 7.13: Comparison between the experimental and predicted Nusselt number results for heated and cooled annulus cases

7.6.3.   Friction factor

The isothermal friction factor correlation, which takes varying geometric dimensions that were considered in this study into account, is presented in Equation 7.3. The associated coefficient, $C_{iso}(\lambda)$ and exponent, $m(\lambda)$ are given by Equation 7.13 and Equation 7.14, respectively. Based on the isothermal friction factor equation, a diabatic friction factor correlation was initially developed, which considered only the variation of annular dimensions the approximately UWT condition ($\tau = 0.99$) data, and is given in Equation 7.4. In the comprehensive friction factor correlation, the effect of wall temperature uniformity is taken into account by τ based on the hypothetical friction factor for $\tau = 1$ so that Equation 7.2 becomes:

$$f = \left[f_{iso} C_f \lambda^{n_f} \left(\tau + 0.01 \right)^{p_f} \right]_{ha/ca} \tag{7.24}$$

The following suitable expressions for C_f, n_f and p_f have been found:

For heated annuli:

$$C_{f,ha} = 205.7 \times 10^6 \left(\mathrm{Gr}^{0.01} \, \mathrm{Pr}^{2.9} \right)^{-3.32}, \quad n_{f,ha} = 660 \left(\mathrm{Gr}^{0.01} \, \mathrm{Pr}^{2.9} \right)^{-1.45}, \quad p_{f,ha} = -6.1 \tag{7.25}$$

For cooled annuli:

$$C_{f,ca} = 2.37 \left(\mathrm{Gr}^{0.01} \, \mathrm{Pr}^{2.9} \right)^{0.47}, \quad n_{f,ca} = 0.3735 \left(\mathrm{Gr}^{0.01} \, \mathrm{Pr}^{2.9} \right)^{0.0546}, \quad p_{f,ca} = 2.92 \tag{7.26}$$

The exponents for Gr and Pr were found iteratively in order to minimise the RMSD of the predicted friction factor values compared to the experimentally obtained values. The ranges for which these equations can be applied are $1\,400 \leq \mathrm{Re} \leq 2\,500$, $130 \leq \mathrm{Gr}^{0.01} \, \mathrm{Pr}^{2.9} \leq 170$, $63 \leq \lambda \leq 145$ and $1 \leq \tau \leq 0.965$ for a heated annulus case and $1\,400 \leq \mathrm{Re} \leq 2\,500$, $70 \leq \mathrm{Gr}^{0.01} \, \mathrm{Pr}^{2.9} \leq 105$, $63 \leq \lambda \leq 145$ and $1 \leq \tau \leq 0.965$ for a cooled annulus case. The agreement between the experimental results and the proposed correlations was good, with 90% of the data points falling within a $\pm10\%$ error band and 98% falling within a $\pm15\%$ error band as shown in Figure 7.14.
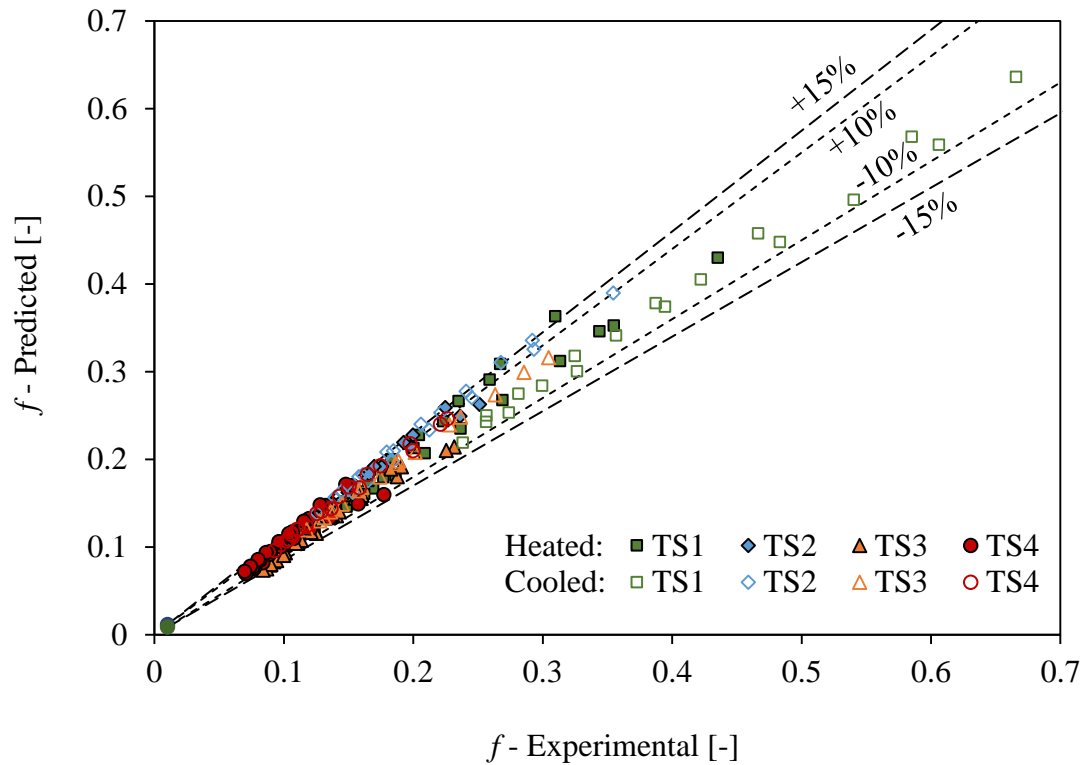
Figure 7.14: Comparison between the results of the experimental and predicted friction factors for the heated and cooled annulus cases with $\tau = 1$, 0.99, 0.975 and 0.965

7.7 Summary

In this chapter, the effect of the geometric dimensions of the annular passage on the Reynolds number limits of the transition regime, heat transfer coefficients and friction factors was discussed. It was learnt that the size of the annular gap had a well-defined influence on the said characteristics. The geometric dimensions of the annular passage were first converted to a dimensionless parameter, which was then used to define the behaviour of the Reynolds number limits of the transition regime, heat transfer coefficients and friction factors.

New correlations were developed to predict the heat transfer coefficients, friction factors and transitional Reynolds number spans. The first set of correlations was that for all test sections, but was based on an approximate UWT boundary condition. Comprehensive correlations that included the effects of the annular dimensions and the thermal boundary conditions were also developed. All the correlations predicted the experimental values very well.

Chapter 8

Conclusions

8.1.   Summary

Generally, most heat exchangers are designed to be operated in either the laminar or the turbulent flow regimes and not in the transition regime. This could mainly be due to a lack of knowledge on the behaviour of heat exchangers in the transition flow regime, or due to the need for higher heat transfer rates associated with turbulent flow, or due to system limitations or characteristics that result in transition flow conditions.

Several researchers have performed work in the transition flow in circular tubes over the years. However, the characteristics of a transition flow regime in the annular passage are still not well understood. As a result, predictions of transition flow behaviour in an annular passage are very difficult. The aim of this study, therefore, was to investigate the characteristics of heat transfer coefficients and friction factors in the transition flow regime of an annular passage. The lower and upper Reynolds number limits of the transition regime were also investigated.

The experimental system comprised tube-in-tube heat exchanger test sections. Four annular passages of different annular diameter ratios and hydraulic diameters were investigated. The investigation also involved varying non-uniform temperatures on the inner annular passage surface, while the outer surface was insulated. Non-uniform temperature was expressed in terms of the degree of wall temperature uniformity, τ. Three different wall temperature uniformities were investigated on each of the four test sections: 0.99 (also referred to as approximate UWT), 0.975 and 0.965. Apart from the diabatic investigations, which involved both the heating and the cooling of annular fluid, isothermal tests were also done for the friction factor analysis.

8.2. Results

8.2.1.   Inlet configuration

Some research shows that the disturbance of fluid flow at the entrance region impacts on the lower and upper Reynolds number limits of transition flow. However, information in this regard

was not found for an annular passage. In order to make an informed design of the inlet for the four test sections, two different inlet configurations were examined. Similar results of friction factors were obtained from the two inlets, indicating that the inlet configuration had no impact on the characteristics of the transition flow regime. Despite the results being similar, only one design was used in the entire study to ensure consistence of the results.

8.2.2. Buoyancy-driven secondary flows

During data analysis, it was realised that buoyancy-driven secondary flows could not be ignored. Therefore, types of convection were analysed for each diabatic test in order to establish the significance of secondary flows in all the flow regimes. Special attention was given to the transition flow regime. It was found that the larger hydraulic diameters and higher degrees of wall temperature uniformity had stronger buoyancy forces. The cooled annulus cases also had stronger buoyancy forces than the heated annulus cases. It was observed later in the data analysis that buoyancy-driven secondary flows had a significant influence on the heat transfer coefficients, the friction factors and the Reynolds number limits of the transition flow regime. A comparison of the friction factors in the low Reynolds numbers showed higher values for the experimental data than those based on forced convection calculations. Similar comparisons for the Nusselt numbers in the laminar region showed higher experimental values than those based on forced convection calculations. The influence of the buoyancy force was also evident in the heat transfer results that were presented in terms of the Colburn *j*-factor. The cooled annulus and heated annulus results in the present study did not fall exactly on one line, as is often the case in fully forced convection turbulent cases.

8.2.3. Influence of degree of wall temperature uniformity

In all four test sections that were considered in this study, the degree of wall temperature uniformity had a significant influence on the heat transfer coefficients and friction factors. The higher the τ value, the larger the heat transfer coefficients and the friction factors. This applies to both the heated and the cooled annulus cases. The lower Reynolds number limits for the three different degrees of wall temperature uniformity were slightly closer to each other, but the upper limit was larger for a higher τ and smaller for a lower τ.

8.2.4. Influence of annular passage dimensions

A significant dependence on the dimensions of the annular passage was observed in both the isothermal and diabatic tests. The dependence was found to be more related to the hydraulic diameter than to the annular diameter ratio. Heat transfer coefficients and friction factors were higher for an annular passage with a larger annular gap size than a smaller gap. The lower Reynolds number limits for the four annular passages were slightly closer to each other, but the upper limit was larger for an annular passage with a larger annular gap size.

Considering the finding of this study and those of others, a dimensionless parameter that combines the existing ratios (annular diameter ratio and length-to-hydraulic diameter ratio) was proposed. In this study, the new dimensionless parameter, which is referred to as annular geometric parameter, λ is the product of the annular diameter ratio and length-to-hydraulic diameter ratio. It was observed that the heat transfer coefficients and friction factors related well with the proposed parameters.

8.2.5. Influence of heating or cooling annular fluid

The heating or cooling of the annular fluid had an influence on the Reynolds number limits of the transition flow regime, the heat transfer coefficients and the friction factors. In all diabatic tests that were considered in this study, the heat transfer coefficients for a heated annulus case were higher than for the cooled annulus case. This was due to the variation of the temperature differences between the bulk annular fluid temperature and the inner wall temperature of the annular passage, as well as the fluid Prandtl and Grashof numbers. However, the friction factors were higher for the cooled annulus case than for the heated annulus case. This was attributed to various factors, including the different viscosity values on the inner wall, as determined by different wall temperature uniformities. The transition flow regime spans, based on either wall temperature uniformity or annular passage dimensions, were larger for the cooled annulus case than for the heated annulus case.

8.2.6.   Heat transfer against pressure drop

The general trend of pressure drop against Reynolds number for all the tests in this investigation occurred as follows: the pressure drop was lowest in the laminar flow regime, as the Reynolds number increased the pressure drop also increased gently in the laminar and transitional flow regimes but steeply in the turbulent flow regime. This trend is similar to that of heat transfer (Nusselt number). This means that the pumping cost is lowest when the heat transfer ability is also lowest and high when the heat transfer ability is high. Therefore, for the annular passage, a better compromise between the heat transfer ability and the pressure drop penalty is in the transitional flow regime.

8.3. Correlations

Since it was evident from the results that the dimensions of the annular passage and thermal boundary condition had a significant impact on the heat transfer coefficients, friction factor and Reynolds number limits of the transition flow regime, three sets of correlations were developed. The first set was developed based on a single annular passage, but taking into account varying degrees of wall temperature uniformity. The second set was based on a single degree of wall temperature uniformity, but varying dimensions of the annular passage. The last set considered that both variables occurred concurrently, therefore they were both taken into account to form comprehensive correlations. Due to the presence of buoyancy-driven secondary flow, the Grashof number was considered in all the diabatic correlations. Correlations for isothermal friction factors were also proposed.

The agreement between the experimental results and the proposed correlations was good for all the correlations that were proposed. The best case had all the data points being predicted within a ±4 % error band, and the worst case had 90 % of the data points being predicted within a ±10% error band.

8.4.Future works

Despite the extensive work that was covered in this study, some critical questions remain unanswered. Thus, future recommended work should include the following:

- Due to the unavailability of information on the influence of inlet disturbances on the Reynolds number limits of transition flow in the annular passage, two inlet configurations were examined in this study. Although similar results were obtained, investigations on more diverse inlet configurations might give varying results.

- In this study, characteristics of the transition flow regime were found to relate with the hydraulic diameter better than the annular dimeter ratio. An investigation into several annular passages with either the same annular diameter ratio but a varying hydraulic diameter, or the same hydraulic diameter but a varying annular diameter ratio, can define this relationship better.

- The transition based on heat transfer and that based on fluid flow occurred at different Reynolds numbers in this study. This is attributed to heat transfer occurring on a single surface, while friction was both on the inner and outer surfaces. It might be interesting to find out the effect of heat transfer occurring on both surfaces as well.

- It is known that the influence of buoyancy force on heat transfer coefficients varies with the orientation of the heat exchanger. Since heat exchangers do not always operate in a horizontal position, as was a case in this study, a wider range of positions would add valuable information to the database.

References

Abed, W.M., Shareef, A.J., and Najeeb, A.A. 2010. Natural convection heat transfer in horizontal concentric annulus between outer cylinder and inner flat tube, *Anbar Journal of Engineering Science,* 3, pp 31–45.

Abraham, J.P., Sparrow, E.M., and Tong, J.C.K. 2009. Heat transfer in all pipe flow regimes – laminar, transitional/intermittent and turbulent, *International Journal of Heat and Mass Transfer,* 52, pp 557–563.

Çengel, Y.A., and Ghajar, A.J. 2011. *Heat and mass transfer*, fourth ed. New York, NY: McGraw-Hill.

Ciampi, M., Faggiani, S., Grassi, W., and Tuoni, G. 1987. Mixed-convection heat transfer in horizontal, concentric annuli for transitional flow conditions, *International Journal of Heat and Mass Transfer,* 30, pp 833–841.

Crookston, R.B., Rothfus, R.R., and Kemode, R.I. 1968. Turbulent heat transfer with annuli with small cores, *International Journal of Heat Mass Transfer,* 11, pp 415–426.

Davis, E.S. 1953. Heat transfer and pressure drop in annuli, *Transactions of the American Society of Mechanical Engineers,* pp 755–760.

Dawood, H.K., Muhammed, H.A., Sidik, N.A.C., Munisamy, K.M., and Wahid, M.A. 2015. Forced, natural and mixed convection heat transfer and fluid flow in annulus: a review, *International Communications in Heat and Mass Transfer,* 62, pp 45–57.

Dirker, J., and Meyer, J.P. 2005. Convective heat transfer coefficients in concentric annuli, *Heat Transfer Engineering,* 26, pp 38–44.

Dirker, J., and Meyer, J.P., and Garach, D.V. 2014. Inlet flow effects in micro-channels in the laminar and transitional regimes on single-phase heat transfer coefficients and friction factors, *International Journal of Heat and Mass Transfer*, 77, pp 612–626.

References

Dirker, J., Van Der Vyver, H., and Meyer, J.P. 2004. Convection heat transfer in concentric annuli, *Experimental Heat Transfer,* 17, pp 19–29.

Dittus, F.W., and Boelter, L.M.K. 1930. *University of California Publications on Engineering,* 2, pp 329–353.

Everts, M., and Meyer, J.P. 2015a. Heat transfer of developing flow in the transitional flow regime, *Proceedings of the first Thermal and Fluid Engineering Summer Conference,* New York, NY, 9–12 August.

Everts, M., and Meyer, J.P. 2015b. Heat transfer of developing flow in the transitional flow regime of solar receiver tube, *Proceedings of the third Southern African Solar Energy Conference,* Kruger National Park, South Africa, 11–13 May.

Everts, M., Ayres, R.S., Houwer, F.A.M., Vanderwagen, C.P., Kotze, N.M., and Meyer, J.P. 2014. The influence of surface roughness on heat transfer in the transitional flow regime, *Proceedings of the fifteenth International Heat Transfer Conference,* Tokyo, Japan, 10–15 August.

Filonenko, G.K. 1954. Hydraulic resistance of pipes (Hydraulilischer widerstand von rohrleitungen), *Teploenergetika,* 1, pp 40–44.

Foust, A.S., and Christian, G.A. 1940. Non-boiling heat transfer coefficients in annuli, *AlChE Journal,* 36, pp 541–554.

Ghajar, A.J., and Madon, K.F. 1992. Pressure drop measurements in the transition region for a circular tube with three different inlet configurations, *Experimental Thermal and Fluid Science*, 15, pp 129–135.

Ghajar, A.J., and Madon, K.F. 1995. Flow regime map for a horizontal pipe with uniform wall heat flux and three inlet configurations, *Experimental Thermal and Fluid Science*, 10, pp 287–297.

References

Ghajar, A.J., and Tam, L. 1997. Effect of inlet geometry and heating on the fully developed friction factor in the transition region of a horizontal tube, *Experimental Thermal and Fluid Science*, 15, pp 52–64.

Ghajar, A.J., and Tam, L. 1994. Heat transfer measurements and correlations in the transition region for a circular tube with three different inlet configurations, *Experimental Thermal and Fluid Science*, 8, pp 79–90.

Ghajar, A.J., and Tam, L. 1995. Flow regime map for a horizontal pipe with uniform wall heat flux and three inlet configurations, *Experimental Thermal and Fluid Science*, 10, pp 287–297.

Gnielinski, V. 1976. New equations for heat and mass transfer in turbulent pipe and channel flow, *International Journal of Chemical Engineering,* 16, pp 359–368.

Gnielinski, V. 2007. Berechnung des druckverlustes in glatten konzentrischen ringspalten bei ausgebildeter laminarer und turbulenter strömung, *Chemie Ingenieur Technik,* 79, pp 91–95.

Gnielinski, V. 2009. Heat transfer coefficients for turbulent flow in concentric annular ducts, *Heat Transfer Engineering,* 30, pp 431–436.

Gnielinski, V. 2010. Heat transfer in laminar flow, *VDI heat atlas,* second ed. Springer Verlag.

Gnielinski, V. 2013. On heat transfer in tubes, *International Journal on Heat and Mass Transfer,* 63, pp 134–140.

Gnielinski, V. 2015. Turbulent heat transfer in annular spaces – a new comprehensive correlation, *Heat Transfer Engineering,* 36, pp 787–789.

Hattori, N. 1979. Combined free and forced convection heat transfer for fully developed laminar flow in horizontal concentric annuli (numerical analysis), *JSME Transactions,* 45, pp 227–239.

Hausen, H. 1943. Darstellung des wärmeüberganges in rohren durch verallgemeinerte pryenzbeziehungen, *Ver. Dtsch. Ing.,* 4, pp 91–134.

References

Heaton, H.S., Reynolds, W.C., and Kays, W.M. 1964. Heat transfer in annular passages – simultaneous development of velocity and temperature fields in laminar flow, *International Journal of Heat and Mass Transfer,* 7, pp 763–781.

Islam, N., Gaitonde, U.N., and Sharma, G.K. 2001. Mixed-convection heat transfer in the entrance region of horizontal annuli, *International Journal of Heat and Mass Transfer,* 44, pp 2107–2120.

Jones, O.C., and Leung, J.C.M. 1981. An improvement in the calculation of turbulent friction in smooth concentric annuli, *Journal of Fluids Engineering,* 103, pp 615–623.

Kakaç, S., Shah, R.K., and Aung, W. 1987. *Handbook of single-phase convective heat transfer,* New York, NY: Wiley Interscience.

Kaneda, M., Yu, B., Ozoe, H., and Churchill, S.W. 2003. The characteristics of turbulent flow and convection in concentric circular annuli, *International Journal of Heat and Mass Transfer,* 46, pp 5045–5057.

Kays, W.M., and Leung, E.Y. 1963. Heat transfer in annular passages – hydrodynamically developed turbulent flow with arbitrarily prescribed heat flux, *International Journal of Heat Mass Transfer,* 6, pp 537–557.

Kays, W.M., and Perkins, H.C. 1972. *Handbook of heat transfer*, Rohsenow, W.M., and Hartnett, J.P. (ed.) New York, NY: McGraw-Hill.

Konakov, P.K. 1946. Eine neue formel für den reibungskoeffizienten glatter rohre (Orig. Russ), *Berichte der Akademie der Wissenschaften der UdSSR*, L1 (7), pp 503-506. A new equation for the frictional resistance in smooth tubes.

Kotake, S., and Hattori, N. 1985. Combined free and forced convection heat transfer for fully developed laminar flow in concentric annuli, *International Journal of Heat and Mass Transfer,* 28, pp 2115–2120.

Lu, G., and Wang, J. 2008a. Experimental investigation on flow characteristics in a narrow annulus, *Heat and Mass Transfer,* 44, pp 495–499.

122

References

Lu, G., and Wang, J. 2008b. Experimental investigation on heat transfer characteristics of water flow in a narrow annulus, *Applied Thermal Engineering,* 28, pp 8–13.

Manglik, R.M., and Bergles, A.E. 1993. Heat transfer and pressure drop correlations for twisted – tape inserts in isothermal tubes: Part1 – laminar flows, *Journal of Heat Transfer,* 115, pp 881–889.

Martinell, R.C., Southwell, C.J., Alves, G., Craig, H.L., Weinberg, E.B., Lansing, N.F., and Boelter, L.M.K. 1942. Heat transfer and pressure drop for a fluid flowing in the viscous region through a vertical pipe. *AIChE Journal,* 38, pp 493–530.

Massey, B. 2006. *Mechanics of fluids,* London: Taylor and Francis.

McAdams, W.H. 1954. *Heat transmission,* New York, NY: McGraw-Hill.

Metais, B., and Eckert, E.R.G. 1964. Forced, mixed and free convection regimes, *Journal of Heat Transfer,* 86, pp 295–296.

Meyer, J.P. 2014. Heat transfer in tubes in the transitional flow regime, *Proceedings of the fifteenth International Heat Transfer Conference,* Kyoto, Japan, 10–15 August.

Moffat, R.J. 1988. Describing the uncertainty in experimental results, *Experimental Thermal Fluids Science*, 105, pp 498–504.

Mohammed, H.A., Campo, A., and Saidur, R. 2010. Experimental study of forced and free convective heat transfer in the thermal entry region of horizontal concentric annuli, *International Communication in Heat and Mass Transfer*, 37, pp 739–747.

Monrad, C.C., and Pelton, J.F. 1942. Heat transfer by convection in annular spaces, *AIChE Journal,* 38, pp 593–611.

Nada, S.A. 2007. Experimental investigation of natural convection heat transfer in horizontal and inclined annular fluid layers, *Heat Mass Transfer*, 44, pp 929–936.

References

Nguyen, T.H., Vasseur, V., Robillard, L., and Chandra, S.B., 1988. Combined free and forced convection of water between horizontal concentric cylinders, *Journal of Heat Transfer,* 1, pp 3–17.

Nunner, W. 1956. Heat transfer and pressure drop in rough tubes, *VDI – Forschungsheft,* 55-B, pp 5–39.

Obot, N.T., Esen, E.B., and Rabas, T.J. 1990. The role of transition in determining friction and heat transfer in smooth and rough passages, *International Journal of Heat Mass Transfer*, 33, pp 2133–2143.

Olivier, J.A., and Meyer, J.P. 2010. Single-phase heat transfer and pressure drop of the cooling of water inside smooth tube for transitional flow with different inlet geometries, *American Society of Heating, Refrigeration and Air-conditioning Engineers*, 16, pp 476–496.

Passerini, A., Ferrario, C., and Thäter, G. 2007. Natural convection in horizontal annuli: a lower bound for the energy, *Journal of Engineering Mathematics,* 62, pp 247–259.

Petukhov, B.S. 1970. *Heat transfer and friction in turbulent pipeflow with variable physical properties*, New York, NY: Academic Press.

Petukhov, B.S., and Roizen, L.I. 1964. Generalized relationships for heat transfer in turbulent flow of gas in tubes of annular section, *High Temperatures,* 2, pp 65–68.

Petukhov, B.S., Polyakov, A.F., and Strigin, B.K. 1969. Heat transfer in tubes with viscous – gravity flow, *Heat Transfer – Soviet Research*, 1, pp 24–31.

Popiel, C.O., and Wojtkowiak, J. 1998. Simple formulas for thermo-physical properties of liquid water for heat transfer calculations (from 0° to 150°), *Heat Transfer Engineering,* 19, pp 87–101.

Prinsloo, F.P.A., Dirker, J., and Meyer, J.P. 2014. Heat transfer and pressure drop characteristics in the annuli of tube-in-tube heat exchangers (horizontal layout). *Proceedings of the fifteenth International Heat Transfer Conference,* Kyoto, Japan, 10–15 August.

References

Rayle, R.E. 1959. Influence of orifice geometry on static pressure measurements, *ASME,* Paper No. 59-A-234.

Reynolds, O. 1883. On the experimental investigation of the circumstances which determine whether the motion of water shall be direct or sinuous, and the law of resistance in parallel channels, *Philosophical Transactions of the Royal Society of London A – Mathematical, Physical And Engineering Science,* 174, pp 935–982.

Sambamuthy, N., Shaija, A., Narasimham, G., and Murthy, M. 2008. Laminar conjugate natural convection in horizontal annuli, *International Journal of Heat Fluid Flow*, 29, pp 1347–1359.

Shigley, J., Mischke, C., and Budynas, R. 2004. *Mechanical Engineering Design,* New York, NY: McGraw-Hill.

Stein, R.P., and W. Begell, 1958. Heat transfer to water in turbulent flow in internally heated annuli, *AIChE Journal.*, 4, pp 127–131.

Sun, Z.N., Sun, L.C., and Yan, C.Q. 2004. Experimental investigation of single flow friction in narrow annuli (in Chinese), *Nuclear Engineering,* 25, pp 123–127.

Swamee, P.K., Aggarwal, N., and Aggarwal, V. 2008. Optimum design of double pipe heat exchanger, *Heat and Mass Transfer,* 51, pp 2260–2266.

Tam, L., and Ghajar, A.J. 1997. Effect of inlet geometry and heating on the fully developed friction factor in the transition region of a horizontal tube, *Experimental Thermal and Fluid Science,* 15, pp 52–64.

Van Zyl, W.R. 2012. *Single-phase convective heat transfer and pressure drop coefficients in concentric annuli.* Master's dissertation, University of Pretoria.

Van Zyl, W.R., Dirker, J., and Meyer, J.P. 2013. Single-phase convective heat transfer and pressure drop coefficients in concentric annuli, *Heat Transfer Engineering*, 34, pp 1112–1123.

References

Wiegand, J.H., Mc Millen, E.L., and Larson, R.E. 1945. Annular heat transfer coefficients for turbulent flow, *AIChE Journal,* 41, pp 147–153.

Withers, J.G. 1980. Tube-side heat transfer and pressure drop for tubes having helical internal ridging with turbulent/transitional flow of single-phase fluid: Part 1 – single-helix ridging, *Heat Transfer Engineering*, 2, pp 48–58.

Zhipeng, D. 2012. New correlative model for fully developed turbulent heat and mass transfer in circular and non-circular ducts, *Transactions of the American Society of Mechanical Engineers Journal of Heat Transfer*, p 134.

Appendix A

Uncertainty analysis of measurements

A.1   Introduction

In order to ascertain the degree of reliability of the results of this experimental study, the uncertainty analysis was performed on the captured data, the calculated heat transfer coefficients and friction factors. The method that was used to determine all the important parameters is discussed in this appendix.

A.2   Theory

Every measurement is subject to some uncertainty. The uncertainty of a measurement describes something about its quality. It is a quantification of the doubt about the measurement result. According to Kline and McClintock (1953), uncertainty is a possible value that an error may have, and identifies an interval around a measured value in which the true value is expected to lie. A measurement result is only complete if it is accompanied by a statement of the uncertainty in the measurement. Uncertainty analysis refers to the process of estimating how great an effect the uncertainties in the individual measurements have on the calculated result (Moffat, 1988).

The analysis of uncertainty of the system has a number of advantages. Among other things, it provides a measure of validity to the experimental results and describes the degree of reliability of the results of the experiment (Coblentz, 2002). When the uncertainty in a measurement is evaluated and stated, the fitness for purpose of the measurement can be properly judged.

A.3   Sources and types of errors

Measurement uncertainties can come from different sources. These are the external system parameters, the internal system parameters, the system model itself and the experimenter's observation of the system. An error source is usually categorised as fixed or random, depending on whether the error it introduces is steady or unsteady during the period of complete experiment. In a fixed error, the same influence affects the result for each of the repeated measurements. An error is inherent in measurement equipment and is normally indicated on the equipment itself. When repeated measurement gives a randomly different result, it is referred to as a random error.

The errors may be caused by equipment fluctuations and various influences of friction. Fixed and random errors are referred to as bias and precision errors, respectively, and are presumed to represent the stationary statistical properties of a Gaussian distributed data set (Moffat, 1988).

A.4   Generalised uncertainty analysis method

Uncertainty analysis on the final result may be done with a common sense analysis or a precise mathematical method. In this study, the precise method of Kline and McClintock (1953) was used. This is based on the careful specification of the uncertainties in the various experimental measurements. Each variable is specified as the measured value plus the uncertainty, and the odds on the uncertainty, written in mathematical form as follows:

$$x_i = x_i(measured) \pm \delta x_i \text{ (95\% confidence)},$$

Where, δx_i is the uncertainty of variable x_i with a confidence interval that the measured value is within this uncertainty of 95%. The measured value x_i represents the observation in a single sample experiment or the mean of a data set in a multi-sample experiment.

According to Moffat (1988), the uncertainty is calculated as the Euclidean norm of the bias (B_{xi}) or fixed errors, and the precision (P_{xi}) or random errors.

$$\delta x_i = \sqrt{B_{xi}^2 + P_{xi}^2} \tag{A.1}$$

Let R be the result of an experiment calculated from a set of measurements. Let it be a function of n variables, $x_1, x_2, ..., x_n$ each with their own uncertainty value. Therefore, it is written mathematically as follows:

$$R = f(x_1, x_2, ..., x_n) \tag{A.2}$$

Assuming that the uncertainties of $x_1, x_2, ..., x_n$ are known, the effect of these uncertainties on the result R is as follows:

$$\delta R_{xi} = \frac{\partial R}{\partial x_i} \delta x_i$$

(A.3)

Here, the partial derivative of R is called the sensitivity coefficient of the result R with respect to x_i. The sensitivity coefficient is the effect that the uncertainty of a single measurement for the variable x_i, with the measurement being in error, has on the overall uncertainty of the result. Equation A.4 is derived by adding all the uncertainties of R to obtain a maximum overall uncertainty and using a root-sum-squared method.

$$\delta R_x = \left\{ \left(\frac{\partial R}{\partial x_1} \delta x_1 \right)^2 + \left(\frac{\partial R}{\partial x_2} \delta x_2 \right)^2 + ... + \left(\frac{\partial R}{\partial x_n} \delta x_n \right)^2 \right\}^{\frac{1}{2}}$$

(A.4)

Equation A.4 is referred to as the absolute uncertainty of R with the engineering units of R. It is only valid under the following conditions:

- Each measurement must be an independent variable.
- If measurements were repeated observations, they would display a Gaussian distribution.
- The uncertainty of each measurement was initially expressed at the confidence level.

If δx_i^2 are taken to be variances, Equation A.4 holds without the need for Gaussian distributed populations.

Some applications require the uncertainty estimate as a relative uncertainty of the result. This approach is simplified if the equation describing the result is of product form as in Equation A.5.

$$R = x_1^a x_2^b .... x_n^m$$

(A.5)

The relative uncertainty can then be found directly from the following:

$$\frac{\delta R}{R} = \left\{ \left(a \frac{\delta x_1}{x_1} \right)^2 + \left(b \frac{\delta x_2}{x_2} \right)^2 + ... + \left(m \frac{\delta x_n}{x_n} \right)^2 \right\}^{\frac{1}{2}}$$

(A.6)

The relative uncertainty of R is expressed as a percentage. In this formulation the exponent of x_i becomes the sensitivity coefficient (Moffat, 1988).

A.5   Quantifying uncertainties

Using the method of Kline and McClintock (1953), the uncertainties of each of the instruments are calculated for their usable ranges. The formulation of the equations used to calculate the uncertainties of all the calculated parameters according to the method of Kline and McClintock (1953) is shown in the following section.

A.5.1   Instruments

The three instruments types used, namely thermocouples, coriolis flow meters and pressure transducer, each had manufacturer's specified accuracy, which was the bias. The precision was obtained by capturing 120 data points. The standard deviation was found using these points and multiplied by two to fall within the 95% confidence interval. Table A.1 provides all the instruments with their ranges, bias, precision and total uncertainty.

Table A.1: Ranges and uncertainties of instruments used in the experimentation

Instrument	Range	Bias	Precision	Uncertainty
Thermocouple (T-type)	-200 – 350 °C	0.1 °C[8]	0.036 °C	0.106 °C
Coriolis flow meters	0 – 1.833 kg/s	0.1%[9]	0.09%	0.13%
	0 – 0.607 kg/s	0.1%[9]	0.05%	0.11%
Pressure transducer	0 – 2.2 kPa	0.25%[10]	2.19%	2.2%

---

[8] Calibrated with a PT 100 with an uncertainty of 0.01 °C.
[9] Percentage of reading.
[10] Percentage of full scale value.

The specifications of thermocouple, coriolis mass flow meters and pressure transducer are respectively presented in Tables A2, A3 and A4.

Thermocouple

Table A.2: Details of type-T thermocouple

Range:		-200 to 350 ℃
Material:	Positive:	Copper
	Negative:	Constantan
Color code	Positive:	Blue
	Negative:	Red

More information may be found on www.thermocoupleinfo.com

Coriolis Mass Flow Meter

Table A.3: Details of coriolis mass flow meters

Performance Specification		Standard	Optional
Range:	CMF025:	0 to 2180 kg/h	
	CMF050:	0 to 6800 kg/h	
Mass/volume flow accuracy:		±0.10% of rate	±0.05% of rate
Mass/volume flow repeatability:		±0.05% of rate	±0.025% of rate
Density accuracy:		±0.0005 g/cm^3	±0.0002 g/cm^3
Density repeatability:		±0.0002 g/cm^3	±0.0001 g/cm^3
Temperature accuracy:		±1 ℃ ±0.5% of reading	
Temperature repeatability:		±0.2 ℃	

More information may be found on www.emerson.com

Pressure Transducer

Table A.4: Details of DP15 Variable Reluctance Differential Pressure Transducer

Standard Ranges:		±0.08 psid FS to 3200 psi FS
Accuracy:		±0.25% FS (including effects of non-linearity, hysteresis and non-repeatability)
Overpressure:		200% FS up to 4000 psi maximum, with less than 0.5% zero shift
Line Pressure:		3200 psig operating
Line Pressure Effect:		Less than 1% FS zero shift/ 1000 psig
Output:		±35 mV/V full-scale nominal
Inductance:		20 mh nominal, each coil
Zero balance:		Within 5 mV/V
Excitation:	Rated:	5 Vrms, 3 kHz to 5 kHz
	Limits:	30 Vrms at 3 kHz
		1 kHz to 20 kHz with 20 mH coils
Temperature:	Operating:	-0.65 to 250 °F
	Specified:	0 to 160 °F
Thermal Zero Shift:		1% FS/100 °F typical
Thermal Sensitivity Shift:		2%/100 °F typical
Pressure Cavity Volume:		1.2×10^{-2} cu. in.
Volumetric Displacement:		6×10^{-4} cu. in.

More information may be found on www.validyne.com

A.5.2   Fluid and tube properties

All fluid properties and their associated uncertainties were calculated from the method of Popiel and Wojtkowiak (1998). Table A.**2**5 shows the uncertainties.

Table A.5: Uncertainty of fluid properties from the correlations of Popiel and Wojtkowiak (1998)

Fluid property	Uncertainty
Density	0.04%
Viscosity	1.00%
Specific heat	0.06%
Thermal conductivity	2.0%

The thermal conductivity of the copper tube was calculated using the method of Abu-Eishah (2001). The uncertainty of this method is given as 0.13%.

A.5.3   Inlet and outlet temperatures

The inlet and outlet of the inner tube were obtained using four thermocouples, while eight thermocouples were used for the annulus at the inlet and outlet. This was done to reduce the uncertainty of the relative temperature readings. The average temperature at a specific point, indicated by a location subscript as *xy*, where *x* is the flow passage and y is either the inlet or the outlet, was then obtained for all the inlets and outlets. Here the inlet of the inner tube is used for illustration.

$$\bar{T}_{ii} = \frac{T_{ii,1} + T_{ii,2} + ... + T_{ii,n}}{n}$$

(A.7)

The uncertainty was then determined by the following:

$$\delta \bar{T}_{ii} = \left\{ \left(\frac{\delta T_{ii,1}}{n} \right)^2 + \left(\frac{\delta T_{ii,2}}{n} \right)^2 + ... + \left(\frac{\delta T_{ii,n}}{n} \right)^2 \right\}^{\frac{1}{2}}$$

(A.8)

Since all the thermocouples are the same type and from the same source, all the uncertainties are equal:

$$\delta T_{ii,1} = \delta T_{ii,2} = ... = \delta T_{ii,n} = \delta T$$

(A.9)

Equation A.8 is then simplified further:

$$\delta \overline{T}_{ii} = \frac{\delta T}{\sqrt{n}}$$

(A.10)

This equation was used to calculate uncertainties for the inlet and outlet temperatures for an inner tube with $n = 4$ and an annular passage with $n = 8$.

The inner tube had two thermocouples at each of the nine stations, which were 550 mm apart, while the outer tube had eight stations also with two thermocouples. Therefore, their uncertainties were determined by Equation A.10, but with n values of 18 and 16 for the inner tube and the outer tube, respectively.

A.5.4   Temperature difference

In the calculations of experimental heat transfer, the temperature difference between the inlet and the outlet of both the inner tube and the annular passage are required. For the inner tube:

$$\Delta T_i = \overline{T}_{ii} - \overline{T}_{io}$$

(A.11)

and for the annular passage:

$$\Delta T_o = \overline{T}_{oo} - \overline{T}_{oi}$$

(A.12)

The uncertainty for the temperature difference of the inner tube is given by the following:

$$\delta \Delta T_i = \sqrt{\delta \overline{T}_{ii}^2 + \delta \overline{T}_{io}^2}$$

(A.13)

and for the annular passage:

$$\delta \Delta T_o = \sqrt{\delta \overline{T}_{oo}^2 + \delta \overline{T}_{oi}^2}$$

(A.14)

A.5.5   Logarithmic mean temperature difference (LMTD)

LMTD is defined numerically as follows:

$$\Delta T_{lm} = \frac{\left(\overline{T}_{ii} - \overline{T}_{oo}\right) - \left(\overline{T}_{io} - \overline{T}_{oi}\right)}{\ln\left[\left(\overline{T}_{ii} - \overline{T}_{oo}\right)/\left(\overline{T}_{io} - \overline{T}_{oi}\right)\right]} \tag{A.15}$$

Let $\left(\overline{T}_{ii} - \overline{T}_{oo}\right) = \overline{T}_1$ and $\left(\overline{T}_{io} - \overline{T}_{oi}\right) = \overline{T}_2$. Then Equation A.15 becomes the following:

$$\Delta T_{lm} = \frac{\left(\overline{T}_1 - \overline{T}_2\right)}{\ln\left(\overline{T}_1/\overline{T}_2\right)} \tag{A.16}$$

Uncertainty for LMTD is determined by the following:

$$\delta T_{lm} = \left\{\left(\frac{\partial T_{lm}}{\partial \overline{T}_{ii}}\delta \overline{T}_{ii}\right)^2 + \left(\frac{\partial T_{lm}}{\partial \overline{T}_{oo}}\delta \overline{T}_{oo}\right)^2 + \left(\frac{\partial T_{lm}}{\partial \overline{T}_{io}}\delta \overline{T}_{io}\right)^2 + \left(\frac{\partial T_{lm}}{\partial \overline{T}_{oi}}\delta \overline{T}_{oi}\right)^2\right\}^{\frac{1}{2}} \tag{A.17}$$

Expanding Equation A.17 results in the following:

$$\delta T_{lm} = \left[\begin{array}{l}\left(\left\{\dfrac{1}{\ln\left(T_1/T_2\right)} - \dfrac{\left(T_1 - T_2\right)}{\ln\left(T_1/T_2\right)^2 T_1}\right\}\delta \overline{T}_{ii}\right)^2 + \left(\left\{-\dfrac{1}{\ln\left(T_1/T_2\right)} + \dfrac{\left(T_1 - T_2\right)}{\ln\left(T_1/T_2\right)^2 T_1}\right\}\delta \overline{T}_{oo}\right)^2 \\[4mm] + \left(\left\{-\dfrac{1}{\ln\left(T_1/T_2\right)} + \dfrac{\left(T_1 - T_2\right)}{\ln\left(T_1/T_2\right)^2 T_2}\right\}\delta \overline{T}_{io}\right)^2 + \left(\left\{\dfrac{1}{\ln\left(T_1/T_2\right)} - \dfrac{\left(T_1 - T_2\right)}{\ln\left(T_1/T_2\right)^2 T_2}\right\}\delta \overline{T}_{oi}\right)^2\end{array}\right]^{\frac{1}{2}} \tag{A.18}$$

A.5.6   Heat transfer rate

A.5.6.1   Inner tube

The heat transfer rate of the inner tube is calculated as follows:

$$\dot{Q}_i = \dot{m}_i C_{p,i}\Delta T_i \tag{A.19}$$

With the uncertainties determined by the following:

$$\delta\dot{Q}_i = \left\{ \left(\frac{\partial \dot{Q}_i}{\partial \dot{m}_i} \delta\dot{m}_i \right)^2 + \left(\frac{\partial \dot{Q}_i}{\partial C_{p,i}} \delta C_{p,i} \right)^2 + \left(\frac{\partial \dot{Q}_i}{\partial \Delta T_i} \delta\Delta T_i \right)^2 \right\}^{\frac{1}{2}}$$

$$= \left\{ \left(C_{p,i} \Delta T_i \delta\dot{m}_i \right)^2 + \left(\dot{m}_i \Delta T_i \delta C_{p,i} \right)^2 + \left(\dot{m}_i C_{p,i} \delta\Delta T_i \right)^2 \right\}^{\frac{1}{2}}$$

(A.20)

A.5.6.2   Annular passage

The heat transfer rate of the annulus is calculated as follows:

$$\dot{Q}_o = \dot{m}_o C_{p,o} \Delta T_o$$

(A.21)

With the uncertainties determined by the following:

$$\delta\dot{Q}_o = \left\{ \left(\frac{\partial \dot{Q}_o}{\partial \dot{m}_o} \delta\dot{m}_o \right)^2 + \left(\frac{\partial \dot{Q}_o}{\partial C_{p,o}} \delta C_{p,o} \right)^2 + \left(\frac{\partial \dot{Q}_o}{\partial \Delta T_o} \delta\Delta T_o \right)^2 \right\}^{\frac{1}{2}}$$

$$= \left\{ \left(C_{p,o} \Delta T_o \delta\dot{m}_o \right)^2 + \left(\dot{m}_o \Delta T_o \delta C_{p,o} \right)^2 + \left(\dot{m}_o C_{p,o} \delta\Delta T_o \right)^2 \right\}^{\frac{1}{2}}$$

(A.22)

A.5.7   Annulus heat transfer coefficient

The annulus heat transfer coefficient is defined as follows:

$$h_o = \frac{\dot{Q}_o}{A_{so} \Delta T_{LMTD}}$$

(A.23)

With the uncertainties determined by the following:

$$\delta h_o = \left\{ \left(\frac{\partial h_o}{\partial \dot{Q}_o} \delta \dot{Q}_o \right)^2 + \left(\frac{\partial h_o}{\partial A_{so}} \delta A_{so} \right)^2 + \left(\frac{\partial h_o}{\partial \Delta T_{LMTD}} \delta \Delta T_{LMTD} \right)^2 \right\}^{\frac{1}{2}}$$

$$= \left\{ \left(\frac{1}{A_{so} \Delta T_{LMTD}} \delta \dot{Q}_o \right)^2 + \left(-\frac{\dot{Q}_o}{A_{so}^2 \Delta T_{LMTD}} \delta A_{so} \right)^2 + \left(-\frac{\dot{Q}_o}{A_{so} \Delta T_{LMTD}^2} \delta \Delta T_{LMTD} \right)^2 \right\}^{0.5}$$

$$(A.24)$$

A.5.8 Physical dimensions

Tube diameters and other smaller dimensions were measured by a Vernier calliper with an uncertainty of 20 µm. The larger dimensions, like the axial length of the tubes, were measured by a measuring tape with an uncertainty of 1 mm.

A.5.8.1 Hydraulic diameter

The hydraulic diameter is defined as follows:

$$D_h = D_0 - D_1 \tag{A.25}$$

With the uncertainties determined by the following:

$$\delta D_h = \left\{ \left(\frac{\partial D_h}{\partial D_0} \delta D_0 \right)^2 + \left(\frac{\partial D_h}{\partial d D_1} \delta D_1 \right)^2 \right\}^{\frac{1}{2}}$$

$$= \left\{ (\delta D_0)^2 + (-\delta D_1)^2 \right\}^{\frac{1}{2}}$$

$$(A.26)$$

A.5.8.2 Heat transfer area

The inner heat transfer area is defined by the following:

$$A_{si} = \pi d_i L_h \tag{A.27}$$

With the uncertainties determined as follows:

$$\delta A_{si} = \left\{ \left(\frac{\partial A_{si}}{\partial d_i} \delta d_i \right)^2 + \left(\frac{\partial A_{si}}{\partial L_h} \delta L_h \right)^2 \right\}^{\frac{1}{2}}$$

$$= \left\{ \left(\pi L_h \delta d_i \right)^2 + \left(\pi d_i \delta L_h \right)^2 \right\}^{\frac{1}{2}} \qquad (A.28)$$

Similarly, the outer heat transfer area is determined by the following:

$$\delta A_{so} = \left\{ \left(\pi L_h \delta d_o \right)^2 + \left(\pi d_o \delta L_h \right)^2 \right\}^{0.5} \qquad (A.29)$$

A.5.8.3   Inner tube cross-sectional area

The cross-sectional area is defined as follows:

$$A_i = \frac{\pi}{4} d_i^2 \qquad (A.30)$$

With the uncertainties determined by the following:

$$\delta A_i = \left\{ \left(\frac{\partial A_i}{\partial d_i} \delta d_i \right)^2 \right\}^{\frac{1}{2}}$$

$$= \left(\frac{\pi}{2} d_i \delta d_i \right) \qquad (A.31)$$

The annulus cross-sectional area is defined as follows:

$$A_o = \frac{\pi}{4} \left(D_i^2 - d_o^2 \right) \qquad (A.32)$$

With the uncertainties determined by the following:

$$\delta A_o = \left\{ \left(\frac{\partial A_o}{\partial D_i} \delta D_i \right)^2 + \left(\frac{\partial A_o}{\partial d_o} \delta d_o \right)^2 \right\}^{\frac{1}{2}}$$

$$= \left\{ \left(\frac{\pi}{2} D_i \delta D_i \right)^2 + \left(\frac{\pi}{2} d_o \delta d_o \right)^2 \right\}^{\frac{1}{2}} \tag{A.33}$$

A.5.9   Reynolds number

The Reynolds number in the inner tube is defined as follows:

$$\mathrm{Re}_i = \frac{\dot{m}_i d_i}{A_i \mu_i} \tag{A.34}$$

With the uncertainties determined by the following:

$$\delta \mathrm{Re}_i = \left\{ \left(\frac{\partial \mathrm{Re}_i}{\partial \dot{m}_i} \delta \dot{m}_i \right)^2 + \left(\frac{\partial \mathrm{Re}_i}{\partial d_i} \delta d_i \right)^2 + \left(\frac{\partial \mathrm{Re}_i}{\partial A_i} \delta A_i \right)^2 + \left(\frac{\partial \mathrm{Re}_i}{\partial \mu_i} \delta \mu_i \right)^2 \right\}^{\frac{1}{2}}$$

$$= \left\{ \left(\frac{d_i}{A_i \mu_i} \delta \dot{m}_i \right)^2 + \left(\frac{\dot{m}_i}{A_i \mu_i} \delta d_i \right)^2 + \left(-\frac{\dot{m}_i d_i}{A_i^2 \mu_i} \delta A_i \right)^2 + \left(-\frac{\dot{m} d_i}{A_i \mu_i^2} \delta \mu_i \right)^2 \right\}^{\frac{1}{2}} \tag{A.35}$$

Similarly, the Reynolds number in the annulus is determined by the following:

$$\delta \mathrm{Re}_{D_h} = \left\{ \left(\frac{D_h}{A_o \mu_o} \delta \dot{m}_o \right)^2 + \left(\frac{\dot{m}_o}{A_o \mu_o} \delta D_h \right)^2 + \left(-\frac{\dot{m}_o D_h}{A_o^2 \mu_o} \delta A_o \right)^2 + \left(-\frac{\dot{m}_o D_h}{A_o \mu_o^2} \delta \mu_o \right)^2 \right\}^{\frac{1}{2}} \tag{A.36}$$

A.5.10   Nusselt number

The Nusselt number in the annulus is defined as follows:

$$Nu_{D_h} = \frac{h_o D_h}{k_o} \qquad (A.37)$$

With uncertainties determined by the following:

$$\delta Nu_{D_h} = \left\{ \left(\frac{\partial Nu_{D_h}}{\partial h_o} \delta h_o \right)^2 + \left(\frac{\partial Nu_{D_h}}{\partial D_h} \delta D_h \right)^2 + \left(\frac{\partial Nu_{D_h}}{\partial k_o} \delta k_o \right)^2 \right\}^{\frac{1}{2}}$$

$$= \left\{ \left(\frac{h_o}{k_o} \delta D_h \right)^2 + \left(\frac{D_h}{k_o} \delta h_o \right)^2 + \left(-\frac{h_o D_h}{k_o^2} \delta k_o \right)^2 \right\}^{\frac{1}{2}} \qquad (A.38)$$

A.5.11   Friction factor

The friction factor in the annulus is expressed as follows:

$$f = \frac{2 D_h \Delta P \rho_o A_o^2}{L_{hp} \dot{m}_o^2} \qquad (A.39)$$

The uncertainty is determined from the following:

$$\delta f = \left\{ \begin{array}{l} \left[\left(\frac{\partial f}{\partial D_h} \delta D_h \right)^2 + \left(\frac{\partial f}{\partial \Delta P} \delta \Delta P \right)^2 + \left(\frac{\partial f}{\partial \rho_o} \delta \rho_o \right)^2 + \left(\frac{\partial f}{\partial A_o} \delta A_o \right)^2 \right]^{\frac{1}{2}} \\ + \left(\frac{\partial f}{\partial L_{hp}} \delta L_{hp} \right)^2 + \left(\frac{\partial f}{\partial \dot{m}_o} \delta \dot{m}_o \right)^2 \end{array} \right\}$$

$$
= \left\{
\begin{array}{l}
\left(\dfrac{2\Delta P \rho_o A_o^2}{L_{hp} \dot{m}_o^2} \delta D_h \right)^2 + \left(\dfrac{2 D_h \rho_o A_o^2}{L_{hp} \dot{m}_o^2} \delta \Delta P \right)^2 + \left(\dfrac{2 D_h \Delta P A_o^2}{L_{hp} \dot{m}_o^2} \delta \rho_o \right)^2 \\[4ex]
+ \left(\dfrac{2 D_h \Delta P \rho_o}{L_{hp} \dot{m}_o^2} \delta A_o^2 \right)^2 + \left(-\dfrac{2 D_h \Delta P \rho_o A_o^2}{L_{hp}^2 \dot{m}_o^2} \delta L_{hp} \right)^2 + \left(-\dfrac{2 D_h \Delta P \rho_o A_o^2}{L_{hp} \dot{m}_o^3} \delta \dot{m}_o \right)^2
\end{array}
\right\}^{\frac{1}{2}}
\tag{A.40}
$$

A.6   References

Abu-Eishah, S.I. 2001. Correlations for the thermal conductivity of metals as a function of temperature, *International Journal of Thermophysics*, 22 (6), pp 1855–1868.

Coblentz, L.C. 2002. Uncertainty analysis of heat exchangers. Master's dissertation, University of Johannesburg.

Kline, F.J., and McClintock, F.F. 1953. Describing uncertainties in single sample experiments, *Mechanical Engineering,* 75, pp 2–8.

Moffat, R.J. 1988. Describing the uncertainty in experimental results. *Experimental Thermal Fluid Science,* 105, pp 498–504.

Popiel, C.O., and Wojtkowiak, J. 1998. Simple formulas for thermophysical properties of liquid water for heat transfer calculations (from 0 ˚C to 150 ˚C), *Heat Transfer Engineering,* 19, pp 87–101.

Appendix B

Results of the influence of the degree of wall temperature uniformity

B.1 Introduction

In this study, the characteristics of the transition flow regime in the annuli of horizontal concentric tube-in-tube heat exchangers was investigated. In Chapter 6, the results of the influence of the degree of wall temperature uniformity on the heat transfer coefficients, friction factors and Reynolds number limits of transition regime for a test section (TS 1) were presented. The results of the other three test sections (TS 2, TS 3 and TS 4) are presented in this appendix based on the isothermal and the three inner wall thermal boundaries that were considered. The correlations based on the degree of wall temperature uniformity are also presented for each of the test sections. The details of these test sections and all calculations and methods used to obtain the respective results are provided in the main text.

Since the flow comprised secondary flows, it was necessary to have a good knowledge of the convection types that were present in the flow regimes. For this purpose, the Richardson numbers for all the relevant data points were calculated and used to determine the approximate cut-off points between the forced, mixed and natural convection types.

B.2 Test Section 2

Test Section 2 (TS 2) had a hydraulic diameter of $D_h = 23$ mm, annular diameter ratio of $a = 0.409$ and a length-to-hydraulic diameter ratio of $L_{hx}/D_h = 221$.

B.2.1 Distribution of convection flow types

Convection types were analysed in order to have a better understanding of the behaviour of the span of the transition flow regime, heat transfer and pressure drop. Figure B.**1** shows the distribution of convection types along the laminar, transition and turbulent flow regimes by using the Richardson number method. The lower and upper Reynolds number limits of the transition

regime in Figure B.1 are the averages for all the lower and upper Reynolds number limits of this test section's transition regime.
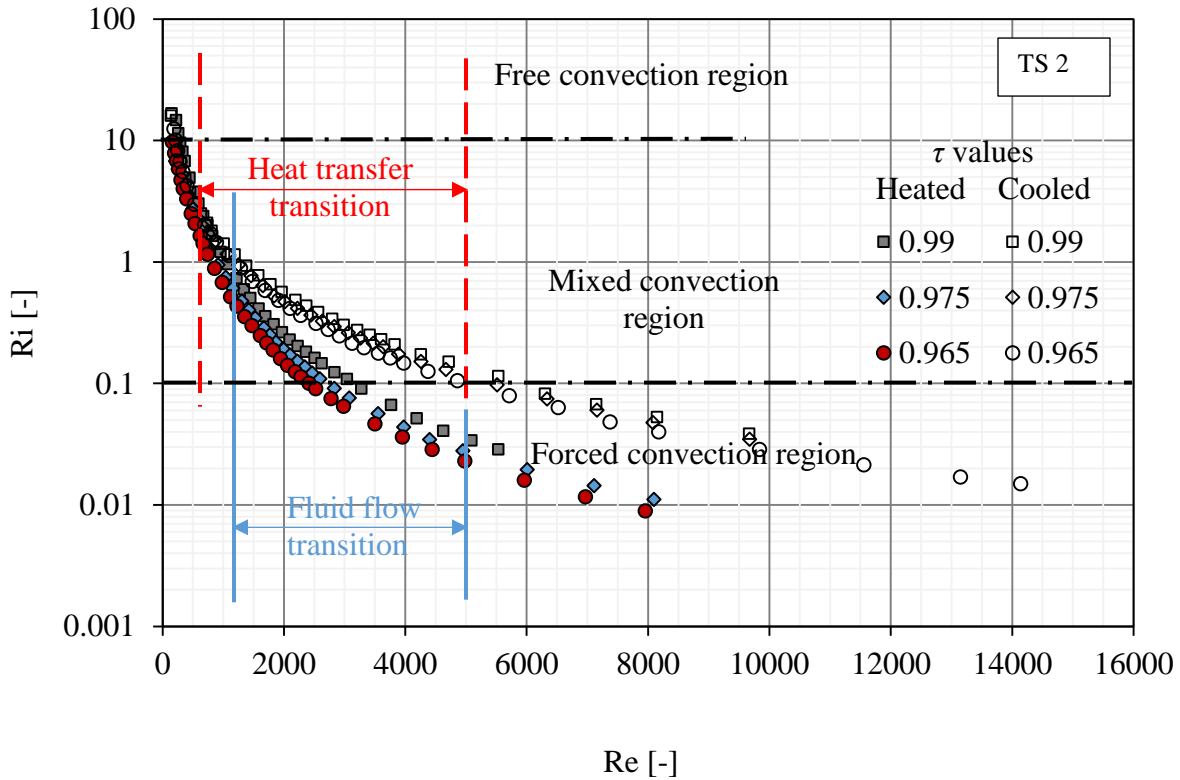

Figure B.1: The distribution of convection types along the laminar, transition and turbulent flow regimes for TS 2

B.2.2   Transition flow regime Reynolds number spans

Figure B.**2**a and Figure B.**2**b show the spans of the Reynolds number transition range based on the heat transfer coefficient and the friction factor, respectively. The Reynolds number limits of the transition regime for the heated and cooled annulus cases depend on the degree of wall temperature uniformity, τ.

a)

b)
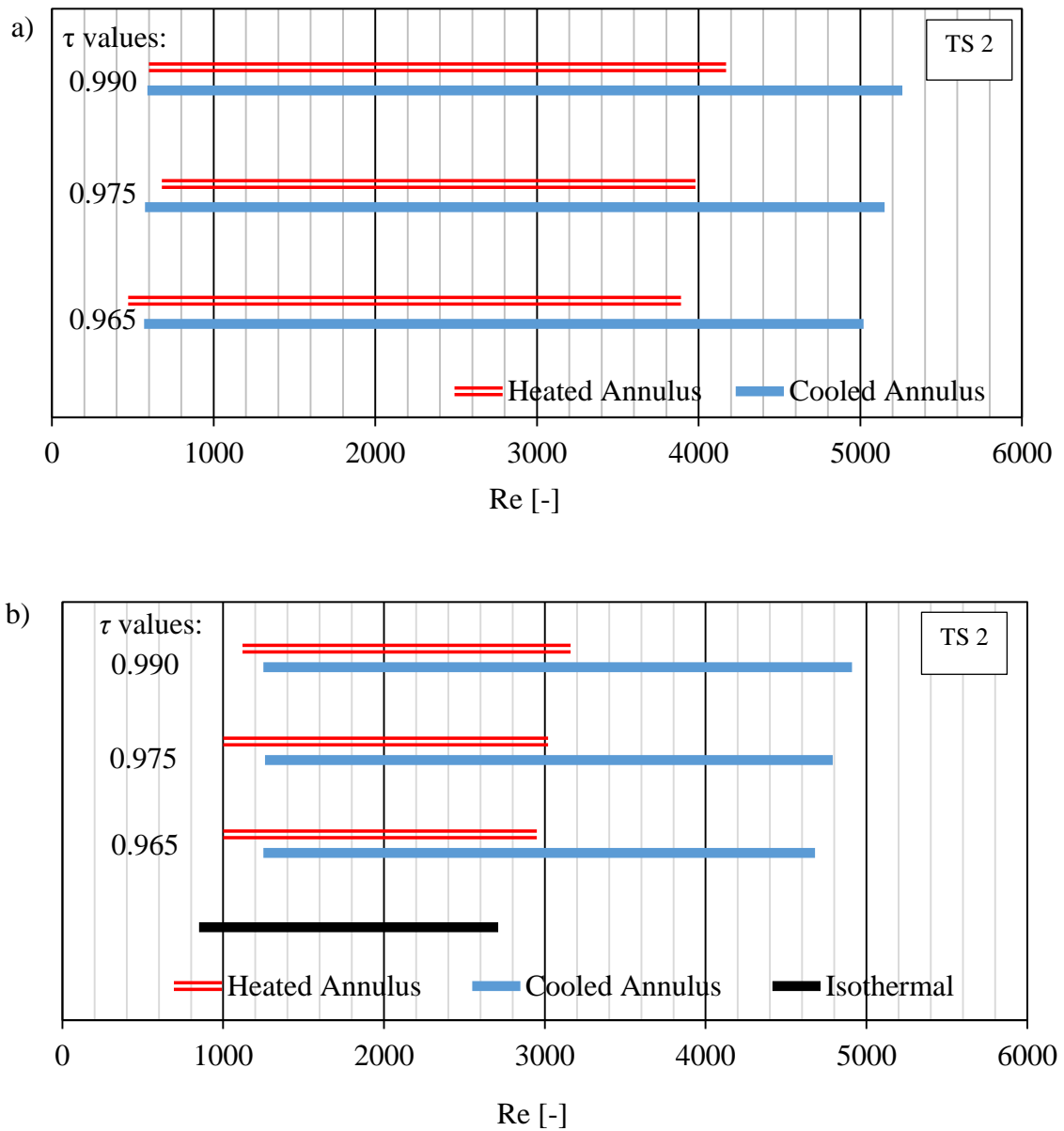
Figure B.2: A graphical representation of transition ranges for (a) heat transfer and (b) fluid flow for TS 2

B.2.3   Heat transfer coefficient

The mean heat transfer coefficient for the cooled and heated annulus cases were calculated with the mean logarithmic mean temperature difference (LMTD) method. Figure B.**3** and Figure

B.**4** give the heat transfer coefficients expressed in terms of the Nusselt number and the Colburn *j*-factor, respectively.

In the transition regime (refer to Figure B.**3**) at a Reynolds number of 2000, the Nusselt numbers for wall temperature uniformities of 0.975 and 0.965 of a heated annulus case were 3.4% and 7.9% lower than the $\tau = 0.99$ case, respectively. For the cooled annulus case, the Nusselt numbers for the wall temperature uniformities of 0.975 and 0.965 were 0.5% and 1.7% lower than for the $\tau = 0.99$ case, respectively.
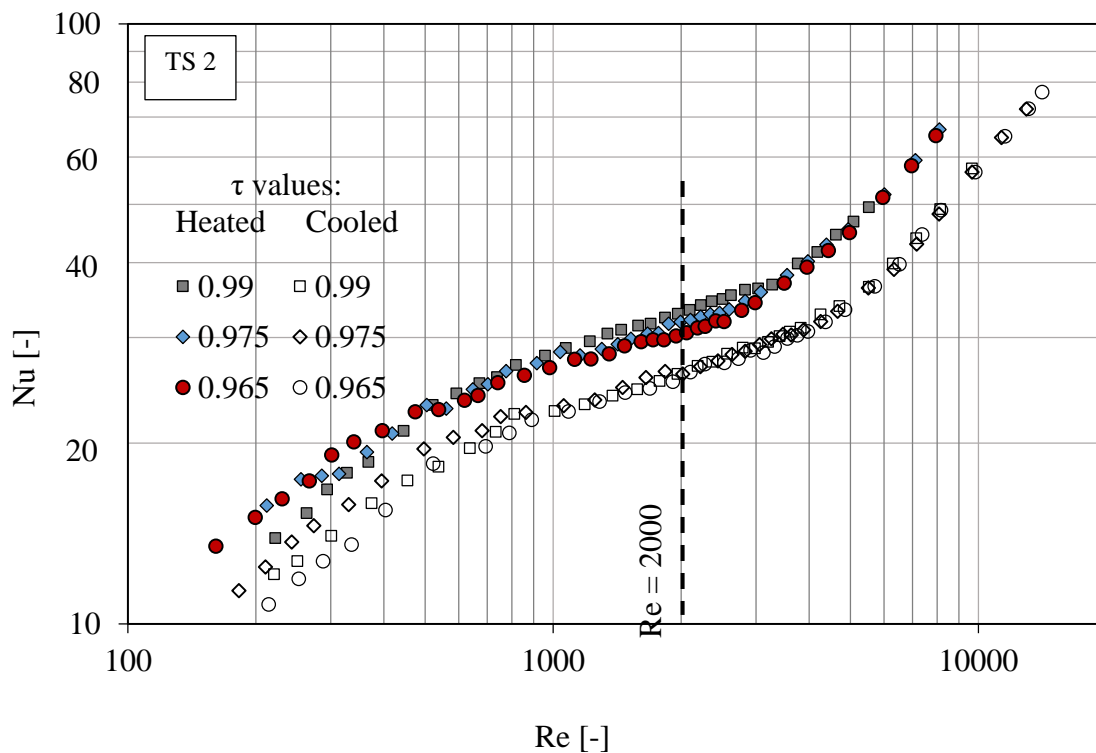
Figure B.3: Nusselt numbers for the heated and cooled annulus cases for different degrees of temperature uniformity on the inner wall for TS 2
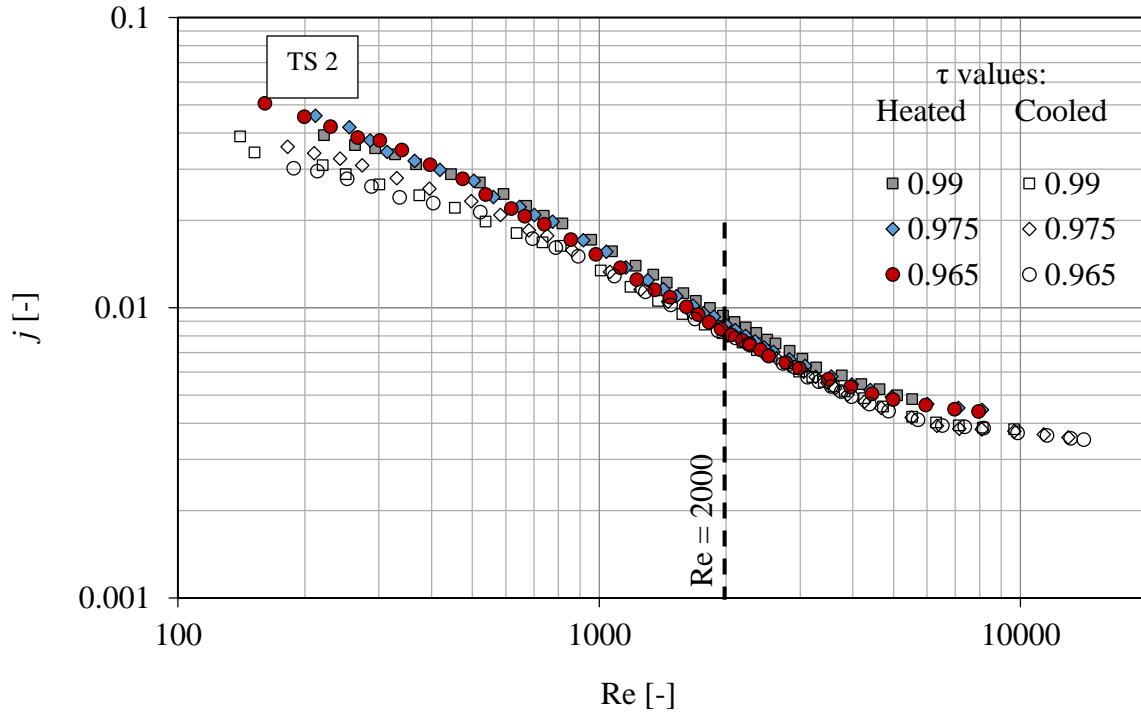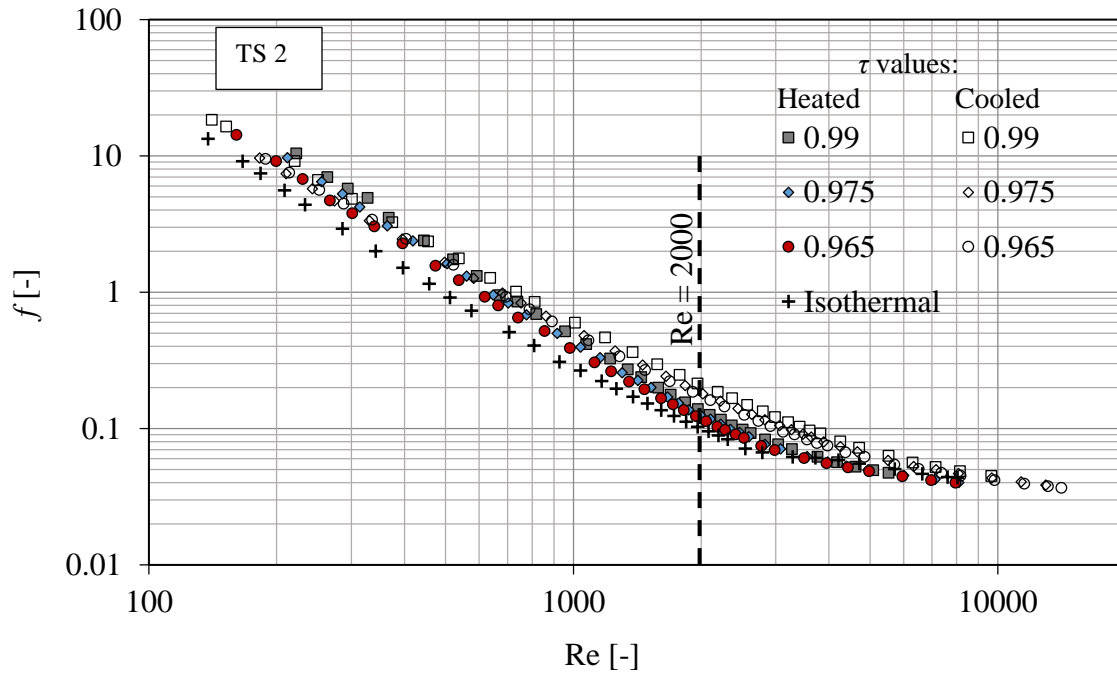
Figure B.4: Colburn *j*-factors for the heated and cooled annulus cases for different degrees of temperature uniformity on the inner wall for TS 2

In the transition regime (refer to Figure B.4) at a Reynolds number of 2000, the Colburn *j*-factor for wall temperature uniformities of 0.975 and 0.965 of a heated annulus case were 5.6% and 10.89% lower than the $\tau = 0.99$ case, respectively. For the cooled annulus case, the Nusselt numbers for the wall temperature uniformities of 0.975 and 0.965 were 0.5% and 0.6% higher than for the $\tau = 0.99$ case, respectively.

At a Reynolds number of 2 000, the Nusselt numbers for the heated cases at $\tau = 0.99$, 0.975 and 0.965 were 26%, 22% and 18%, higher than for the cooled case counterparts, respectively. The Colburn *j*-factors for the heated annulus for $\tau = 0.99$, 0.975 and 0.965 were +15%, +4% and +2% higher than for the cooled annulus counterparts, respectively.

B.2.4   Friction factor

The mean friction factors for the cooled, heated and isothermal annulus cases were calculated from the pressure drop measurement between the inlet and the outlet of the annular passage and are plotted against the Reynolds number, as shown in Figure B.**5**.

Figure B.5: Friction factors for heated, cooled and isothermal annulus cases for different degrees of temperature uniformity on the inner wall for TS 2

At a Reynolds number of 2 000, the average friction factor for the heated cases with τ values of 0.99, 0.975 and 0.965 were 35%, 24% and 18% higher than for the isothermal case, respectively. For the cooled annulus cases, the average friction factors for τ values of 0.99, 0.975 and 0.965 were 108%, 82% and 73% higher than for the isothermal case, respectively.

B.3 Test Section 3

Test Section 3 (TS 3) had a hydraulic diameter of $D_h = 20.2$ mm, an annular diameter ratio of $a = 0.386$ and a length-to-hydraulic diameter ratio of $L_{hx}/D_h = 251$.

B.3.1 Distribution of convection types

Convection types were analysed in order to have a better understanding of the behaviour of the span of transition regime, heat transfer and pressure drop. Figure B.6 shows the distribution of convection types along the laminar, transition and turbulent regimes using the Richardson number method. The lower and upper Reynolds number limits of the transition regime in Figure B.6 are the averages for all the lower and upper Reynolds number limit data of the transition regime of this test section.
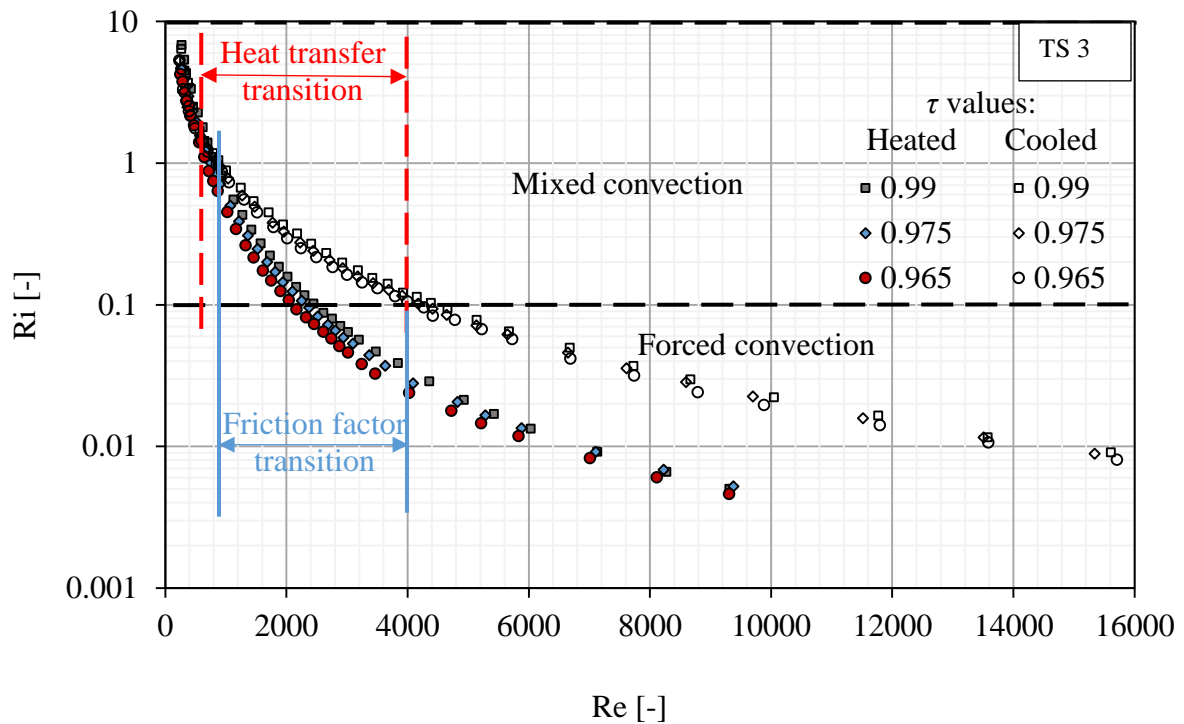
Figure B.6: The distribution of convection types along the laminar, transition and turbulent regimes for TS3

B.3.2 Transition flow regime Reynolds number spans

Figure B.**7**a and Figure B.**7**b show the spans of the Reynolds number transition range based on heat transfer and friction factor, respectively. The Reynolds number limits of the transition regime for the heated and cooled annulus cases depend on the degree of wall temperature uniformity, τ.
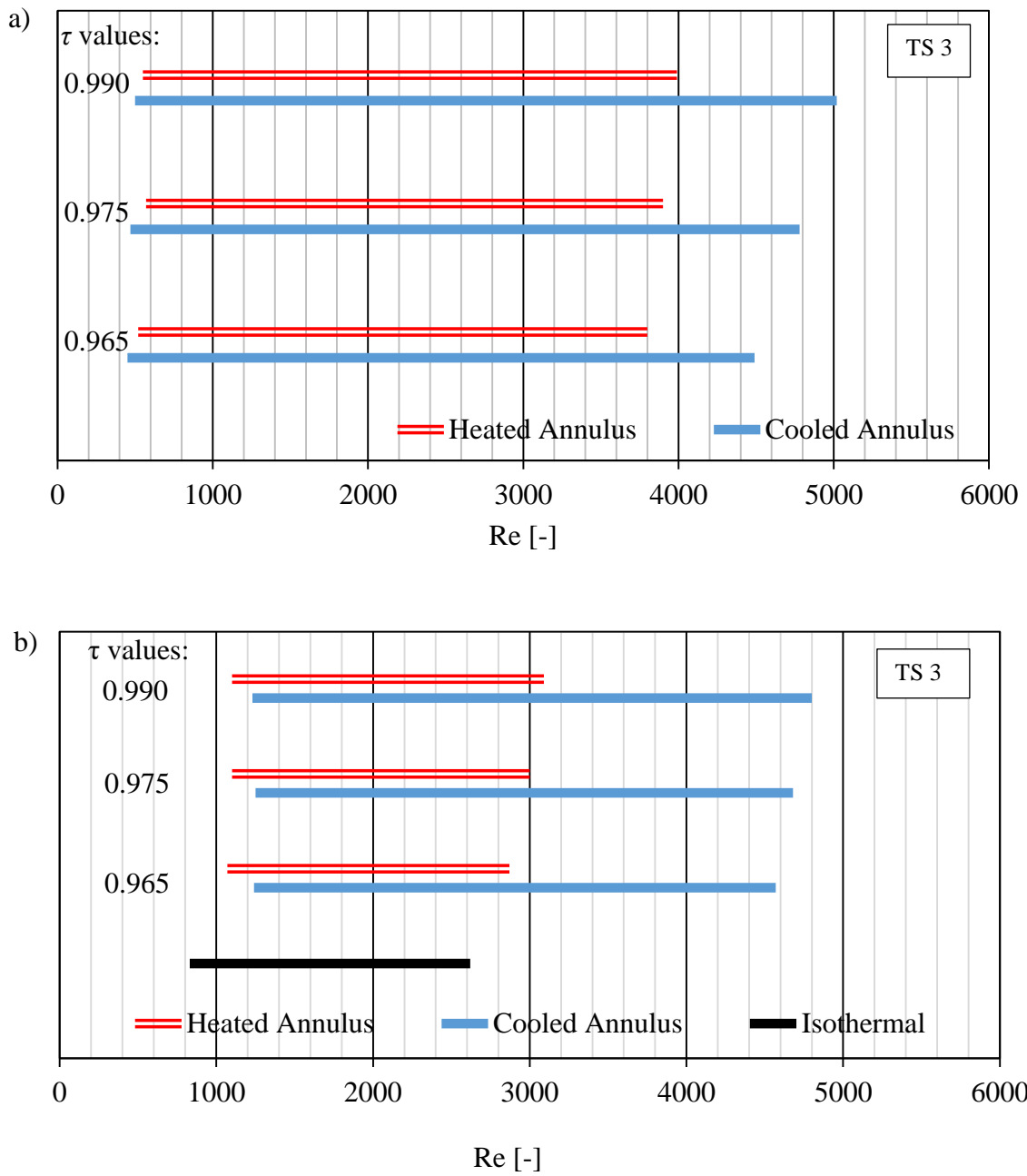
Figure B.7: A graphical representation of transition ranges for (a) heat transfer and (b) friction factor for TS 3

B.3.3 Heat transfer coefficient

The mean heat transfer coefficient for the cooled and heated annulus cases was calculated using the mean LMTD method. Figure B.8 and Figure B.9 give the heat transfer coefficients expressed in terms of the Nusselt number and the Colburn *j*-factor, respectively.
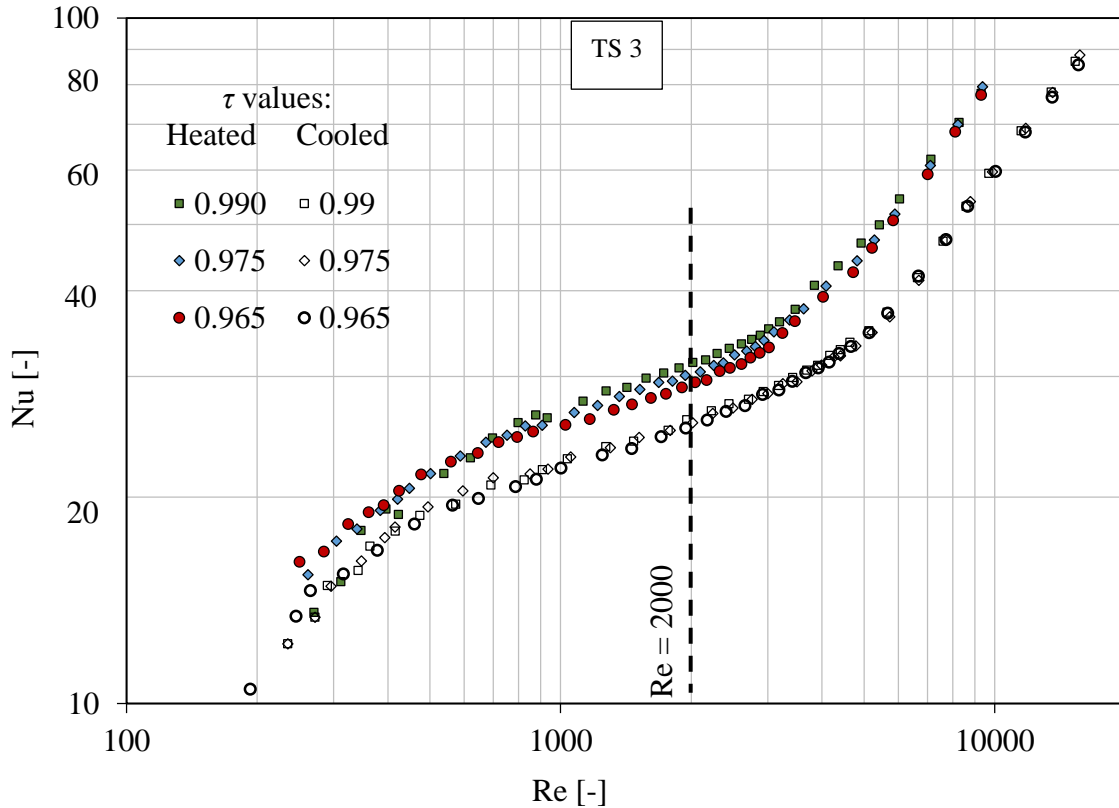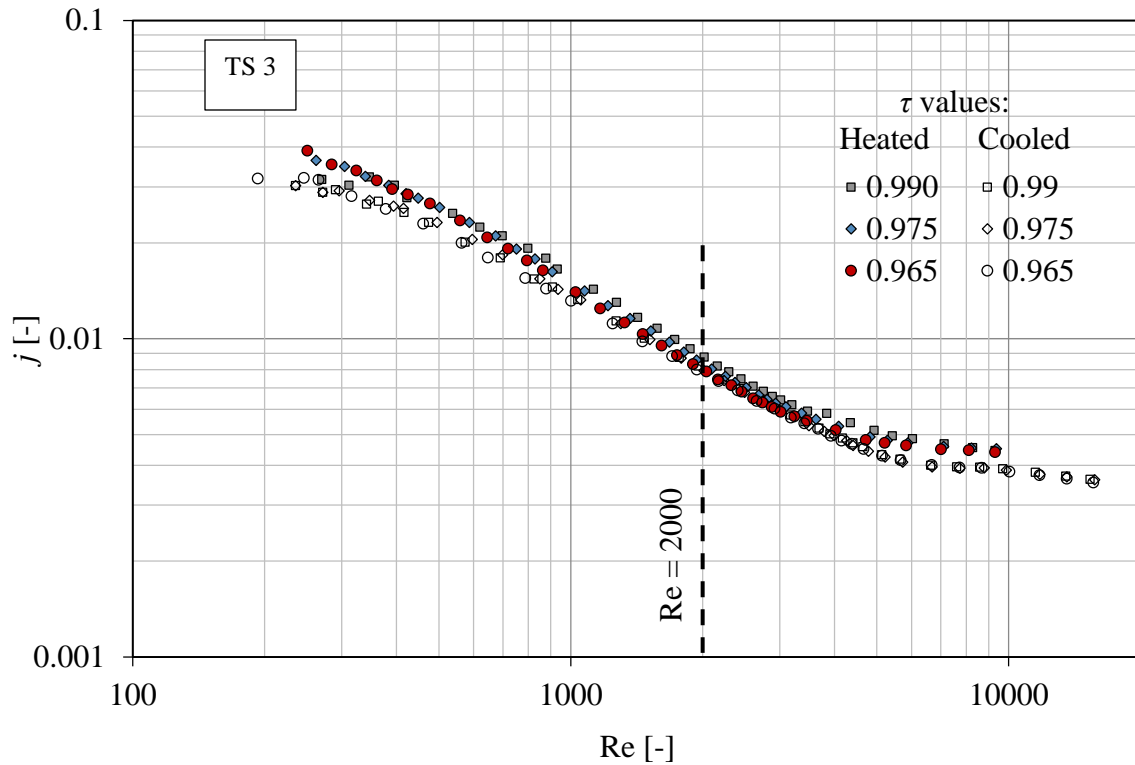

Figure B.8: The Nusselt numbers for heated and cooled annulus cases for different degrees of temperature uniformity on the inner wall for TS 3

In the transition regime (refer to Figure B.8) at a Reynolds number of 2 000, the Nusselt numbers for wall temperature uniformities of 0.975 and 0.965 for a heated annulus case were 3.5% and 6.7% lower than for the $\tau = 0.99$ case, respectively. For the cooled annulus case, the Nusselt numbers for the wall temperature uniformities of 0.975 and 0.965 were 0.6% and 1.9% lower than for the $\tau = 0.99$ case, respectively.

Figure B.9: Colburn *j*-factors for the heated and cooled annulus cases for different degrees of temperature uniformity on the inner wall

In the transition regime (refer to Figure B.9) at a Reynolds number of 2000, the Colburn *j*-factor for wall temperature uniformities of 0.975 and 0.965 of a heated annulus case were 5.2% and 9.2% lower than for the $\tau = 0.99$ case, respectively. For the cooled annulus case, the Nusselt numbers for the wall temperature uniformities of 0.975 and 0.965 were 1.9% and 3.1% lower than for the $\tau = 0.99$ case, respectively.

At a Reynolds number of 2 000, the Nusselt numbers for the heated cases with $\tau = 0.99$, 0.975 and 0.965 were 18%, 15% and 12% higher, respectively, than for the cooled case counterparts. The Colburn *j*-factors for the heated annulus cases with $\tau = 0.99$, 0.975 and 0.965 were +12%, +4 and +0.4% higher than for the cooled annulus counterparts, respectively.

B.3.4 Friction factor

The mean friction factors for cooled, heated and isothermal annulus cases were calculated from the pressure drop measurement between the inlet and outlet of the annular passage and are plotted against the Reynolds number as shown in B.10.
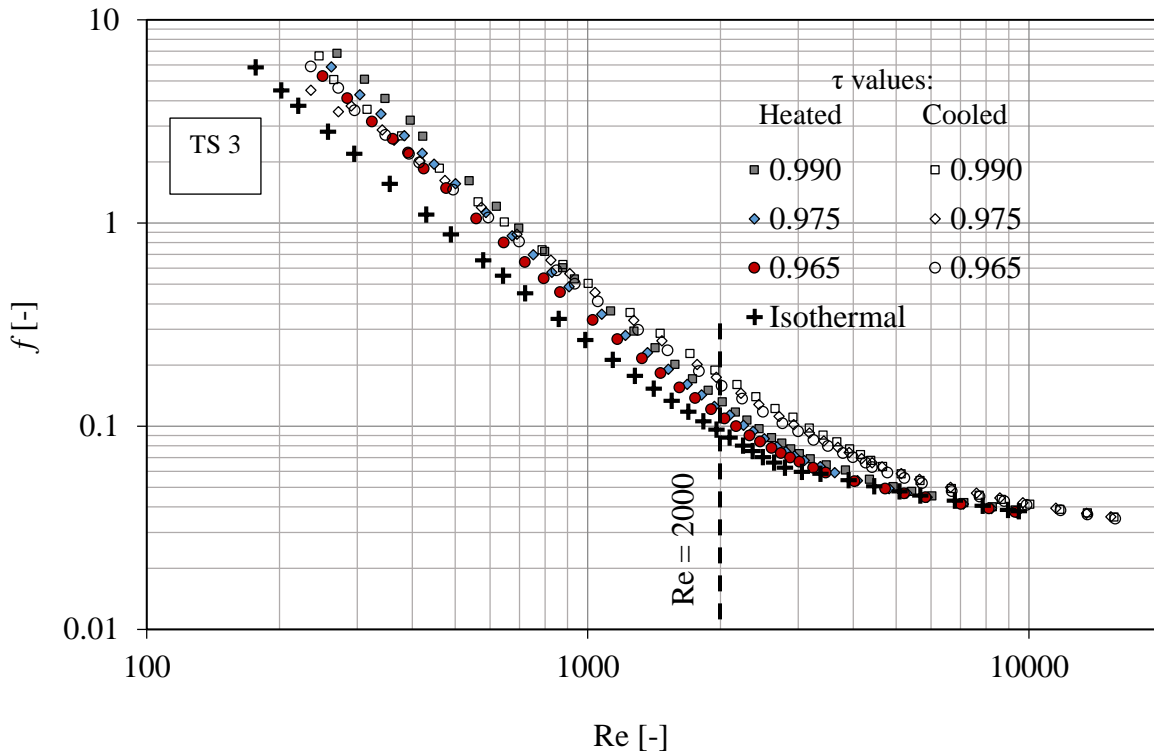

Figure B.10: Friction factors for the heated, cooled and isothermal annulus cases for different degrees of temperature uniformity on the inner wall for TS 3

At a Reynolds number of 2 000, the average friction factors for the heated cases with τ values of 0.99, 0.975 and 0.965 were 43%, 29% and 20% higher than for the isothermal case, respectively. For the cooled annulus cases, the average friction factors for τ values of 0.99, 0.975 and 0.965 were 94%, 81% and 70% higher than for the isothermal case, respectively.

B.4 Test Section 4

Test Section 4 (TS 4) had a hydraulic diameter of $D_h = 17$ mm, annular diameter ratio of $a = 0.483$ and a length-to-hydraulic diameter ratio of $L_{hx}/D_h = 299$.

B.4.1   Distribution of convection flow types

Convection types were analysed in order to have a better understanding of the behaviour of the span of transition regime, heat transfer and pressure drop. Figure B.11 shows the distribution of convection types along the laminar, transition and turbulent regimes by using the Richardson number method. The lower and upper Reynolds number limits of transition regime in Figure B.11 are the averages for all the lower and upper Reynolds number limit data of the transition regime of this test section.
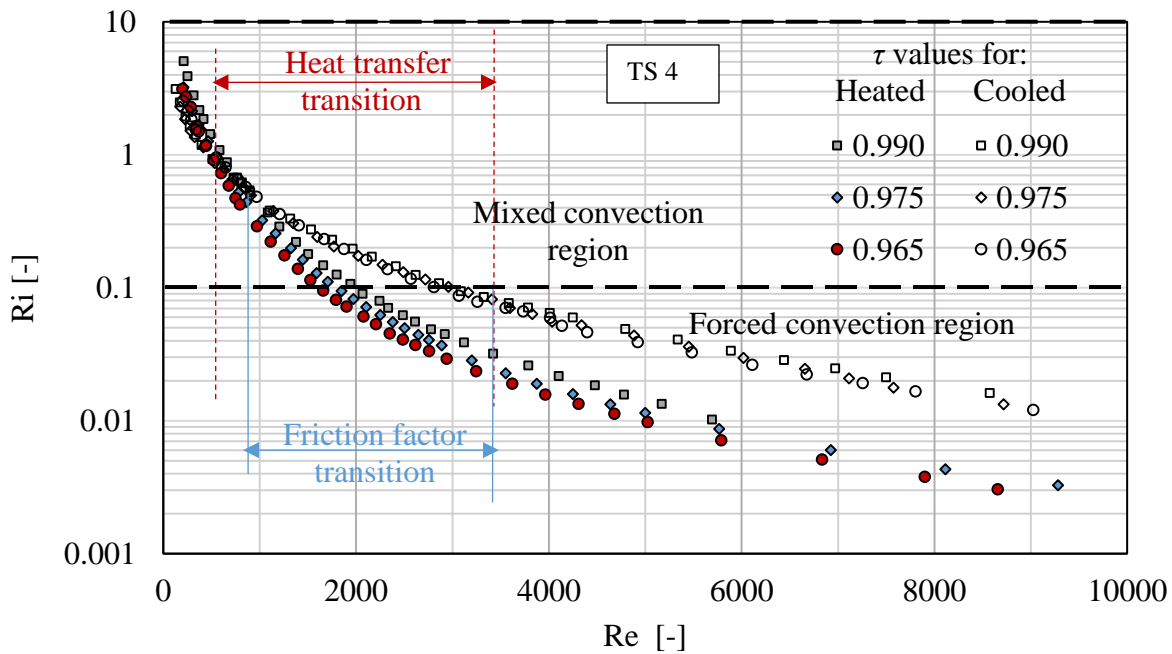
Figure B.11: Distribution of convection types along the laminar, transition and turbulent regimes for TS 4

B.4.2   Transition flow regime Reynolds number spans

Figure B.12a and Figure B.12b show the Reynolds number spans of the transition range based on the heat transfer coefficient and friction factor, respectively. The Reynolds number limits of the transition regime for the heated and cooled annulus cases depend on the degree of wall temperature uniformity, τ.
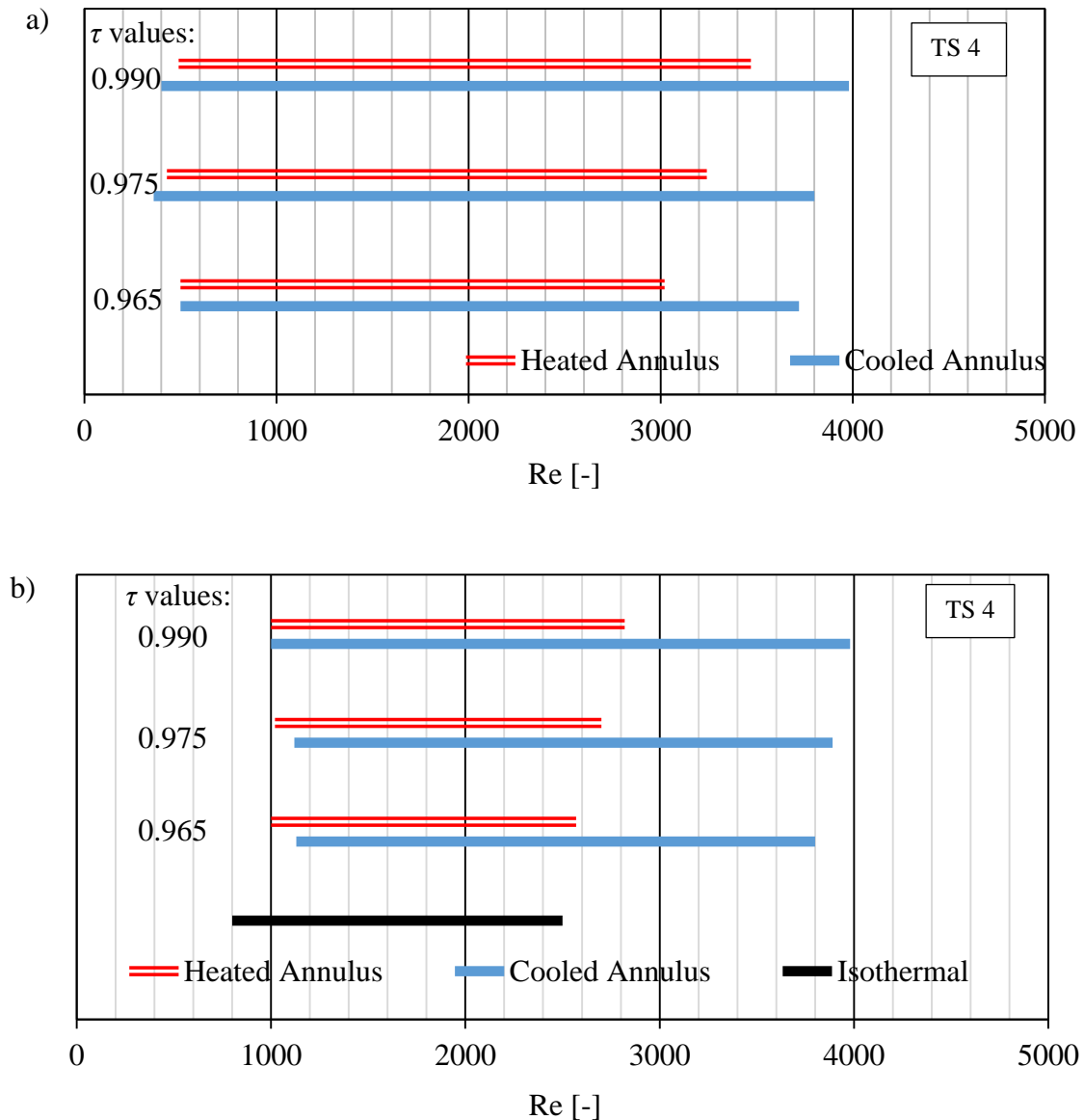

Figure B.12: A graphical representation of transition ranges for (a) heat transfer and (b) fluid flow for TS 4

B.4.3   Heat transfer coefficient

The mean heat transfer coefficient for the cooled and heated annulus cases was calculated using the mean LMTD method. Figure B.13 and Figure B.14 give the heat transfer coefficients expressed in terms of the Nusselt number and the Colburn *j*-factor, respectively.
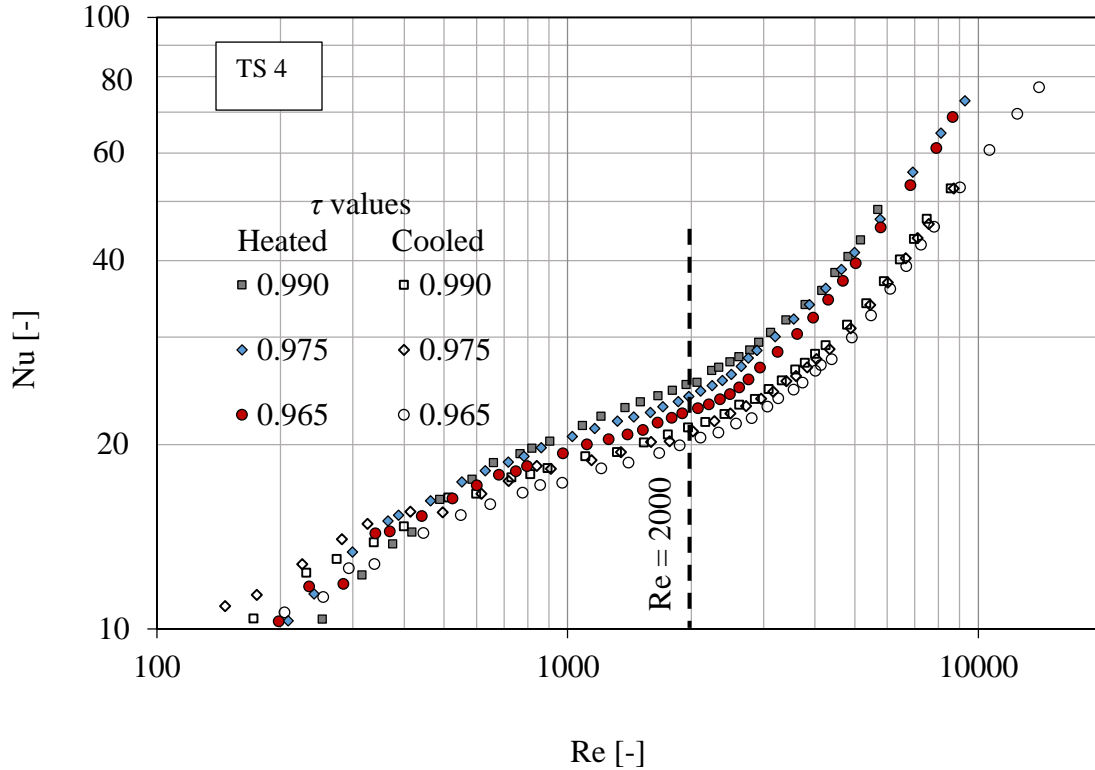

Figure B.13: The Nusselt numbers for heated and cooled annulus cases for different degrees of temperature uniformity on the inner wall for TS 4

In the transition regime (refer to Figure B.13) at a Reynolds number of 2 000, the Nusselt numbers for the wall temperature uniformities of 0.975 and 0.965 of a heated annulus case were 4.4% and 9.6% lower than the $\tau = 0.99$ case, respectively. For the cooled annulus case, the Nusselt numbers for the wall temperature uniformities of 0.975 and 0.965, were 2.1% and 5.4% lower than for the $\tau = 0.99$ case, respectively.
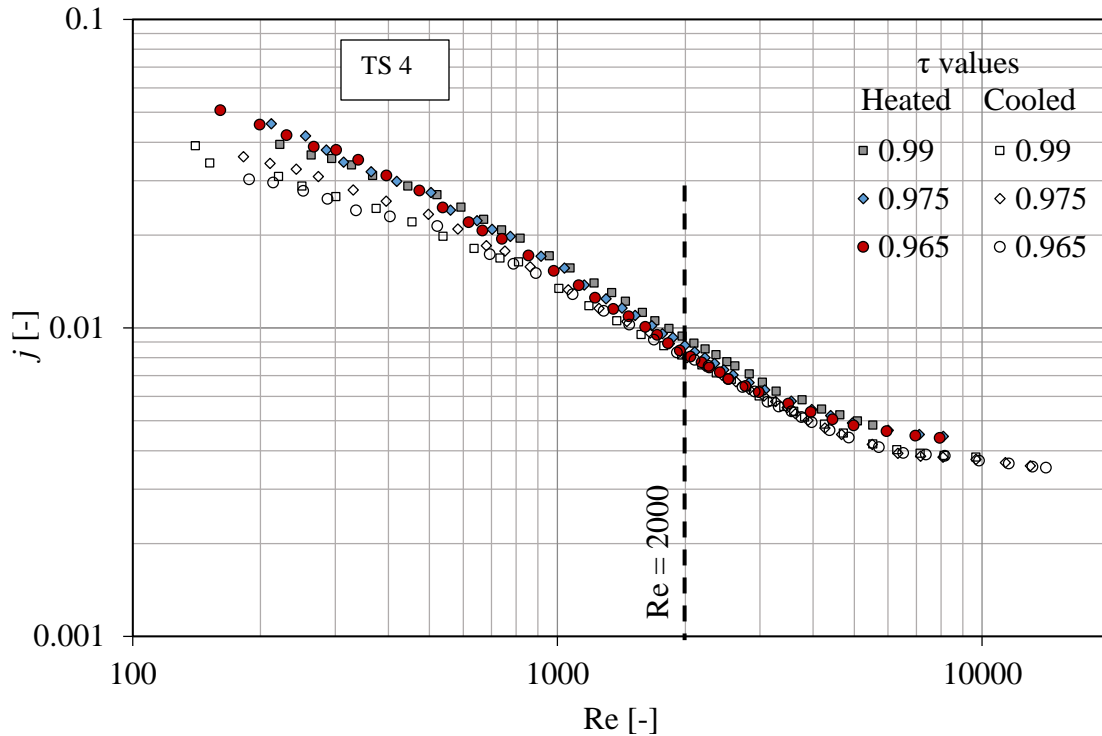
Figure B.14: The Colburn *j*-factors for the heated and cooled annulus cases for different degrees of temperature uniformity on the inner wall for TS 4

In the transition regime (refer to Figure B.14) at a Reynolds number of 2 000, the Colburn *j*-factor for wall temperature uniformities of 0.975 and 0.965 of a heated annulus case were 6.4% and 13% , respectively for the $\tau = 0.99$ case. For the cooled annulus case, the Nusselt numbers for the wall temperature uniformities of 0.975 and 0.965 were 1.2% and 2.9% lower than for the $\tau = 0.99$ case, respectively. At a Reynolds number of 2 000, the Nusselt numbers for the heated cases with $\tau = 0.99$, 0.975 and 0.965 were 18%, 15% and 12%, higher, respectively, than for the cooled case counterparts. The Colburn *j*-factors for the heated annulus cases with $\tau = 0.99$, 0.975 and 0.965 were +9%, +3.3 and +1% higher than for the cooled annulus counterparts, respectively.

B.4.4   Friction factor

The mean friction factors for cooled, heated and isothermal annulus cases were calculated from the pressure drop measurement between the inlet and the outlet of the annular passage and are plotted against the Reynolds number as shown in Figure B.15.
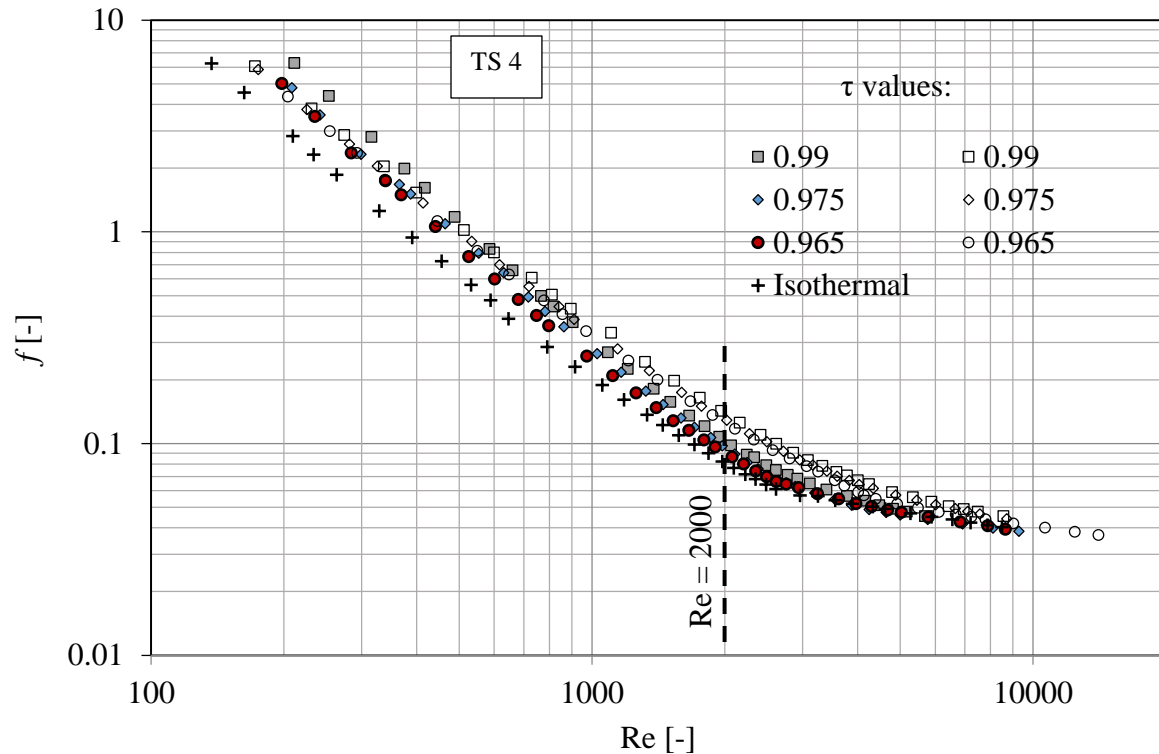
Figure B.15: The friction factors for the heated, cooled and isothermal annulus cases for different degrees of temperature uniformity on the inner wall for TS 4

At a Reynolds number of 2 000, the average friction factor for the heated case for τ values of 0.99, 0.975 and 0.965 were 27%, 18% and 12% higher than the isothermal friction factor case, respectively, while for the cooled annulus case, the average friction factor for τ values of 0.99, 0.975 and 0.965 were 72%, 61% and 56% higher than the isothermal friction factor case, respectively.

B.5 New correlations

B.5.1 Nusselt number

The mathematical formulation for the correlations for TS 2, TS 3 and TS 4 are the same as for TS 1, which is described in Chapter 6. However, the constants and exponents of the correlations were recalculated for each test section as presented in Table B.1.

Table B.1: Constants, exponents and application ranges of the proposed Nusselt number correlations for the heated and cooled annulus cases

TS	Case	Constants			Exponent	Application range
		B_1	B_2	z_1	z_2	
2	Heated annulus	294.52	13.3	-0.266	-0.088	$650 \leq Re \leq 3\ 600$ $4.6 \leq Pr \leq 6.5$ $1\ 000 \leq GrPr/Re \leq 7\ 700$ $0.965 \leq \tau \leq 0.990$
	Cooled annulus	2580.7	12437	-0.543	-0.983	$630 \leq Re \leq 4\ 800$ $3.8 \leq Pr \leq 5.0$ $1900 \leq GrPr/Re \leq 7\ 200$ $0.965 \leq \tau \leq 0.990$
3	Heated annulus	294.64	24.86	-0.292	-0.243	$630 \leq Re \leq 3\ 500$ $4.4 \leq Pr \leq 6.7$ $750 \leq GrPr/Re \leq 4\ 900$ $0.965 \leq \tau \leq 0.990$
	Cooled annulus	1430	583.32	-0.501	-0.69	$600 \leq Re \leq 4\ 480$ $3.87 \leq Pr \leq 5.07$ $1400 \leq GrPr/Re \leq 4\ 800$ $0.965 \leq \tau \leq 0.990$
4	Heated annulus	417.42	132.24	-0.39	-0.415	$570 \leq Re \leq 3\ 000$ $4.3 \leq Pr \leq 6.2$ $520 \leq GrPr/Re \leq 2\ 900$ $0.965 \leq \tau \leq 0.990$
	Cooled annulus	1466	356.34	-0.566	-0.597	$540 \leq Re \leq 3\ 700$ $3.8 \leq Pr \leq 5.2$ $960 \leq GrPr/Re \leq 2\ 500$ $0.965 \leq \tau \leq 0.990$

Figure B.16, Figure B.17 and Figure B.18 show the comparison between the experimental results and the predicted Nusselt number for TS 2, TS 3 and TS 4, respectively. The agreement between the experimental results and the proposed correlations was good, with almost all the data points being predicted within a ±6 % error band.
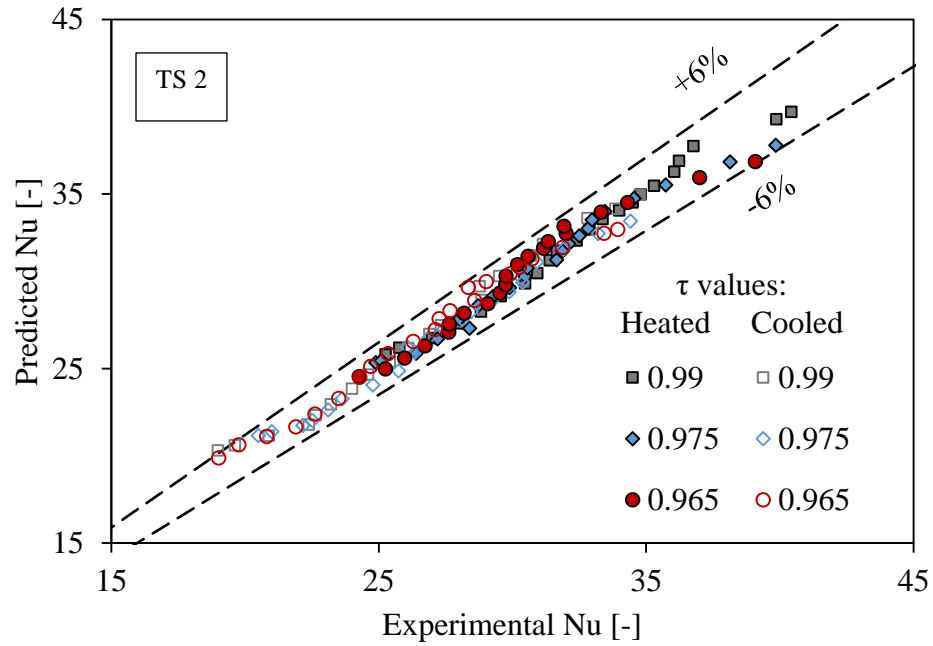
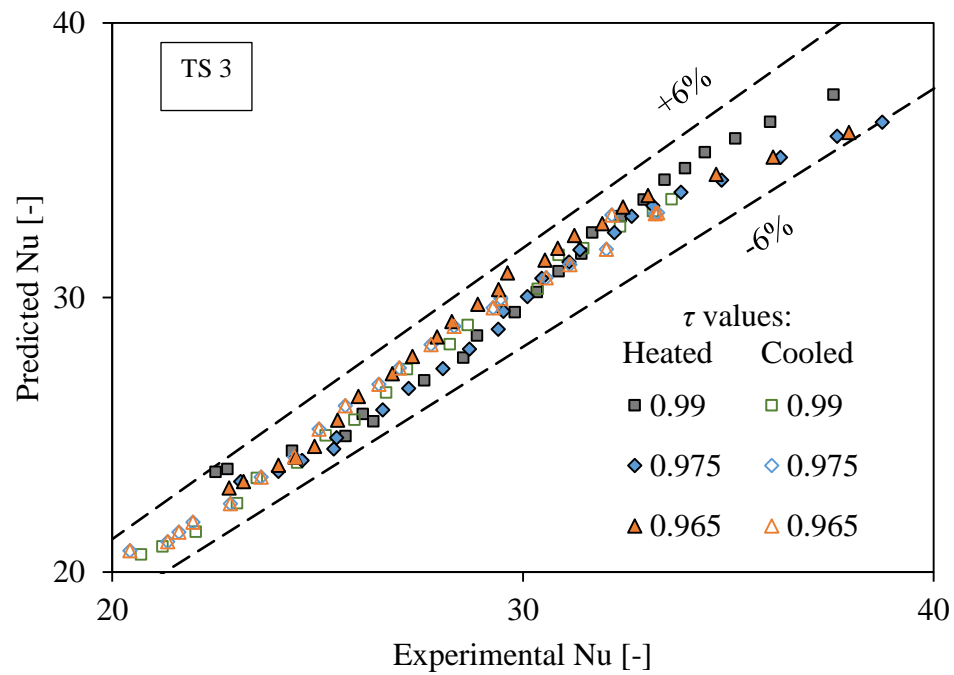Figure B.16: Comparison between the experimental and predicted Nusselt numbers for TS 2

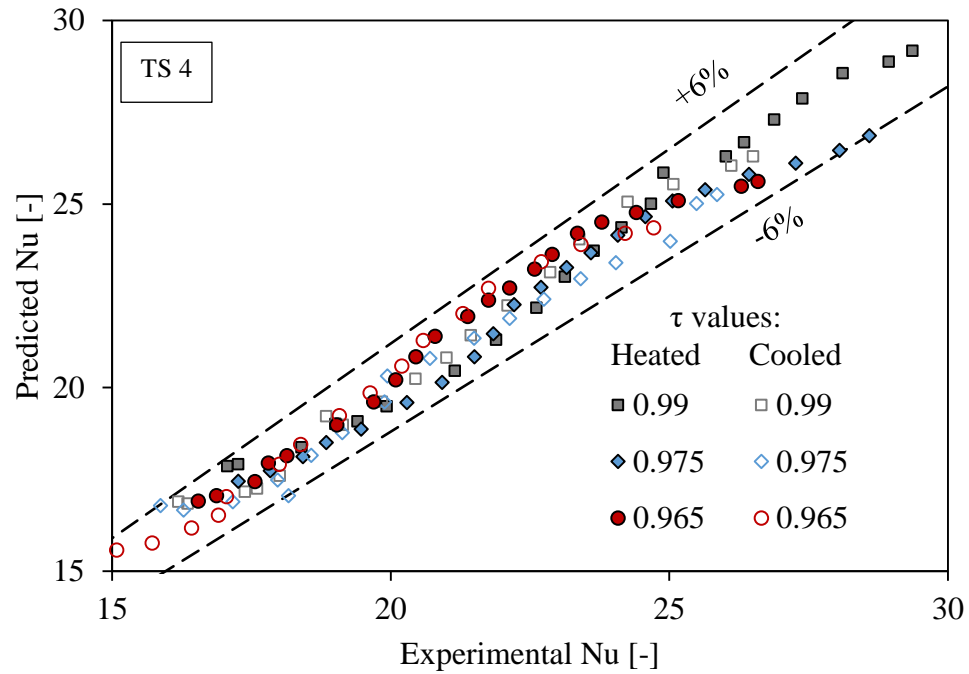Figure B.17: Comparison between the experimental and predicted Nusselt numbers for TS 3

Figure B.18: Comparison between the experimental and predicted Nusselt numbers for TS 4

B.5.2   Friction factor

The correlation for the diabatic friction factor is of the form $f_{iso} = f_a\, C\, (\mu_b/\mu_{iw})\, \tau^p$ where C and p are a function of $(GrPr)$. The constants and exponents for heated and cooled cases of the three test sections are presented in Table B.2.

Table B.2:The constants, exponents and application ranges of the proposed friction factor correlations for the heated and cooled annulus cases

TS	Case	Constants			Exponents			Application range
		B_1	B_2	B_3	u	v	z_3	
2	Heated annulus	5.68×10^3	-1.65	28.82	0.07	1.12	-3.0	$1\,260 \leq Re \leq 2\,700$, $16.90 \leq Gr^u\,Pr^v \leq 20.15$, $1.36 \leq \mu_b/\mu_{iw} \leq 1.51$, $0.990 \leq \tau \leq 0.965$
	Cooled annulus	34.02	-1.17	28.96	0.07	1.12	-0.86	$1\,260 \leq Re \leq 2\,700$, $12.75 \leq Gr^u\,Pr^v \leq 14.74$, $0.64 \leq \mu_b/\mu_{iw} \leq 0.78$, $0.990 \leq \tau \leq 0.965$
3	Heated annulus	2.35×10^3	-0.75	11.36	0.07	1.12	-2.73	$1\,250 \leq Re \leq 2\,600$, $15.98 \leq Gr^u\,Pr^v \leq 19.44$, $1.35 \leq \mu_b/\mu_{iw} \leq 1.6$, $0.990 \leq \tau \leq 0.965$
	Cooled annulus	37.82	-1.45	29.33	0.07	1.12	-1.08	$1\,250 \leq Re \leq 2\,600$, $12.79 \leq Gr^u\,Pr^v \leq 14.32$, $0.66 \leq \mu_b/\mu_{iw} \leq 0.77$, $0.990 \leq \tau \leq 0.965$
4	Heated annulus	265	-0.038	-1.66	0.07	1.12	-2.03	$1\,200 \leq Re \leq 2\,500$, $15.24 \leq Gr^u\,Pr^v \leq 18.20$, $1.32 \leq \mu_b/\mu_{iw} \leq 1.50$, $0.990 \leq \tau \leq 0.965$
	Cooled annulus	4.23	-0.14	10.2	0.07	1.12	-0.17	$1\,200 \leq Re \leq 2\,500$, $12.17 \leq Gr^u\,Pr^v \leq 14.09$, $0.65 \leq \mu_b/\mu_{iw} \leq 0.78$, $0.990 \leq \tau \leq 0.965$

Figure B.19, Figure B.20 and Figure B.21 show the comparison between the experimental results and the predicted friction factors for TS 2, TS 3 and TS 4. The agreement between the experimental results and the proposed correlations was good, with almost all the data points predicted within a $\pm 5\%$ error band.
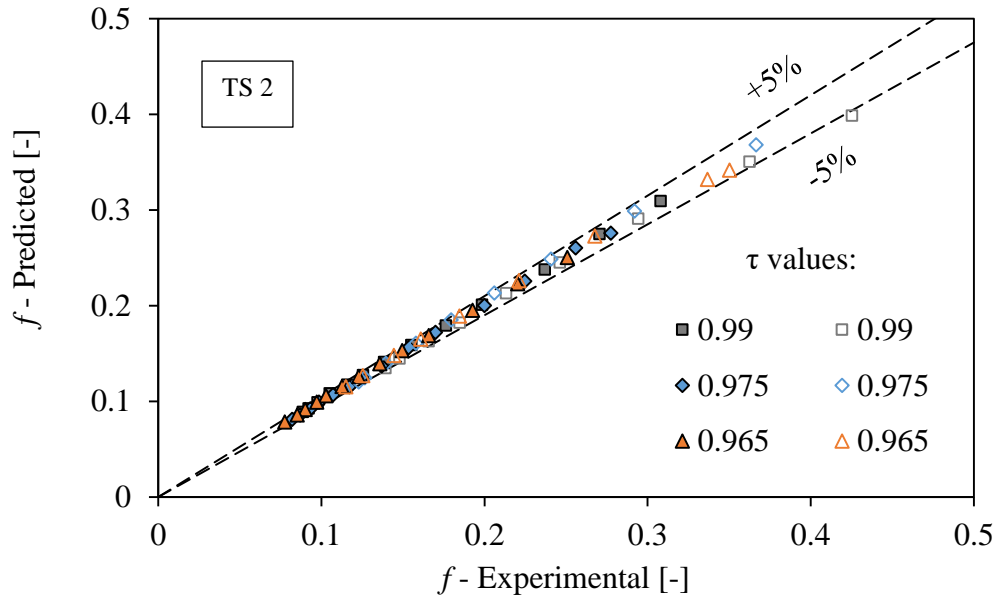

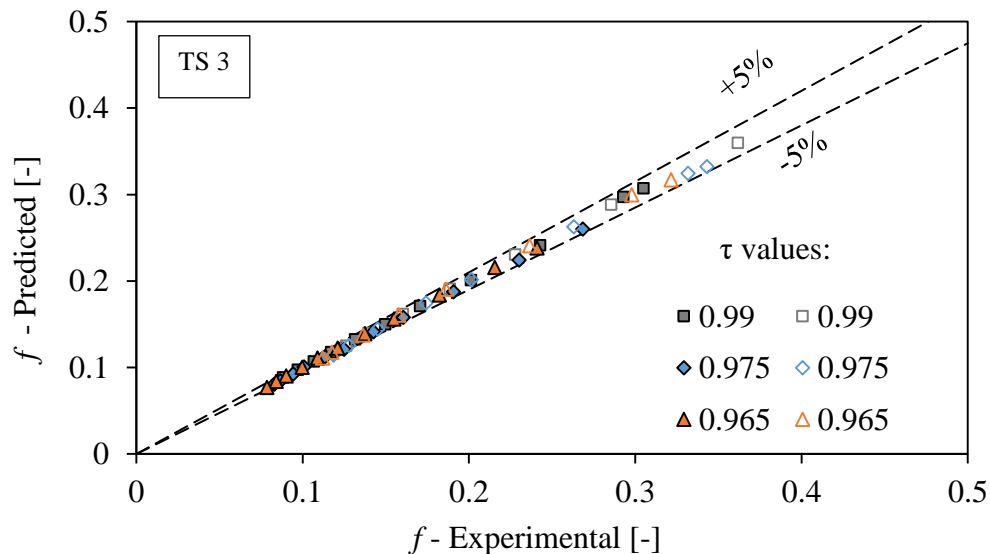Figure B.19: Comparison between the experimental and predicted friction factors for TS 2

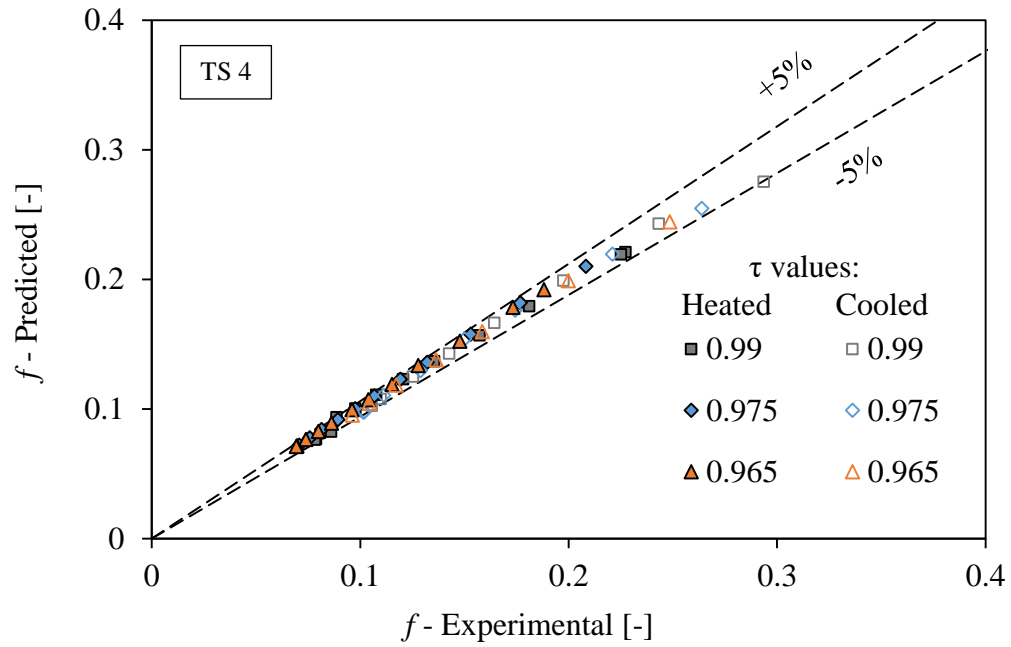Figure B.20: Comparison between the experimental and predicted friction factors for TS 3

Figure B.21: Comparison between the experimental and predicted friction factors for TS 4

Appendix C

Results of the influence of annular geometrical size

C.1.   Introduction

In this study, the characteristics of the transition flow regime in the annuli of horizontal concentric tube-in-tube heat exchangers were investigated. In Chapter 7, the results of the influence of the annular passage dimensions on the heat transfer coefficients, friction factors and Reynolds number limits of the transition regime for the approximately UWT ($\tau = 0.990$) boundary condition were presented. The results of the other two wall boundary conditions ($\tau = 0.975$ and $\tau = 0.965$) for the four test sections that were considered are presented in this appendix. The correlations based on the annular geometric parameter, λ, are also presented for each τ value. The details of these test sections and all calculations and methods used to obtain the respective results are provided in the main text.

C.2. $\tau = 0.975$

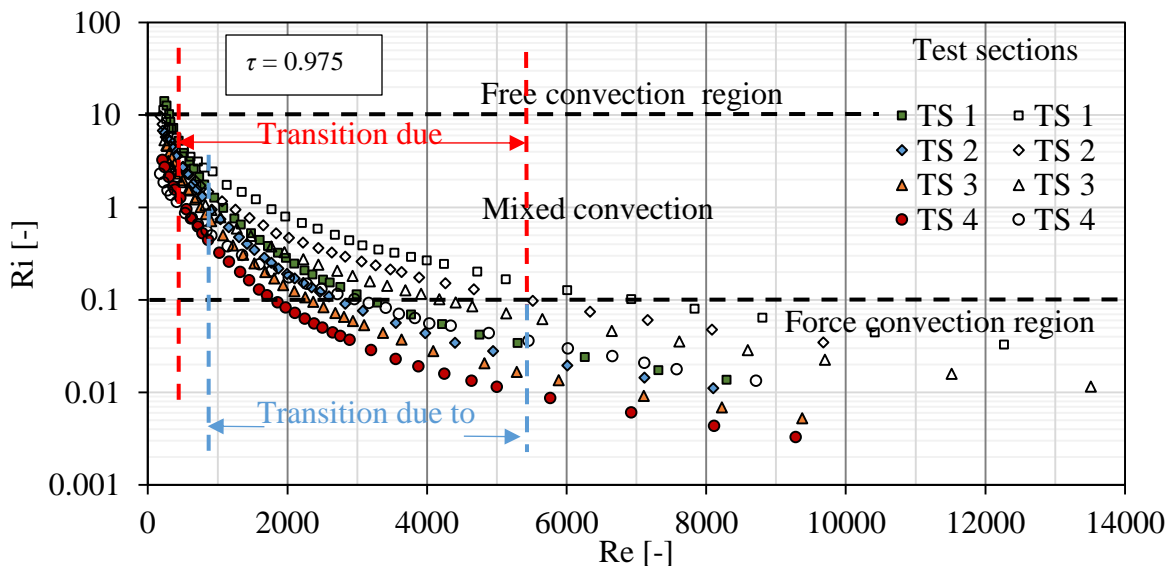#### C.2.1.   Distribution of convection flow types

Figure C.1: Distribution of convection types along the laminar, transition and turbulent regimes for $\tau = 0.975$

Convection types were analysed in order to have a better understanding of the characteristics of the Reynolds number limits of the transition regime, heat transfer coefficients and friction factors. Figure C.1 shows the distribution of convection types along the laminar, transition and turbulent flow regimes by using the Richardson number method. The lower and upper Reynolds number limits of transition flow regime in Figure C.1 are the average values for all the lower and upper Reynolds number limit data of the transition regime for the thermal boundary, $\tau = 0.975$.

The proportion of the transition flow regime data points that fall within mixed convection is presented as a percentage in Table C.1.

Table C.1: Heat transfer and flow transition ranges for the heated and cooled annuli and mixed-convection size for the approximately UWT case, $\tau = 0.975$

Heated annulus						
TS	**Transition based on Nusselt number**			**Transition based on friction factor**		
	Re_1	**Re_2**	**Mixed convection in the transition regime**	**Re_1**	**Re_2**	**Mixed convection in the transition regime**
1	700	4 790	86%	1 260	3 560	88%
2	680	3 980	83%	1 000	3 020	82%
3	570	3 880	64%	1 100	3 000	67%
4	430	3 240	55%	1 020	2 700	50%
Cooled annulus						
1	540	5 900	100%	1 510	5 770	100%
2	575	5 150	100%	1 260	4 790	100%
3	470	4 900	95%	1 250	4 680	87%
4	360	3 800	77%	1 120	3 890	60%

C.2.2.   Transition regime

Figure C.2a and Figure C.2b show the Reynolds number spans of the transition regime of the test sections based on heat transfer and friction factor, respectively. The transitions for the heated and cooled annulus cases depend on the annular geometric dimensions.
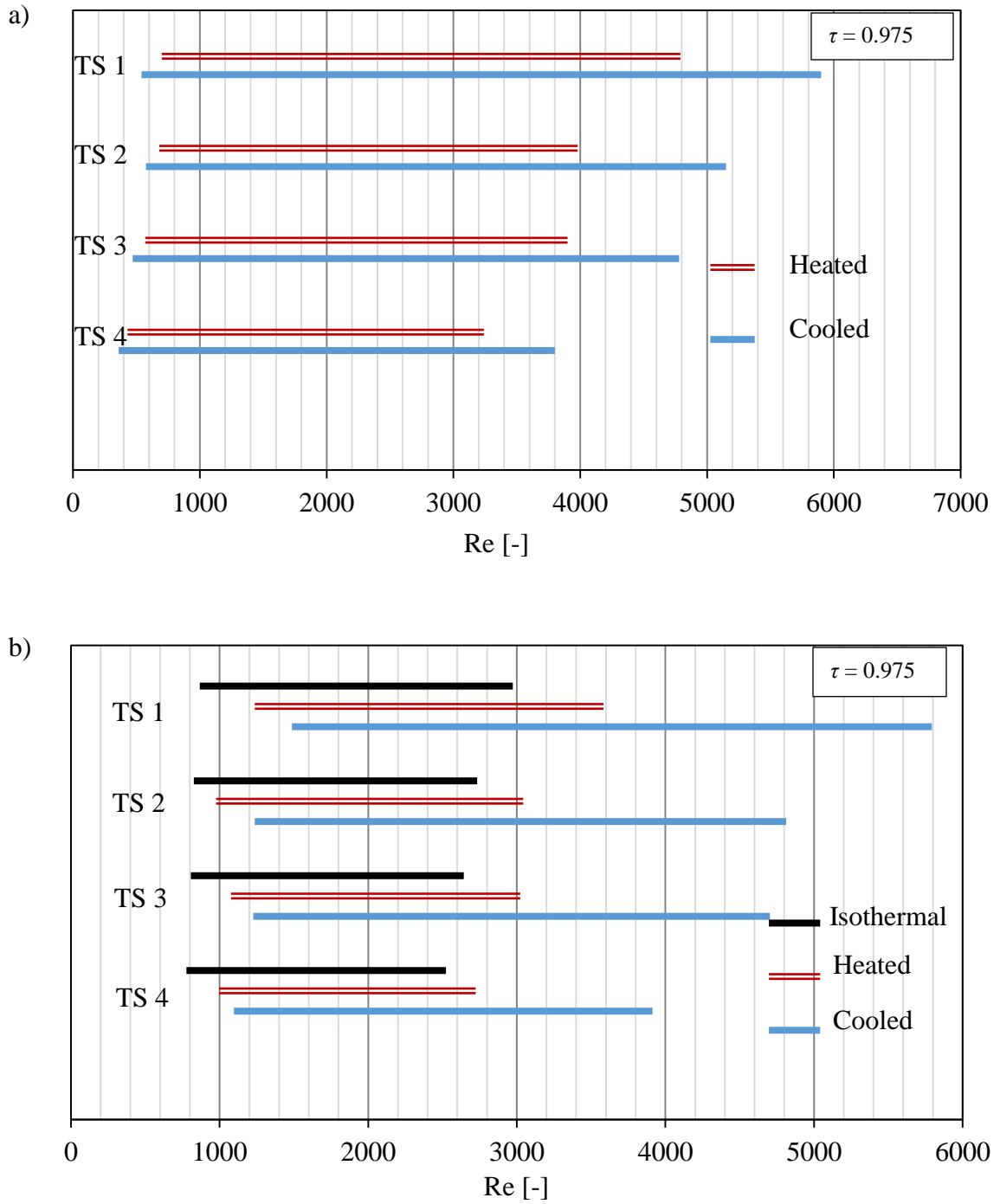
Figure C.2: A graphic representation of Reynolds number spans of the transition ranges for the (a) heat transfer and (b) friction factor for $\tau = 0.975$

C.2.3.   Heat transfer coefficient

The mean heat transfer coefficient for the cooled and heated annulus cases calculated using the mean LMTD method. Figure C.3 and Figure C.4 are heat transfer coefficients expressed in terms of the Nusselt number and the Colburn *j*-factor, respectively.

In the transition regime (refer to Figure C.3) at a Reynolds number of 2 000, the Nusselt numbers for TS 2, TS 3 and TS 4 of a heated annulus case were 15%, 19% and 37% lower than for TS 1, respectively. For the cooled annulus cases, the Nusselt numbers for test sections TS 2, TS 3 and TS 4 were 17%, 19% and 35% lower than the TS 1, respectively.

In the transition regime (refer to Figure C.4) at a Reynolds number of 2 000, the Colburn *j*-factor for test sections TS 2, TS 3 and TS 4 for the heated cases were 15%, 19% and 37% lower than for TS 1, respectively. For the cooled annulus cases, the Colburn *j*-factor for test sections TS 2, TS 3 and TS 4 were 17%, 19% and 35% lower than for TS 1, respectively. As it was observed for $\tau = 0.99$, the results of the comparisons between TS 1 and the other test section for the Nusselt number and Colburn *j*-factor results are also similar for $\tau = 0.975$. The small differences in these values could be due to the measurement uncertainties.

At a Reynolds number of 2 000, the Nusselt numbers for heated cases of TS 1, TS 2, TS 3 and TS 4 were 18%, 19%, 16% and 15% higher, respectively, than for the cooled case counterparts. The Colburn *j*-factors for heated cases of TS 1, TS 2, TS 3 and TS 4 were +4%, +4%, +3% and +3% higher for the cooled counterparts.
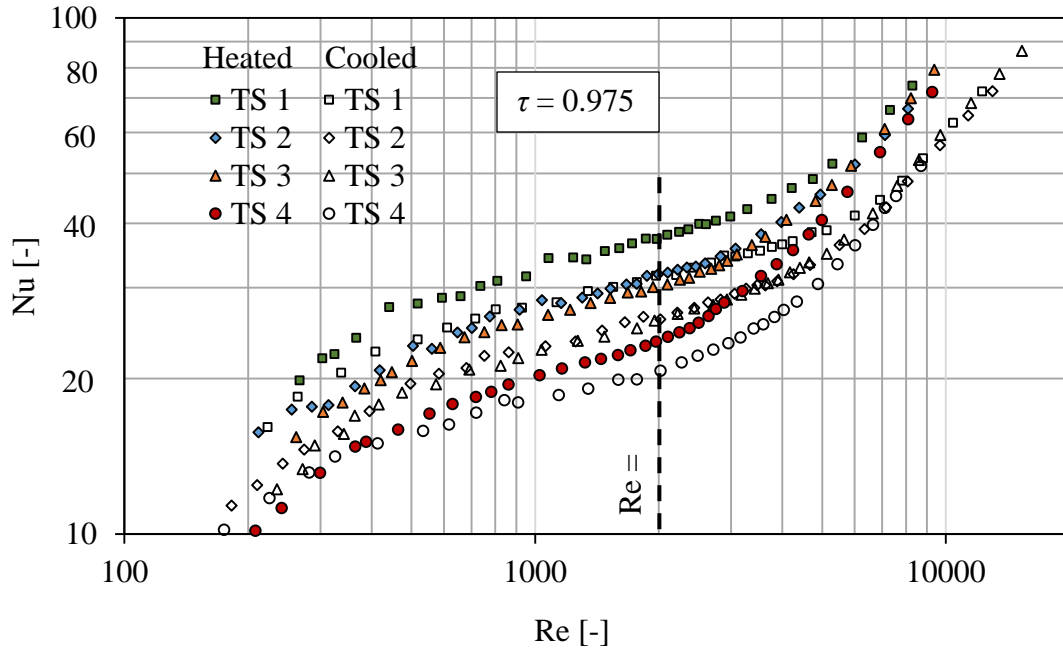
Figure C.3: The Nusselt numbers for the different test sections for the heated and cooled annulus cases for $\tau = 0.975$
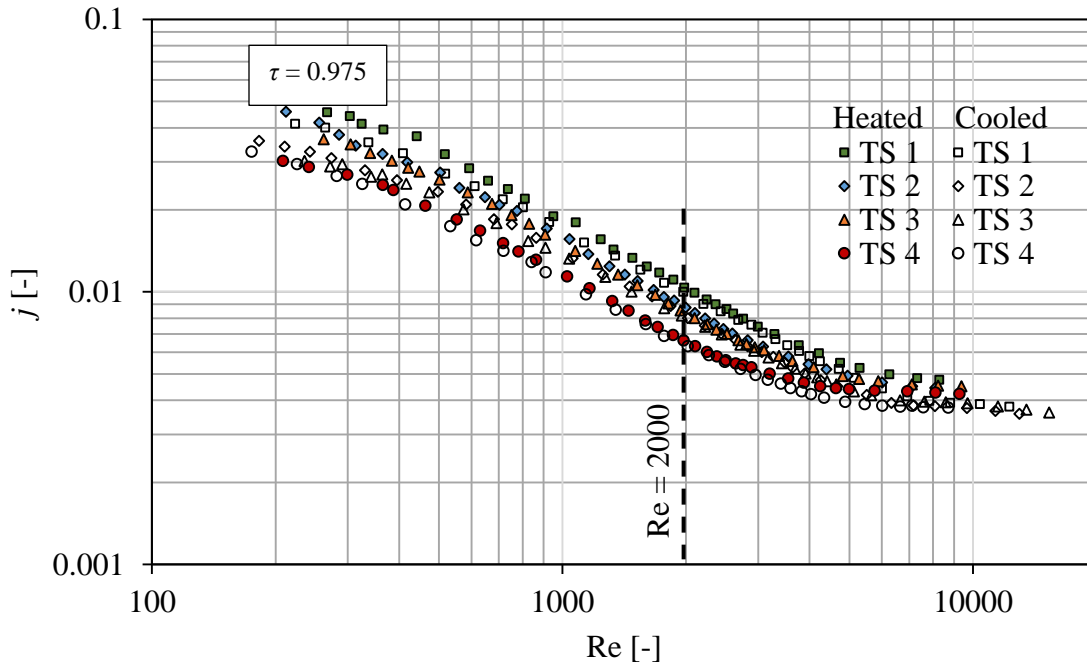

Figure C.4: The Colburn j-factor values for the different test sections for the heated and cooled annulus cases for $\tau = 0.975$

C.2.4.   Friction factors

The mean friction factors for heated and cooled annulus cases were calculated from the pressure drop measurement between the inlet and the outlet of the annular passage.
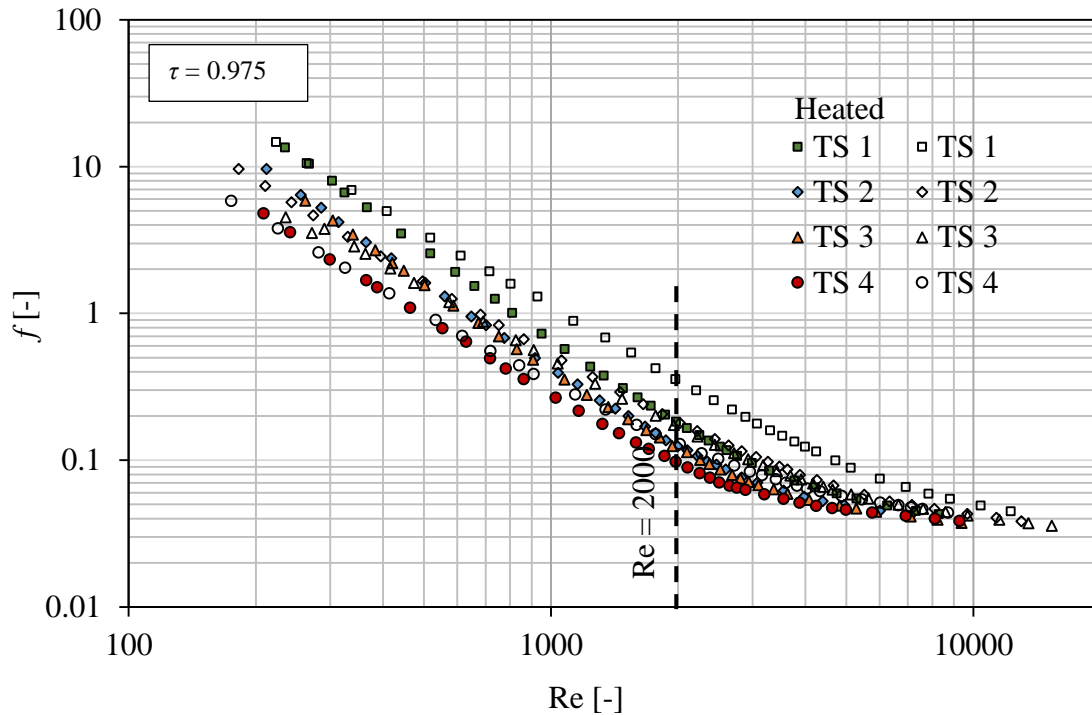

Figure C.5: Friction factors for the different test sections for the heated and the cooled annulus cases for $\tau = 0.975$

At a Reynolds number of 2 000, the average friction factor for the heated cases of TS 2, TS 3 and TS 4 were 31%, 33% and 47% lower than for TS 1, respectively. For the cooled cases, the average friction factor for TS 2, TS 3 and TS 4 were 48%, 52% and 63% lower than for TS 1, respectively.

C.3. $\tau = 0.965$

C.3.1.   The distribution of convection flow types

Figure C.6 shows the distribution of convection types along the laminar, transition and turbulent regimes by using the Richardson number method. The lower and upper Reynolds number limits of the transition flow regime in Figure C.6 are the average values for all the lower and upper Reynolds number limit data of the transition regime for the thermal boundary, $\tau = 0.965$.
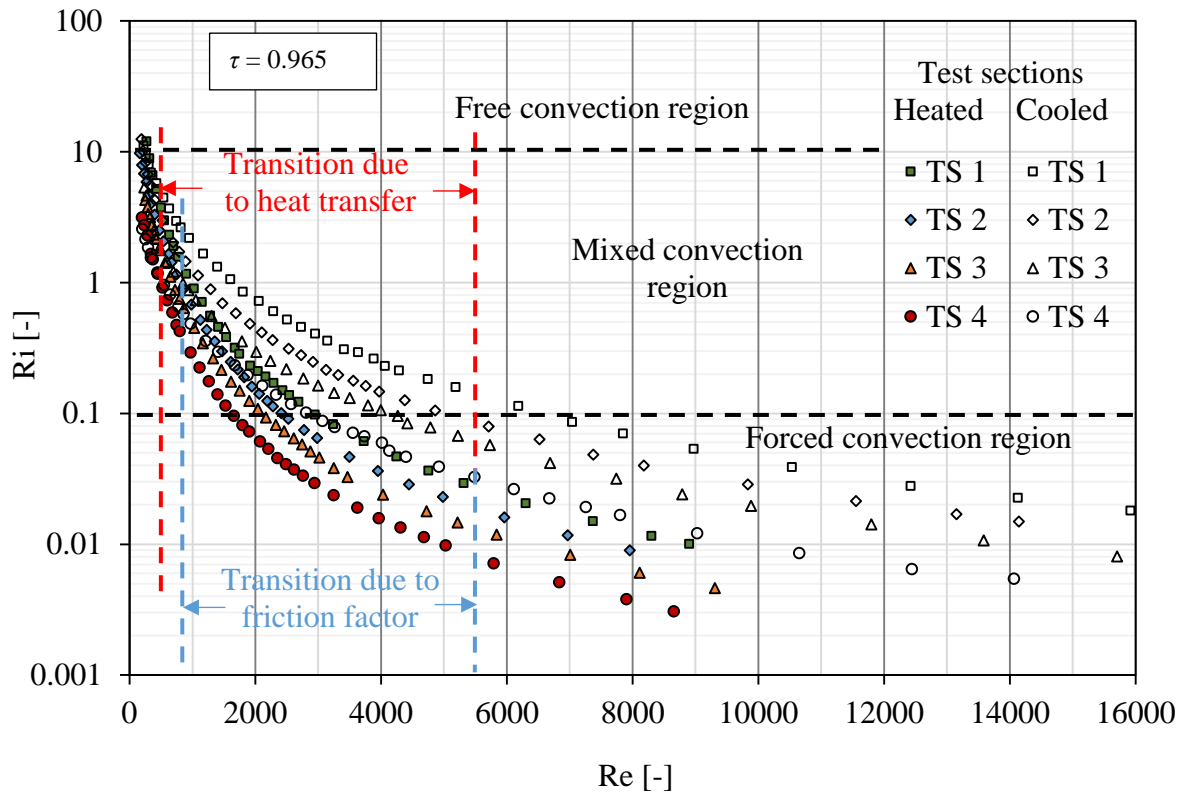

Figure C.6: Distribution of convection types along laminar, transition and turbulent regimes for $\tau = 0.975$

The proportion of the transition flow regime data points that fall within mixed convection are presented as a percentage in Table C.2.

Table C.2: Heat transfer and flow transition ranges for the heated and cooled annuli and mixed-convection size for the approximately UWT case, $\tau = 0.965$

Heated annulus						
TS	**Transition based on Nusselt number**			**Transition based on friction factor**		
	Re_1	**Re_2**	**Mixed convection in the transition regime**	**Re_1**	**Re_2**	**Mixed convection in the transition regime**
1	740	4 680	84%	1 240	3 350	82%
2	470	3 890	80%	1 000	2 950	80%
3	520	3 800	61%	1 070	2 870	60%
4	500	3 020	52%	1 000	2 570	47%
Cooled annulus						
1	520	5 650	100%	1 520	5 640	100%
2	570	5 020	100%	1 250	4 680	100%
3	450	4 780	85%	1 240	4 570	86%
4	500	3 720	76%	1 130	3 800	54%

C.3.2.   Transition regime

Figure C.7a and Figure C.7b show the Reynolds number spans of the transition regime of test sections based on the heat transfer and friction factor, respectively. The transitions for the heated and cooled annulus cases depend on the annular geometric dimensions.
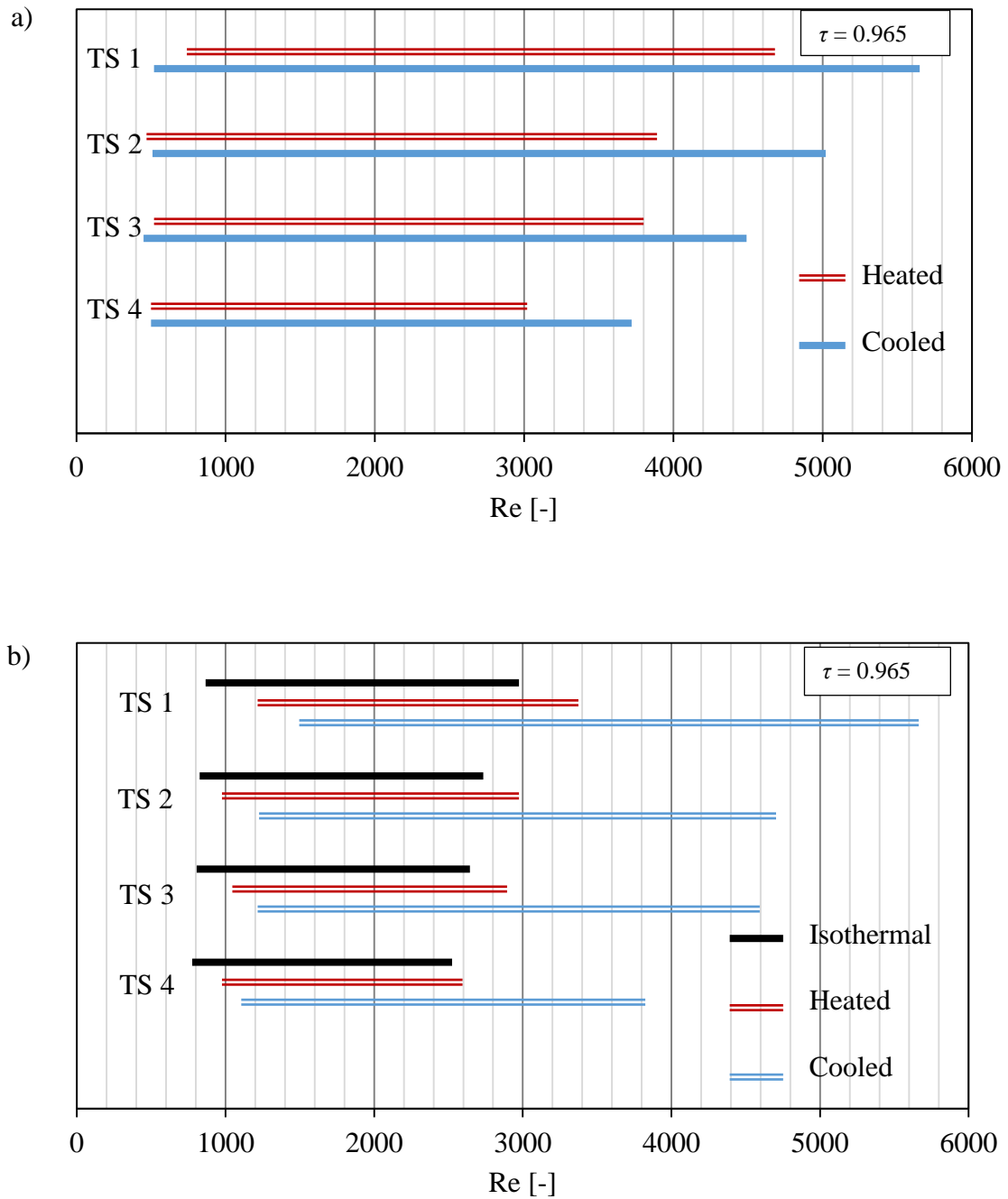
a)

b)

Figure C.7: A graphical representation of the Reynolds number spans of the transition ranges for (a) heat transfer and (b) friction factor for $\tau = 0.965$

C.3.3. Heat transfer coefficient

The mean heat transfer coefficient for the cooled and heated annulus cases calculated using the mean LMTD method. Figure C.8 and Figure C.9 are heat transfer coefficients expressed in terms of the Nusselt number and Colburn *j*-factor, respectively.
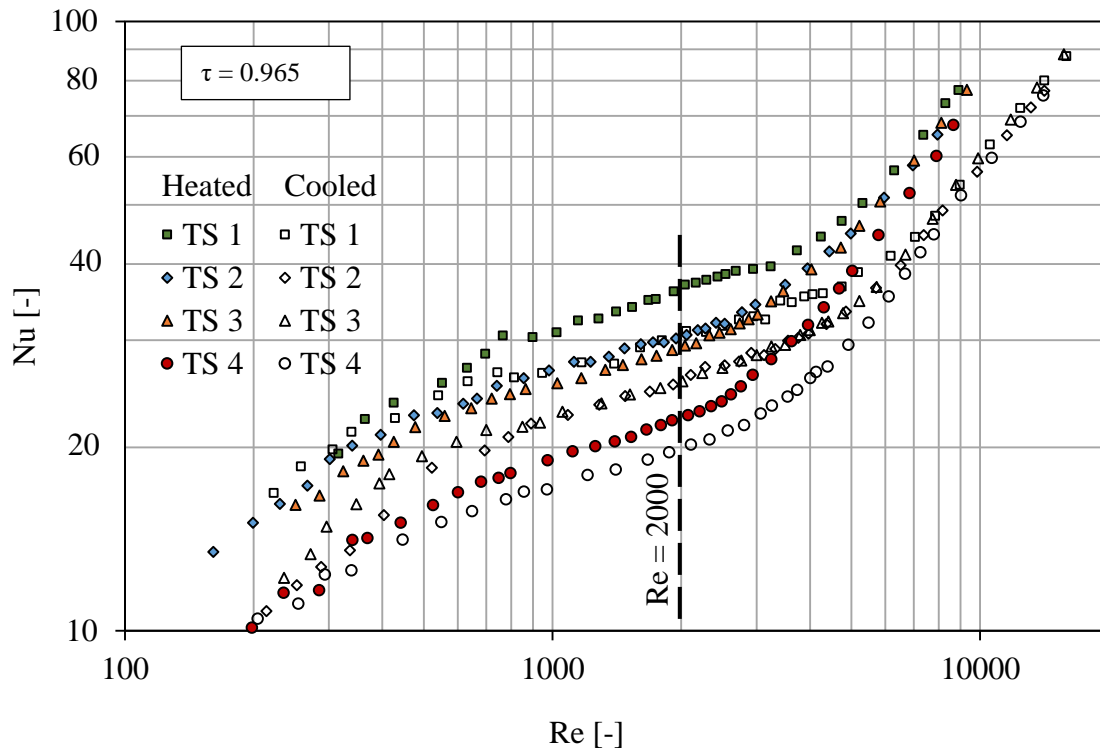

Figure C.8: Nusselt numbers for the different test sections for the heated and cooled annulus cases for $\tau = 0.965$

In the transition regime (refer to Figure C.8) at a Reynolds number of 2 000, the Nusselt numbers for test sections TS 2, TS 3 and TS 4 of a heated annulus case were 17%, 20% and 39% lower than for TS 1, respectively. For the cooled annulus cases, the Nusselt numbers for test sections TS 2, TS 3 and TS 4 were 16%, 17% and 35% lower than the TS 1, respectively.
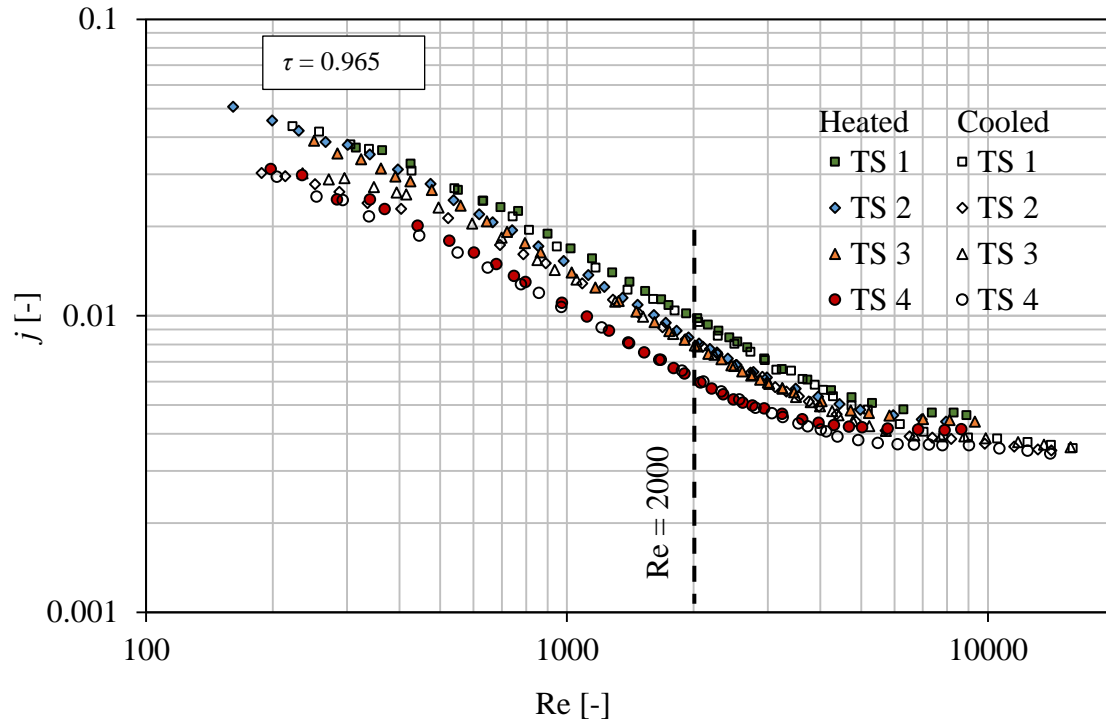
Figure C.9: Colburn *j*-factor values for the different test sections for the heated and cooled annulus cases for $\tau = 0.965$

In the transition regime (refer to Figure C.9) at a Reynolds number of 2 000, the Colburn *j*-factor for test sections TS 2, TS 3 and TS 4 for heated cases were 17%, 20% and 39% lower than for TS 1, respectively. For the cooled annulus case, the Colburn *j*-factor for test sections TS 2, TS 3 and TS 4 were 17%, 18% and 36% lower than for TS 1, respectively. As was observed for $\tau = 0.99$ and $\tau = 0.975$, the results of the comparisons between TS 1 and the other test section for the Nusselt number and Colburn *j*-factor results are also similar for $\tau = 0.965$. The small differences in these values could be due to the measurement uncertainties.

At a Reynolds number of 2 000, the Nusselt numbers for the heated cases of TS 1, TS 2, TS 3 and TS 4 were 19%, 18%, 14% and 12% higher, respectively, than for their cooled case counterparts. The Colburn *j*-factors for the heated cases of TS 1, TS 2, TS 3 and TS 4 were +2%, +2%, 0% and 1% higher for their cooled annulus counterparts.

C.3.4.   Friction factors

The mean friction factors for the heated and cooled annulus cases were calculated from the pressure drop measurement between the inlet and the outlet of the annular passage.
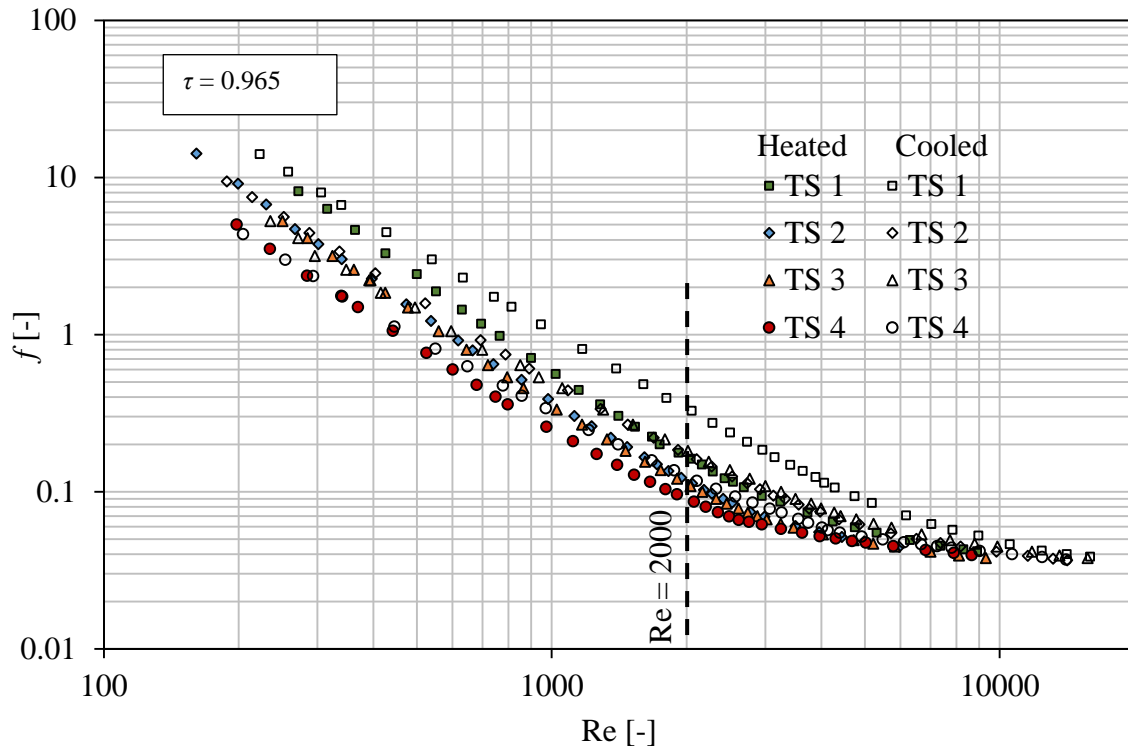

Figure C.10: The friction factors for the different test sections for the heated and the cooled annulus cases for $\tau = 0.965$

At a Reynolds number of 2 000, the average friction factor for the heated cases of TS 2, TS 3 and TS 4 were 30%, 33% and 46% lower than for TS 1, respectively. For the cooled cases, the average friction factors for TS 2, TS 3 and TS 4 were 49%, 53% and 63% lower than for TS 1, respectively.

C.4. New correlations

C.4.1. Coefficients and exponents for the Nusselt number correlations

C.4.1.1. For $\tau = 0.975$

Expressions for the coefficient and exponent in Equation 7.1 in the main document for the heated and the cooled annulus cases were obtained as follows:

For heated annuli:

$$C = 367.08\left(\frac{\mathrm{Gr\,Pr}}{\mathrm{Re}}\right)^{0.253} \tag{C.1}$$

$$z = 0.402\left(\frac{\mathrm{Gr\,Pr}}{\mathrm{Re}}\right)^{0.116} \tag{C.2}$$

For an applicable range of $700 \leq \mathrm{Re} \leq 3\,200$, $590 \leq \mathrm{GrPr/Re} \leq 8\,400$ and $63 \leq \lambda \leq 145$.

For cooled annuli:

$$C = 323.57\left(\frac{\mathrm{Gr\,Pr}}{\mathrm{Re}}\right)^{0.396} \tag{C.3}$$

$$z = 0.435\left(\frac{\mathrm{Gr\,Pr}}{\mathrm{Re}}\right)^{0.132} \tag{C.4}$$

For an applicable range of $640 \leq \mathrm{Re} \leq 3\,750$, $1\,000 \leq \mathrm{GrPr/Re} \leq 10\,200$ and $63 \leq \lambda \leq 145$.

C.4.1.2. For $\tau = 0.965$

For heated annuli:

$$C = 2637.7\left(\frac{\mathrm{Gr\,Pr}}{\mathrm{Re}}\right)^{-0.013} \tag{C.1}$$

$$z = 0.665\left(\frac{\mathrm{Gr\,Pr}}{\mathrm{Re}}\right)^{0.051} \tag{C.2}$$

For an applicable range of $680 \leq \mathrm{Re} \leq 3\,000$, $520 \leq \mathrm{GrPr/Re} \leq 7\,400$ and $63 \leq \lambda \leq 145$.

For cooled annuli:

$$C = 218.74\left(\frac{\mathrm{Gr\,Pr}}{\mathrm{Re}}\right)^{0.718} \tag{C.3}$$

$$z = 0.509\left(\frac{\mathrm{Gr\,Pr}}{\mathrm{Re}}\right)^{0.14} \tag{C.4}$$

For an applicable range of $600 \leq \mathrm{Re} \leq 3\,700$, $960 \leq \mathrm{GrPr/Re} \leq 11\,000$ and $63 \leq \lambda \leq 145$.

Figure C.11 and Figure C.12 show the comparison between experimental results and the predicted Nusselt number for $\tau = 0.975$ and $\tau = 0.965$, respectively. The agreement between the experimental results and the proposed correlations was good, with almost 97% of the data points being predicted within a $\pm 8\%$ error band.
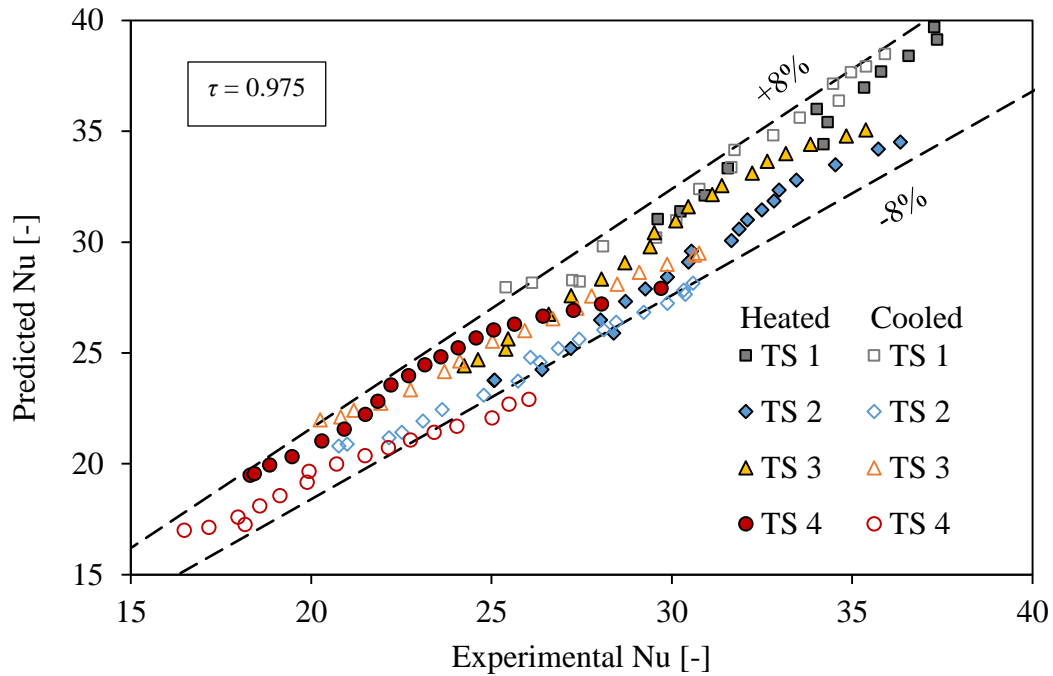
Figure C.11: Comparison between the experimental and predicted Nusselt numbers for $\tau = 0.975$
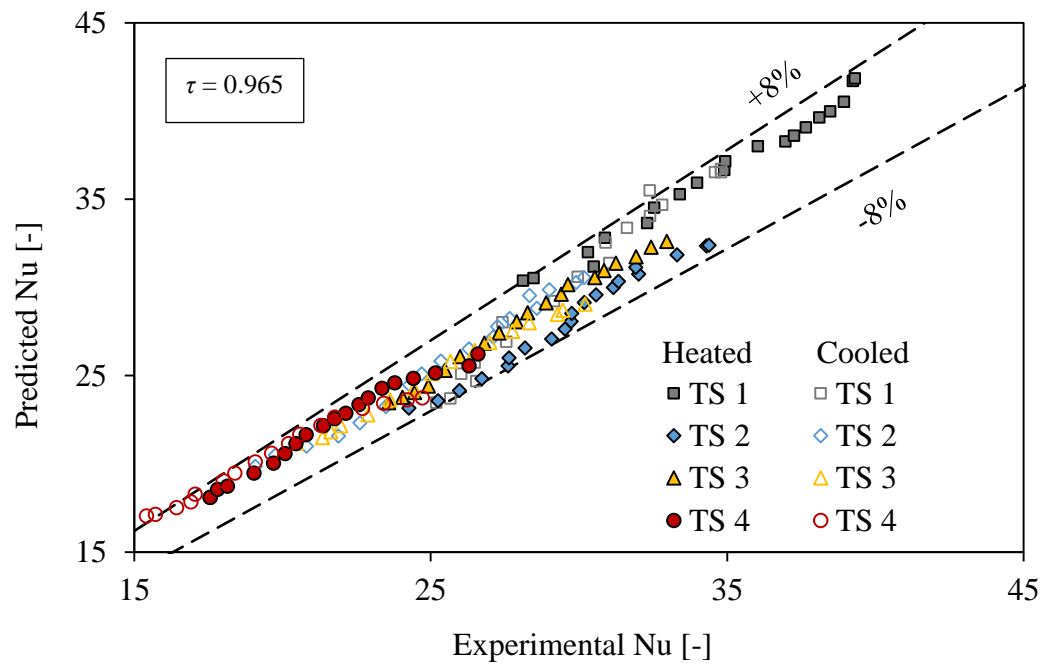

Figure C.12: Comparison between the experimental and predicted Nusselt numbers for $\tau = 0.965$

C.4.2. Coefficients and exponents for friction factor correlations

C.4.2.1. For $\tau = 0.975$

Expressions for the coefficient and exponent for the diabatic friction factor Equation 7.3 in the main document were obtained as follows:

For heated annuli:

$$C_d = 92 \times 10^3 \left(Gr^{0.01} \, Pr^{2.9} \right)^{-1.935} \tag{C.5}$$

$$z = 1.6 \times 10^{-3} \left(Gr^{0.01} \, Pr^{2.9} \right) - 0.535 \tag{C.6}$$

For an applicable range of $1\,400 \leq Re \leq 2\,500$, $157 \leq Gr^{0.01} \, Pr^{2.8} \leq 225$ and $64 \leq \lambda \leq 144$.

For cooled annuli:

$$C_d = 0.31 \left(Gr^{0.01} \, Pr^{2.9} \right)^{0.94} \tag{C.7}$$

$$z = -1.82 \times 10^3 \left(Gr^{0.01} \, Pr^{2.9} \right) - 0.355 \tag{C.8}$$

For an applicable range of $1\,400 \leq Re \leq 2\,500$, $64 \leq Gr^{0.01} \, Pr^{2.8} \leq 87$ and $64 \leq \lambda \leq 144$.

C.4.2.2. For $\tau = 0.965$

Expressions for the coefficient and exponent for the diabatic friction factor Equation 7.3 in the main document were obtained as follows:

For heated annuli:

$$C_d = 37 \times 10^3 \left(Gr^{0.01} \, Pr^{2.9} \right)^{-1.74} \tag{C.9}$$

$$z = 1.3 \times 10^{-3} \left(Gr^{0.01} \, Pr^{2.9} \right) - 0.50 \tag{C.10}$$

For an applicable range of $1\,400 \le \mathrm{Re} \le 2\,500$, $187 \le \mathrm{Gr}^{0.01}\,\mathrm{Pr}^{2.8} \le 243$ and $64 \le \lambda \le 144$.

For cooled annuli:

$$C_d = 0.86\left(\mathrm{Gr}^{0.01}\,\mathrm{Pr}^{2.9}\right)^{0.37} \tag{C.11}$$

$$z = -0.48 \times 10^3 \left(\mathrm{Gr}^{0.01}\,\mathrm{Pr}^{2.9}\right) - 0.66 \tag{C.12}$$

For an applicable range of $1\,400 \le \mathrm{Re} \le 2\,500$, $60 \le \mathrm{Gr}^{0.01}\,\mathrm{Pr}^{2.8} \le 75$ and $64 \le \lambda \le 144$.

Figure C.13 and Figure C.14 show the comparison between experimental results and the predicted friction factors for $\tau = 0.975$ and $\tau = 0.965$, respectively. The agreement between the experimental results and the proposed correlations was good, with all the data points being predicted within a $\pm 11\%$ error band for both $\tau = 0.975$ and $\tau = 0.965$.
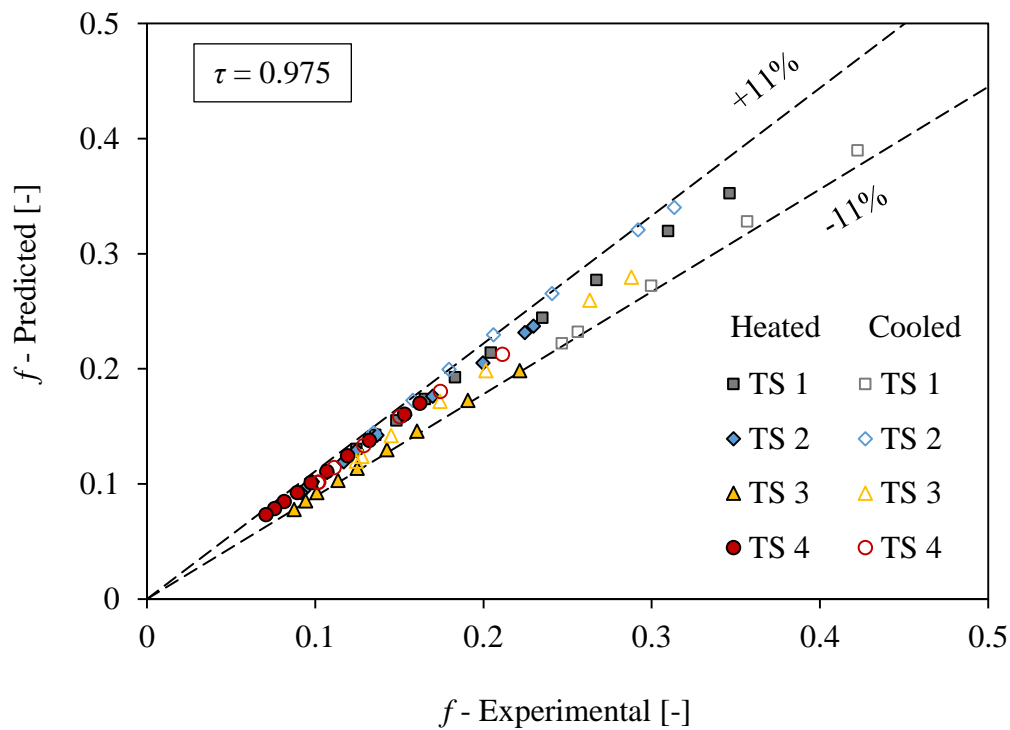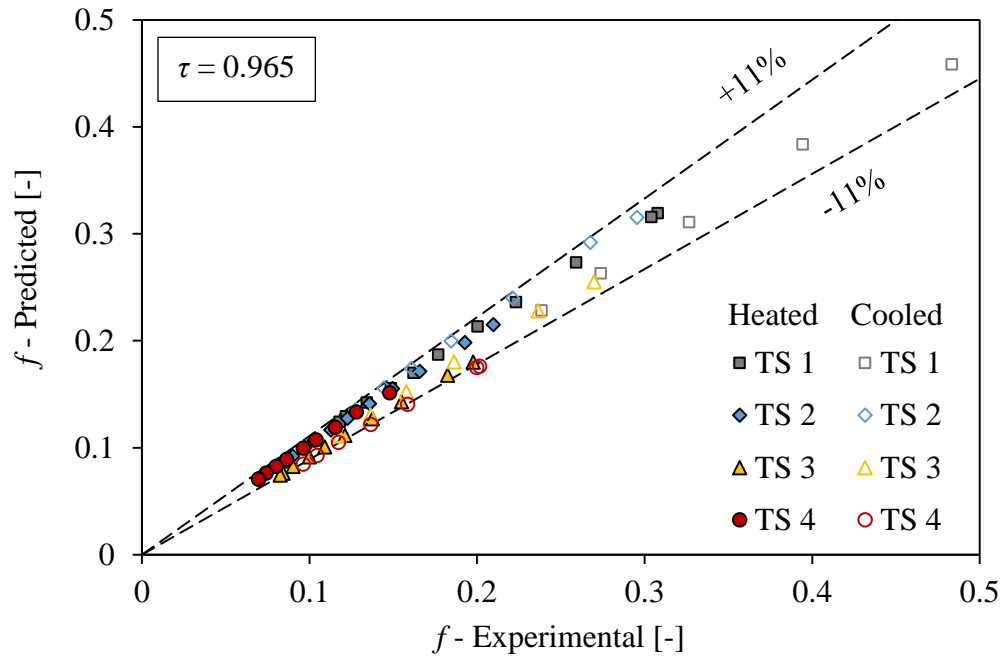

Figure C.13: Comparison between the experimental and predicted friction factors for $\tau = 0.975$

Figure C.14: Comparison between the experimental and predicted friction factors for $\tau = 0.965$